Proceedings of
the 25th Workshop on General Relativity and Gravitation in Japan

7—11 December 2015

Yukawa Institute for Theoretical Physics, Kyoto University
Kyoto, Japan

Volume 3

Oral Presentations: Third Day

Contents

Oral Presentations: Third Day

Wednesday 9 December

Plenary Session 5 [Chair: Takahiro Tanaka]

9:30 Hideo Kodama (KEK) [Invited]
"Is Higher-Dimensional Theory Tool or Reality? – Compactification By Non-Compact Space –"
[JGRG25(2015)I07]

10:30 Short poster talks (3/3)

10:45-11:00 Caffee break

Parallel Session 4a [Chair: Akihiro Ishibashi]

11:00 Tetu Makino (Yamaguchi U.)
"On mathematical study of the Einstein-Euler-de Sitter equations"
[JGRG25(2015)4a1]

11:15 Kentaro Tomoda (Kobe U.)
"Antisymmetric tensor generalisations of affine vector fields"
[JGRG25(2015)4a2]

11:30 Benson Way (DAMTP)
"The Black Ring is Unstable"
[JGRG25(2015)4a3]

11:45 Kentaro Tanabe (KEK)
"Evolution and endpoint of the black string instability: Large D solution"
[JGRG25(2015)4a4]

12:00 Masato Nozawa (U. of Milan, INFN)
"Black holes with scalar hair in N=2 supergravity"
[JGRG25(2015)4a5]

12:15 Yasufumi Kojima (Hiroshima U.)
"Origin of outgoing electromagnetic power by a black hole rotation"
[JGRG25(2015)4a6]

Parallel Session 4b [Chair: Hideki Ishihara]

11:00 Ryotaro Kase (TUS)
"Existence and disappearance of conical singularities in GLPV theories"
[JGRG25(2015)4b1]

11:15 Norihiro Tanahashi (DAMTP)
"Causality, Hyperbolicity & Shock formation in Lovelock Theories"
[JGRG25(2015)4b2]

11:30 Katsuki Aoki (Waseda U.)
"Relativistic Stars in the Bigravity Theory"
[JGRG25(2015)4b3]

11:45 Kazufumi Takahashi (RESCEU)
"Universal instability of hairy black holes in Lovelock-Galileon theories in D dimensions"
[JGRG25(2015)4b4]

12:00 Kohji Yajima (Rikkyo U.)
"Suppressing the primordial tensor amplitude without changing the scalar sector in quadratic curvature gravity"
[JGRG25(2015)4b5]

12:15 Daisuke Yoshida (Kobe U.)
"Quasi-Normal Modes of Lovelock Black Hole"
[JGRG25(2015)4b6]

12:30-14:30 Lunch & poster view

Parallel Session 5a [Chair: Yasufumi Kojima]

14:00 Shinsuke Kawai (Sungkyunkwan U.)
"Holographic Reheating"
[JGRG25(2015)5a1]

14:15 Motoyuki Saijo (Waseda U.)
"Unstable Mechanism of Low T/W Dynamical Instability"
[JGRG25(2015)5a2]

14:30 Hajime Sotani (NAOJ)
"Oscillation spectra of neutron stars with highy tangled magnetic fields"
[JGRG25(2015)5a3]

14:45 Nami Uchikata (Rikkyo U.)
"Deformation of thin-shell gravastars"
[JGRG25(2015)5a4]

15:00 Yuji Akita (Rikkyo U.)
"Primordial non-Gaussianities of gravitational waves beyond Horndeski"
[JGRG25(2015)5a5]

15:15 Yoshimune Tomikawa (Nagoya U.)
"New definition of wormhole throat"
[JGRG25(2015)5a6]

Parallel Session 3b [Chair: Ken-ichi Nakao]

14:00 E. P. Berni Ann Thushari (Kyushu U.)
"Observational constraints on variable equation of state parameters of dark energy"
[JGRG25(2015)5b1]

14:15 Atsushi Naruko (TiTech)
"Gravitational scalar-tensor theory"
[JGRG25(2015)5b2]

14:30 Taishi Katsuragawa (Nagoya U.)
"Compact stars in massive gravity"
[JGRG25(2015)5b3]

14:45 Sakine Nishi (Rikkyo U.)
"Matter Creation in Generalized Galilean Genesis"
[JGRG25(2015)5b4]

15:00 Hiromu Ogawa (Rikkyo U.)
"Instability of hairy black holes in shift-symmetric Horndeski theories"
[JGRG25(2015)5b5]

15:15 Sirachak Panpanich (Waseda U.)
"Effects of Vainstein Screening on LSB Galaxies and Milky Way"
[JGRG25(2015)5b6]

15:30-16:30 Coffee break & poster view

Plenary Session 4 [Chair: Kei-ichi Maeda]

16:30 Takashi Nakamura (Kyoto U.) [Invited]
"Some Topics of Sources of Gravitational Waves and available Physics from them"
[JGRG25(2015)I08]

18:00 Banquet

“Is Higher-Dimensional Theory Tool or Reality? – Compactification By Non-Compact Space –”

by Hideo Kodama (invited)

[JGRG25(2015)I07]

Is Higher-Dimensional Theory Tool or Reality? -- Compactification By Non-Compact Space --

Hideo Kodama

Theory Center, KEK

JGRG25, YITP, 9 December 2015

Maximal Symmetry Principle

Personal Great Ansatz

Maximal local symmetry is realized in the ultimate theory.

$$\mathscr{L} = (\mathrm{ST\ sym.} \oplus \mathrm{Internal\ sym.}) \oplus \mathrm{SUSY}$$

Maximal SUSY:	N=8 SUSY
Maximal ST sym.:	D=11 Lorentz
Maximal Internal sym.:	???

SSB & decoupling

Low energy 4D real world with lower symmetry

High Energy

Low Energy

Plan of the Talk

- Introduction
  - Maximal symmetry principle ?
- Do we have a successful influm in string/M theory?
  - No-Go theorems against cosmic acceleration
  - Remaining options
- Inflation in 4D supergravity
  - N=8 gauged supergravity
  - Inflation in the SO(4,4) gauged maximal supergravity
- Can we uplift a maximal supergravity influm to 11D?
  - Uplift of the SO(8) gauged theory
  - Uplift of the SO(4,4) gauged theory
- Summary

» De we have a successful influm in string/M theory?

SEC

Raychaudhuri Equations [1955]

$$n\frac{\ddot{\ell}}{\ell} = -\sigma^2 + \omega^2 - R_{\mu\nu}V^\mu V^\nu$$

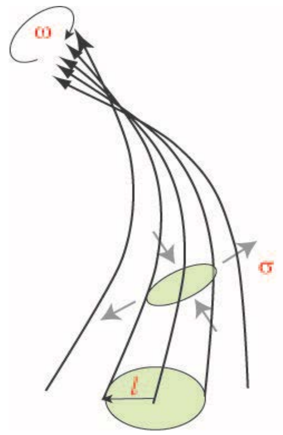

Strong Energy Condition
=Timelike convergence condition

For any timelike vector V,

$$\mathrm{Ric}(V,V) = R_{\mu\nu}V^\mu V^\nu \geq 0$$

Implications
If the strong energy condition is satisfied;
- gravity becomes attractive;
- the cosmic expansion decelerates.

Gibbons' No-Go Theorem

Theorem For a compactification $M_{n+4} = X_4 \times Y_n$ of a higher dimensional theory by a classical solution satisfying the following conditions, the strong energy condition is satisfied in the four-dimensional spacetime X_4:

1. The spacetime metric has the structure
$$ds^2(M_{n+4}) = W(y)^{1/2} ds^2(X_4) + ds^2(Y_n).$$
2. The internal space Y_n is a smooth compact manifold without bounary, and its metric is static.
3. The warp factor $W(y)$ is regular and bounded everywhere.
4. The original higher-dimensional theory satisfies the SEC.
(This is the case for all 10D/11D supergravities.)

Gibbons GW (1984): Aspects of Supergravity Theories, Three lectures given at GIFT Seminar on Theoretical Physics, San Feliu de Guixols, Spain, Jun 4-11, 1984.

Proof

From the assumptions, we have

$$R_{VV}(X) = R_{VV} - \frac{1}{4W}\triangle_Y W$$

for any timelike vector V parallel to X. By integrating this equation over Y, we obtain

$$R_{VV}(X)\int_Y d\Omega(Y)W = \int_Y d\Omega(Y)\left[W\,R_{VV} - \frac{1}{4}\triangle_Y W\right]$$

If $R_{VV} \geq 0$ and W is regular and bounded everywhere, the right-hand side of this equation is non-negative. Hence, we obtain

$$R_{VV}(X) \geq 0$$

Q.E.D.

Accelerating 4D Universe from 10/11D

- To circumvent the No-Go theorem, at least one of the following conditions must be violated:

1. Semi-classical description of the internal structures .
2. Warped compactification: $ds^2(M_D) = W(y)^2\, g(X_4) + g(Y_n)$.
3. Y_n: stationary, compact and closed.
4. W(y): a smooth, non-vanishing and bounded function.
5. The original semi-classical HD theory satisfies the strong energy condition.

Maldacena-Nunez's No-Go Theorem

[Maldacena JM, Nunez G (2001): IJMPA16, 822.]

Theorem For a compactification $M_D = X_d \times Y_n$ of a higher dimensional theory by a classical solution satisfying the following conditions, X_d cannot be de Sitter spacetime:

1. The spacetime metric has the structure
$$g(M_D) = \Omega(y)^2 \left[g(X_d) + \hat{g}(Y_n)\right].$$
2. Near the boundary of Y_n or singularities of Ω, Ω decreases monotonically toward them.
3. The Newton constant in X_d is finite:
$$\int_Y d\mu_{\hat{g}} \Omega^{D-2} < \infty.$$
4. In the original higher-dimensional theory, the potential is non-positive and all massless bosonic fields have positive kinetic terms.

Note: A stronger result can be obtained for the massive IIA supergravity.

No-Go Theorems for Corrections to HD Theories

No SO(4,1)-invariant compactification for the following modifications

- IIB
  - adding smeared D-branes and anti-D-branes
  - without O-planes, α' corrections, NP corrections, loop corrections

  [Dasgupta et al 2014; Giα' ddings, Kachru, Polchinski 2002]
- Heterotic
  - adding gaugino condensates and perturbative α' corrections
  - No stringy loop or non-perturbative correction

  [Gautason, Junghans, Zagermann 2012;Quigley 2015]
- Heterotic or type IIB with no RR fluxes
  - all perturbative α' corrections and WS NP effects
  - no stringy loop or non-perturbative correction

  [Kutasov et al 2015]

Remaining possibilities

- Stringy higher-loop/non-perturbative effects

  ⇒ ???

- Higher-order α' corrections with RR fluxes (type II SST)

  ⇒ Kaehler uplifting of the KKLT-type compactifications.

  KKLT-type LVS in the type IIB

  – CY compactif of a no-scale IIB w SD flux + NP qn effects (D-instantons/gaugino condensates) + D-branes+O-plane + higher-order alpha' corrections (+ string loop corrections)

    => Effective 4D N=1 sugra models

- Non-compact internal space

» Inflation in 4D Supergravity

Basic 4D Supergravity Theories

	N	classification	mult.	$N=8 \rightarrow N'$	Scalar Manifold	dim
	8	unique	$[2]_8$		SymS: $E_{7(7)}/SU(8)$	70
	6	unique	$[2]_6$	$+2[3/2]_6$	SymS: $SO^*(12)/U(6)$	30
Unique	5	unique	$[2]_5$	$+3[3/2]_5$	SymS: $SU(5,1)/U(5)$	10
	4	n = #of vector multiplets	$[2]_4$ $+n\,[1]_4$	(n=6) $+4[3/2]_4$	SymS: $SU(1,1)/U(1)$ $\times SO(6,n)/(SU(4)\times SO(n))$	6n+2
No Func.	3	n= # of vector mulltiplets	$[2\text{-}1/2]_3$ $+ n\,[1]_3$	(n=4) $+6[1]_3$ $+5[3/2]_3$	SymS: $SU(3,n)/(U(3)\times SU(n))$	6n
V=0	2	Prepotential F(Z) (h_{uv},J^I)	$[2\text{-}1]_2$ $+n_V\,[1]_2$ $+2n_H[1/2]_2$		Special Kaehler x Quaternion-Kaehler	$2n_V$ $+4n_H$
	1	$K(Z,Z^*)$ $W(Z)$ $N_{AB}(Z)$	$[2\text{-}3/2]_1$ $+n_V[1\text{-}1/2]_1$ $+ n_c\,[1/2]_1$		Kaehler-Hodge	$2n_c$

Influm by N=1 Supergravity

- The η-problem
- Shift symmetry
- Instability problem
- Stabilizer problem
- Uplift problem

Gauging

D=4 N=8 ungauged SUGRA

$$(g_{\mu\nu},\ A^M_\mu,\ \mathscr{V};\psi^a_\mu,\ \chi^{abc})$$

D=4 N=8 gauged SUGRA

Duality Group $E_{7(7)}$

$$\mathscr{V} \in \boldsymbol{E_{7(7)}/\mathrm{SU}(8)}$$

Gauge Group (28 dim) $G \subset E_{7(7)}$

$$A^M = \begin{cases} \text{electric}: A^{[ab]} \in \mathbb{R}^{28} \\ \text{magnetic}: A_{[ab]} \in \mathbb{R}^{28} \end{cases}$$

$$N_{\Lambda\Sigma}F^{(+)\Sigma} = F^{(+)}_\Lambda$$

$$\mathscr{A} = A^M X_M \in \mathrm{ad}(G) \subset \rho_{56}(E_{7(7)})$$

$$D\mathscr{V} = (\partial + g\mathscr{A})\mathscr{V}$$

Abelian gauge fields are uncoupled to the other fields.

No potential.
All fields are massless.

Non-Abelian gauge fields are coupled to the scalar fields.

Non-trivial potential and mass terms.

Classification of the SL8-type Gaugings

- Dyonic gauging

$$\mathscr{A} = \begin{pmatrix} -(\theta A_e + A_m\xi)\wedge 1 & 0 \\ 0 & -(A_e\theta + \xi A_m)\wedge 1 \end{pmatrix} \in M(56,\mathbb{R}), \quad \theta,\xi \in \mathrm{S}(8)$$

- Non-degenerate cases: $\theta\xi=1$

$$\theta \cong \boldsymbol{s} I_{p,q}, \quad \xi \cong \boldsymbol{s}^{-1} I_{p,q}$$

Deformation parameter s

$$G = \mathrm{SO}(p,q) \quad (p+q=8)$$

[Dall'Agata, Inverso 2012; HK, Nozawa 2013]

- Degenerate cases: $\theta\xi=0$

$$\theta \cong I_{p,q} \oplus 0_{r+s+t}, \quad \xi \cong 0_{p+q+r} \oplus I_{s,t} \quad (p+q+r+s+t=8)$$

$$G \cong \mathrm{SO}(p,q) \times \mathrm{SO}(s,t) \ltimes \mathbb{R}^{(p+q+r)(r+s+t)-r^2}$$

Electric gauging : $\xi = 0 \Rightarrow \quad G = \mathrm{CSO}(p,q,r) \cong \mathrm{SO}(p,q) \ltimes \mathbb{R}^{r(p+q)}$

Special SL8-type Gaugings

Special SL8-type gauging ⇔ SL8-type gauging in which one of the critical point can be moved to the base point by a SL8 transformation.

All special SL8-type dyonic gaugings are classified (GTTO):

[HK, M Nozawa (2013) ; G Dall'Agata, G Inverso (2012)]

$\theta\xi=1:$ $\quad \mathrm{SO}(8), \quad \mathrm{SO}(7,1), \quad \mathrm{SO}(6,2), \quad \mathrm{SO}(5,3), \quad \mathrm{SO}(4,4)$

$\theta\xi=0:$ $\quad \mathrm{SO}(4)\times\mathrm{SO}(2,2)\ltimes\mathbb{R}^{16}, \quad \mathrm{SO}(6)\times\mathrm{SO}(1,1)\ltimes\mathbb{R}^{12},$
$\mathrm{SO}(2)^2\ltimes\mathbb{R}^{20}, \quad \mathrm{SO}(7)\ltimes\mathbb{R}^{7}$

Inflationary Universe in the 4D Maximal Sugra

- Only three dS vacua have been found up to this point:
  - SO(4,4) gauging: HW saddle point and DI saddle point
  - SO(5,3) gauging: HW saddle point.
- Stable Starobinsky-type inflation in the SO(4,4) gauging
  - Attractor slow roll trajectories consistent with observations exist for the deformation parameter s around its critical value.

$$V=\frac{3}{2}(\sqrt{2}-1)\left(1-2e^{-\sqrt{2}\phi}+\frac{8}{3}e^{-2\sqrt{2}\phi}\right).$$

[HK, M Nozawa 2015]

Is there an uplift of this theory to the 11D sugra?

Inflation in the SO(4,4) Maximal Sugra

HK, M Nozawa: JCAP 15025, 028 (2015) arXiv: 1502.01378

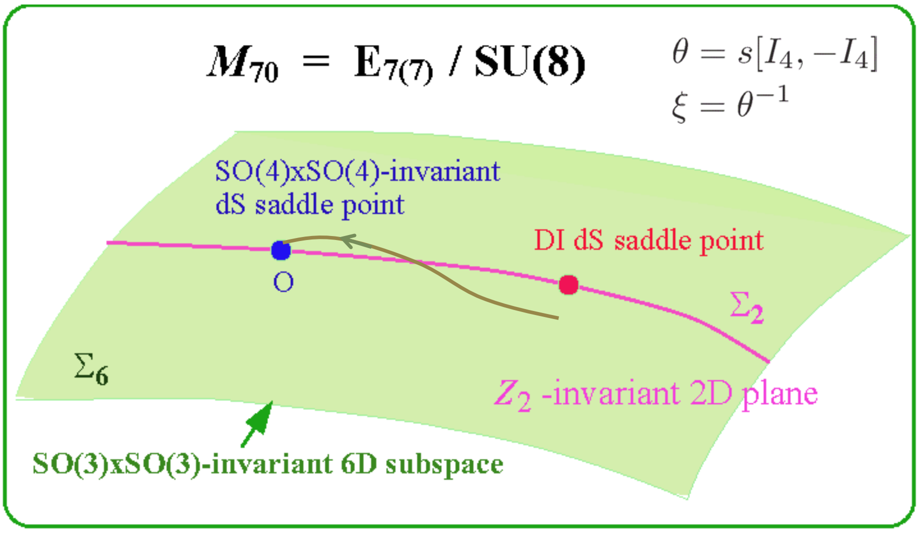

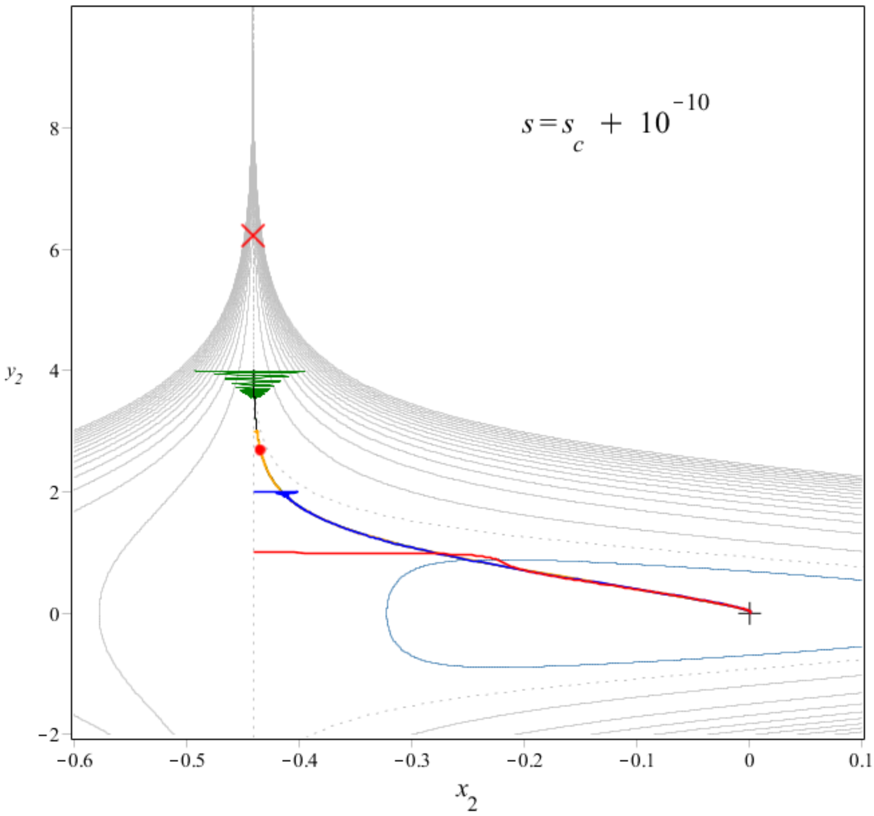

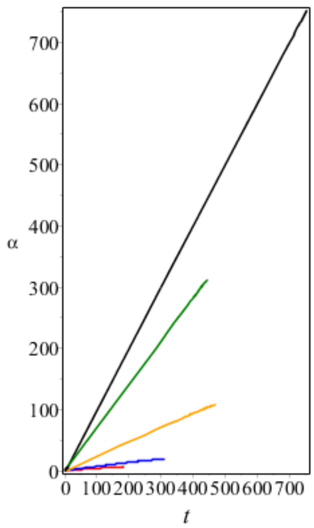

Can we uplift a maximal sugra influm to 11D?

D=11 Supergravity

[Cremmer, Julia, Scherk 1978]

- Fundamental fields

$$\text{Metric/frame field}: \quad e_A = (e_A^M); \quad g^{MN} = \eta^{AB} e_A^M e_B^N, \quad \theta^A(e_B) = \delta_B^A,$$

$$\text{Form gauge fields}: \quad A_3 = \frac{1}{3!} A_{MPQ} dx^M \wedge dx^P \wedge dx^Q,$$

$$\text{Majorana } 3/2 \text{ field}: \quad \Psi_M; \quad \Gamma_{(11)}\Psi_M = +\Psi_M.$$

- Action

$$\begin{aligned}
2\kappa^2 S = & \int d^{11}x|\theta| \Big[R_s(g) - \frac{1}{2}|F_4|^2 + \frac{1}{6} * (F_4 \wedge F_4 \wedge A_3) \\
& -i\bar{\Psi}_M \Gamma^{MNP} D_N \Psi_P + \Psi^4 \text{ terms} \\
& + \frac{i}{96} \left(\bar{\Psi}_M \Gamma^{MN****} \Psi_N + 12 \bar{\Psi}^* \Gamma^{**} \Psi^* \right) F_{****} \Big].
\end{aligned}$$

Uplifting of 4D maximal sugra to 11D (1)

- Ungauged => **M / T^7**

  [Cremmer, Julia 1978]

- Nil gauging => **M / Twisted T^7 (no gauge flux)**
  - Some stable Minkowski vacua: with geometrical flux

    [Cremmer, Scherk 1979; Schwarz 1979 ; Kaloper, Myers 1999]

- SO(8)-gauging => **M / S^7**
  - SO(8)-inv. stable adS vacuum : round S7 with no torsion
  - SO(7)-inv. unstable adS vacua: round S7 with parallelising torsion

    [Englert et al 1983; de Wit, Nicolei 1984]
  - Full uplifting for the electric SO(8)-gauging.

    [de Wit, Nicolei 1987; Nicoli, Pilch 2012; de Wit, Nicolei 2013]

Uplift of the SO(8)-inv. critical point

- SO(8)-invariant critical point of the 4D SO(8) theory.
  - Potential: $V_0 = -3g^2/4$ => adS vacuum
  - Masses: OSp(4|8) massless multiplet.
    - scalar: $m_s^2/|V_0| = -2/3 > -3/4$ [35+35] (BF bound)
    - vector, ½ field, graviton: massless [28, 56, 1]
    - 3/2 field: $m_{3/2}^2/|V_0| = 1/3$ [8]
- Uplift to 11D
  - Geometry: $M_{11} = adS_4 \times$ round S^7 with $\Lambda = -12/\ell^2$ ⇒ $g = \dfrac{4}{\ell}$
  - Flux: $F = f\,\Omega(X_4)$ with $f = 6/\ell$
  - Masses of perturbations: "The lowest supermultiplet" has the same spectrum as above. [Duff, Nilsson, Pope: PLC130, 1 (1986)]

➢ The gauge coupling constant corresponds to the curvature scale of Y_7.

➢ The gauge group is the isometry group of Y_7.

KK tower at the SO(8)-inv point

◆ D=4 N=8 SO(8) sugra is not a simple KK reduction of D=11 Sugra.

- Each massive supermultiplet contains fields with different masses.
- A negative mass^2 mode and zero mass mode are contained in massive supermultiplet.

Level n	mass spectrum
-2	0^+: **8** [1]
-1	½: **1** [8_c], 0^+: **3** [8_v] <= Gauge modes
0	2: **0** [1], 1^-: **0** [28_{adj}], 0^+: **0** [35], 0^-: **0** [35] 3/2: **0** [8_s], ½: **0** [56]
1	2: **7** [8_v], 1^-: **3** [160], 1^+: **15** [56], 0^+: **-1** [112], 0^-: **3** [210] 3/2: **1** [56], **49** [8_c], ½: **1** [126], **9** [160]
2	2: **16** [126], 1^-: **8** [105], **48** [28], 1^+: **24** [56], 0^+: **0** [294], **24** [50], **80** [1], 0^-: **8** [560], 0^-: **48** [15] 3/2: **4** [70], **64** [56], ½: **4** [112], **16** [280], **36** [160], **64** [8_s]
3	….

Uplifting of 4D maximal sugra to 11D (2)
-- Non-compact semi-simple gauging --

- HW dS vacua
  - SO(4,4) gauging: SO(4)xSO(4)-inv.
  - SO(5,3) gauging : SO(5)xSO(3) –inv.

  => **M / $H_E^{p,q}$: 'Non-compact' internal space**

  [Hull, Warner 1988]

- DI dS vacuum
  - SO(4,4) gauging: New SO(3)xSO(3)-inv. dS vacuum

  => **M/deformed $H_E^{4,4}$ with internal 3-form flux**

  [Baron, Dall'Agata: arXiv: 1410.8823]

$H^{p,q}{}_E$

- Generalised hyperboloid: $H_{+/-}{}^{p,q} \subset E^{p,q}$

$$H^{p,q}_{\pm}: \quad \eta_{ab}X^a X^b = \pm A^2$$

$$\mathrm{Isom}_0(H^{p,q}_{\pm}) = \mathrm{SO}(p,q)$$

- Embedding to the Euclidean space E^{p+q}

$$j: H^{p,q}_{\pm} \to E^{p+q} \Rightarrow \quad H^{p,q}_{\pm E} \cong S^{p-1} \times S^{q-1} \times \mathbb{R}$$

$$\mathrm{Isom}_0(H^{p,q}_{\pm E}) = \mathrm{SO}(p) \times \mathrm{SO}(q)$$

$$g(H^{p,q}_{+E}) = \cosh(2\psi)d\psi^2 + \cosh^2(\psi)g(S^{p-1}) + \sinh^2(\psi)g(S^{q-1})$$

Questions

- Scalar field mass

Scalar fields have (mass)^2 of the order of g^2.

✔How do these mass arise by mass-less truncation in the KK reduction?

Is there a mass gap for perturbations in 11D for 'open compatif' ?

- Scalar potential

Where does the potential come from?

Why is the potential unbounded in the gauged extended sugra?

Can we avoid the unbounded potential from 11D perspective?

- Local Susy

Non-compact internal spaces has no global Killing spinor.

Where does the N=8 local susy come from?

Uplift Prescription for the SO(p,q) gauging

[Baron, Dall'Agata: JHEP1502, 003 (2015)]

- To realise SO(p,q) gauge symmetry,

embed the Killing vectors of the indefinite metric space $H^{p,q}$ to $H_E^{p,q}$:

$$K^m_{[AB]}:\ 28\ \text{generators of}\ \mathrm{SO}(p,q) \hookrightarrow \mathscr{X}(H_E^{p,q}).$$

$$K_{mn}^{[AB]} \equiv R^{-1} \overset{o}{g}{}^{(L)}_{mp} \eta^{AC} \eta^{BD} \overset{o}{\nabla}{}^{(L)}_n K^p_{[CD]}; \quad \eta = [I_p, -I_q]$$

- 11D metric

$$ds^2(M_{11}) = \Delta(x,y)^{-1} g_X(x) + g_{mn}(x,y)(dy^m + B^m)(dy^n + B^n)$$

$$\boldsymbol{\Delta^{-1} g^{mn}} = -2K^{(m}_{AB}(y) K^{n)}_{CD}(y) \boldsymbol{\mathscr{V}^{[AB]ij}(x) \mathscr{V}^{[CD]}{}_{ij}(x)}.$$ 35 scalars

$$\Delta(x,y) = \left[\det g_{mn}(x,y)/|\det g^{(L)}_{mn}(y)|\right]^{1/2}$$

$$\boldsymbol{B^m} = -\frac{1}{2} K^m_{AB}(y) \boldsymbol{A^{[AB]}(x)}$$ 'Electric' gauge fields

- Form gauge fields

35 axionic fields

$$\boldsymbol{A_{mnp}} = \frac{1}{\sqrt{2}} \Delta(x,y) g_{pq}(x,y) K^{AB}_{mn}(y) K^q_{CD}(y) \boldsymbol{\mathscr{V}_{[AB]ij}(x) \mathscr{V}^{[CD]ij}(x)},$$

$$\boldsymbol{A_{\mu mn} - B^p_\mu A_{mnp}} = -\frac{1}{2\sqrt{2}} K^{AB}_{mn}(y) \boldsymbol{A_{\mu[AB]}(x)},$$ 'Magnetic' gauge fields

$$\boldsymbol{F_{\mu\nu\lambda\sigma}} = f_{\mathrm{FR}} \epsilon_{\mu\nu\lambda\sigma}.$$ 11D Einstein eqs

- Spinor fields

Not determined yet!

Can we utilise the Killing spinor on $H^{4,4}$ with indefinite metric?

Example: SO(4,4) gauging

- HW dS critical point: SO(4)xSO(4) invariant
  - 4D

$$\begin{aligned} \text{Metric} &: \quad X_4 = \mathrm{dS}^4; \quad \Lambda = \tfrac{1}{4}g^2, \\ \text{Scalar field} &: \quad \mathscr{V} = \mathscr{V}(0) = \tfrac{1}{\sqrt{2}}\left(\begin{smallmatrix} -i & -i \\ -1 & 1 \end{smallmatrix}\right) \otimes I_{28}, \\ \text{Gauge fields} &: \quad A^M = 0. \end{aligned}$$

  - 11D

$$ds^2(M^{11}) = W(y)^2 g(\mathrm{dS}^4(\Lambda)) + \ell^2 W(y)^{-1} g(H_E^{4,4});$$

$$W(y) = \cosh^{1/3}(2y),$$

$$F_{[4]} = f\Omega(X^4); \quad f = \tfrac{2}{\ell}, \quad \ell = \frac{4}{g}, \quad \Lambda = \frac{4}{\ell^2}.$$

- DI dS critical point: SO(3)xSO(3) invariant

An uplifting solution with cohomogeneity 2 non-compact internal space and an internal flux was constructed. [Baron, Dall'Agata 2015]

The Origin of Potential and its Unboundedness

- The Origin in D=11 supergravity

$$S_B = \int d^{11}x\sqrt{-g}\left[\frac{1}{2}R_s(g) - \frac{1}{2}|F_4|^2 + \frac{1}{6}\cancel{*(F_4 \wedge F_4 \wedge A_3)}\right]$$

$$ds^2(M_{11}) = W(y,\phi(x))^2 g_X(x) + \hat{g}_{mn}(y,\phi(x))(dy^m + B^m)(dy^n + B^n)$$

  - Scalar curvature

$$\sqrt{-g}R_s(M^{11}) \to V_R = \int d\mu_Y \left[-\frac{W^4}{2}R_s(Y) - 6W^2(\hat{\nabla}W)^2\right] + \boldsymbol{V_R^\partial}$$

Contribution from the boundary ∂ Y at infinity

  - Flux

$$F_{[4]} = f\Omega(X_4) + \hat{F}_{[4]} + \cdots$$

$$\sqrt{-g}|F_{[4]}|^2 \to V_F = \int d\mu_Y \, \frac{1}{2}\left(-\frac{f^2}{W^4} + W^4\hat{F}^2\right)$$

- Estimation for the SO(4,4) uplift

All integrals diverge. So, regularisation is required.

– The gravitational constant

$$\frac{1}{\kappa^2} = \int d\mu_Y W^2 = \Omega^2 \int_0^L dy \frac{1}{8}\ell^7 \sinh^3(2y) \sim \frac{\ell^7}{48} e^{6L}\Omega^2 \quad (\Omega = \mathrm{vol}(S^3))$$

– V_R

$$V_R^0 = \Omega^2 \int_0^L dy \left(-\frac{\ell^5}{8}\right) \frac{\sinh^3(2y)(8\cosh^2(2y)+1)}{\cosh^2(2y)} \sim -\frac{\ell^5}{6} e^{6L}\Omega^2,$$

$$V_R^\partial = \int_{y=L} d\Sigma W^4 K \sim \frac{\ell^5}{4} e^{6L}\Omega^2,$$

$$V_R \sim \frac{\ell^5}{12} e^{6L}\Omega^2.$$

– V_F

$$V_F = \Omega^2 \int_0^L dy \frac{\ell^5}{64} \frac{\sinh^3(2y)}{\cosh^2(2y)} \sim \frac{\ell^5}{2} e^{2L}\Omega^2$$

– Cosmological constant

$$\Lambda = \kappa^2 V = \frac{4}{\ell^2}$$

- Scaling behavior

$$g(Y_7) \quad \to \quad \lambda^2 g(Y_7) \qquad g(X) \to \lambda^{-7} g(X), \quad W \to W$$

– Internal geometry

$$d\mu_X d\mu_Y \to \lambda^{-7} d\mu_X d\mu_Y, \quad R_s(Y) \to \lambda^{-2} R_s(Y), \quad (\hat\nabla W)^2 \to \lambda^{-2}(\hat\nabla W)^2$$

$$V_R = \int d\mu_Y \left[-\frac{W^4}{2} R_s(Y) - 6W^2(\hat\nabla W)^2 + \hat\triangle(W^4)\right] \to \frac{1}{\lambda^9} V_R$$

– Flux

$$d(W^4 *_Y \hat F) = f\hat F \Rightarrow \quad f \to \lambda^{-1} f, \quad \hat F_4 \to \hat F_4$$

$$V_F \to \int d\mu_Y \, \frac{1}{2}\left(-\frac{1}{\lambda^9}\frac{f^2}{W^4} + \frac{1}{\lambda^{15}} W^4 \hat F^2\right)$$

The potential diverges in the small internal space limit $\lambda \to 0$.

Harmonic Analysis on $H^{4,4}_E$

- **Scalar Laplace-Beltrami operator**
  - 11D metric: (y=2ψ)

$$ds^2(M^{11}) = \cosh^{2/3}(y) g(\mathrm{dS}^4) + \ell^2 \cosh^{-1/3}(y) g(H_E^{4,4})$$

  - Harmonic expansion:

$$\Box_{M^{11}}\phi = 0 \Rightarrow \quad \phi = \sum_j \phi_j(x) u_j(y); \quad \left(\Box_{dS^4} - m_j^2\right)\phi_j = 0$$

where

$$\mathcal{L}^{\mathrm{HW}}_{4,4} u_j = \lambda_j u_j \Rightarrow \quad \frac{m_j^2}{\Lambda} = \lambda_j,$$

$$\mathcal{L}^{\mathrm{HW}}_{4,4} \equiv -\frac{1}{\sinh^3 y}\partial_y\left(\sinh^3 y \partial_y\right) - \frac{\cosh y}{2(\cosh y + 1)}\triangle_{S_1^3} - \frac{\cosh y}{2(\cosh y - 1)}\triangle_{S_2^3}$$

$$z = \cosh y$$

$$L = -\frac{1}{z^2-1}\frac{d}{dz}\left((z^2-1)^2\frac{d}{dz}\right) + \ell_1(\ell_1+2)\frac{z}{2(z+1)} + \ell_2(\ell_2+2)\frac{z}{2(z-1)}.$$

- **Spectrum**
  - Normalisation

$$\|u\|^2 = \int_1^\infty dz(z^2-1)|u(z)|^2.$$

  - Continuous spectrum

$$\lambda \geq \frac{\ell_1(\ell_1+2) + \ell_2(\ell_2+1)}{2} + \frac{9}{4}$$

  - Discrete spectrum: $\ell_1 > \ell_2+1$

$$\lambda = \frac{\ell_1(\ell_1+2) + \ell_2(\ell_2+1)}{2} + \frac{9}{4} - \alpha^2; \quad \alpha = 0, 1, \cdots, [\tfrac{\ell_1-\ell_2-1}{2}]$$

  - Low lying modes
    - $\ell_2=0, \ell_1=0,1$: no discrete spectrum

      Continuous spectrum: $\lambda \geq 9/4$

    - $\ell_2=0, \ell_1=2$:

      Continuous spectrum: $\lambda \geq 25/4$

      Discrete spectrum: $\lambda = 6$.

The lowest mode $\lambda=0$ (u=const) is not contained in the spectrum because it is not normalisable.

Gravitational tensor perturbation wrt S^3_1, but no counterpart in the spectrum of the 4D theory.

The Origin of the Maximal Local SUSY

- **SO(8) gauging**

  In the case of compactification on S^7, local SUSY transformations are defined after the deviation of the internal geometry from the round sphere is "gauged away" with the help of the generalised frame field.

- **SO(p,q) gauging**

  The number of local SUSY is determined not by the real structure of the internal space, but rather by its maximal geometry, which need not be Riemannian.

These examples suggest that the maximal number of local SUSY is determined by the topology of the internal space, but we cannot give a definite argument to support this.

» Conclusion

- 4D vs High D
  - Four-dimensional supergravity theory may not be a simple low energy effective theory of a compactified higher-dimensional theory.
  - This implies that either of them is not reality.
- Compactification by non-compact space
  - If you believe that higher-dimensional unified theory describes reality, compactification by non-compact space can be a very fascinating remaining option to realise an inflationary universe.
  - Lots of work have to be done to confirm this possibility:
    - Clarify the geometrical meaning of the deformation parameter in the dyonic SO(p,q)-gaugings.
    - Complete the embedding formula of 4D to 11D/10D.
    - Check the stability of the embedding -- the complete spectrum of perturbations.
    - List up all critical points of the potential for non-compact semi-simple gaugings.
    - Explore non-SL8 gaugings.

» Backup slides

Killing spinors

- Killing spinor in 11D

$$\tilde{D}_M\tilde{\epsilon} \equiv \tilde{\nabla}_M\tilde{\epsilon} + \frac{1}{288}\left(\tilde{\Gamma}_M{}^{****} - 8\delta^*_M\tilde{\Gamma}^{***}\right)F_{****}\,\tilde{\epsilon} = 0.$$

- Freund-Rubin type warped compactification

$$\boxed{\begin{aligned}\tilde{g}(M^{11}) &= W^2(y)g(X_4) + \hat{g}(Y_7),\\ F_{[4]} &= f\Omega(X_4) + \hat{F}_{[4]}(y).\end{aligned}}$$

$$\Gamma^\alpha = \gamma^\alpha \otimes 1 \ (\alpha = 0, \cdots, 3), \quad \Gamma^a = \gamma_5 \otimes \hat{\gamma}^a \ (a = 4, \cdots, 10)$$

$$\tilde{\epsilon} = \epsilon_+(x) \otimes \eta_+(y) + \epsilon_-(x) \otimes \eta_-(y); \quad \gamma_5\epsilon_\pm = \pm\epsilon_\pm$$

$$\Rightarrow \boxed{\begin{aligned}&\hat{D}_m\eta_\pm \equiv (\hat{\nabla}_m + T_m)\eta_\pm = 0;\\ &T_m \equiv \frac{if}{12W^4}\hat{\gamma}_m \pm \frac{1}{72}\left\{3i\hat{\gamma}^{pq}(\,*_Y\hat{F})_{pqm} - 2\hat{\gamma}^{npq}\hat{F}_{mnpq}\right\}.\end{aligned}}$$

Condition for Maximal Susy on Y_7

f ≠ 0 case:

$$[\hat{D}_m, \hat{D}_n] = 0 \Rightarrow \quad dW = 0, \quad \hat{F} = 0$$

$$\Rightarrow \quad \hat{D}_m = \hat{\nabla}_m + \frac{if}{12}\hat{\gamma}_m \Rightarrow \quad [\hat{D}_m, \hat{D}_n] = \frac{1}{4}\hat{R}_{mnab}\hat{\gamma}^{ab} - \frac{f^2}{72}\hat{\gamma}_{mn}$$

$$[\hat{D}_m, \hat{D}_n] = 0 \Rightarrow \quad \hat{R}_{mn}{}^{pq} = \frac{f^2}{36}\delta^{pq}_{mn} \Rightarrow \quad f = \pm\frac{6}{\ell}$$

Therefore, for the maximal susy with f ≠ 0,

- No warp,
- Y_7 must be a round sphere S^7,
- the internal flux should vanish: F=f dΩ(X_4).

(T^7 can also have the maximal susy for F=0.)

Uplift Ansatz: Linear level

[B. Biran, F. Englert, B. de Wit, H. Nicolai (1983)]

- Spinor fields

$$\Psi_\mu(x,y) = \psi'_\mu(x,y) + \frac{1}{2}\gamma_5\gamma_\mu\hat{\gamma}^m\psi'_m(x,y),$$
$$\Psi_m(x,y) = \psi'_m(x,y)$$

$$\Uparrow \qquad \eta_m^{IJK}(y) = -i\eta_+^{[I}(y)K_{+m}^{JK]}$$

$$\psi'_\mu = \boldsymbol{\psi^I_\mu(x)} \otimes \eta_+^I(y) + \cdots,$$
$$\psi'_m = \boldsymbol{\chi^{IJK}(x)} \otimes \left(\eta_m^{IJK}(y) - \tfrac{1}{9}\hat{\gamma}_m\hat{\gamma}^n\eta_n^{IJK}(y)\right) + \cdots$$

  – susy trf

$$\epsilon = \epsilon_I(x) \otimes \eta_+^I(y) + \cdots$$

$$\Rightarrow \quad \delta\psi^I_\mu = (\nabla_\mu - m_7\gamma_\mu\gamma_5)\epsilon_I,$$
$$\delta\chi^{IJK} = 2\sqrt{2}\gamma^\mu\mathscr{P}_\mu^{LIJK}\epsilon_L + \tfrac{3}{2}F^{+[IJ}_{\mu\nu}\gamma^{\mu\nu}\epsilon^{K]} - 2gA_{2L}{}^{IJK}\epsilon^L + \cdots$$

- Metric

$$h_{\mu\nu}(x,y) = h'_{\mu\nu}(x,y) - \frac{1}{2}\overset{(0)}{g}_{\mu\nu}(x)h'^m{}_m(x,y),$$
$$h_{mn}(x,y) = h'_{mn}(x,y), \quad h_{\mu m}(x,y) = h'_{\mu m}(x,y)$$

$$h'_{\mu\nu} = \boldsymbol{h_{\mu\nu}(x)} + \cdots,$$
$$h'_{m\mu} = \boldsymbol{A^{IJ}_\mu(x)}K_{IJm}(y) + \cdots,$$
$$h'_{mn} = -\boldsymbol{A_{IJKL}(x)}\left\{K_m^{[IJ}K_n^{KL]} - \tfrac{1}{9}\overset{(0)}{g}_{mn}K^{l[IJ}K_l{}^{KL]}\right\} + \cdots$$

- Form gauge field

$$A_{\mu\nu\rho}(x,y) = \overset{(0)}{A}_{\mu\nu\rho}(x) + \frac{1}{3!}\epsilon_{\mu\nu\rho\sigma}t^\sigma(x,y);$$
$$\nabla\cdot t(x,y) = \nabla\cdot t'(x) + \frac{3m_7}{\sqrt{2}}[h'^\mu_\mu(x,y) - h'^m_m(x,y)],$$
$$A_{mnp}(x,y) = i\boldsymbol{B_{IJKL}(x)}\Omega^{[IJ}_{[mn}(y)K^{KL]}_{p]}(y)$$

Non-linear Uplifting Prescription

[H. Nicolai, K. Pilch (2012); B. de Wit, H. Nicolai (1987)]

- Ansatz on the 11D sector
  - Bosonic fields

$$g_{M_{11}}(x,y) = \Delta^{-1} g_{X_4}(x) + g_{Y_7}(x,y)$$
$$F_{[4]}(x,y) = f\Delta^{-2}\Omega(X_4) + \hat{F}_{[4]}(x,y)$$

where

$$\Delta(x,y) \equiv \det S; \quad \theta_m{}^a(x,y) = \overset{o}{\theta}_m{}^b(y) S_b{}^a(x,y),$$
$$f_0 \equiv f\Delta^{-2} : \text{FR parameter}$$

  - Spinor fields

$$\boxed{\begin{aligned} &\frac{i^{-1/2}}{2}(1+\gamma_5)\left(\boldsymbol{\Psi_\alpha^A} - \tfrac{1}{2}\gamma_5\gamma_\alpha\hat{\gamma}^a\boldsymbol{\Psi_a^A}\right) = \Delta(x,y)^{1/4}\boldsymbol{\psi_\alpha^i(x)}\eta_i^A(y), \\ &\frac{3\sqrt{2}i^{1/2}}{4}(1+\gamma_5)\Gamma^a_{[AB}\boldsymbol{\Psi_{|a|C]}} = \Delta(x,y)^{1/4}\boldsymbol{\chi^{ijk}(x)}\eta_i^A(y)\eta_j^B(y)\eta_k^C(y)\end{aligned}}$$

- Generalised frame field

$$\boxed{\begin{aligned} &e^m_{AB}(x,y) \equiv i e^m_a \Delta^{-1/2}({}^T\Phi\Gamma^a\Phi)_{AB} \\ &e^{mAB} = (e^m_{AB})^*\end{aligned}}$$

where $\Phi(x,y) \in SU(8)$

$$\mathrm{SO}(10,1) \Downarrow \mathrm{SO}(3,1)\times\mathrm{SO}(7) \Downarrow \mathrm{SO}(3,1)\times\mathrm{SU}(8)$$

- 4D -> $e^m{}_{AB}$

$$\mathscr{V}(x) = \begin{pmatrix} u & v \\ v^* & u^* \end{pmatrix} \in E_{7(7)} \to e^m_{ij}(x,y) = K^{mIJ}(y)(u+v)_{ij}{}^{IJ}(x)$$

$$\Rightarrow \quad e^m_{AB}(x,y) = e^m_{ij}(x,y)\eta^i_A(y)\eta^j_B(y)$$

- Metric <= "Non-linear metric ansatz"

$$\boxed{\begin{aligned} 8(\boldsymbol{\Delta^{-1}g^{mn}})(x,y) &= e^m_{ij}e^{nij} \\ &= K^{mIJ}(y)K^{nKL}(y)[\,{}^T\boldsymbol{(u+v)(u^*+v^*)}]_{IJKL}(x)\end{aligned}}$$

- Generalised Vielbein Postulate

$$\overset{o}{D}_m e^n_{AB} + \mathscr{B}_m{}^C{}_{[A} e^n_{B]C} + \mathscr{A}_{mABCD} e^{nCD} = 0$$

where

$$\begin{aligned}
\mathscr{B}_m{}^A{}_B &= \frac{1}{2}(S^{-1}\overset{o}{D}_m S)_{ab}\Gamma^{ab}_{AB} + \frac{i\sqrt{2}}{14} f e_{ma}\Gamma^a_{AB} - \frac{\sqrt{2}}{48} e^a_m F_{abcd}\Gamma^{bcd}_{AB}, \\
\mathscr{A}_{mABCD} &= -\frac{3}{4}(S^{-1}\overset{o}{D}_m S)_{ab}\Gamma^a_{[AB}\Gamma^b_{CD]} + \frac{i\sqrt{2}}{56} e_{ma} f \Gamma^{ab}_{[AB}\Gamma^b_{CD]} + \frac{\sqrt{2}}{32} e_m{}^a F_{abcd}\Gamma^{bc}_{[AB}\Gamma^d_{CD]}
\end{aligned}$$

- Flux <= "A-eqs"

$$gA_1{}^{ij} = \mathfrak{A}_1{}^{ij} \equiv -\frac{\sqrt{2}}{4}\left(e^{mik}\mathscr{B}_m{}^j{}_k + \mathscr{A}_m{}^{ijkl} e^m_{kl}\right)$$

$$gA_{2l}{}^{ijk} = \mathfrak{A}_{2l}{}^{ijk} \equiv -\frac{\sqrt{2}}{4}\left(3e^{m[ij}\mathscr{B}^{k]}_{ml} - 3e^m_{pq}\mathscr{A}_m{}^{pq[ij}\delta^{k]}_l - 4\mathscr{A}_m{}^{hjkl} e^m_{hl}\right)$$

$$\boxed{\begin{aligned}
\boldsymbol{f} &= -\frac{\sqrt{2}}{48\cdot 5!}\Delta^4 g^{mn}\epsilon_{mnpqrst} e^n_{ij}(e^{[p}\bar{e}^q\bar{e}^s e^{t]})_{kl}\mathscr{A}_{\boldsymbol{u}}{}^{\boldsymbol{ijkl}} \\
\hat{\boldsymbol{F}}_{\boldsymbol{mnpq}} &= -\frac{i}{144}\Delta^4 g_{rw} e^r_{ij}(e^{[s}\bar{e}^t\bar{e}^v e^{w]})_{kl}\epsilon_{stuw[mnp}\mathscr{A}_{\boldsymbol{q}]}{}^{\boldsymbol{ijkl}}
\end{aligned}}$$

SO(7)-invariant solutions in 4D and 11D

- 4D SO(8)-gauging [de Wit-Nicolai 1984]

$$\Lambda_{\mathrm{SO(7)+}} = -2\cdot 5^{3/4} g^2 = \frac{5^{3/4}}{3}\Lambda_{\mathrm{SO(8)}}$$ SL8-type

$$\frac{m_s^2}{|\Lambda|} = \begin{cases} \text{even parity} & : 2(1),\ -4/5(27_s),\ 0(7_s) \\ \text{odd parity} & : -2/5(35_{3a}) \end{cases}$$

$$\Lambda_{\mathrm{SO(7)-}} = -\frac{25}{8}\sqrt{5}g^2 = \frac{25\sqrt{5}}{48}\Lambda_{\mathrm{SO(8)}}$$ non-SL8-type

- 11D S^7 compactification [Englert 1982; de Wit-Nicolai 2012]

It was confirmed that the non-linear uplift formula correctly gives the known solutions in D=11 supergravity.

SO(7)$_+$ => Deformed S^7 with no internal flux

SO(7)$_-$ => Round S^7 with internal flux

However, the mass spectrum has not been calculated.

“On mathematical study of the Einstein-Euler-de Sitter equations”

by Tetu Makino

[JGRG25(2015)4a1]

On mathematical study of the Einstein-Euler-de Sitter equations

Tetu Makino
(Yamaguchi University, Japan)

December 9, 2015 / JGRG25 at Kyoto

1

1 Introduction

The Einstein-de Sitter equation:

$$R_{\mu\nu} - \frac{1}{2}g_{\mu\nu}(g^{\alpha\beta}R_{\alpha\beta}) - \Lambda g_{\mu\nu} = \frac{8\pi G}{c^4}T_{\mu\nu}$$

The energy-momentum tensor of a perfect fluid

$$T^{\mu\nu} = (c^2\rho + P)U^\mu U^\nu - Pg^{\mu\nu}.$$

2

Assumption. *P is a given analytic function of $\rho > 0$ such that $0 < P, 0 < dP/d\rho < c^2$ for $\rho > 0$, and $P \to 0$ as $\rho \to +0$. Moreover there are positive constants A, γ and an analytic function Ω on a neighborhood of $[0, +\infty[$ such that $\Omega(0) = 1$ and*

$$P = A\rho^\gamma \Omega(A\rho^{\gamma-1}/c^2).$$

We assume that $1 < \gamma < 2$ and $\dfrac{1}{\gamma - 1}$ is an integer.

Spherically symmetric metric:

$$ds^2 = e^{2F(t,r)}c^2dt^2 - e^{2H(t,r)}dr^2 - R(t,r)^2(d\theta^2 + \sin^2\theta d\phi^2).$$

co-moving :

$$U^{ct} = e^{-F}, \qquad U^r = U^\theta = U^\phi = 0.$$

$\rightsquigarrow$

Equations on $\{\rho > 0\}$:

$$e^{-F}\frac{\partial R}{\partial t} = V \tag{1a}$$

$$\begin{aligned} e^{-F}\frac{\partial V}{\partial t} &= -GR\Big(\frac{m}{R^3} + \frac{4\pi P}{c^2}\Big) + \frac{c^2\Lambda}{3}R + \\ &\quad -\Big(1 + \frac{V^2}{c^2} - \frac{2Gm}{c^2R} - \frac{\Lambda}{3}R^2\Big)\frac{P'}{R'(\rho + P/c^2)} \end{aligned} \tag{1b}$$

$$e^{-F}\frac{\partial \rho}{\partial t} = -(\rho + P/c^2)\Big(\frac{V'}{R'} + \frac{2V}{R}\Big) \tag{1c}$$

$$e^{-F}\frac{\partial m}{\partial t} = -\frac{4\pi}{c^2}R^2PV \tag{1d}$$

Here X' stands for $\partial X/\partial r$.

5

Put

$$m = 4\pi\int_0^r \rho R^2 R' dr,$$

supposing that ρ is continuous at $r = 0$.

$$e^{2H} = \Big(1 + \frac{V^2}{c^2} - \frac{2Gm}{c^2R} - \frac{\Lambda}{3}R^2\Big)^{-1}(R')^2.$$
$$e^{2F} = \kappa_+ e^{-2u/c^2}$$

with

$$u := \int_0^\rho \frac{dP}{\rho + P/c^2} = \frac{\gamma A}{\gamma - 1}\rho^{\gamma-1}\Omega_u(A\rho^{\gamma-1}/c^2).$$

6

Note

$$\rho = A_1 u^{\frac{1}{\gamma-1}} \Omega_\rho(u/c^2), \quad P = A A_1^\gamma u^{\frac{\gamma}{\gamma-1}} \Omega_P(u/c^2)$$

with $A_1 := \Big(\dfrac{\gamma - 1}{\gamma A}\Big)^{\frac{1}{\gamma-1}}$.

2 Equilibrium

The Tolman-Oppenheimer-Volkoff-de Sitter equation:

$$\frac{dm}{dr} = 4\pi r^2 \rho, \tag{2a}$$

$$\frac{dP}{dr} = -(\rho + P/c^2) \frac{G\Big(m + \dfrac{4\pi r^3}{c^2} P\Big) - \dfrac{c^2\Lambda}{3} r^3}{r^2\Big(1 - \dfrac{2Gm}{c^2 r} - \dfrac{\Lambda}{3} r^2\Big)}. \tag{2b}$$

For arbitrary positive central density ρ_c there exists a unique solution germ $(m(r), P(r)), 0 < r \ll 1$, such that

$$m = \frac{4\pi}{3}\rho_c r^3 + [r^2]_2 r, \tag{3a}$$

$$P = P_c - (\rho_c + P_c/c^2)\Big(\frac{4\pi G}{3}(\rho_c + 3P_c/c^2) - \frac{c^2\Lambda}{3}\Big)\frac{r^2}{2} + [r^2]_2. \tag{3b}$$

Here $[X]_Q$ denotes a convergent power series of the form $\sum_{k\geq Q} a_k X^k$.

We denote

$$\kappa(r.m) := 1 - \frac{2Gm}{c^2 r} - \frac{\Lambda}{3}r^2,$$

$$Q(r, m, P) := G\Big(m + \frac{4\pi r^3}{c^2}P\Big) - \frac{c^2\Lambda}{3}r^3.$$

Definition 1. *A solution* $(m(r), P(r)), 0 < r < r_+$*, such that* $\rho > 0, \kappa(r, m) > 0$ *of (2a)(2b) is said to be* **monotone-short** *if* $r_+ < \infty$*,* $dP/dr < 0$ *for* $0 < r < r_+$*, that is,* $Q(r, m(r), P(r)) > 0$*, and* $P \to 0$ *as* $r \to r_+ - 0$ *and if*

$$\kappa_+ := \lim_{r\to r_+ - 0} \kappa(r, m(r)) = 1 - \frac{2Gm_+}{c^2 r_+} - \frac{\Lambda}{3}r_+^2$$

and

$$Q_+ := \lim_{r\to r_+ - 0} Q(r, m(r), P(r)) = Gm_+ - \frac{c^2\Lambda}{3}r_+^3$$

are positive. Here

$$m_+ := \lim_{r\to r_+ - 0} m(r) = 4\pi\int_0^{r_+} \rho(r) r^2 dr.$$

Suppose that there is a monotone-short solution $(\bar{m}(r), \bar{P}(r)), 0 < r < r_+$, **satisfying (3a)(3b), and fix it. Then the associated function** $u = \bar{u}(r)$ **turns out to be analytic on a neighborhood of** $[0, r_+]$ **and**

$$\bar{u}(r) = \frac{Q_+}{r_+^2 \kappa_+}(r_+ - r) + [r_+ - r]_2$$

as $r \to r_+ - 0$**.**

3 Equations for the small perturbation from the equilibrium

Solutions of (1a)-(1d) of the form

$$R = r(1 + y), \qquad V = rv$$

with small unknowns y, v

$\rightsquigarrow$

$$e^{-F}\frac{\partial y}{\partial t} = \Big(1+\frac{P}{c^2\rho}\Big)v, \tag{4a}$$

$$\begin{aligned} e^{-F}\frac{\partial v}{\partial t} &= \frac{(1+y)^2}{c^2}\frac{P}{\bar\rho}v\frac{\partial}{\partial r}(rv) + \\ &-G(1+y)\Big(\frac{m}{r^3(1+y)^3}+\frac{4\pi}{c^2}P\Big)+\frac{c^2\Lambda}{3}(1+y)+ \\ &-\Big(1+\frac{r^2v^2}{c^2}-\frac{2Gm}{c^2r(1+y)}-\frac{\Lambda}{3}r^2(1+y)^2\Big)\times \\ &\times\Big(1+\frac{P}{c^2\rho}\Big)^{-1}\frac{(1+y)^2}{\bar\rho r}\frac{\partial P}{\partial r}. \end{aligned} \tag{4b}$$

Here $m = \bar{m}(r)$ is a given function and ρ is considered as given functions of r and the unknowns $y, z(:= r\partial y/\partial r)$ as

$$\rho = \bar\rho(r)(1+y)^{-2}(1+y+z)^{-1}$$

4 Analysis of the linearized equation

The linearized wave equation of (4a)(4b):

$$\frac{\partial^2 y}{\partial t^2} + \mathcal{L}y = 0 \quad \text{with} \quad \mathcal{L}y = -\frac{1}{b}\frac{d}{dr}a\frac{dy}{dr} + Qy,$$

where

$$\begin{aligned} a &= e^{\bar H+\bar F}\frac{\overline{P\Gamma}r^4}{\overline{\overline{1+P/c^2\rho}}} \\ b &= e^{3\bar H-\bar F}\frac{r^4\bar\rho}{\overline{\overline{1+P/c^2\rho}}}, \\ Q &\in C([0,r_+]). \end{aligned}$$

Proposition 1. *The operator* $\mathfrak{T}_0, \mathcal{D}(\mathfrak{T}_0) = C_0^\infty(0, r_+)$, $\mathfrak{T}_0 y = \mathcal{L}y$ *in the Hilbert space* $L^2((0, r_+); b(r)dr)$ *admits the Friedrichs extension* $\mathfrak{T}$, *a self adjoint operator, whose spectrum consits of simple eigenvalues* $\lambda_1 < \lambda_2 < \cdots < \lambda_\nu < \cdots \to +\infty$.

$$x := \frac{\tan^2\theta}{1+\tan^2\theta} \quad \text{with} \quad \theta := \frac{\pi}{2\xi_+}\int_0^r \sqrt{\frac{\bar{\rho}}{\Gamma \bar{P}}} e^{-\bar{F}+\bar{H}} dr.$$

$\rightsquigarrow$

$$r = C_0\sqrt{x}(1+[x]_1) \quad \text{as} \quad x \to 0,$$
$$r_+ - r = C_1(1-x)(1+[1-x]_1) \quad \text{as} \quad x \to 1$$

$$\mathcal{L}y = -x(1-x)\frac{d^2y}{dx^2} - \Big(\frac{5}{2}(1-x) - \frac{N}{2}x\Big)\frac{dy}{dx} + L_1(x)x(1-x)\frac{dy}{dx} + L_0(x)y,$$

Here $L_1(x), L_0(x)$ are analytic functions on a neighborhood of $[0,1]$, and

$$N := \frac{2\gamma}{\gamma-1}.$$

Note

$$X\frac{d^2}{dX^2}+\frac{N}{2}\frac{d}{dX}=\frac{d^2\xi}{d\xi^2}+\frac{N-1}{\xi}\frac{d}{d\xi}=\triangle_\xi^{(N)} \quad \text{for} \quad X=\frac{\xi^2}{4}$$

5 Rewriting (4a)(4b) using $\mathcal{L}$

Putting

$$J := e^F(1+P/c^2\rho),$$

we rewrite the system of equations (4a)(4b) as

$$\frac{\partial y}{\partial t}-Jv=0, \tag{5a}$$

$$\frac{\partial v}{\partial t}+H_1\mathcal{L}y+H_2=0. \tag{5b}$$

Here H_1, H_2 are analytic functions of x in a neighborhood of $[0,1]$ and $y, z = x\partial y/\partial x, v, w = x\partial v/\partial x$ in a neighborhood of $(0,0,0,0)$. Moreover

$$H_1(x,0,0,0) = \frac{1}{J(x,0,0,0)}$$

and

$$H_2(x,0,\cdots,0) = \partial_y H_2(x,0,\cdots,0) = \cdots = \partial_w H_2(x,0,\cdots,0) = 0$$

.

6 Main results

(I). Let us fix a time periodic solution of the linearized equation:

$$Y_1 = \sin(\sqrt{\lambda}t + \Theta_0)\psi(x),$$

where λ is a positive eigenvalue of the operator $\mathfrak{T}$ and ψ is an associated eigenfunction. We seek a solution of the form

$$R = r(1+y) = r(1+\varepsilon Y_1 + \varepsilon^2 \check{y}), \qquad V = r(\varepsilon V_1 + \varepsilon^2 \check{v}),$$

where

$$V_1 = e^{-\bar{F}}(1 + \overline{P/c^2\rho})^{-1}\frac{\partial Y_1}{\partial t}.$$

Theorem 1. *Given $T > 0$, there is a positive number ϵ_0 such that, for $|\varepsilon| \leq \epsilon_0$, there is a solution $(\check{y}, \check{v}) \in C^\infty([0,T] \times [0,1])$ such that*

$$\sup_{j+k \leq n} \Big\| \Big(\frac{\partial}{\partial t}\Big)^j \Big(\frac{\partial}{\partial x}\Big)^k (\check{y}, \check{v}) \Big\|_{L^\infty([0,T]\times[0,1])} \leq C(n).$$

Note that

$$R(t, r_+) = r_+(1 + \varepsilon \sin(\sqrt{\lambda} t + \Theta_0) + O(\varepsilon^2)),$$

provided that ψ has been normalized as $\psi(x = 1) = 1$, and that the density distribution enjoys the 'physical vacuum boundary' condition:

$$\rho(t, r) = \begin{cases} C(t)(r_+ - r)^{\frac{1}{\gamma - 1}}(1 + O(r_+ - r)) & (0 \leq r < r_+) \\ 0 & (r_+ \leq r) \end{cases}$$

with a smooth function $C(t)$ of t such that

$$C(t) = \Big(\frac{\gamma - 1}{A\gamma} \frac{Q_+}{r_+^2 \kappa_+}\Big)^{\frac{1}{\gamma-1}} + O(\varepsilon).$$

(II). Also we can consider the Cauchy problem

$$\frac{\partial y}{\partial t} - Jv = 0, \qquad \frac{\partial v}{\partial t} + H_1\mathcal{L}y + H_2 = 0,$$
$$y\Big|_{t=0} = \psi_0(x), \qquad v\Big|_{t=0} = \psi_1(x).$$

Then we have

Theorem 2. *Given $T > 0$, there exits a small positive δ such that if $\psi_0, \psi_1 \in C^\infty([0,1])$ satisfy*

$$\max_{k \leq \mathfrak{K}} \left\{ \left\| \left(\frac{d}{dx}\right)^k \psi_0 \right\|_{L^\infty}, \left\| \left(\frac{d}{dx}\right)^k \psi_1 \right\|_{L^\infty} \right\} \leq \delta,$$

then there exists a unique solutuon (y, v) of the Cauchy problem in $C^\infty([0,T] \times [0,1])$. Here $\mathfrak{K}$ is sufficiently large number.

7 Metric in the exterior domain

The Schwarzschild-de Sitter metric:

$$ds^2 = \kappa^\sharp c^2 (dt^\sharp)^2 - \frac{1}{\kappa^\sharp}(dR^\sharp)^2 - (R^\sharp)^2(d\theta^2 + \sin^2\theta d\phi^2)$$

Here $t^\sharp = t^\sharp(t,r), R^\sharp = R^\sharp(t,r)$ are smooth functions of $0 \leq t \leq T, r_+ \leq r \leq r_+ + \delta$, δ being a small positive number, and

$$\kappa^\sharp = 1 - \frac{2Gm_+}{c^2 R^\sharp} - \frac{\Lambda}{3}(R^\sharp)^2.$$

The patched metric:

$$ds^2 = g_{00}c^2dt^2 + 2g_{01}cdtdr + g_{11}dr^2 + g_{22}(d\theta^2 + \sin^2\theta d\phi^2),$$

where

$$g_{00} = \begin{cases} e^{2F} = \kappa_+ e^{-2u/c^2} & (r \leq r_+) \\ \kappa^\sharp (\partial_t t^\sharp)^2 - \dfrac{1}{c^2 \kappa^\sharp} (\partial_t R^\sharp)^2 & (r_+ < r) \end{cases}$$

$$g_{01} = \begin{cases} 0 & (r \leq r_+) \\ c\kappa^\sharp (\partial_t t^\sharp)(\partial_r t^\sharp) - \dfrac{1}{c\kappa^\sharp} (\partial_t R^\sharp)(\partial_r R^\sharp) & (r_+ < r) \end{cases}$$

$$g_{11} = \begin{cases} -e^{2H} = -\Big(1 + \dfrac{V^2}{c^2} - \dfrac{2Gm}{c^2 R} - \dfrac{\Lambda}{3} R^2\Big)^{-1} (\partial_r R)^2 & (r \leq r_+) \\ c^2 \kappa^\sharp (\partial_r t^\sharp)^2 - \dfrac{1}{\kappa^\sharp} (\partial_r R^\sharp)^2 & (r_+ < r) \end{cases}$$

$$g_{22} = \begin{cases} -R^2 & (r \leq r_+) \\ -(R^\sharp)^2 & (r_+ < r). \end{cases}$$

Let $R = R^\sharp$ and $\partial_r R = \partial_r R^\sharp$ along $r = r_+$ in order that g_{22} be of class C^1.

Moreover

$$\frac{\partial t^\sharp}{\partial t}, \quad \frac{\partial t^\sharp}{\partial r}, \quad \frac{\partial^2 t^\sharp}{\partial r^2}, \quad \frac{\partial^2 R^\sharp}{\partial r^2} \quad \text{at} \quad r = r_+ + 0$$

are uniquely determined in order that g_{00}, g_{01}, g_{11} be of class C^1 across $r = r_+$.

$\rightsquigarrow$

$$\frac{\partial^2 R^\sharp}{\partial r^2}\Big|_{r_+ +0} - \frac{\partial^2 R}{\partial r^2}\Big|_{r_+ -0} = \mathcal{A}\Big(\frac{\partial R}{\partial r}\Big)^2,$$

with

$$\mathcal{A} = -\frac{V^2}{c^2}\Big(\Big(\frac{Gm_+}{c^2R^2} - \frac{\Lambda}{3}R + \frac{1}{\sqrt{\kappa_+}}\frac{1}{c^2}\frac{\partial V}{\partial t}\Big)\Big(1 + \frac{V^2}{c^2} - \frac{2Gm_+}{c^2R} - \frac{\Lambda}{3}R^2\Big)^{-2}\Big|_{r_+ -0}.$$

$\rightsquigarrow$

$$\frac{\partial^2 R^\sharp}{\partial r^2} \equiv \frac{\partial^2 R}{\partial r^2} \quad \Leftrightarrow \quad \frac{\partial R}{\partial t} \equiv 0 \quad \text{at} \quad r = r_+$$

THANK YOU
FOR YOUR ATTENTION!

PLEASE VISIT MY HOME PAGE

‘Arkivo de Tetu MAKINO’:

(http://hc3.seikyou.ne jp/home/Tetu.Makino)

“Antisymmetric tensor generalisations of affine vector fields”

by Kentaro Tomoda

[JGRG25(2015)4a2]

2015/12/09 JGRG25 @ Kyoto

Antisymmetric tensor generalisations of affine vector fields

Kentaro Tomoda
(Kobe Univ.)

based on a work with
T. Houri and Y. Morisawa [arXiv:1510.03538]

Killing Vectors

- Classifications of spacetimes
- Conserved quantities

There are many generalisations of KVs

Purpose of this talk

To present

Affine Killing-Yano Tensors

and their properties

Purpose of this talk

To present

Affine Killing-Yano Tensors

and their properties

- conserved quantity along geodesics!
- a method to find AKYTs

Related works

S. A. Cook and T. Dray,
“Tensor generalizations of affine symmetry vectors”,
J. Math. Phys. **50** 122506 (2009).

T. Houri and Y. Yasui,
“A simple test for spacetime symmetry”,
Class. Quant. Grav. **32** 055002 (2015).

Affine Killing Vectors

Killing Vectors

$$\nabla_{(a}\xi_{b)} = 0$$

Conformal Killing Vectors

$$\nabla_{(a}\xi_{b)} = \phi\, g_{ab}$$

Affine Killing Vectors

$$\nabla^a\nabla_{(b}\xi_{c)} = 0$$

Killing Vectors

$$\Leftrightarrow\ \mathcal{L}_\xi g_{ab} = 0$$

Conformal Killing Vectors

$$\Leftrightarrow\ \mathcal{L}_\xi g_{ab} = \phi\, g_{ab}$$

Affine Killing Vectors

$$\Leftrightarrow\ \mathcal{L}_\xi \Gamma^a_{bc} = 0$$

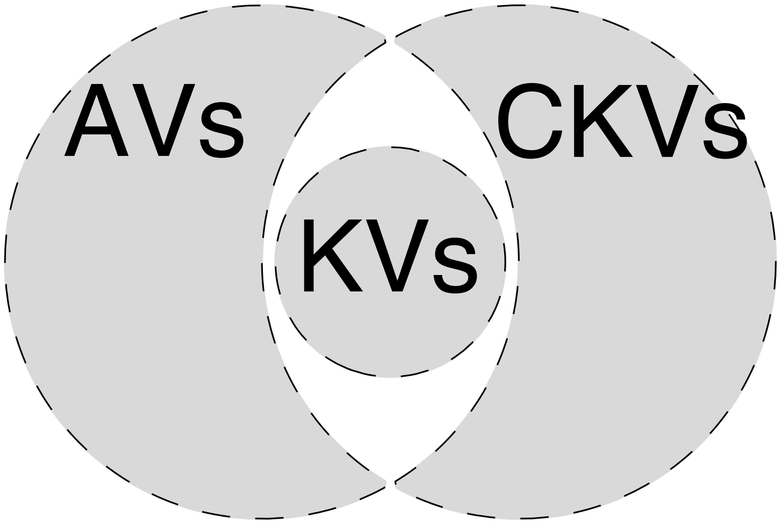

Fig: Venn diagram for KVs, CKVs and AVs

Affine Killing Vectors

$$\nabla^a \nabla_{(b}\xi_{c)} = 0$$

Example: Minkowski spacetime

$$\xi^a = P^a{}_b x^b + P^a \qquad (P_{ab} = -P_{ba})$$

Affine Killing Vectors

$$\nabla^a \nabla_{(b}\xi_{c)} = 0$$

Example: Minkowski spacetime

$$t\,\partial_t, \qquad t\,\partial_x,$$
$$x\,\partial_t, \qquad x\,\partial_x, \qquad \ldots$$

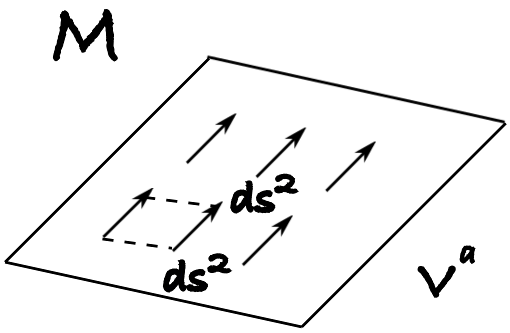

Fig: KVs

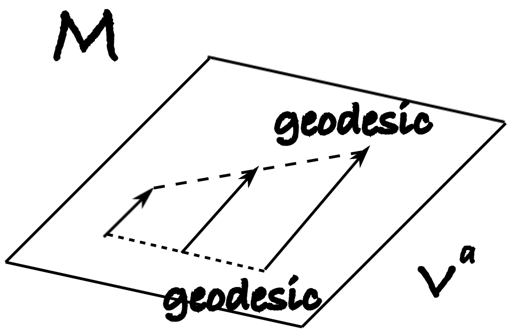

Fig: AVs

Affine Killing-Yano Tensors

Killing-Yano Tensors

$$\nabla_{(a}K_{b_1)\cdots b_p} = 0$$

Conformal Killing-Yano Tensors

$$\nabla_{(a}K_{b_1)\cdots b_p} = g_{a[b_1}\phi_{b_2\cdots b_p]}$$

where

$$K_{b_1\cdots b_p} = K_{[b_1\cdots b_p]}, \quad \phi_{b_1\cdots b_{p-1}} = \phi_{[b_1\cdots b_{p-1}]}$$

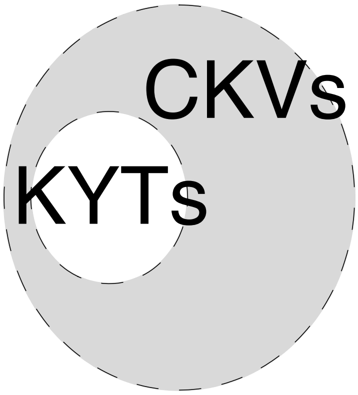

Fig: Venn diagram for KYTs and CKYTs

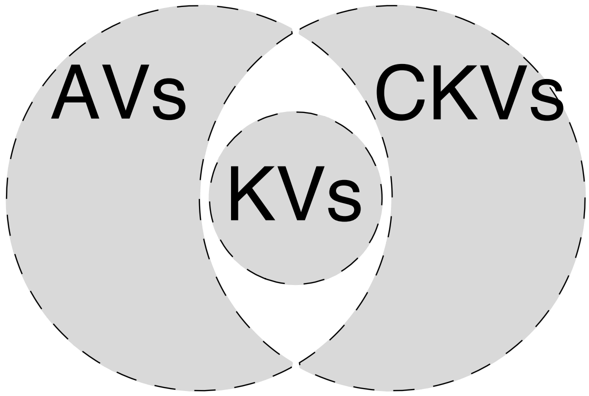

Fig: Venn diagram for KVs, CKVs and AVs

Killing-Yano Tensors

$$\nabla_{(a}K_{b_1)\cdots b_p} = 0$$

Conformal Killing-Yano Tensors

$$\nabla_{(a}K_{b_1)\cdots b_p} = g_{a[b_1}\phi_{b_2\cdots b_p]}$$

Affine Killing-Yano Tensors

$$\boxed{\nabla_a\nabla_{(b}K_{c_1)c_2\cdots c_p} = 0}$$

Properties

Affine Killing-Yano Tensors

$$\boxed{\nabla_a \nabla_{(b} K_{c_1) c_2 \cdots c_p} = 0}$$

Parallelly transported tensor

$$T^{a_1 \cdots a_{p-1}} := V^b V^c \nabla_{(b} K_{c)}{}^{a_1 \cdots a_{p-1}}$$

$$\Rightarrow \quad V^b \nabla_b T^{a_1 \cdots a_{p-1}} = 0$$

where V^a is a geodesic tangent

Conserved quantity

$$\boxed{Q := T^{a_1\cdots a_{p-1}}T_{a_1\cdots a_{p-1}}}$$

$$\Rightarrow V^a\nabla_a Q = 0$$

where V^a is a geodesic tangent and

$$T^{a_1\cdots a_{p-1}} = V^b V^c \nabla_{(b}K_{c)}{}^{a_1\cdots a_{p-1}}$$

$$\nabla_a\nabla_{(b}K_{c_1)c_2\cdots c_p} = 0$$

How to find AKYTs?

- $\nabla_a K_{b_1\cdots b_p} = F_{ab_1\cdots b_p} + \dfrac{2p}{p+1}N_{a[b_1\cdots b_p]}$
- $\nabla_a F_{b_1\cdots b_{p+1}} = (p+1)\; R_{a[b_1 b_2}{}^{c}\,K_{|c|b_3\cdots b_{p+1}]}$
- $\nabla_a N_{b_1\cdots b_{p+1}} = 0$

where

$$F_{a_1\cdots a_{p+1}} = \nabla_{[a_1}K_{a_2\cdots a_{p+1}]}$$

$$N_{a_1\cdots a_{p+1}} = \nabla_{(a_1}K_{a_2)\cdots a_{p+1}}$$

Applying ∇_a ...

- $R_{ab[c_1}{}^d K_{|d|c_2\cdots c_p]} = \dfrac{p+1}{p}\Big(R_{a[bc_1}{}^d K_{|d|c_2\cdots c_p]} - R_{b[ac_1}{}^d K_{|d|c_2\cdots c_p]}\Big)$
- $R_{ab[c_1}{}^d F_{|d|c_2\cdots c_{p+1}]}$
  $= \Big(\nabla_a R_{b[c_1c_2}{}^d - \nabla_b R_{a[c_1c_2}{}^d\Big) K_{|d|c_3\cdots c_{p+1}]}$
  $+ R_{a[c_1c_2}{}^d F_{|db|c_3\cdots c_{p+1}]} - R_{b[c_1c_2}{}^d F_{|da|c_3\cdots c_{p+1}]}$
  $- \dfrac{2p}{p+1}\Big(R_{a[c_1c_2}{}^d N_{|db|c_3\cdots c_{p+1}]} - R_{b[c_1c_2}{}^d N_{|da|c_3\cdots c_{p+1}]}\Big)$
- $2R_{ab(c_1}{}^d N_{|d|c_2)c_3\cdots c_{p+1}} = -(p-1) R_{ab[c_3}{}^d N_{|c_1c_2d|c_4\cdots c_{p+1}]}$

Applying ∇_a ...

- $R_{ab[c_1}{}^d K_{|d|c_2\cdots c_p]} = \dfrac{p+1}{p}\Big(R_{a[bc_1}{}^d K_{|d|c_2\cdots c_p]} - R_{b[ac_1}{}^d K_{|d|c_2\cdots c_p]}\Big)$
- $R_{ab[c_1}{}^d F_{|d|c_2\cdots c_{p+1}]}$
  $= \Big(\nabla_a R_{b[c_1c_2}{}^d - \nabla_b R_{a[c_1c_2}{}^d\Big) K_{|d|c_3\cdots c_{p+1}]}$
  $+ R_{a[c_1c_2}{}^d F_{|db|c_3\cdots c_{p+1}]} - R_{b[c_1c_2}{}^d F_{|da|c_3\cdots c_{p+1}]}$
  $- \dfrac{2p}{p+1}\Big(R_{a[c_1c_2}{}^d N_{|db|c_3\cdots c_{p+1}]} - R_{b[c_1c_2}{}^d N_{|da|c_3\cdots c_{p+1}]}\Big)$
- $2R_{ab(c_1}{}^d N_{|d|c_2)c_3\cdots c_{p+1}} = -(p-1) R_{ab[c_3}{}^d N_{|c_1c_2d|c_4\cdots c_{p+1}]}$

$\Rightarrow$ algebraic equations!

In most cases, these eqs determine AKYTs

Affine Killing-Yano Tensors

$$\boxed{\nabla_a \nabla_{(b} K_{c_1)c_2\cdots c_p} = 0}$$

Example: pp-wave spacetimes

$$ds^2 = H(u,x,y)du^2 + 2dudv + dx^2 + dy^2$$

rank-1	$u(du)_a$
rank-2	$u(du)_a \wedge (dx)_b$
	$u(du)_a \wedge (dy)_b$
rank-3	$u(du)_a \wedge (dx)_b \wedge (dy)_c$

Summary

- Affine Killing-Yano Tensors are presented
- Conserved quantities can be constructed by using of AKYTs
- pp-wave spacetimes have non-trivial AKYTs

“The Black Ring is Unstable”

by Benson Way

[JGRG25(2015)4a3]

The Black Ring Is Unstable

Benson Way (DAMTP)

Jorge Santos and B.W., Phys.Rev.Lett. 114 (2015) 221101 [arXiv:1503.00721]

Gravity in Four Dimensions

(Stationary, asymptotically flat, vacuum) black holes are simple.

- Spherical: Topologically S^2.
- Special: Uniquely specified by E and J.
- Stable: Mode-stable, likely nonlinearly stable.

“Black holes have no hair.”

Gravity in More Dimensions

Black holes are NOT simple.

- Not Spherical: e.g. $S^{p_1} \times \ldots \times S^{p_q}$.
- Not Special: e.g. turning points in phase diagram.
- Not Stable: Gregory-Laflamme instability.

Gravity in All Dimensions?

Are STABLE black holes simple?

Myers-Perry seems simple for slow rotation.

- Spherical: Topologically S^{d-2}.
- Special: Uniquely specified by E and J_i.
- Stable: Good numerical evidence.

Dynamical No Hair Conjecture

Dynamical no hair conjecture: Slowly rotating Myers-Perry is the unique stable solution.

Difficult to prove. Requires showing all non-spherical or non-special black holes are unstable.

Dynamical No Hair Conjecture

Dynamical no hair conjecture: Slowly rotating Myers-Perry is the unique stable solution.

Difficult to prove. Requires showing all non-spherical or non-special black holes are unstable.

Focus on five dimensions:

- All known black holes have topology S^3 or $S^1 \times S^2$.
- S^3 black holes are unique, $S^1 \times S^2$ black rings are not.

Are black rings unstable?

R. Emparan, H.S. Reall hep-th/0110260

5D Phase Diagram

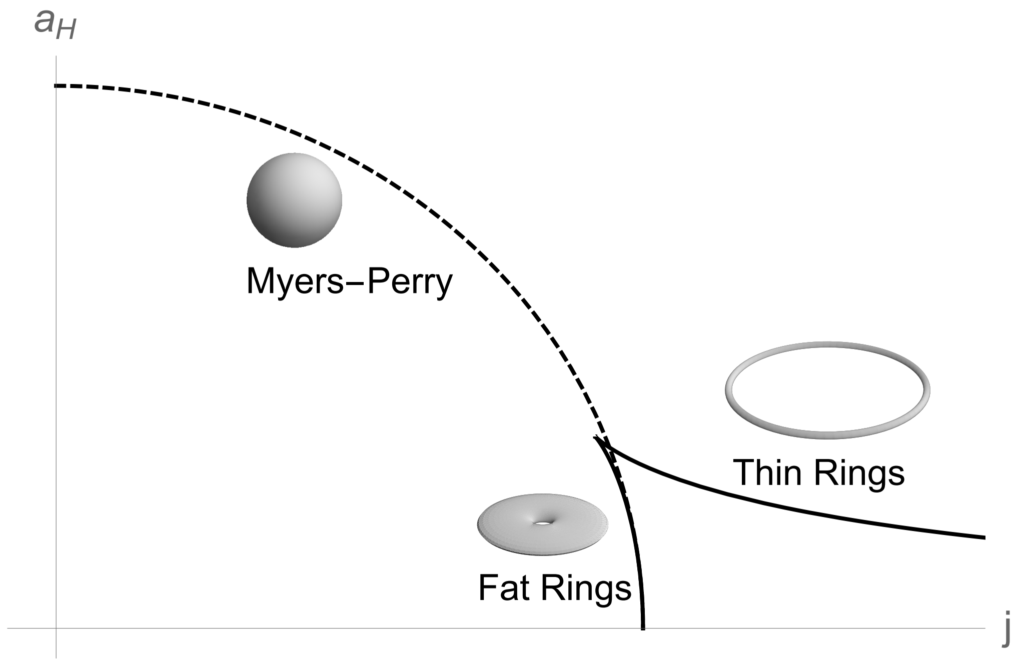

Instability of Fat Rings

Heuristic Argument:

- Use singular configurations of the black ring to derive an effective potential.

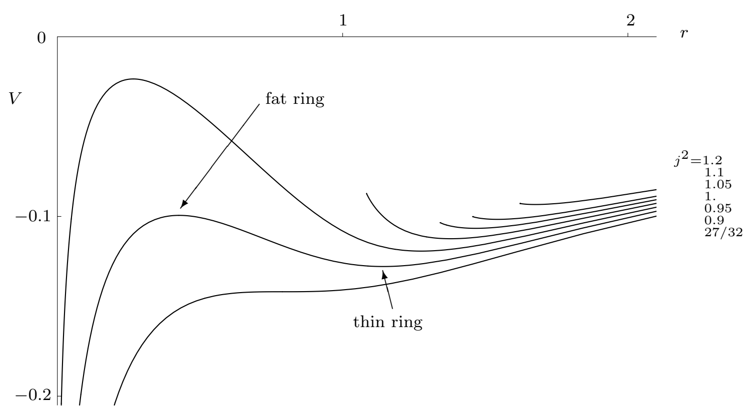

H. Elvang, R. Emparan, A. Virmani hep-th/0608076

Instability of Fat Rings

Instability of fat rings demonstrated using local Penrose inequalities.

- Assuming stability, derive a local Penrose inequality.

$$A_{\text{app}} \leq A_{BH}(E, J_i)$$

- If initial data describing a perturbation violates this inequality, solution is unstable.

- Initial data must have rotational symmetry in order to derive a useful Penrose inequality.

P. Figueras, K. Murata, H.S. Reall arXiv:1107.5785

Instability of Very Thin Rings

- Black strings suffer from the Gregory-Laflamme instability.

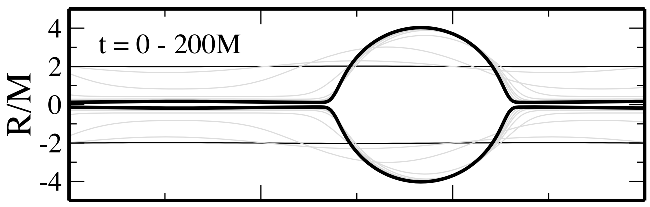

- Very thin rings resemble black strings, so they should be unstable. Perturbations must break rotational symmetry.

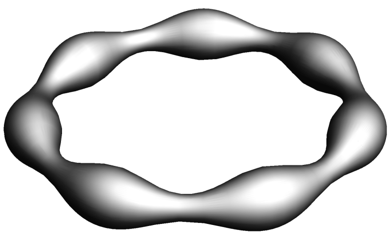

- Direct comparison difficult due to boundary conditions.

R. Gregory, L. Laflamme hep-th/9301052 L. Lehner, F. Pretorius arXiv:1006.5960

Window of Stability?

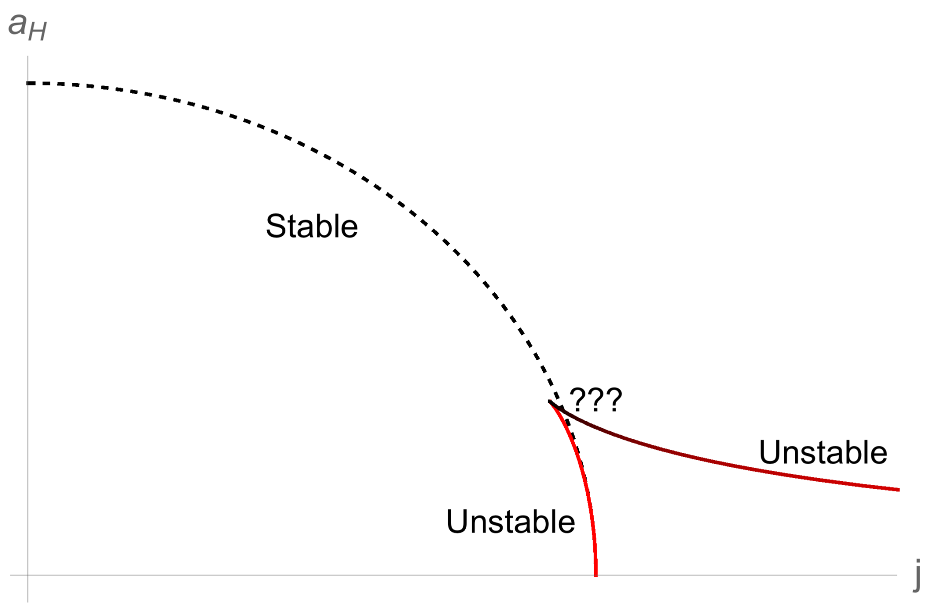

Perturbative Calculation

Fix $T = 1/2\pi$. Solve linearised Einstein equations in transverse-traceless gauge.

$$(\triangle_L h)_{ab} = 0 \qquad \nabla^a h_{ab} = 0 \qquad h^a{}_a = 0$$

Perform mode decomposition.

$$h_{ab} = e^{i\omega t + im\psi} \widetilde{h}_{ab}$$

Get quadratic eigenvalue problem.

$$(\mathcal{L}_0 + \omega \mathcal{L}_1 + \omega^2 \mathcal{L}_2) h_{ab} = 0$$

Choose m=2.

Boundary Conditions

Regularity at axes; ingoing at horizon; outgoing at infinity.

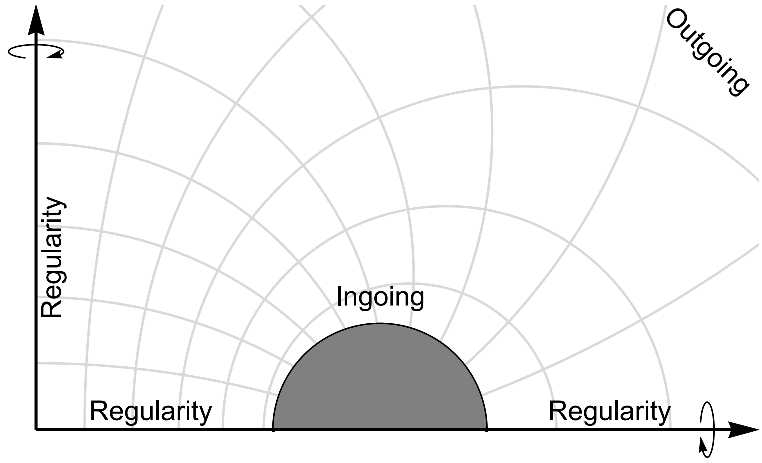

How do we impose five boundary conditions?

Coordinate Patches

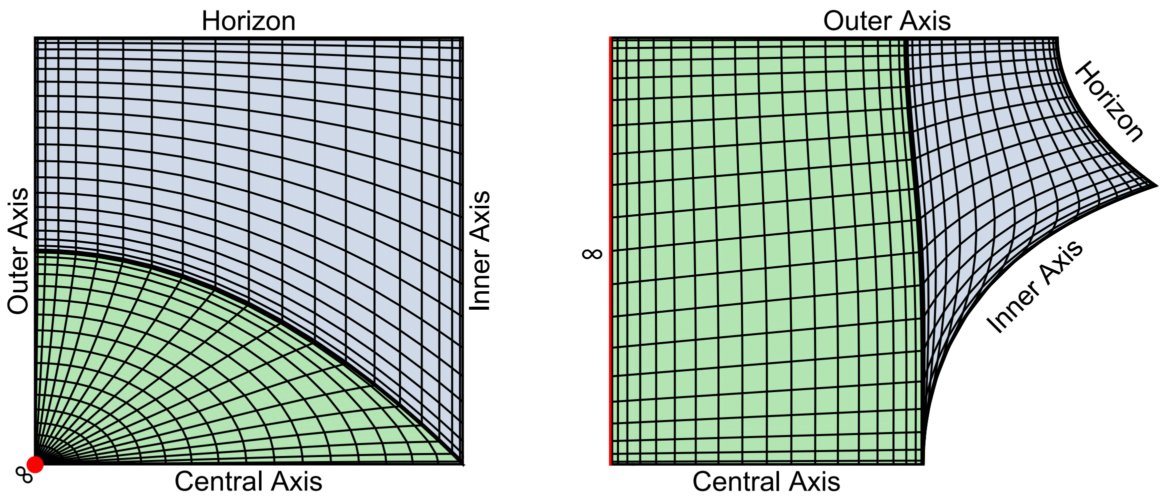

Solving the Eigenvalue Problem

First, solve an easier problem.

- Introduce a conical singularity to get a static ring.
- Onset of instability has $\omega = 0$, so set $\omega = 0$ and solve for negative modes

$$(\triangle_L h)_{ab} = -k^2 h_{ab}$$

- This a linear (not quadratic) eigenvalue problem in k^2 with *real,* positive eigenvalues. It also has fewer functions and real matrices.
- Solve matrix eigenvalue problem with QZ factorisation.

$$M_0 + k^2 M_1 = 0$$

Newton-Raphson

Use Newton-Raphson to obtain desired solution.

$$\omega = 0, \quad \alpha \neq 0, \quad \Omega = 0 \qquad (\triangle_L h)_{ab} = -k^2 h_{ab}$$

$$\text{increase } \Gamma, \text{solve } k^2$$

$$\omega = i\Gamma, \quad \alpha \neq 0, \quad \Omega = 0 \qquad (\triangle_L h)_{ab} = 0$$

$$\text{vary } \{\alpha, \Omega\}, \text{solve } \omega$$

$$\omega \neq 0, \quad \alpha = 0, \quad \Omega \neq 0 \qquad (\triangle_L h)_{ab} = 0$$

Results

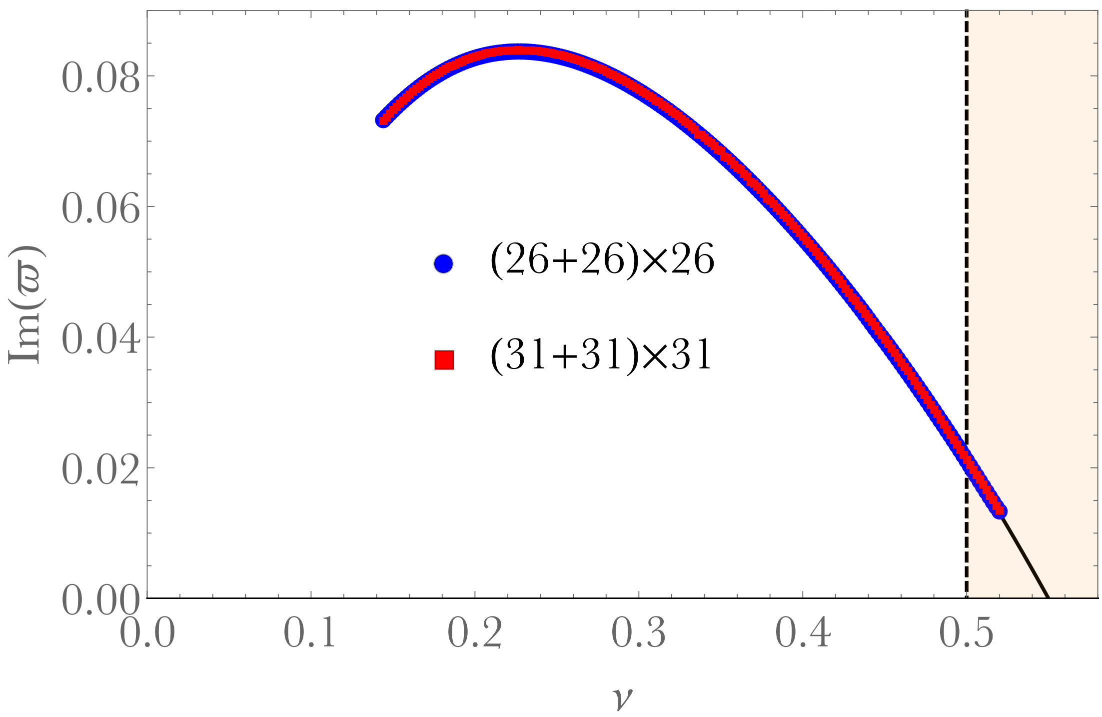

Results

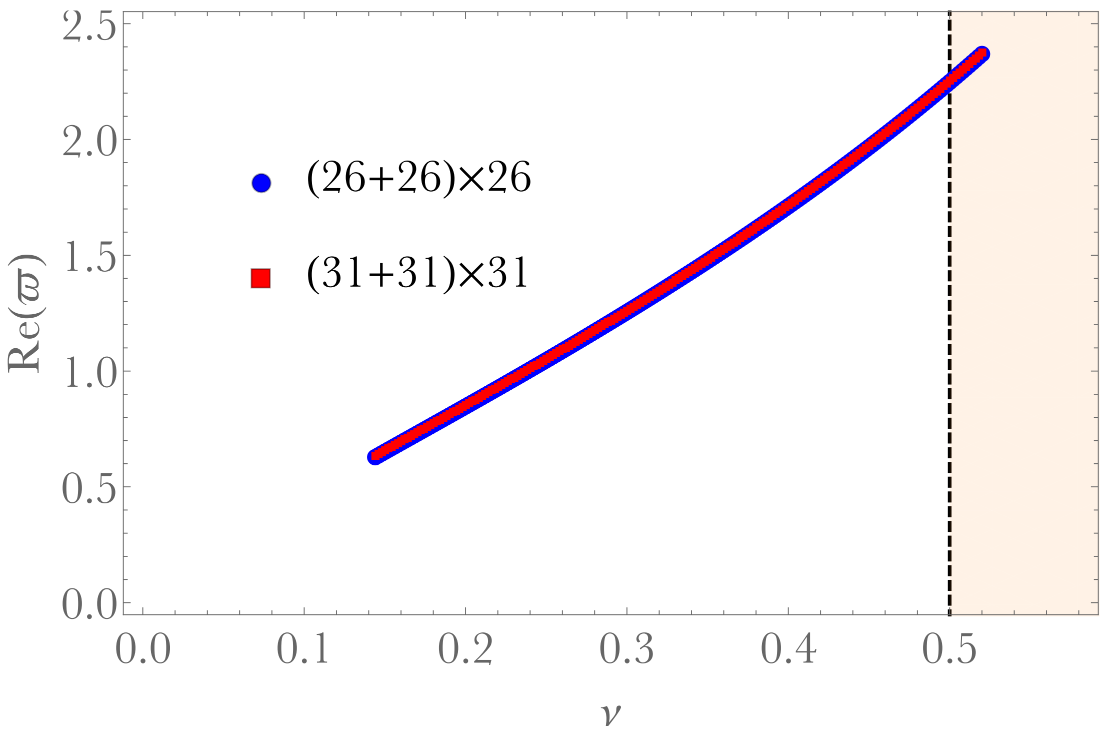

Embedding

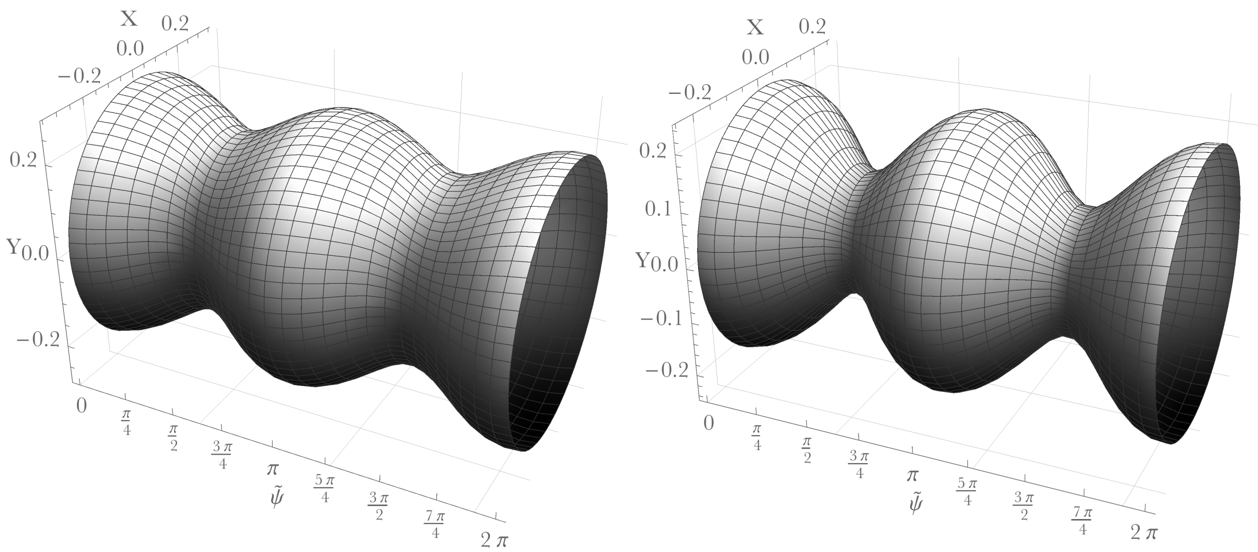

$\nu = 0.5$ $\nu = 0.2$

Eigenfunctions

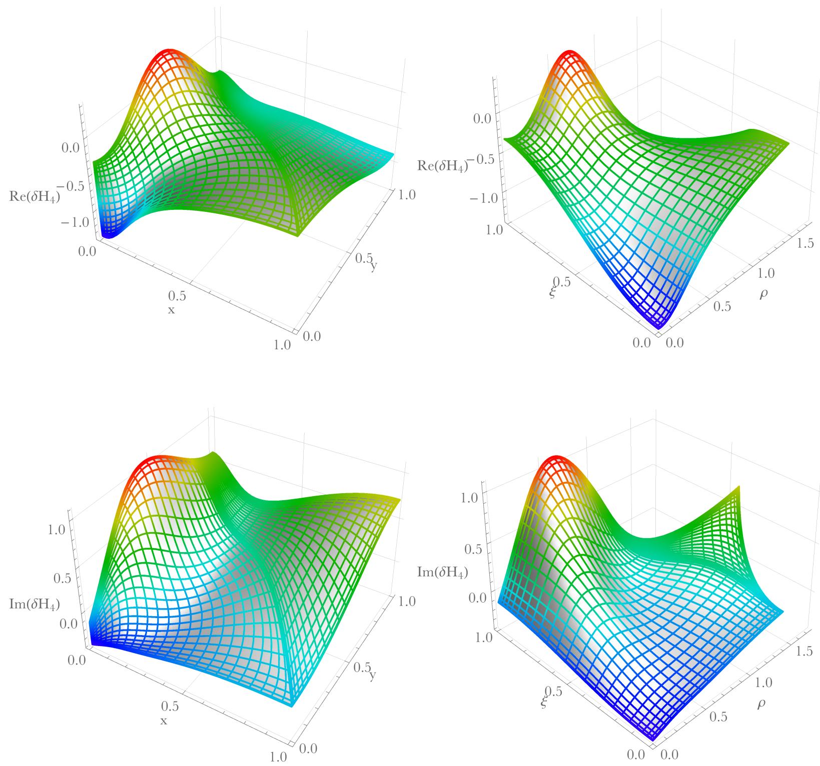

Remaining 5D Solutions

- Double-spin: Kerr-string is more unstable (higher growth rate), so double-spinning ring likely unstable.
- Multi-horizon solutions: contain ring components with their own instabilities. Also typically requires delicate balancing.

There is now good evidence for the dynamical no-hair conjecture in 5D.

Future and Ongoing Work

- Other m modes: How does m=0 compete with m=2? Is there an m=1 instability?
- Superradiant instabilities for double-spinning ring.
- Higher dimensions, Large D limit.
  K.Tanabe arXiv:1510.02200
- Addition of matter? Supersymmetric rings?

What is the endpoint?

Work in progress by **`GRChombo`** collaboration.

P. Figueras, M. Kunesch, S. Tunyasuvunakool, to appear

- Very fat rings likely go towards Myers-Perry.
- Thin rings may possibly violate cosmic censorship.

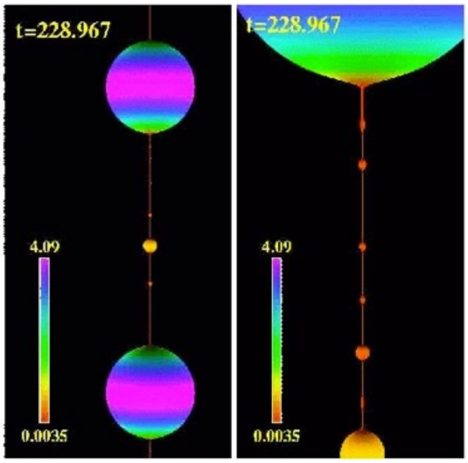

L. Lehner, F. Pretorius arXiv:1006.5960

Thank you

“Evolution and endpoint of the black string instability: Large D solution”

by Kentaro Tanabe

[JGRG25(2015)4a4]

EVOLUTION AND ENDPOINT OF THE BLACK STRING INSTABILITY: LARGE D SOLUTION

KENTARO TANABE (KEK)

based on arXiv:1506.06772 (PRL 115 091102)
with Roberto Emparan and Ryotaku Suzuki

PURPOSE

- **We want to solve the Einstein equation for some dynamical black holes**

$$R_{\mu\nu} = 0 \quad (G_{\mu\nu} + \Lambda g_{\mu\nu} = T_{\mu\nu})$$

- Non-linear Partial Differential Equations
- We need a technique to solve the equation
  - Numerical method (one by one)
  - (Semi-)Analytical method (approximations to the system : perturbation, symmetry,…)

PURPOSE

☐ We want to solve the Einstein equation for some dynamical black holes

$$R_{\mu\nu} = 0 \quad (G_{\mu\nu} + \Lambda g_{\mu\nu} = T_{\mu\nu})$$

- Non-linear Partial Differential Equations
- We need a technique to solve the equation
  - ➢ Numerical method (one by one)
  - ➢ (Semi-)Analytical method (approximations to the system : perturbation, symmetry,…)

METHOD

☐ We use the Large D expansion method

- 1/D expansion of the Einstein equation in D dimension

  [Asnin et.al. (2007), Emparan-Suzuki-KT (2013)]
- Analytic formulae of QNM frequencies (linear problem)
  - ➢ Instabilities of rotating black holes in higher dimensions, black ring, black brane and de Sitter charged black holes,…
  - ➢ Good accuracies by including higher order corrections in 1/D

    e.g., within a few percent error in D=6,7,.. for Schwarzschild BH
- Apply to non-linear problems

LARGE D EXPANSION

☐ Why can we solve Einstein equations ?

$$f = 1 - \left(\frac{r_0}{r}\right)^{D-3}$$ Gravitational potential in D dimension

- Radial gradient becomes large and dominant at large D

$$\partial_r = O(D) \qquad \partial_t = O(1) \qquad \partial_\theta = O(1)$$

- Einstein equation is reduced to **Ordinary Differential Equation**

$$R_{\mu\nu}[g_{\mu\nu}(t,r,\theta)] = 0 \;\xrightarrow{\text{r-integration}}\; \hat{R}_{\mu\nu}\;[\hat{g}_{\mu\nu}\;(t,\theta)] = 0$$

MEMBRANE AT LARGE D

☐ "membrane paradigm" for large D black holes

[Minwalla et.al. (2015), Emparan-Shiromizu-Suzuki-Tanaka-KT (2015)]

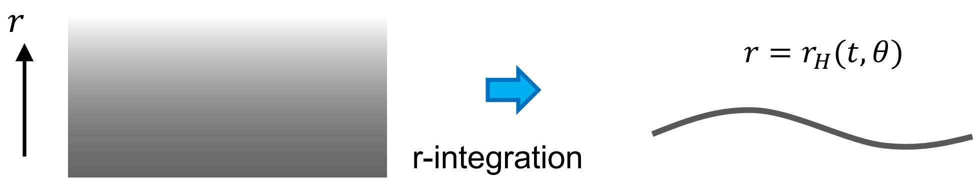

TODAY'S SYSTEM

☐ Apply to the black string instability

- Black string is unstable [Gregory-Laflamme (1994)]

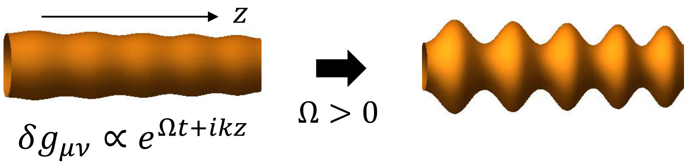

- What is the endpoint of this instability ?
  - ➢ Instability stops or does not stop?
  - ➢ We should solve the Einstein equation in nonlinear way
  - ➢ Large D expansion method can give answer ?

NUMERICAL SOLUTION

☐ A numerical study for five dimensional case

[Lehner-Pretorius (2010)]

- It is a very hard task, and there is only one result
  - ➢ Result in 5 dimensions
  - ➢ Instability **does not** stop
    - Fractal behavior ?
    - What is the endpoint ?

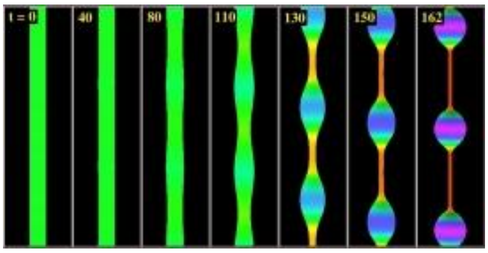

- An analytic approach would be helpful.

LARGE D SOLUTION

□ "dynamical black string solution" at large D

- Black String solution (exact solution)

$$ds^2 = -\left(1 - \frac{m}{r^n}\right) dt^2 + 2dtdr + dz^2 + r^2 d\Omega_{D-3}^2 \qquad n = D - 4$$

- Leading order solution in 1/D expansions (by r-integrations)

$$ds^2 = -\left(1 - \frac{\boldsymbol{m(t,z)}}{\boldsymbol{r^n}}\right) dt^2 + 2dtdr + \frac{dz^2}{n} + \frac{\boldsymbol{2p(t,z)}}{\boldsymbol{r^n}} \frac{dtdz}{n\sqrt{n}} + r^2 d\Omega_{D-3}^2$$

➢ Solution can have a dynamical mass $\boldsymbol{m(t,z)}$ and momentum $\boldsymbol{p(t,z)}$ at large D (time dependent solution)

EFFECTIVE EQUATION

□ Effective equations for dynamical black string

- Consider 1/D corrections to the solution

$$ds^2 = -\left(1 - \frac{\boldsymbol{m(t,z)}}{\boldsymbol{r^n}}\right) dt^2 + 2dtdr + \frac{dz^2}{n} + \frac{\boldsymbol{2p(t,z)}}{\boldsymbol{r^n}} \frac{dtdz}{n\sqrt{n}} + r^2 d\Omega_{D-3}^2 \quad + \frac{1}{D} \boldsymbol{\delta g_{\mu\nu}} dx^\mu dx^\nu$$

- Momentum constraint gives Large D effective equations

$$\boldsymbol{\partial_t m - \partial_z^2 m = -p \qquad \partial_t p - \partial_z^2 p = \partial_z \left[m - \frac{p^2}{m} \right]}$$

➢ "Einstein equation" reduces to simple "diffusion equations" at large D

SOLVING

- ☐ **Dynamical equations can be soled easily by *Mathematica***

$$\partial_t m - \partial_z^2 m = -p \qquad \partial_t p - \partial_z^2 p = \partial_z \left[m - \frac{p^2}{m} \right]$$

```
eq1 = ∂t m[t, z] - ∂z,z m[t, z] + ∂z p[t, z];
eq2 = ∂t p[t, z] - ∂z,z p[t, z] - ∂z m[t, z] + ∂z p[t, z]^2 / m[t, z];

tmax = 1455;
k = 0.995;
Ls = 2 π / k;
pertm = 0.05 Cos[k z];
pertp = 0;

pde = {eq1 == 0, eq2 == 0};
icbc = {m[0, z] == 1 + pertm, p[0, z] == pertp, m[t, -Ls/2] == m[t, Ls/2], p[t, -Ls/2] == p[t, Ls/2]};

sol = NDSolve[{pde, icbc}, {m, p}, {t, 0, tmax}, {z, -Ls/2, Ls/2}, MaxStepSize → 0.1];
```

SOLUTION

- ☐ Plot of the numerical solutions

  - Imposing periodic boundary conditions

$$m(t,z) = m(t, z + L_s)$$

  - Initial perturbations satisfy Gregory-Laflamme instability condition ("thin" black string)

$$r_{BS} < L_s = 2\pi k^{-1} \qquad \delta m\Big|_{v=0} = m_0 + \delta m \, e^{ikz}$$

  - Plot of the horizon position $r^n = m(t,z)$
  - The endpoint is (stable) **Non Uniform Black String**
  - This result does not have dimensional dependence

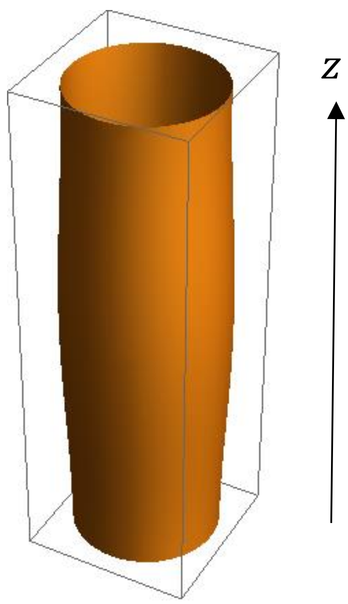

RESULTS AND SUMMARY

- **Large D non-linear dynamical black string solution of the Einstein equation**

  - Capture the black string instability (Gregory-Laflamme instability) by simple **diffusion equations**

  - The endpoint of the instability is a **non-uniform black string (NUBS)** solution (static and stable)

  - Large D results is **not inconsistent** with numerical results
    - Numerical results (instability does not stop) is in **five** dimensions
    - Large D result (instability does stop) is in **higher** dimensions

  - Stability of NUBS changes in dimensions (critical dimension)
    - Stable in D>13, unstable in D <13 [Sorkin (2004)]

EXTENSIONS

- **Various extensions**

  - In similar settings (dynamical non-linear solutions)

    Observe the critical dimension by 1/D corrections

    Charged (dilatonic) black branes in Einstein-Maxwell-dilaton system

    Dynamical black hole solutions (Myers-Perry BH, black ring,…)

    [These results will appear (or appeared) on arXiv]

  - In a bit different settings (ongoing work)

    Non-linear dynamics of black holes/branes in background matter field

    e.g., (AdS) black brane in background electric field (polarized black hole in background electric field,…)

"Black holes with scalar hair in N=2 supergravity"

by Masato Nozawa

[JGRG25(2015)4a5]

Black holes with scalar hair in N=2 supergravity

Masato Nozawa

University of Milan/INFN

Reference:
F.Faedo-D.Klemm-MN
JHEP 11 045 (2015)

Black hole uniqueness

Uniqueness theorem

An asymptotically flat, stationary and rotating black hole solution to vacuum Einstein's equations is only the Kerr-family

Hawking, Sudarsky-Wald, Israel, Carter, Robinson, Mathur,...

No hair conjecture

Ruffini & Wheeler 1971

gravitational collapse settles to equilibrium BH characterized by conserved charges (M, J, Q)

Supporting evidences:

- Price's law   Price 1973
- instability of `colored' black hole   Bizon-Wald 1991

Question: generalization to other asymptotics/matter fields

this talk: black holes with scalar field in asymptotically AdS space

Anti-de Sitter: ugly duckling

- our universe allows $\Lambda>0$
- nonglobally hyperbolic space

- AdS/CFT correspondence

  instability of BHs $\longleftrightarrow$ bound state of boundary tachyon

  Gubser-Mitra 2001

- condensed matter applications

  neutral BHs $\longleftrightarrow$ bulk scalar operator

Black holes w/ scalar hair in AdS

AdS black holes have richer spectrum than asy flat solutions

- limited version of uniqueness in Einstein-scalar system

  spherical sym. + potential is convex + "standard" asymptotic AdS

  $\Rightarrow$ Schwarzschild-AdS   Bekenstein 1974 & many others

Some scalar-haired black holes found

- Einstein-scalar system   Anabalon+ 2012
- Einstein-conformal scalar system   Caldarelli+ 2013

Here:

construct exact scalar haired black holes in N=2 gauged SUGRA
for which 'gauging' provides a scalar potential

N=2 gauged supergravity

N=2 gauged SUGRA w/abelian Fayet-Iliopoulous gaugings   Andrianopoli+ 1996

$$\mathcal{L} = \frac{1}{2}(R-2V)\star 1 - g_{\alpha\bar{\beta}}\mathrm{d}z^{\alpha}\wedge\star\mathrm{d}\bar{z}^{\bar{\beta}} + \frac{1}{2}(\mathrm{Im}\mathcal{N})_{IJ}F^{I}\wedge\star F^{J} - \frac{1}{2}(\mathrm{Re}\mathcal{N})_{IJ}F^{I}\wedge F^{J}$$

- special-Kahler metric $g_{\alpha\bar{\beta}}$

  covariantly holomorphic symplectic section $\mathcal{V} = \begin{pmatrix} X^I \\ F_I \end{pmatrix} = e^{\mathcal{K}/2}\begin{pmatrix} Z^I(z) \\ \frac{\partial}{\partial Z^I}F(Z) \end{pmatrix}$

  $\mathcal{D}_{\bar{\alpha}}\mathcal{V} = 0\,. \quad \langle\mathcal{V},\bar{\mathcal{V}}\rangle = i\,,$ $\lambda^2 F(X) = F(\lambda X)$: prepotential

- gauge kinetic fun $F_I = \mathcal{N}_{IJ}X^J\,, \quad \mathcal{D}_{\bar{\alpha}}\bar{F}_I = \mathcal{N}_{IJ}\mathcal{D}_{\bar{\alpha}}\bar{X}^J\,.$

- potential $V = -2g_I g_J[(\mathrm{Im}\mathcal{N})^{-1IJ} + 8\bar{X}^I X^J]\,,$ g_I: gauge couplings

Our model: $F(X) = -\frac{i}{4}(X^0)^n(X^1)^{2-n}\,,$ $0<n<2$:parameter

- truncation of STU model $F \propto (X^0X^1X^2X^3)^{1/2}$ $X^2 = (X^0)^{2n-1}\,,$ $X^3 = (X^1)^{3-2n}\,,$

- set $Z^0=1, Z^1=z$ and assume $F^I=0, z=z^*$

Einstein-Scalar system

$\phi = \lambda_n^{-1}\ln z\,,$ $\lambda_n = \sqrt{\frac{2}{n(2-n)}}\,,$ → $\mathcal{L} = \frac{1}{2}(R-2V)\star 1 - \frac{1}{2}\mathrm{d}\phi\wedge\star\mathrm{d}\phi\,, \quad V = 4\left[2(\partial_\phi W)^2 - 3W^2\right]\,,$

superpotential: $W(\phi) = g_1 e^{n\lambda_n\phi/2} + g_0 e^{(n-2)\lambda_n\phi/2}\,.$

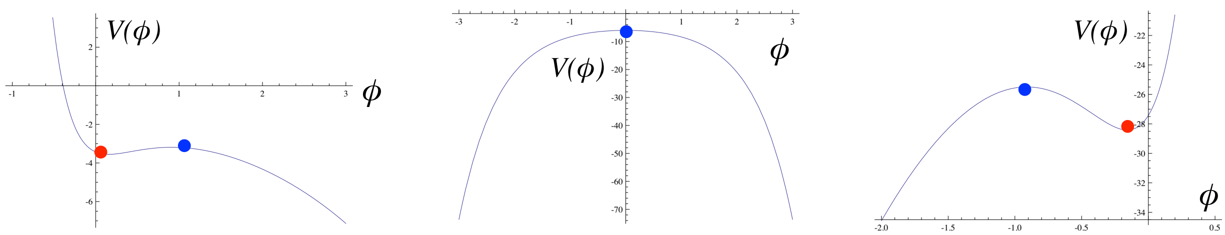

(i) 0<n<1/2   (ii) 1/2≤n≤3/2   (iii) 3/2<n<2

non SUSY vacuum $m^2 = 6/\ell^2$

SUSY vacuum $m^2 = -2/\ell^2$

look for a BH solution which asymptotes to SUSY vacuum at infinity

Hairy black hole

Static & (pseudo-)spherically symmetric $\mathrm{d}\Sigma_k^2 = \frac{\mathrm{d}\chi^2}{1-k\chi^2} + \chi^2 \mathrm{d}\varphi^2 \,,$ k=0,±1

$$\mathrm{d}s^2 = -f(r)\mathrm{d}t^2 + \frac{\mathrm{d}r^2}{f(r)} + \rho(r)^2 \mathrm{d}\Sigma_k^2 \qquad \phi = \phi(r)\,,$$

ansatz deduced from SUSY solutions c.f. Klemm-Vaughan 2013

$$f(r) = \Delta(r)/\rho(r)^2\,, \qquad \rho(r)^2 = f_1(r)^n f_2(r)^{2-n}\,, \qquad F(X) = -\frac{i}{4}(X^0)^n (X^1)^{2-n}\,,$$

$$f_1 = \frac{n}{\sqrt{2}}\left(r + \frac{2\beta}{n}\right), \qquad f_2 = \frac{2-n}{\sqrt{2}}\frac{g_0}{g_1}\left(r - \frac{2\beta}{2-n}\right), \qquad e^{\lambda_n \phi} = \frac{g_0(2-n)}{g_1 n}\frac{r - 2\beta/(2-n)}{r + 2\beta/n}\,,$$

$$\Delta = 8g_0^2\left(r + \frac{2\beta}{n}\right)\left(r - \frac{2\beta}{2-n}\right)\left(r^2 - \frac{4(1-n)}{n(2-n)}\beta r + 4\frac{5n^2-10n+4}{n^2(2-n)^2}\beta^2 + \frac{k}{8g_0^2}\right)$$

- includes 5 parameters (n, k, g_0, g_1, β)

  β=0 corresponds to (SUSY) AdS $\Rightarrow \beta$ ~mass

- ϕ=const. is achieved only for β=0 ⇔ AdS

  disconnected w/ Schwarzchild-AdS

Horizon structure

For certain range of β, our solution admits regular horizons $\Delta(r_\pm)=0$

$$\mathrm{d}s^2 = -\frac{\Delta}{\rho^2}\mathrm{d}t^2 + \frac{\rho^2}{\Delta}\mathrm{d}r^2 + \rho(r)^2 \mathrm{d}\Sigma_k^2\,,$$

	(i) 0<n<1/2	(ii) 1/2<n<3/2	(iii) 3/2<n<2
k=1	BH	Naked singularity	BH
k=0	BH	Naked singularity	BH
k=-1	BH	BH	BH

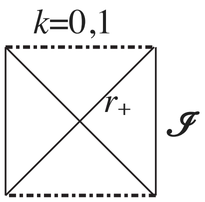

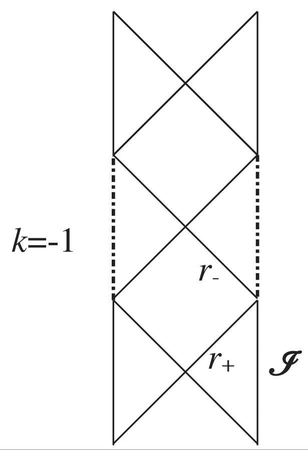

Asymptotics

Asymptotic expansion by areal radius $\rho = \sqrt{f_1^n f_2^{2-n}}$.

$$\mathrm{d}s^2 \simeq -\left(k + \frac{\rho^2}{\ell^2} - \frac{2\mu_1}{\rho}\right)\mathrm{d}\tau^2 + \left(k + \gamma + \frac{\rho^2}{\ell^2} - \frac{2\mu_2}{\rho}\right)^{-1}\mathrm{d}\rho^2 + \rho^2 \mathrm{d}\Sigma_k^2 ,$$

$$\phi \simeq \phi_1 + \frac{\phi_-}{\rho} + \frac{\phi_+}{\rho^2} + \mathcal{O}(1/\rho^3) , \qquad \tau = \rho_0^{-1} t, \quad \ell = \frac{\rho_0}{2\sqrt{2} g_0}, \quad \rho_0 \equiv \frac{n}{\sqrt{2}}\left(\frac{(2-n)g_0}{n g_1}\right)^{1-n/2} .$$

$$\gamma \equiv \frac{32 g_0^2 \beta^2}{n(2-n)} . \qquad \mu_1 = \frac{1}{12}\rho_0 \lambda_n^6 (n-1)\beta[3kn^2(n-2)^2 + 128 g_0^2 \beta^2 (3-2n)(1-2n)] , \quad \phi_+ = -2(n-1)\lambda_n^3 \beta^2 \rho_0^2 .$$

$$\mu_2 = \frac{1}{12}\rho_0 \lambda_n^6 (n-1)\beta[3kn^2(n-2)^2 + 128 g_0^2 \beta^2 (5n^2 - 10n + 3)] . \quad \phi_- = -2\lambda_n \beta \rho_0 ,$$

▸nonstandard fall-off behavior for $\gamma \neq 0$ Hertog-Maeda 2004

the slowly decaying mode ϕ_- is also normalizable for $m_{\mathrm{BF}}^2 \le m^2 \le m_{\mathrm{BF}}^2 + \frac{1}{\ell^2}$.

$m^2 = -2/\ell^2$, $m_{\mathrm{BF}}^2 = -9/4\ell^2$, Breitelohner-Freedman 1982

▸boundary condition is specified by a single parameter α Ishibashi-Wald 2003

$$\alpha \equiv \frac{\phi_+}{\phi_-^2} \longrightarrow \alpha = \frac{1}{2}(1-n)\lambda_n . \qquad \lambda_n = \sqrt{\frac{2}{n(2-n)}} ,$$

Hamiltonian formulation for conserved quantities

Various definitions of asymptotic AdS for $\alpha = \infty$ (Dirichlet b.c)

- 2nd order Einstein's tensor Abott-Deser 1982
- spinor Gibbons-Hull-Warner 1983
- electric part of Weyl tensor Ashtekar-Magnon 1984
- surface term of Hamiltonian Henneaux-Teitelboim 1985
- covariant phase space Hollands-Ishibashi-Marolf 2005

generalized AdS invariant boundary condition Hertog-Maeda 2004

$$h_{tt} = O(1/r^{d-3}) , \quad h_{ij} = O(1/r^{d-3}) , \quad h_{ti} = O(1/r^{d-3}) , , \quad \lambda_\pm = \frac{1}{2}[d - 1 \pm \sqrt{(d-1)^2 + 4m^2\ell^2}] ,$$

$$h_{rr} = -\frac{\alpha^2 \ell^2 \lambda_-}{(d-2) r^{2(1+\lambda_-)}} + O(1/r^{d+1}) , \quad h_{tr} = O(1/r^{d-2}) , \quad h_{ri} = O(1/r^{d-2}) .$$

$$Q[\xi] = Q_{\mathrm{HT}}[\xi] + \frac{\lambda_-}{2\ell^{d-3}} \int \mathrm{d}\Omega_{d-2} \xi^{\perp} r^{d-2} \left(\phi^2 + \frac{2\alpha(\lambda_+ - \lambda_-)}{d-1}\phi^{(d-1)/\lambda_-}\right) .$$

Q_{HT}: Henneaux-Teitelboim charge

$$M = Q[\partial_\tau] = \frac{\Sigma_k \mu_1}{4\pi} , \qquad \mathrm{d}s^2 \simeq -\left(k + \frac{\rho^2}{\ell^2} - \frac{2\mu_1}{\rho}\right)\mathrm{d}\tau^2 + \left(k + \gamma + \frac{\rho^2}{\ell^2} - \frac{2\mu_2}{\rho}\right)^{-1}\mathrm{d}\rho^2 + \rho^2 \mathrm{d}\Sigma_k^2 ,$$

c.f Martinez's talk

Thermodynamics

(M,A,κ) obey 1st law of black hole thermodynamics

$$\delta M = \frac{\kappa}{8\pi}\delta A\,. \qquad A = \Sigma_k \rho^2(r_+)$$
$$\kappa^2 = -\frac{1}{2}\nabla_\mu \xi_\nu \nabla^\mu \xi^\nu\,,$$

entropy $S=A/4$ is always smaller than the Schwarzschild-AdS

indication of instability

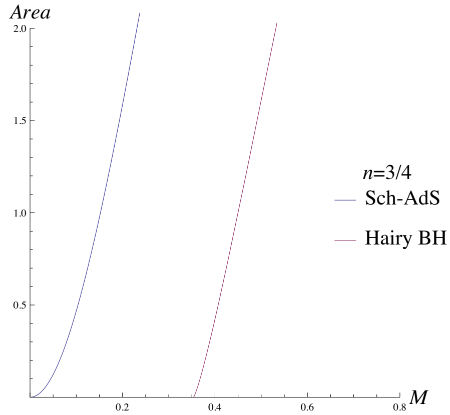

Linear instability

Spherically symmetric perturbations $\quad g^{(0)} = -f(r)\mathrm{d}t^2 + \mathrm{d}r^2/f(r) + \rho(r)^2\mathrm{d}\Omega_2^2$

$$g_{\mu\nu} \simeq g^{(0)}_{\mu\nu} + g^{(1)}_{\mu\nu}(r)e^{-i\omega t}\,, \qquad \phi \simeq \phi^{(0)} + \phi^{(1)}(r)e^{-i\omega t}\,,$$

- reduce to the Schrodinger-type equation

$$\left(-\frac{\mathrm{d}^2}{\mathrm{d}r_*^2} + U(r)\right)\Phi = \omega^2\Phi\,, \qquad \Phi = \rho\phi^{(1)}, \quad r_* = \int \mathrm{d}r/f(r)$$

$$U = \frac{f}{2\rho\rho'^2}[f\rho^3(\phi^{(0)})'^4 + 2\rho'^2(f\rho')' - 2\rho\rho'(f\rho)'(\phi^{(0)})'^2 + 4\rho^2\rho'(\phi^{(0)})'V_\phi + 2\rho\rho'^2 V_{\phi\phi}]\,,$$

- boundary conditions

horizon: $\quad \Phi \sim \exp(-i\omega r_*) \qquad r_* \to -\infty$

infinity: $\quad \dfrac{\mathrm{d}}{\mathrm{d}r_*}\Phi \simeq -\dfrac{2\alpha\phi_-^{(0)}}{\rho_0\ell^2}\Phi \qquad r_* \to 0 \qquad \phi \sim \dfrac{\phi_-}{\rho} + \dfrac{\alpha\phi_-^2}{\rho^2}\,,$

look for a pure imaginary mode σ=-iω>0

Linear instability

$$\Phi \to \Phi(r)e^{-i\omega t} = \Phi(r)e^{\sigma t}$$

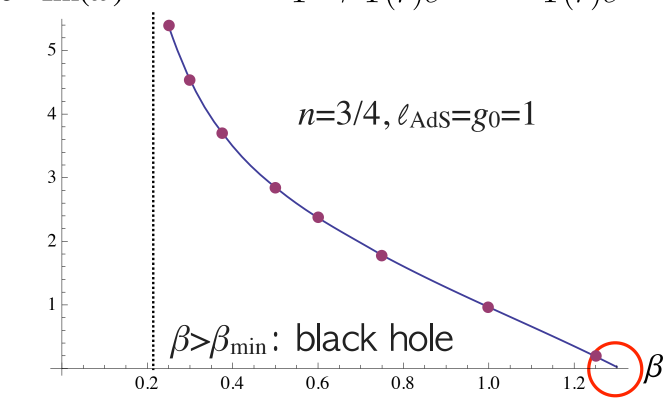

Zero mode exists

c.f Gregory-Laflamme instability

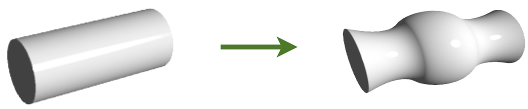

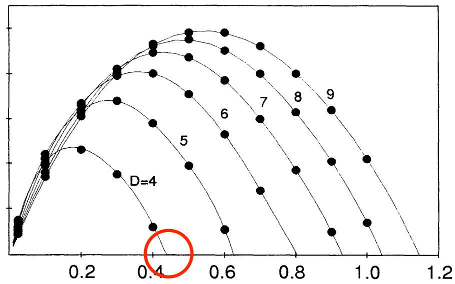

indicates a branch of more stable static bhs

Concluding remarks

constructed a family of static black holes in N=2 gauged SUGRA

$$ds^2 = -\frac{\Delta(r)}{\rho(r)^2}dt^2 + \frac{\rho(r)^2}{\Delta(r)}dr^2 + \rho(r)^2 d\Sigma_k^2 ,$$

$$f_1 = \frac{n}{\sqrt{2}}\left(r + \frac{2\beta}{n}\right), \quad f_2 = \frac{2-n}{\sqrt{2}}\frac{g_0}{g_1}\left(r - \frac{2\beta}{2-n}\right), \quad e^{\lambda_n \phi} = \frac{g_0(2-n)}{g_1 n}\frac{r - 2\beta/(2-n)}{r + 2\beta/n},$$

$$\Delta = 8g_0^2\left(r + \frac{2\beta}{n}\right)\left(r - \frac{2\beta}{2-n}\right)\left(r^2 - \frac{4(1-n)}{n(2-n)}\beta r + 4\frac{5n^2 - 10n + 4}{n^2(2-n)^2}\beta^2 + \frac{k}{8g_0^2}\right)$$

- provides a valuable example of neutral black hole w/scalar hair
- various applications in condensed matter physics
- well-defined mass & horizon structure clarified
- linearized spherical instability found

“Origin of outgoing electromagnetic power by a black hole rotation”

by Yasufumi Kojima

[JGRG25(2015)4a6]

Origin of outgoing electromagnetic power by a black hole rotation

Yasufumi Kojima

Ref: MNRAS,454(2015),3902

arXiv:1509.04793

JGRG25 2015 Dec. 7-11 Kyoto

HIROSHIMA UNIVERSITY

広島大学 極限宇宙研究拠点 CORE-U Core of Research for the Energetic Universe HIROSHIMA UNIVERSITY

Motivation

A fundamental problem in Blandford-Znajek process

- What is origin of outgoing EM power from a BH?

  Answer

  Spin of a black hole

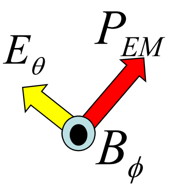

$$P = -\oint_r d\theta d\phi (\sqrt{-g} T_t^{\,r})$$

- How?

$$= -\tfrac{1}{2}\int d\theta (S\Phi_{,\theta}) \propto \int d\theta (E \times B)_r$$

$$\underbrace{B_\phi (j_p)}_{} \qquad \qquad E_\theta$$

>> EM field structure near horizon?

Event horizon is passive BC, determined by the exterior (behavior outside BH) $r > r_H$

What's new?

Because there are so many works.

(Microscopic) two fluids treatment!

$$\rho_e = e(n_+ - n_-)$$
$$j = e(n_+ v_+ - n_- v_-)$$

✓ It never needs ideal MHD condition, which may be broken elsewhere.

Ideal MHD

$$\vec{E}\cdot\vec{B} = 0 \Rightarrow \Phi(G), \vec{\nabla}\Phi = \Omega\vec{\nabla}G$$

✓It differs from force-free approximation, which may be invalid near horizon.

FF approx.

$$\Rightarrow S(G)$$

Approximations simplify the problem, but are questioned.

$$P = -\tfrac{1}{2}\int d\theta (S\Phi_{,\theta}) \propto \int d\theta (E\times B)_r$$

Model

Radial magnetic field, split-monopole

In spherically symmetric case, radial accretion even for charged fluids

$$\vec{E} = 0, \vec{j} = 0, \rho_e = 0$$

everywhere

Taking into account B.H. spin (a) up to the first order

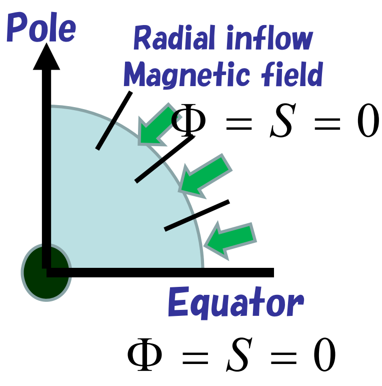

$$P = -\tfrac{1}{2}\int d\theta (S\Phi_{,\theta}) \propto \int d\theta (E\times B)_r$$

Straightforward calculation

MNRAS,454（2015）,3902

Stationary axially symmetric EM and flows determined by four functions G,Φ,F_+,F_-

- Spherical case as background
  -> Radial flow with no charge and current
- Linear pert. w.r.t. spin parameter a*
- Mode decomposition w.r.t. sym. $\delta G = 0$
  -> a coupled ord. diff. eqs for $\delta\Phi, \delta F(=\delta F_+, -\delta F_-)$
- Large/small number χ,κ involved
  -> WKB approximation $\propto \exp(i\chi W(r))$
  Many solutions, e.g. Locally oscillating plasma
- Single out radiating mode relevant to BZ
  Results in next page

Results

Electric potential & current function, toroidal magnetic field

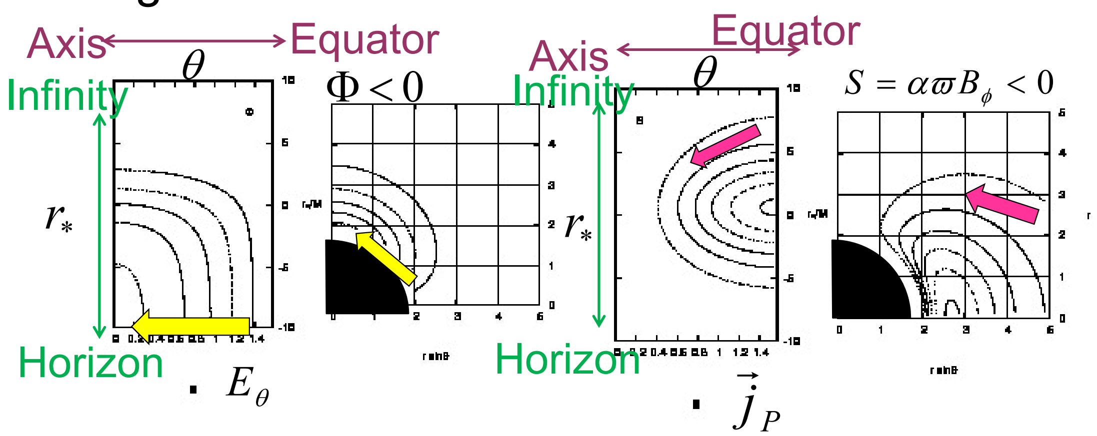

Finite electric field Zero current at horizon

Poynting flux

Outgoing EM Power

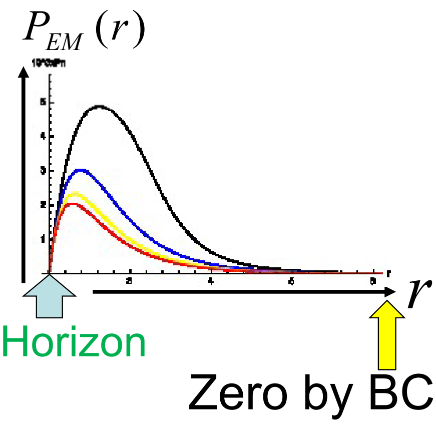

EM power through radius r

$$P_{EM}(r) = -\tfrac{1}{2}\int d\theta (S\Phi_{,\theta})$$

Maximum at $r/M \approx 2.5$

Four models shown by colored lines

EM power originates outside horizon, (ergo-region?)

Conclusion

BZ Power

$$P_{BZ} = \tfrac{2}{3}\underbrace{(\Omega_F - \omega_H)\Omega_F}_{\text{parameter}} B_n{}^2$$

Maximum $\Rightarrow \tfrac{1}{6}(a_* B_n GM)^2 c^{-3}$ $\quad 1/6 \approx 0.16$

Present work $\approx 0.08(a_* B_n GM)^2 c^{-3}$

Power is the same order, although EM fields depend on microscopic parameter.

$$\boxed{\begin{gathered}\delta B_\phi \propto \kappa a_*, \delta\Phi \propto \kappa^{-1} a_* \\ \kappa = \omega_p (GM/c^3) >> 1, \omega_p^2 = 4\pi e^2 n/m\end{gathered}}$$

“Existence and disappearance of conical singularities in GLPV theories”

by Ryotaro Kase

[JGRG25(2015)4b1]

JGRG25

Existence and disappearance of conical singularities in GLPV theories

A. De Felice, R. Kase and S. Tsujikawa, arXiv:1508.06364

Tokyo University of Science
Ryotaro Kase

1. Introduction

- **Horndeski theories**

$$S=\int d^4x\sqrt{-g}\sum_{i=2}^{5}L_i+S^M$$

$\boxed{G_{i,X}\equiv \partial G_i/\partial X}$

$X=g^{\mu\nu}\nabla_\mu\phi\nabla_\nu\phi$

$$L_2=G_2(\phi,X)\,,$$
$$L_3=G_3(\phi,X)\Box\phi\,,$$
$$L_4=G_4(\phi,X)R-2G_{4,X}(\phi,X)\left[(\Box\phi)^2-\phi^{;\mu\nu}\phi_{;\mu\nu}\right]\,,$$
$$L_5=G_5(\phi,X)G_{\mu\nu}\phi^{;\mu\nu}+\frac{1}{3}G_{5,X}(\phi,X)\left[(\Box\phi)^3-3(\Box\phi)\phi^{;\mu\nu}\phi_{;\mu\nu}+2\phi_{;\mu\nu}\phi^{;\mu\sigma}\phi^{;\nu}{}_{;\sigma}\right]\,.$$

- Quintessence and K-essence $\quad G_2=G_2(\phi,X)\,,\quad G_3=0\,,\quad G_4=\frac{M_{\rm pl}^2}{2}\,,\quad G_5=0$
- $f(R)$ and Brans-Dicke gravity $\quad G_2=G_2(\phi,X)\,,\quad G_3=0\,,\quad G_4=F(\phi)\,,\quad G_5=0$
- covariant Galileon $\quad G_2=c_2X\,,\quad G_3=\frac{c_3}{M^3}\,,\quad G_4=\frac{M_{\rm pl}^2}{2}+\frac{c_4}{M^6}X^2\,,\quad G_5=\frac{c_5}{M^9}X^2$

Horndeski theories are the most general second-order scalar-tensor theories on the general background.

1. Introduction

- **3+1 decomposition in unitary gauge** $(\phi = \phi(t))$

$$L = A_2 + A_3 K + A_4(K^2 - \mathcal{S}) + B_4 \mathcal{R} + A_5 K_3 + B_5(\mathcal{U} - K\mathcal{R}/2)$$

$K_{\mu\nu}$: extrinsic curvature

$\mathcal{R}_{\mu\nu}$: intrinsic curvature

$$K \equiv K^\mu_\mu\,, \quad \mathcal{S} \equiv K^\mu_\nu K^\nu_\mu\,,$$
$$\mathcal{R} \equiv \mathcal{R}^\mu_\mu\,, \quad \mathcal{U} \equiv \mathcal{R}_{\mu\nu} K^{\mu\nu}\,,$$
$$K_3 = 3H(2H^2 - 2HK + K^2 - \mathcal{S})$$

Horndeski theories satisfy the following relations:

$$A_4 = 2XB_{4,X} - B_4\,, \quad A_5 = -XB_{5,X}/3$$

1. Introduction

- **3+1 decomposition in unitary gauge** $(\phi = \phi(t))$

$$L = A_2 + A_3 K + A_4(K^2 - \mathcal{S}) + B_4 \mathcal{R} + A_5 K_3 + B_5(\mathcal{U} - K\mathcal{R}/2)$$

$K_{\mu\nu}$: extrinsic curvature

$\mathcal{R}_{\mu\nu}$: intrinsic curvature

$$K \equiv K^\mu_\mu\,, \quad \mathcal{S} \equiv K^\mu_\nu K^\nu_\mu\,,$$
$$\mathcal{R} \equiv \mathcal{R}^\mu_\mu\,, \quad \mathcal{U} \equiv \mathcal{R}_{\mu\nu} K^{\mu\nu}\,,$$
$$K_3 = 3H(2H^2 - 2HK + K^2 - \mathcal{S})$$

Horndeski theories satisfy the following relations:

$$A_4 = 2XB_{4,X} - B_4\,, \quad A_5 = -XB_{5,X}/3$$

Gleyzes, Langlois, Piazza, and Vernizzi (GLPV) minimally extended Horndeski theories in the way that the above relations are not necessarily satisfied.

J. Gleyzes, D. Langlois, F. Piazza and F. Vernizzi, PRL(2015)

1. Introduction

- GLPV theories (covariant form)

$$S = \int d^4x\sqrt{-g}\sum_{i=2}^{5} L_i + S^M$$

$$L_2 = A_2(\phi, X)\,,$$
$$L_3 = [C_3(\phi, X) + 2XC_{3,X}(\phi, X)]\Box\phi + XC_{3,\phi}(\phi, X)\,,$$
$$L_4 = B_4(\phi, X)R - \frac{B_4(\phi, X) + A_4(\phi, X)}{X}\left[(\Box\phi)^2 - \phi^{;\mu\nu}\phi_{;\mu\nu}\right]$$
$$+\frac{2\,\boxed{[B_4(\phi, X) + A_4(\phi, X) - 2XB_{4,X}(\phi, X)]}}{X^2}\left(\phi^{;\mu}\phi^{;\nu}\phi_{;\mu\nu}\Box\phi - \phi^{;\mu}\phi_{;\mu\nu}\phi_{;\sigma}\phi^{;\nu\sigma}\right)\,,$$

This term vanishes in Horndeski theories.

$$\left(A_3 = 2|X|^{3/2}\left[C_{3,X} + \frac{B_{4,\phi}}{X}\right]\right)$$

Here we focus on theories with $L_5 = 0$ since it tends to disturb the screening mechanism of the fifth force being at work.

Kimura et al. PRD (2012), Koyama et al. PRD (2013), Kase and Tsujikawa, JCAP (2013).

1. Introduction

- **GLPV theories on the spherically symmetric background**

・**Kase and Tsujikawa, PRD (2014)**
On the cosmological background, EOMs are determined by A_{2-5} while B_4 , B_5 appear only at the perturbation level.

・**Kase et al. PRD (2014)**
In contrast, B_4 , B_5 appear in BG EOMs on the spherically symmetric background.

On the spherically symmetric background, we can clarify effects of the deviation from Horndeski theories even at the BG level.

・**Kobayashi, Watanabe and Yamauchi, PRD (2015)**
In GLPV theories, the new derivative interactions give rise to a partial breaking of the screening mechanism inside a source.

・**Saito, Yamauchi, Mizuno, Gleyzes and Langlois, JCAP (2015)**
The partial breaking of the screening mechanism modifies structures of astrophysical bodies.

We want to show how this partial breaking would be constrained.

2. Interior Schwarzschild solutions

- Background equations of motion

•Action

$$S=\int d^4x\sqrt{-g}\sum_{i=2}^{4}L_i+\int d^4x\sqrt{-g}L_m(g_{\mu\nu},\Psi_m)\,.$$

•Metric

$$ds^2=-e^{2\Psi(r)}dt^2+e^{2\Phi(r)}dr^2+r^2(d\theta^2+\sin^2\theta\,d\phi^2)\,,$$

•(t,t)

$$\left(\frac{4e^{-2\Phi}A_4}{r}-\mathcal{C}_1+4\mathcal{C}_2\right)\Phi'-A_2+\mathcal{C}_3-\mathcal{C}_4-\frac{2A_4}{r^2}\left(e^{-2\Phi}-1-\alpha_{\rm t}\right)=-\rho_m\,,$$

•(r,r)

$$\left(\frac{4e^{-2\Phi}A_4}{r}-\mathcal{C}_1+4\mathcal{C}_2\right)\Psi'+A_2-2XA_{2,X}-\frac{2\mathcal{C}_1}{r}+\frac{2}{r^2}\left[A_4(e^{-2\Phi}-1-\alpha_{\rm H})+r\mathcal{C}_2\right]=-P_m\,,$$

$$\alpha_{\rm H}\equiv\frac{2XB_{4,X}-B_4}{A_4}-1\,,\quad \alpha_{\rm t}\equiv-\frac{B_4}{A_4}-1\,,\quad \mathcal{C}_1\equiv 2e^{-\Phi}XA_{3,X}\,,\quad \mathcal{C}_2\equiv\frac{2e^{-2\Phi}XA_{4,X}}{r}\,,$$

$$\mathcal{C}_3\equiv e^{-\Phi}\phi'\left(A_{3,\phi}+2e^{-2\Phi}\phi''A_{3,X}\right)\,,\quad \mathcal{C}_4\equiv\frac{4e^{-2\Phi}\phi'\left(A_{4,\phi}+2e^{-2\Phi}\phi''A_{4,X}\right)}{r}\,.$$

2. Interior Schwarzschild solutions

- Background equations of motion

•Action

$$S=\int d^4x\sqrt{-g}\sum_{i=2}^{4}L_i+\int d^4x\sqrt{-g}L_m(g_{\mu\nu},\Psi_m)\,.$$

•Metric

$$ds^2=-e^{2\Psi(r)}dt^2+e^{2\Phi(r)}dr^2+r^2(d\theta^2+\sin^2\theta\,d\phi^2)\,,$$

•(t,t)

•(r,r)

It represents the deviation from Horndeski theories ($\alpha_{\rm H}=0$)

It represents the deviation of the squared propagation speed of the odd-mode perturbations from 1.

$$\alpha_{\rm t}=1/c_{\rm t}^2-1$$

$$\boxed{\alpha_{\rm H}\equiv\frac{2XB_{4,X}-B_4}{A_4}-1\,,}\quad \boxed{\alpha_{\rm t}\equiv-\frac{B_4}{A_4}-1\,,}\quad \mathcal{C}_1\equiv 2e^{-\Phi}XA_{3,X}\,,\quad \mathcal{C}_2\equiv\frac{2e^{-2\Phi}XA_{4,X}}{r}\,,$$

$$\mathcal{C}_3\equiv e^{-\Phi}\phi'\left(A_{3,\phi}+2e^{-2\Phi}\phi''A_{3,X}\right)\,,\quad \mathcal{C}_4\equiv\frac{4e^{-2\Phi}\phi'\left(A_{4,\phi}+2e^{-2\Phi}\phi''A_{4,X}\right)}{r}\,.$$

2. Interior Schwarzschild solutions

- Solutions around the origin

In order to derive solutions around the origin, we expand $\Phi(r)$, $\Psi(r)$ and $\phi(r)$. As long as fields are analytic, they can be expanded as

$$\boxed{\Phi(r) = \Phi_0 + \sum_{i=2}^{\infty} \Phi_i r^i\,, \quad \Psi(r) = \Psi_0 + \sum_{i=2}^{\infty} \Psi_i r^i\,, \quad \phi(r) = \phi_0 + \sum_{i=2}^{\infty} \phi_i r^i\,.}$$

They respect the regular boundary conditions, i.e., $\Phi'(0) = \Psi'(0) = \phi'(0) = 0$. We also assume that A_{2-5}, B_{4-5} are finite at the origin. Then...

・(t,t)

$$\left(\frac{4e^{-2\Phi}A_4}{r} - \mathcal{C}_1 + 4\mathcal{C}_2\right)\Phi' - A_2 + \mathcal{C}_3 - \mathcal{C}_4 - \frac{2A_4}{r^2}\left(e^{-2\Phi} - 1 - \alpha_{\rm t}\right) = -\rho_m\,,$$

・(r,r)

$$\left(\frac{4e^{-2\Phi}A_4}{r} - \mathcal{C}_1 + 4\mathcal{C}_2\right)\Psi' + A_2 - 2XA_{2,X} - \frac{2\mathcal{C}_1}{r} + \frac{2}{r^2}\left[A_4(e^{-2\Phi} - 1 - \alpha_{\rm H}) + r\mathcal{C}_2\right] = -P_m\,,$$

$$\boxed{\alpha_{\rm H} \equiv \frac{2XB_{4,X} - B_4}{A_4} - 1\,,} \quad \boxed{\alpha_{\rm t} \equiv -\frac{B_4}{A_4} - 1\,,} \quad \mathcal{C}_1 \equiv 2e^{-\Phi}XA_{3,X}\,, \quad \mathcal{C}_2 \equiv \frac{2e^{-2\Phi}XA_{4,X}}{r}\,,$$

$$\mathcal{C}_3 \equiv e^{-\Phi}\phi'\left(A_{3,\phi} + 2e^{-2\Phi}\phi'' A_{3,X}\right)\,, \quad \mathcal{C}_4 \equiv \frac{4e^{-2\Phi}\phi'\left(A_{4,\phi} + 2e^{-2\Phi}\phi'' A_{4,X}\right)}{r}\,.$$

2. Interior Schwarzschild solutions

- Solutions around the origin

In order to derive solutions around the origin, we expand $\Phi(r)$, $\Psi(r)$ and $\phi(r)$. As long as fields are analytic, they can be expanded as

$$\boxed{\Phi(r) = \Phi_0 + \sum_{i=2}^{\infty} \Phi_i r^i\,, \quad \Psi(r) = \Psi_0 + \sum_{i=2}^{\infty} \Psi_i r^i\,, \quad \phi(r) = \phi_0 + \sum_{i=2}^{\infty} \phi_i r^i\,.}$$

They respect the regular boundary conditions, i.e., $\Phi'(0) = \Psi'(0) = \phi'(0) = 0$. We also assume that A_{2-5}, B_{4-5} are finite at the origin. Then...

・(t,t)

$$\frac{2A_4(1 + \alpha_{\rm H} - e^{-2\Phi_0})}{r^2} + \rho_m - A_2 + 12A_4e^{-2\Phi_0}\Phi_2 + \mathcal{O}(r) = 0\,,$$

・(r,r)

$$-\frac{2A_4(1 + \alpha_{\rm H} - e^{-2\Phi_0})}{r^2} - \rho_m + \rho_c e^{-\Psi_0} + A_2 - 4A_4e^{-2\Phi_0}(\Phi_2 - 2\Psi_2) + \mathcal{O}(r) = 0\,,$$

$$P_m' + \Psi'(\rho_m + P_m) = 0$$

$$\to P_m = -\rho_m + \rho_c e^{-\Psi}\,,$$

ρ_c : an integration constant

2. Interior Schwarzschild solutions

- Solutions around the origin

$$\Phi(r) = -\frac{1}{2}\ln(1+\alpha_{\mathrm{H}}) + \frac{\rho_m - A_2}{12B_4}r^2 + \dots\,,$$
$$\Psi(r) = \Psi_0 + \frac{2A_2 - 2\rho_m + 3\rho_c e^{-\Psi_0}}{24B_4}r^2 + \dots\,,$$
$$\phi(r) = \phi_0$$

Ricci scalar:

$$R = -\frac{2\alpha_{\mathrm{H}}}{r^2} + \frac{4A_2 - 4\rho_m + 3\rho_c e^{-\Psi_0}}{A_4} + \mathcal{O}(r)\,.$$

Thus the Ricci scalar diverges at the origin as long as $\alpha_{\mathrm{H}} \neq 0\,.$
This singularity is originated from the so-called conical singularity.

2. Interior Schwarzschild solutions

- Conical singularity

For simplicity, let us consider the case with $A_2 = \rho_m = 0\,.$
Then the three-dimensional spatial line-element is given as

$$ds^2_{(3)} = (1+\alpha_{\mathrm{H}})^{-1}dr^2 + r^2(d\theta^2 + \sin^2\theta\, d\varphi^2)$$

Defining $\hat{r} = r/\sqrt{1+\alpha_{\mathrm{H}}}\,,\ \hat{\varphi} = \sqrt{1+\alpha_{\mathrm{H}}}\,\varphi\,,$ the two dimensional metric in the $\theta = \pi/2$ plane is represented as

$$ds^2_{(2)} = d\hat{r}^2 + \hat{r}^2 d\hat{\varphi}^2$$

Conical singularity: The angle $\hat{\varphi} = \sqrt{1+\alpha_{\mathrm{H}}}\varphi$ is not restricted between 0 and 2π as long as $\alpha_{\mathrm{H}} \neq 0\,.$

e.g.) $-1 < \alpha_{\mathrm{H}} < 0$

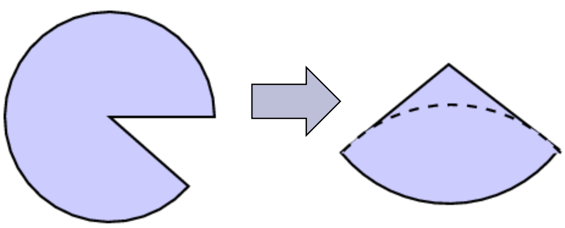

3. Conditions to avoid the conical singularity

In order to avoid the appearance of the conical singularity, $\alpha_{\rm H} \to 0$ is required for the limit $r \to 0$.

$$\boxed{\alpha_{\rm H} \equiv \frac{2XB_{4,X} - B_4}{A_4} - 1\,,}$$

Let us consider the following case:

$$A_4 = -\frac{1}{2}M_{\rm pl}^2 F_1(\phi) + f_1(X)\,, \qquad B_4 = \frac{1}{2}M_{\rm pl}^2 F_2(\phi) + f_2(X)\,,$$

$$\alpha_{\rm H} = \frac{1}{A_4}\left[\frac{M_{\rm pl}^2}{2}(F_1 - F_2) - (f_1 + f_2 - 2Xf_{2,X})\right],$$

e.g.) GR: $A_4 = -M_{\rm pl}^2/2\,,\ B_4 = M_{\rm pl}^2/2\,,$

Brans-Dicke: $A_4 = -M_{\rm pl}^2 F(\phi)/2\,,\ B_4 = M_{\rm pl}^2 F(\phi)/2\,,$

covariant Galileon: $A_4 = -M_{\rm pl}^2/2 + 3c_4X^2\,,\ B_4 = M_{\rm pl}^2/2 + c_4X^2\,,$

$\Bigg\}\ \alpha_{\rm H} = 0$

3. Conditions to avoid the conical singularity

In order to avoid the appearance of the conical singularity, $\alpha_{\rm H} \to 0$ is required for the limit $r \to 0$.

$$\boxed{\alpha_{\rm H} \equiv \frac{2XB_{4,X} - B_4}{A_4} - 1\,,}$$

Let us consider the following case:

$$A_4 = -\frac{1}{2}M_{\rm pl}^2 F_1(\phi) + f_1(X)\,, \qquad B_4 = \frac{1}{2}M_{\rm pl}^2 F_2(\phi) + f_2(X)\,,$$

$$\alpha_{\rm H} = \frac{1}{A_4}\left[\frac{M_{\rm pl}^2}{2}(F_1 - F_2) - (f_1 + f_2 - 2Xf_{2,X})\right],$$

1) $F_1(\phi) \neq F_2(\phi)$

At the origin $(\phi(r) = \phi_0)$, we have $\alpha_{\rm H} = F_2(\phi_0)/F_1(\phi_0) - 1 \neq 0$ leading to the appearance of the conical singularity.

2) $F_1(\phi) = F_2(\phi)$

As long as $f_1(X)$ and $f_2(X)$ are positive power low functions of X, $\alpha_{\rm H}$ vanishes at the origin. Thus the model is free of the conical singularity.
e.g.) $f_1(X) = a_4 X^m\,,\ f_2(X) = b_4 X^n\,,$

4. Conclusions

1. In GLPV theories where the deviation from Horndeski theories is weighed by the parameter $\alpha_{\rm H}$, we have shown that the conical singularity arises at the origin of a spherically symmetric body for nonzero constant $\alpha_{\rm H}$ around the origin.

2. The conical singularity is absent for the models described by $A_4 = -\frac{1}{2}M_{\rm pl}^2 F_1(\phi) + f_1(X)$, $B_4 = \frac{1}{2}M_{\rm pl}^2 F_2(\phi) + f_2(X)$, with $F_1(\phi) = F_2(\phi)$.

3. Under the weak gravity approximation, we found that the Vainshtein mechanism sufficiently suppresses the propagation of the fifth force inside/outside the compact object in the above model.

“Causality, Hyperbolicity & Shock formation in Lovelock Theories”

by Norihiro Tanahashi

[JGRG25(2015)4b2]

Norihiro Tanahashi [DAMTP]

with H. S. Reall & B. Way

arXiv: 1406.3379
1409.3874

Causality Hyperbolicity & Shock formation in Lovelock Theories

Causality, Hyperbolicity & Shock formation in Lovelock Theories

- Lovelock Theories
  = GR + (higher-curvature corrections)
  - EoM up to 2nd derivatives → Avoids ghost instability
  - From string theory?

- GR: Gravity propagate at c
- Lovelock: Faster/slower propagation than c

→ Causality in Lovelock theories?
Does EoM remain hyperbolic?
Shock formation due to variable sound speed?

Lovelock theories

- Lovelock theories in d dimensions ($p \le (d-1)/2$)

$$\mathcal{L} = R - \sum_p 2k_p \delta^{c_1 \ldots c_{2p}}_{d_1 \ldots d_{2p}} R_{c_1 c_2}{}^{d_1 d_2} \ldots R_{c_{2p-1} c_{2p}}{}^{d_{2p-1} d_{2p}}$$
$$= R - 8k_2 \left(R^2 - 4R_{ab}R^{ab} + R_{abcd}R^{abcd}\right) + \cdots$$
$$\left(\delta^{c_1 \cdots c_n}_{d_1 \cdots d_n} \equiv n! \delta^{c_1}_{[d_1} \ldots \delta^{c_n}_{d_n]}\right)$$

- EoM = Einstein eq. + correction

$$E^a{}_b \equiv G^a{}_b + B^a{}_b = 0$$

where

$$B^a{}_b = \sum_{p \ge 2} k_p \delta^{a c_1 \ldots c_{2p}}_{b d_1 \ldots d_{2p}} R_{c_1 c_2}{}^{d_1 d_2} \ldots R_{c_{2p-1} c_{2p}}{}^{d_{2p-1} d_{2p}}$$

- A signal propagates on ***characteristic surface***

EoM of ψ : $\quad 0 = \nabla^2 \psi = g^{tt} \partial_t^2 \psi + \cdots$

- $g^{tt} \neq 0$: $\quad \partial_t^2 \psi$ uniquely determined
  → usual time evolution
- $g^{tt} = 0$: $\quad \partial_t^2 \psi$ non-unique
  → $t =$ const. surface is *characteristic*

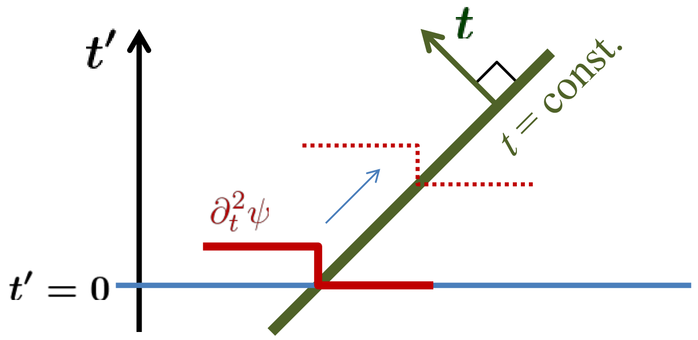

- Characteristics in Lovelock theories [Aragone '87] [Choquet-Bruhat'88]

$$0 = G_{ab} + B_{ab} = P_{ab}{}^{cd}\,\partial_t{}^2 g_{cd} + \cdots$$

$$P^{abcd} \sim g^{tt} g^{c(a} g^{b)d} + \mathcal{R}^{abcd}$$

Characteristic $\Leftrightarrow$ $\det P = 0$

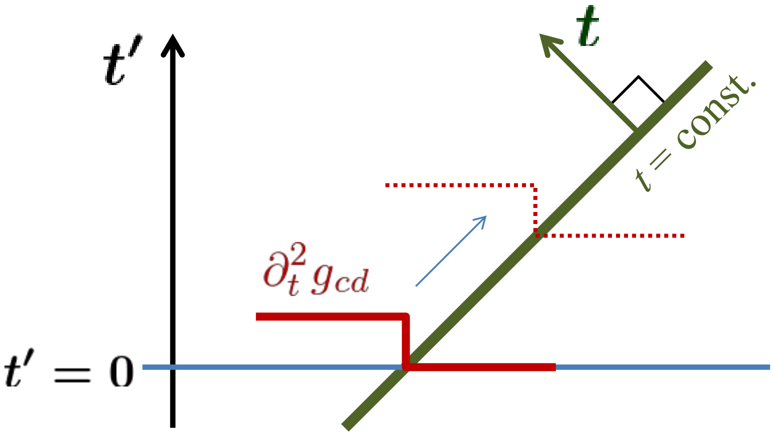

GW Propagation on *plane wave solutions*

$$ds^2 = a_{ij} x^i x^j du^2 + 2dudv + \delta_{ij} dx^i dx^j$$

$$\Rightarrow \begin{cases} R_{\ell i \ell j} \propto a_{ij} \\ \text{Other components} = 0 \end{cases}$$

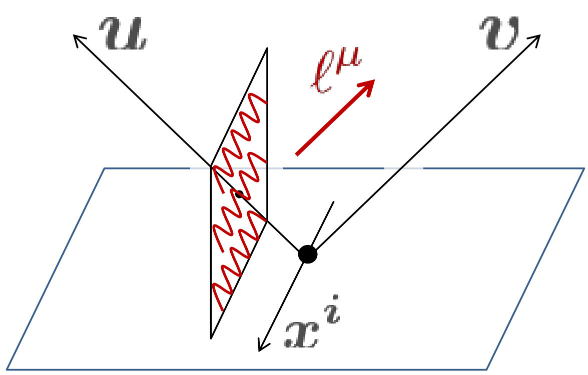

GW Propagation on *plane wave solutions*

Characteristic surfaces are null w.r.t. "effective metrics":

$$G_I^{ab} = g^{ab} + \omega_I(R_{\ell i \ell j})\,\ell^a \ell^b \qquad \left(I = 1, \ldots, \frac{1}{2}d(d-3)\right)$$

✓ $\det P = \prod_I G_I^{ab}\xi_a\xi_b = 0$

✓ ℓ : null w.r.t. G_I

$\Rightarrow$ Characteristic cones tangent to ℓ

✓ Nested characteristic cones

✓ Causality w.r.t. the largest cone

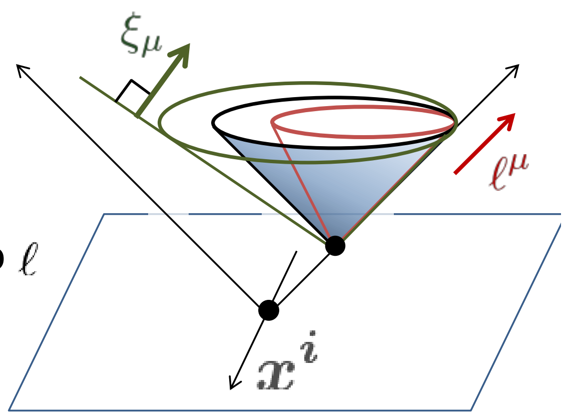

GW Propagation *around BH*

metric: $$ds^2 = -f(r)dt^2 + \frac{dr^2}{f(r)} + r^2 d\Omega^2$$

Effective metric: $$G_{\mu\nu}dx^\mu dx^\nu = -f(r)dt^2 + \frac{dr^2}{f(r)} + \frac{r^2}{c(r)}d\Omega^2$$

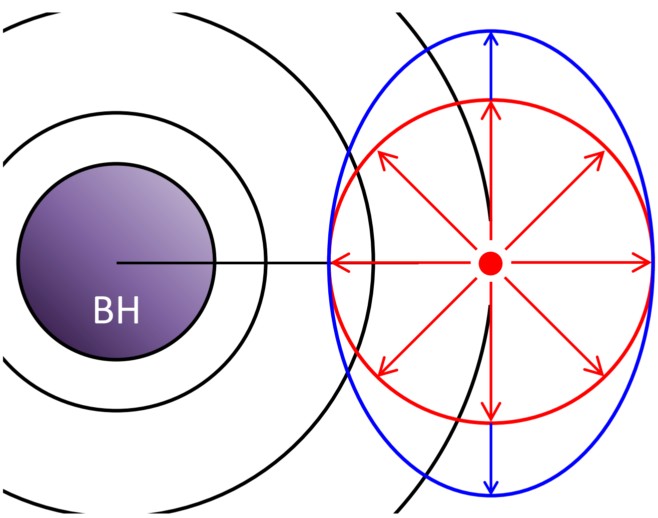

- Light cone and Gravity cone
  - coincide in r direction
  - deviate in Ω direction
- $c(r) > 1 \Rightarrow$ superluminal GW
- $c(r) < 0$ near small BH
  $\Rightarrow$ Hyperbolicity violation?

- Small BH $\Rightarrow c(r) < 0$ near horizon

  $\Rightarrow$ Violation of hyperbolicity

$$\left(-\frac{\partial^2}{\partial t^2} + \frac{\partial^2}{\partial r_*^2} + \frac{f(r)c(r)}{r^2}\frac{\partial^2}{\partial \Omega^2}\right)\Psi = f(r)G^{\mu\nu}\partial_\mu\partial_\nu\Psi$$

$$\frac{\partial^2}{\partial \Omega^2} \sim -l^2$$

✓ $\omega^2 \sim -l^2 \Rightarrow$ growing mode $\sim \exp(lt)$

✓ Consider initial value problem. Perturb initial data with this mode as

$$\delta g_{\mu\nu}(t,r,x) \sim e^{-\sqrt{l}} e^{-lt} \quad \Rightarrow \begin{cases} \bullet\ t=0: & \delta g, \partial^n \delta g = 0 \\ \bullet\ t>0: & \delta g \to \infty \end{cases}$$

with $l \to \infty$

$\therefore$ Solution is not continuous w.r.t. initial data

Solutions do not exist generically

(Initial value problem not well-posed)

Shock formation in Lovelock theories

- Sound speed $\neq$ const.
- Waveform distortion → Shock formation?

ex.) Burgers' equation $\quad \partial_t u + u\, \partial_x u = 0$

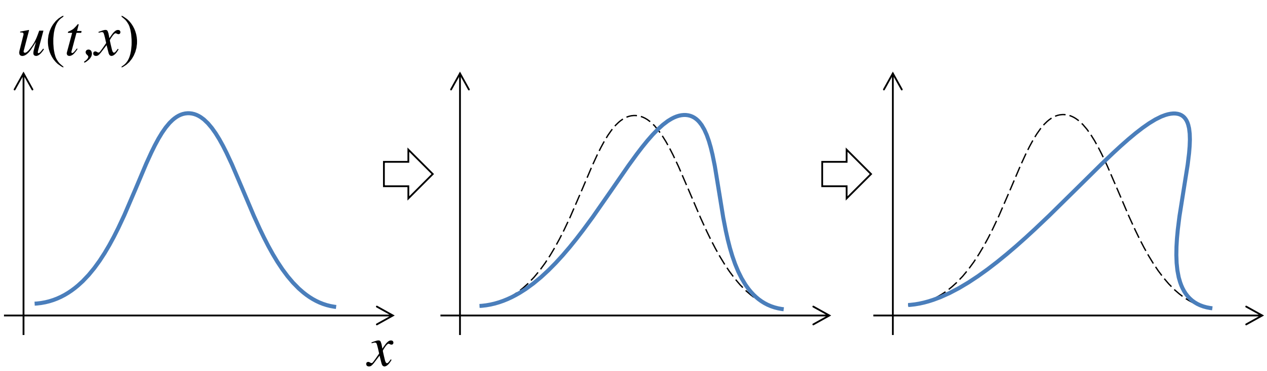

- Propagation of discontinuity in $\partial^2 g_{ab}$

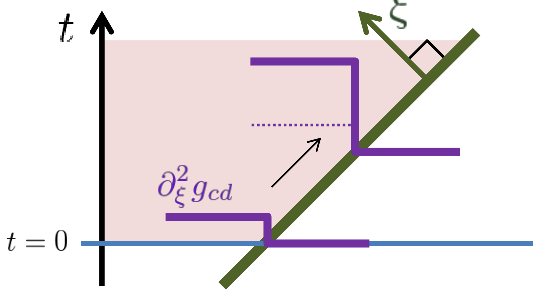

- Transport eq. of discontinuity amplitude $\Pi(t)$

$$[\partial_\xi E_{ab}] = 0 \quad \Rightarrow \quad \dot{\Pi} + M\,\Pi + N\,\Pi^2 = 0$$

$$\left(N = 4\sum_{p\geq 2} p(p-1)k_p\,\delta^{0ikmpr_5\ldots p_{2p}}_{1jlnqs_5\ldots s_{2p}}\,\Gamma^0_{ij'}g^{jj'}\,r^l_k r^n_m r^q_p\,R^{s_5 s_6}_{r_5 r_6}\ldots R^{s_{2p-1}s_{2p}}_{r_{2p-1}r_{2p}} \right)$$

$$\Rightarrow \quad \Pi(t) = \frac{\Pi(0)e^{-\Phi(t)}}{1+\Pi(0)\displaystyle\int_0^t N(t')e^{-\Phi(t')}dt'}$$

- Nonlinear term N term makes $\Pi \to \infty \Rightarrow$ Shock formation

✓ GR: $N=0$ → No shock

✓ Lovelock, Minkowski BG: $N=0$ → No shock

✓ Lovelock, generic BG: $N \neq 0$ → Shock formation

✓ Propagation on plane wave solution

– Along ℓ^μ : $N=0$ → No shock

– Along other directions: $N \neq 0$ → Shock formation

$$\Pi(t) \sim \frac{1}{t-t_0}$$

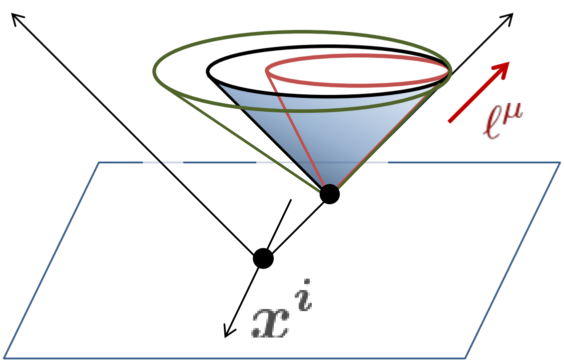

Summary

- Characteristics in Lovelock theories
  - ✓ Characteristics obeys effective metrics
  - ✓ Causality w.r.t. the largest cone
  - ✓ Hyperbolicity violation near small BH horizons

- Shock formation in Lovelock theories
  - ✓ $\exists$ nonlinear term $\Rightarrow$ shock formation
  - ✓ Shock = Naked singularity.
    Violation of cosmic censorship?
  - ✓ Minkowski BG $\rightarrow$ no nonlinear term, no shock formation.
    Is Minkowski stable in Lovelock theories?

?: Hyperbolicity violation & Shock formation in scalar-tensor theories?
(see Seiju Ohashi's poster)

“Relativistic Stars in the Bigravity Theory”

by Katsuki Aoki

[JGRG25(2015)4b3]

Relativistic Stars in the Bigravity Theory

JGRG25@Kyoto University

Katsuki Aoki,
Waseda University

KA, K. Maeda, and M. Tanabe, in preparation.

Why bigravity?

Why modified gravity? Why massive graviton?

What is graviton?

- It should be spin-2 field.
- Massless field or Massive field? How many gravitons?

Experimental constraint
e.g., $m < 7.1 \times 10^{-23}\mathrm{eV}$ (from solar-system experiment)

GR is consistent with many observations.
However, dark components hint us that
GR should be modified at large scale.

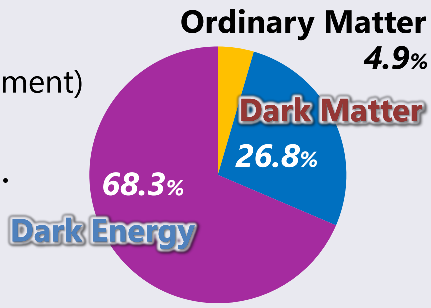

Non-linear bigravity theory (Hassan,Rosen, '11)

contains a massive graviton as well as a massless graviton.

$m \sim 10^{-33}$eV ⇒ DE or $m \gtrsim 10^{-27}$eV ⇒ DM

$$S = \frac{1}{2\kappa_g^2}\int d^4x\sqrt{-g}R(g) + \frac{1}{2\kappa_f^2}\int d^4x\sqrt{-f}\mathcal{R}(f)$$

Gives accelerating expansion

$$-\frac{m^2}{\kappa^2}\int d^4x\sqrt{-g}\sum_{i=0}^{4}\boxed{b_i\mathscr{U}_i(g,f)} + S^{[\mathrm{m}]}(g,f,\psi) \qquad \kappa^2 = \kappa_g^2 + \kappa_f^2$$

$$\gamma^{\mu}{}_{\alpha}\gamma^{\alpha}{}_{\nu} = g^{\mu\alpha}f_{\alpha\nu} \qquad \mathscr{U}_n(g,f) = -\frac{1}{n!(4-n)!}\epsilon^{\cdots\cdot}\epsilon_{\cdots\cdot}(\gamma^{\mu}{}_{\nu})^n$$

$$S^{[\mathrm{m}]} = S_g^{[\mathrm{m}]}(g,\psi_g) + \boxed{S_f^{[\mathrm{m}]}(f,\psi_f)}$$

Physical matter Dark matter (KA and K. Maeda, '14)

Massless limit = GR?

Bigravity → adding mass term of graviton

GR should be recovered in massless limit.

Linear theory (FP theory) → vDVZ discontinuity

Non-linear theory → Vainshtein mechanism

Bigravity is restored to GR in weak gravitational field.

(e.g., Babichev and Crisostomi '13)

How about **"relativistic"** effect? Restoration of **"GR"** ?

$\left\{\begin{array}{l}\text{Cosmological background?}\\ \text{Strong gravity effect?}\end{array}\right.$

Linear theory is unstable on FLRW

Effective action of scalar graviton on curved background

$$\mathcal{L}_{\rm eff} = -\frac{3}{4}(\partial\phi)^2 + \frac{c_{\rm NL}}{\Lambda^3}(\partial\phi)^2\Box\phi + \cdots$$
$$+\frac{\bar{R}^{\mu\nu}}{2m^2}\partial_\mu\phi\partial_\nu\phi + \frac{\tilde{c}_{\rm NL}}{\Lambda^3}\frac{\bar{R}^{\mu\nu\rho\sigma}}{m}\partial_\mu\phi\partial_\rho\phi\,\partial_\nu\partial_\sigma\phi + \cdots + \kappa\phi\delta T$$

When $\bar{R}_0 \gg m^2\,, \quad \bar{R}_0 \sim \bar{R}_{\mu\nu} \qquad \kappa_{\rm eff} = \frac{m}{\sqrt{\bar{R}_0}}\kappa \ll \kappa$

Fifth force can be screened even at quadratic order.

However, third term produces an instability

e.g., $\bar{R}^{\mu\nu}\nabla_\mu\phi\nabla_\nu\phi = +\Lambda_g(\partial\phi)^2$ → Higuchi ghost

Ghost condensation + Vainshtein

Linear instability does not conclude instability of system.

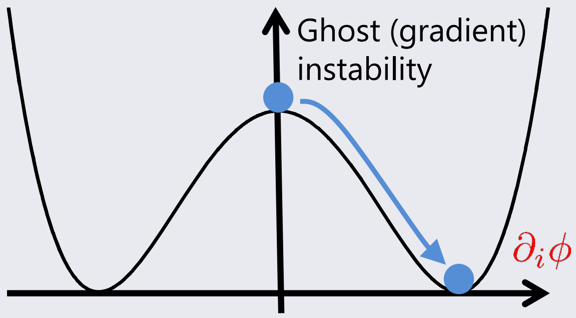

We should take into account non-linear kinetic terms

Non-zero $\langle\dot{\phi}\rangle$ can stabilize in the ghost condensation
(Arkani-Hamed, et al., 2004)

Non-zero expectation value $\langle\partial_i\phi\rangle$ can stabilize in bigravity.

KA, K. Maeda, and R. Namba, PRD 92, 044054 (2015).

Although the scalar mode has an inhomogeneity,
the spacetime is homogenous due to the screening mechanism.

Massless limit = GR?

Bigravity → adding mass term of graviton

GR should be recovered in massless limit.
Linear theory (FP theory) → vDVZ discontinuity
Non-linear theory → Vainshtein mechanism

Bigravity is restored to GR in weak gravitational field.
(e.g., Babichev and Crisostomi '13)

How about **"relativistic"** effect? Restoration of **"GR"** ?

- Cosmological background → **Vainshtein + condensation**
  KA, K. Maeda, and R. Namba, PRD 92, 044054 (2015)
- Strong gravity effect?

Static spherically symmetric spacetime

Bi-diagonal ansatz

$$ds_g^2 = -N_g^2(r)dt^2 + \frac{dr^2}{F_g^2(r)} + r^2 d\Omega^2 \,,$$

$$ds_f^2 = -N_f^2(r)dt^2 + \frac{dr_f^2}{F_f^2(r)} + r_f^2(r) d\Omega^2 \,,$$

Define $\mu(r) := \frac{r_f}{r} - 1$ → Stueckelberg field

When $N_g/N_f = F_g/F_f = r/r_f = 1$ → Minkowski spacetime

We study a relativistic star in g-spacetime
(assuming only g-matter for simplicity).

Basic equations

Einstein equations

$$G^{\mu}{}_{\nu} = \kappa_g^2 (T_g^{[\gamma]\mu}{}_{\nu} + T^{[\mathrm{m}]\mu}{}_{\nu}),$$

$$\mathcal{G}^{\mu}{}_{\nu} = \kappa_f^2 \mathcal{T}_f^{[\gamma]\mu}{}_{\nu}$$

Conversation laws

$$\overset{(g)}{\nabla}_{\mu} T^{[\mathrm{m}]\mu}{}_{\nu} = 0\,,$$

$\overset{(g)}{\nabla}_{\mu} T_g^{[\gamma]\mu}{}_{\nu} = 0$ | Absent in GR → Additional constraint

$$ds_g^2 = -N_g^2(r)dt^2 + \frac{dr^2}{F_g^2(r)} + r^2 d\Omega^2\,,$$

$$ds_f^2 = -N_f^2(r)dt^2 + \frac{dr_f^2}{F_f^2(r)} + r_f^2(r) d\Omega^2\,,$$

$$\mu(r) := \frac{r_f}{r} - 1$$

N_g, F_g, N_f, F_f are determined by Einstein equations.

The variable μ is determined by the additional constraint.

In massless limit

Einstein equations

$$G^{\mu}{}_{\nu} = \kappa_g^2 (\cancel{T_g^{[\gamma]\mu}{}_{\nu}} + T^{[\mathrm{m}]\mu}{}_{\nu}),$$

$$\mathcal{G}^{\mu}{}_{\nu} = \kappa_f^2 \cancel{\mathcal{T}_f^{[\gamma]\mu}{}_{\nu}}$$

Conversation laws

$$\overset{(g)}{\nabla}_{\mu} T^{[\mathrm{m}]\mu}{}_{\nu} = 0\,,$$

$\overset{(g)}{\nabla}_{\mu} T_g^{[\gamma]\mu}{}_{\nu} = 0$ | Absent in GR → Additional constraint

$$ds_g^2 = -N_g^2(r)dt^2 + \frac{dr^2}{F_g^2(r)} + r^2 d\Omega^2\,,$$

$$ds_f^2 = -N_f^2(r)dt^2 + \frac{dr_f^2}{F_f^2(r)} + r_f^2(r) d\Omega^2\,,$$

$$\mu(r) := \frac{r_f}{r} - 1$$

N_g, F_g, N_f, F_f are given by GR solutions.

The variable μ is determined by the additional constraint.

Relativistic star in g-spacetime

We find two cases:

$$\beta_2 = \frac{b_2 + b_3}{b_1 + 2b_2 + b_3}\,, \beta_3 := \frac{b_3}{b_1 + 2b_2 + b_3}$$

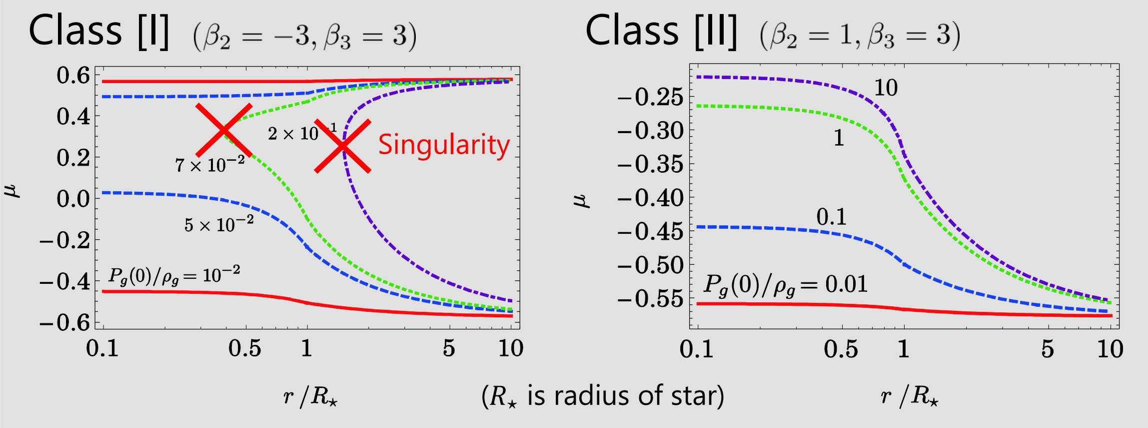

For class [I], there is a critical value of the pressure, beyond which the star solution disappears. → Result is not GR

Classification of coupling constants

We can classify coupling constants into two classes:

Class [I] → $\beta_2^2 - \beta_3 > 0$ + other constraints

There is a critical value

Class [III] → $\beta_2^2 - \beta_3 \leq 0$ + other constraints

No critical value

$$\beta_2 = \frac{b_2 + b_3}{b_1 + 2b_2 + b_3}\,, \beta_3 := \frac{b_3}{b_1 + 2b_2 + b_3}$$

Cosmology vs Astrophysics

We can classify coupling constants into two classes:

Class [I] → $\beta_2^2 - \beta_3 > 0$ + other constraints

There is a critical value

Class [II] → $\beta_2^2 - \beta_3 \leq 0$ + other constraints

No critical value

$$\beta_2 = \frac{b_2 + b_3}{b_1 + 2b_2 + b_3}, \beta_3 := \frac{b_3}{b_1 + 2b_2 + b_3}$$

Stability constraint of the early Universe → $\beta_2^2 - \beta_3 > 0$

Class [I] is favored from cosmological aspect.

→ Maximum mass of neutron star is constrained for Class [I] ?

Maximum mass of the neutron star

We assume a polytropic star

$$P_g = \mathcal{K}\rho_g^2$$

GR (and Class [II]) → $\sim 2M_\odot$

Class [I] → typically $\sim 1M_\odot$

and at most $1.7M_\odot$

Class [I] cannot give $2M_\odot$

The result is also confirmed numerically without massless limit.

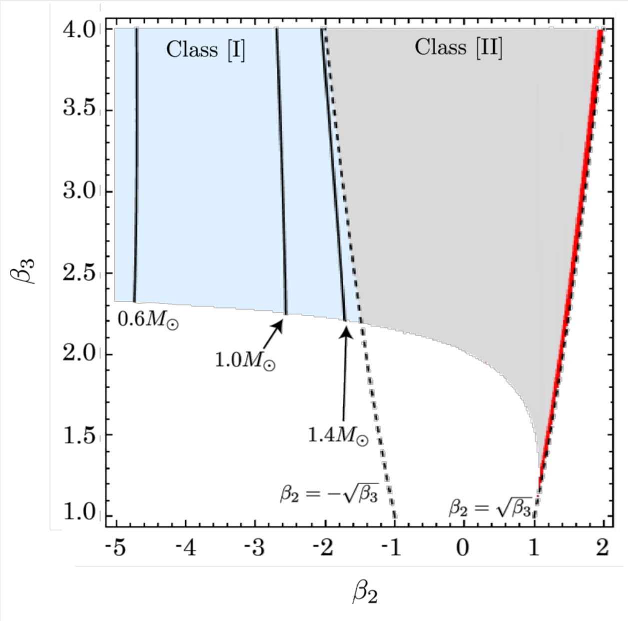

Summary

For Class [I], the maximum mass is constrained.
The simple EoS cannot give $2M_\odot$ even if it can do in GR

Class [II] → No problem from neutron star
However, the instability is problematic in the early Universe

Why not GR? We assume static configuration.
→ It is not necessary that Stueckelberg field is static.
(c.f., Cosmology → homogeneous scalar graviton is unstable
inhomogeneous scalar graviton is stable)

We hope there is a massive neutron star (and black hole) with dynamical Stueckelberg field in Class [I].

“Universal instability of hairy black holes in Lovelock-Galileon theories in D dimensions”

by Kazufumi Takahashi

[JGRG25(2015)4b4]

Universal instability of hairy black holes in Lovelock-Galileon theories in D dimensions

Kazufumi Takahashi

The University of Tokyo, RESCEU

Based on work with

Teruaki Suyama (RESCEU) & Tsutomu Kobayashi (Rikkyo Univ.)

arXiv: 1511.06083

➢ BH with scalar hair

- Many scalar-tensor theories have been considered. (inflation, late-time acceleration, ⋯)

  ➡ Horndeski theory ⋯ the most general theory with second-order EOMs

- When we consider a scalar-tensor theory, it is important to check if the black hole solutions can have scalar hair or not.

- Consider a theory

$$S = \int dx^4 \sqrt{-g}\left(a_0 + a_1 R - \frac{b_0}{2} g^{\alpha\beta}\phi_{;\alpha}\phi_{;\beta} + b_1 G^{\alpha\beta}\phi_{;\alpha}\phi_{;\beta}\right),$$

which is a subclass of the Horndeski class.

➡ This theory has static and spherically symmetric BH solutions with linearly time-dependent scalar hair. (Babichev and Charmousis, 2014)

$$\phi(t,r) = qt + \psi(r) \quad (q = \text{const.} \neq 0)$$

Some properties of the theory

- Consider a theory

$$S = \int dx^4 \sqrt{-g}\left(a_0 + a_1 R - \frac{b_0}{2} g^{\alpha\beta}\phi_{;\alpha}\phi_{;\beta} + b_1 G^{\alpha\beta}\phi_{;\alpha}\phi_{;\beta}\right).$$

- This theory has the following mathematical properties:
  - The first 2 terms are the only quantities which involve only $g_{\mu\nu}$ giving second-order EOMs in 4 dimensions.
  - The tensors coupled to the derivative of the scalar field $\phi_{;\alpha}\phi_{;\beta}$ are derived from the variation of the former 2 terms.

const. $\leftrightarrow$ $g_{\alpha\beta}$

R $\leftrightarrow$ $G_{\alpha\beta}$

- This correspondence can be extended to higher dimensions:
  - Consider the most general theory which involves only $g_{\mu\nu}$ giving second-order field equations in D dimensions.
  - Vary the action to construct rank-2 tensors and couple them to $\phi_{;\alpha}\phi_{;\beta}$.

Lovelock-Galileon theories

- In D-dimensional spacetime, the Lovelock invariants

$$\mathcal{R}^{(n)} \equiv \frac{1}{2^n}\delta^{\alpha_1\alpha_2\cdots\alpha_{2n-1}\alpha_{2n}}_{\beta_1\beta_2\cdots\beta_{2n-1}\beta_{2n}} R^{\beta_1\beta_2}{}_{\alpha_1\alpha_2}\cdots R^{\beta_{2n-1}\beta_{2n}}{}_{\alpha_{2n-1}\alpha_{2n}}$$

are the only quantities giving second-order field equations.

$\mathcal{R}^{(0)}$: const
$\mathcal{R}^{(1)}$: Ricci scalar
$\mathcal{R}^{(2)}$: Gauss-Bonnet scalar

- Variation w.r.t. $g^{\mu\nu}$ gives the Lovelock tensors:

$$H^{(n)\mu}{}_{\nu} \equiv -\frac{1}{2^{n+1}}\delta^{\mu\alpha_1\alpha_2\cdots\alpha_{2n-1}\alpha_{2n}}_{\nu\beta_1\beta_2\cdots\beta_{2n-1}\beta_{2n}} R^{\beta_1\beta_2}{}_{\alpha_1\alpha_2}\cdots R^{\beta_{2n-1}\beta_{2n}}{}_{\alpha_{2n-1}\alpha_{2n}}.$$

- We can consider the following theory (= Lovelock-Galileon theory):

$$S_{\rm LG} = \int d^D x\sqrt{-g}\sum_{n=0}^{M}\left(a_n\mathcal{R}^{(n)} + b_n H^{(n)\alpha\beta}\phi_{;\alpha}\phi_{;\beta}\right),$$

with

$$M \equiv \left\lfloor\frac{D-1}{2}\right\rfloor,$$

since $n > M$ terms do not contribute to the EOMs.

EOMs in Lovelock-Galileon theory

- The EOMs are of second order:

$$\sum_{n=0}^{M}\left(a_n H^{(n)}_{\mu\nu} + b_n E^{(n)}_{\mu\nu}\right) = 0, \qquad \sum_{n=0}^{M} b_n J^{(n)\alpha}{}_{;\alpha} = 0,$$

where

$$H^{(n)\mu}{}_{\nu} \equiv -\frac{1}{2^{n+1}}\delta^{\mu\alpha_1\alpha_2\cdots\alpha_{2n-1}\alpha_{2n}}_{\nu\beta_1\beta_2\cdots\beta_{2n-1}\beta_{2n}} R^{\beta_1\beta_2}_{\alpha_1\alpha_2}\cdots R^{\beta_{2n-1}\beta_{2n}}_{\alpha_{2n-1}\alpha_{2n}}$$

$$\begin{aligned} E^{(n)}_{\mu\nu} \equiv & -\frac{1}{2} g_{\mu\nu} H^{(n)\alpha\beta}\phi_{;\alpha}\phi_{;\beta} + H^{(n)\alpha}{}_{(\mu}\phi_{;\nu)}\phi_{;\alpha} \\ & - \frac{n}{2^{n+1}} g_{\lambda(\mu}\delta^{\alpha_1\alpha_2\cdots\alpha_{2n-1}\alpha_{2n}\alpha}_{\nu)\beta_2\cdots\beta_{2n-1}\beta_{2n}\beta} R^{\lambda\beta_2}_{\alpha_1\alpha_2} R^{\beta_3\beta_4}_{\alpha_3\alpha_4}\cdots R^{\beta_{2n-1}\beta_{2n}}_{\alpha_{2n-1}\alpha_{2n}}\phi_{;\alpha}\phi^{;\beta} \\ & - \frac{n}{2^{n+1}} g_{\alpha_1(\mu}\delta^{\alpha_1\alpha_2\cdots\alpha_{2n-1}\alpha_{2n}\alpha}_{\nu)\beta_2\cdots\beta_{2n-1}\beta_{2n}\beta} R^{\beta_3\beta_4}_{\alpha_3\alpha_4}\cdots R^{\beta_{2n-1}\beta_{2n}}_{\alpha_{2n-1}\alpha_{2n}} R^{\beta_2\beta}_{\alpha_2\lambda}\phi_{;\alpha}\phi^{;\lambda} \\ & - \frac{n}{2^{n}} g_{\alpha_1(\mu}\delta^{\alpha_1\alpha_2\cdots\alpha_{2n-1}\alpha_{2n}\alpha}_{\nu)\beta_2\cdots\beta_{2n-1}\beta_{2n}\beta} R^{\beta_3\beta_4}_{\alpha_3\alpha_4}\cdots R^{\beta_{2n-1}\beta_{2n}}_{\alpha_{2n-1}\alpha_{2n}}\phi_{;\alpha}{}^{;\beta_2}\phi^{;\beta}{}_{;\alpha_2}, \end{aligned}$$

$$J^{(n)\alpha} \equiv -H^{(n)\alpha\beta}\phi_{;\beta}.$$

- This second-order nature follows from the Bianchi identity.

Stability of BH?

- BH solutions in $D = 5$ case have been found recently. (Charmousis and Tsoukalas, 2015)
- Once we obtain a solution, its stability should be checked.
- BH solutions in 4 dimensions are unstable. (Ogawa, Kobayashi, and Suyama, 2015)
- The following questions may arise:
  - Are the BH solutions in 5 dimensions unstable?
  - Can the BH solutions be generalized into higher dimensions?
  - If so, does the instability arise in the generalized solutions?

➢ Stability of BH?

- BH solutions in $D = 5$ case have been found recently. (Charmousis and Tsoukalas, 2015)
- Once we obtain a solution, its stability should be checked.
- BH solutions in 4 dimensions are unstable. (Ogawa, Kobayashi, and Suyama, 2015)
- The following questions may arise:
  - Are the BH solutions in 5 dimensions unstable?
  - Can the BH solutions be generalized into higher dimensions?
  - If so, does the instability arise in the generalized solutions?

YES!

- We argue the solutions for $D = 5$ are unstable. Furthermore, we generalize the solutions into higher dimensions and show the instability cannot be avoided in any dimension.

➢ Review of the BH solutions in 5 dimensions

- Action

$$S \equiv \int d^5x\sqrt{-g}\left(a_0 + a_1 R + a_2\mathcal{R}^{(2)} - \frac{b_0}{2}\phi_{;\alpha}\phi^{;\alpha} + b_1 G^{\alpha\beta}\phi_{;\alpha}\phi_{;\beta} + b_2 H^{(2)\alpha\beta}\phi_{;\alpha}\phi_{;\beta}\right),$$

$$\mathcal{R}^{(2)} = R^2 - 4R_{\alpha\beta}R^{\alpha\beta} + R_{\alpha\beta\gamma\delta}R^{\alpha\beta\gamma\delta},$$

$$H^{(2)}_{\mu\nu} = -\frac{1}{2}g_{\mu\nu}\mathcal{R}^{(2)} + 2RR_{\mu\nu} - 4R_{\mu\alpha}R_\nu{}^\alpha + 4R_{\mu\alpha\nu\beta}R^{\alpha\beta} + 2R_{\mu\alpha\beta\gamma}R_\nu{}^{\alpha\beta\gamma}.$$

- The metric was assumed to be static and spherically symmetric, and the scalar field is linearly time-dependent:

$$ds^2 = -h(r)dt^2 + \frac{dr^2}{f(r)} + r^2\bar{\gamma}_{ij}\,dx^i dx^j,$$

$$\phi(t,r) = qt + \psi(r),$$

where $\bar{\gamma}_{ij}$ is the metric of a 3-dimensional maximally symmetric space with special curvature κ.

- Since only $\nabla_\mu\phi$ appears in the action, the linear dependence on time does not violate the staticity of the metric.

Review of the BH solutions in 5 dimensions

- the tr-component of the metric equation

$$-\frac{b_0}{6}+b_1\left(\frac{fh'}{2rh}-F\right)+2b_2\frac{fh'}{rh}F=0 \Longrightarrow f=f[h,h']$$

quadratic equation

$$F\equiv\frac{\kappa-f}{r^2}$$

- The rr-component

$$-\frac{1}{6}\left(a_0+\frac{b_0q^2}{2h}\right)+\left(a_1-\frac{b_1q^2}{2h}\right)\frac{fh'}{2rh}-\left(a_1+\frac{b_1q^2}{2h}\right)F$$
$$+\left(a_2-\frac{b_2q^2}{2h}\right)\frac{2fh'}{rh}F+f^2\psi'^2\left[\frac{b_1}{2}\left(\frac{h'}{rh}+\frac{2}{r^2}\right)+2b_2\left(\frac{h'}{rh}F-\frac{fh'}{r^3h}\right)\right]=0 \Longrightarrow \psi'=\psi'[h,h']$$

- The tt-component

$$-\frac{1}{6}\left(a_0-\frac{b_0q^2}{2h}\right)+\left(a_1-\frac{b_1q^2}{2h}\right)\left(\frac{f'}{2r}-F\right)+\left(a_2-\frac{b_2q^2}{2h}\right)\frac{2f'}{r}F$$
$$+(b_1+4b_2F)\frac{f^2}{2r}(\psi'^2)'+f^2\psi'^2\left[(b_1+4b_2F)\left(\frac{3}{4}\frac{f'}{rf}+\frac{1}{4}\frac{h'}{rh}\right)+\frac{b_1}{r^3}-\frac{2b_2}{r^3}f'\right]=0$$

$\Longrightarrow$ Second-order ODE w.r.t. h

Instability of the solution ($\rightarrow$ our work)

- We consider the tensor perturbation of the form:

$$\delta g_{ab}=\delta g_{ai}=0, \qquad \delta g_{ij}=r^2\chi(t,r)\bar{h}_{ij}(x^k),$$

$a,b=(t,r)$
$i,j,\cdots$: angular coordinates

where χ represents the dynamical DOF and $\bar{h}_{ij}$ are symmetric tensor spherical harmonics:

$$\bar{\nabla}^k\bar{\nabla}_k\bar{h}_{ij}=-\gamma\bar{h}_{ij}, \qquad \bar{\nabla}^i\bar{h}_{ij}=0, \qquad \bar{h}^i_i=0.$$

positive eigenvalue

Note that $\delta\phi=0$.

- The second-order action

background dependent coefficient

$$S^{(2)}=\int d^5x\sqrt{-\bar{g}}\left(\frac{\lambda_0}{2}\dot{\chi}^2-\frac{\lambda_1}{2}\chi'^2+\frac{\lambda_2}{2}\dot{\chi}\chi'-\frac{\lambda_3}{2}\chi^2\right)\bar{h}^{kl}\bar{h}_{kl}$$

- Introducing the canonical momentum π conjugate to χ, the Hamiltonian is given by

$$H=\int d^5x\sqrt{-\bar{g}}\left[\frac{1}{2\lambda_0}\left(\frac{\pi}{\sqrt{-\bar{g}}\bar{h}^{kl}\bar{h}_{kl}}-\frac{\lambda_2}{2}\chi'\right)^2+\frac{\lambda_1}{2}\chi'^2+\frac{\lambda_3}{2}\chi^2\right]\bar{h}^{kl}\bar{h}_{kl}.$$

For this Hamiltonian to be bounded below, it is necessary that $\lambda_0,\lambda_1,\lambda_3>0$.

Instability of the solution

- The coefficients λ_0 and λ_1 are written in terms of the background solution as

$$\lambda_0 = \frac{a_1}{2h} - a_2\frac{f'}{rh} + \frac{r^2}{h}\left[-\frac{q^2}{h}\left(\frac{b_1}{2} - b_2\frac{fh'}{rh}\right) + X\left(\frac{b_1}{2} + b_2\frac{f'}{r}\right) + 2b_2\frac{f}{r}X'\right],$$

$$\lambda_1 = \frac{a_1}{2}f - a_2\frac{f^2h'}{rh} + r^2 f\left[\frac{q^2}{h}\left(\frac{b_1}{2} - b_2\frac{fh'}{rh}\right) - X\left(\frac{b_1}{2} - 3b_2\frac{fh'}{rh}\right)\right],$$

where

$$X \equiv -\frac{1}{2}\phi_{;\alpha}\phi^{;\alpha} = \frac{q^2}{2h} - \frac{f\psi'^2}{2}.$$

- In the vicinity of the (Killing) horizon where $h \simeq 0$, λ_0 and λ_1 can be approximated as

$$\lambda_0 \approx -\frac{q^2r^2}{h^2}\left(\frac{b_1}{2} - b_2\frac{fh'}{rh}\right), \qquad \lambda_1 \approx \frac{q^2r^2f}{h}\left(\frac{b_1}{2} - b_2\frac{fh'}{rh}\right).$$

$\Rightarrow$ $\lambda_0\lambda_1 \approx -\frac{q^4r^4f}{h^3}\left(\frac{b_1}{2} - b_2\frac{fh'}{rh}\right)^2 < 0$ ⋯ Either λ_0 or λ_1 is negative

$\Rightarrow$ **Ghost/gradient instability!** (for $q \neq 0$)

Extension to higher dimensions

- We consider the full Lovelock-Galileon action in D dimensions:

$$S_{\rm LG} = \int d^Dx\sqrt{-g}\sum_{n=0}^{M}\left(a_n\mathcal{R}^{(n)} + b_nH^{(n)\alpha\beta}\phi_{;\alpha}\phi_{;\beta}\right),$$

with the metric and the scalar field of the form

$$ds^2 = -h(r)dt^2 + \frac{dr^2}{f(r)} + r^2\bar{\gamma}_{ij}\,dx^idx^j,$$
$$\phi(t,r) = qt + \psi(r).$$

- The solution is obtained in the same way as in 5-dimensional case:

tr-component $\rightarrow$ (Solve an algebraic eq. of M-th order) $f = f[h,h']$

rr-component $\rightarrow$ $\psi' = \psi'[h,h']$ (using $f = f[h,h']$)

$f = f[h,h']$, $\psi' = \psi'[h,h']$ $\rightarrow$ tt-component $\Rightarrow$ 2nd-order ODE w.r.t. h

EOMs in terms of h, f, and ψ

- If we find a solution which satisfies the tt, rr, and tr-components of the Einstein eq., then it solves all the other components of the Einstein eq. and the scalar EOM.

$$F \equiv \frac{\kappa - f}{r^2}$$

$$tr:\ \sum_{n=0}^{M} \frac{b_n F^{n-1}}{(D-2n-1)!}\left[n\frac{fh'}{rh} - (D-2n-1)F\right] = 0\,, \Rightarrow f = f[h,h']$$

M-th order algebraic equation

$$rr:\ \sum_{n=0}^{M} \frac{F^{n-2}}{(D-2n-1)!}\left\{n\left(a_n - \frac{b_n q^2}{2h}\right)\frac{fh'}{rh}F - (D-2n-1)\left(a_n + \frac{b_n q^2}{2h}\right)F^2 + nb_n f^2\psi'^2\left[\frac{h'}{rh}F + (D-2n-1)\frac{F}{r^2} - (n-1)\frac{fh'}{r^3 h}\right]\right\} = 0,$$

$$\Rightarrow \psi' = \psi'[h,h']$$

$$tt:\ \sum_{n=0}^{M} \frac{F^{n-2}}{(D-2n-1)!}\left\{\left(a_n - \frac{b_n q^2}{2h}\right)\left[\frac{fh'}{rh}F - (D-2n-1)F^2\right] + nb_n\frac{f^2}{r}F(\psi'^2)' + nb_n f^2\psi'^2\left[\frac{3}{2}\frac{f'}{rf}F + \frac{1}{2}\frac{h'}{rh}F + (D-2n-1)\frac{F}{r^2} - (n-1)\frac{f'}{r^3}\right]\right\} = 0,$$

$\Rightarrow$ Second-order ODE w.r.t. h

Universal instability

- Consider the same type of perturbation as we did in 5 dimensions and construct

$$S_{\rm LG}^{(2)} = \int d^D x\sqrt{-\bar{g}}\left(\frac{\lambda_0}{2}\dot{\chi}^2 - \frac{\lambda_1}{2}\chi'^2 + \frac{\lambda_2}{2}\dot{\chi}\chi' - \frac{\lambda_3}{2}\chi^2\right)\bar{h}^{kl}\bar{h}_{kl}$$

λ_0 and λ_1 determine the presence of ghost/gradient instability

$$F \equiv \frac{\kappa - f}{r^2}$$

- Near the horizon, we obtain

$$\lambda_0 \approx \frac{q^2 r^2}{2h^2}\sum_{n=1}^{M}\frac{(D-4)!\,nb_n F^{n-2}}{(D-2n-1)!}\left[(n-1)\frac{fh'}{rh} - (D-2n-1)F\right],$$

$$\lambda_1 \approx -\frac{q^2 r^2 f}{2h}\sum_{n=1}^{M}\frac{(D-4)!\,nb_n F^{n-2}}{(D-2n-1)!}\left[(n-1)\frac{fh'}{rh} - (D-2n-1)F\right],$$

$$\Rightarrow \lambda_0\lambda_1 \approx -\frac{q^4 r^4 f}{4h^3}\left\{\sum_{n=1}^{M}\frac{(D-4)!\,nb_n F^{n-2}}{(D-2n-1)!}\left[(n-1)\frac{fh'}{rh} - (D-2n-1)F\right]\right\}^2 < 0.$$

$\Rightarrow$ We cannot avoid instability!

➢ Summary

- We analyzed static and spherically symmetric solutions in a class of Lovelock-Galileon theories, which is a scalar-tensor theory with second-order EOMs in arbitrary dimensions.

- Our ansatz is that the metric is static and spherically symmetric, and the scalar field is linearly time-dependent.

- We showed the known 5-dimensional BH solutions are unstable under tensor perturbations.

- We generalized the solutions to higher dimensions, but the instability cannot be avoided.

Appendices

➢ Simple case (1) : ℓ-th-order Lovelock-galileon

- Action

$$\int d^D x\sqrt{-g}\left(a_\ell \mathcal{R}^{(\ell)} + b_\ell H^{(\ell)\alpha\beta}\phi_{;\alpha}\phi_{;\beta}\right)$$

- Solution

$$h = C_0 - \frac{C_1}{r^{(D-2\ell-1)/\ell}},$$

$$f = \frac{\kappa}{C_0}h,$$

$$\psi'^2 = \frac{q^2}{\kappa h^2}\frac{C_1}{r^{(D-2\ell-1)/\ell}}.$$

- In the case of $\kappa = 1$, one can rescale t to have $C_0 = 1$ and $f = h$, leading to

$$h = f = 1 - \frac{C_1}{r^{(D-2\ell-1)/\ell}},$$

Generalizes the Schwarzscild BH in GR

$$\psi' = \pm\frac{q}{h}\frac{\sqrt{C_1}}{r^{(D-2\ell-1)/2\ell}}.$$

➢ Simple case (2): Schwarzschild-like metric

- Assuming $h = f$, the functional form of f is obtained by solving an algebraic equation

$$\sum_{n=0}^{M}\frac{b_n}{(D-2n-1)!}\left(\frac{\kappa - f}{r^2}\right)^n = \frac{\mu}{r^{D-1}},$$

where μ is an integration constant.

- The radial part of the scalar field can be expressed by f as follows:

$$\psi' = \pm\frac{q}{f}\sqrt{1-\frac{f}{\kappa}}.$$

- This type of solution is possible only when a_n's and b_n's satisfy specific conditions:

$$\frac{a_j}{b_j} - 2X_0 j = -\frac{\nu}{\mu}, \text{for all non} - \text{vanishing pairs of } (a_j, b_j)$$

where X_0 and ν are integration constants.

- When the scalar field is expressed in terms of the Eddington-Finkelstein and the radial coordinate, one can show that its radial part remains finite even at the horizon.

  ⟹ Any freely-infalling observer records the finite value of the scalar field on the horizon!

➢ Full expressions for λ_0 and λ_1

$$\lambda_0 = \sum_{n=0}^{M} \frac{(D-4)!\, nF^{n-2}}{(D-2n-1)!} \frac{r^2}{4h} \left\{ -\frac{2a_n}{r^2} \left[(n-1)\frac{f'}{r} - (D-2n-1)F \right] + 4(n-1)b_n \frac{f}{r} X' \right.$$
$$+2b_n X \left[(D-2n-1)\left(2(n-1)\frac{f}{r^2} + F \right) + (n-1)\frac{f'}{rF}\left(F - 2(n-2)\frac{f}{r^2} \right) \right]$$
$$\left. -\frac{2b_n q^2}{h} \left[(D-2n-1)\left((n-1)\frac{f}{r^2} + F \right) - (n-1)\frac{f}{rF}\left(\frac{h'}{h}F + (n-2)\frac{f'}{r^2} \right) \right] \right\}$$

$$\lambda_1 = \sum_{n=0}^{M} \frac{(D-4)!\, nF^{n-2}}{(D-2n-1)!} \frac{r^2 f}{4} \left\{ -\frac{2a_n}{r^2} \left[(n-1)\frac{fh'}{rh} - (D-2n-1)F \right] \right.$$
$$+2b_n X \left[(D-2n-1)\left(2(n-1)\frac{f}{r^2} - F \right) + (n-1)\frac{fh'}{rhF}\left(3F - 2(n-2)\frac{f}{r^2} \right) \right]$$
$$\left. -\frac{2b_n q^2}{h} \left[(D-2n-1)\left((n-1)\frac{f}{r^2} - F \right) + (n-1)\frac{fh'}{rhF}\left(F - (n-2)\frac{f}{r^2} \right) \right] \right\}$$

where X is the canonical kinetic term of the scalar field:

$$X \equiv -\frac{1}{2}\nabla^\mu \phi \nabla_\mu \phi = \frac{q^2}{2h} - \frac{f\psi'^2}{2}.$$

“Suppressing the primordial tensor amplitude without changing the scalar sector in quadratic curvature gravity”

by Kohji Yajima

[JGRG25(2015)4b5]

Suppressing the primordial tensor amplitude without changing the scalar sector in quadratic curvature gravity

Kohji Yajima (Rikkyo University)

Tsutomu Kobayashi (Rikkyo University)

Based on Phys. Rev. D **92**, 103503
[arXiv : 1508.07412]

JGRG 25 @YITP
9 Dec. 2015

Constraints on Inflation model

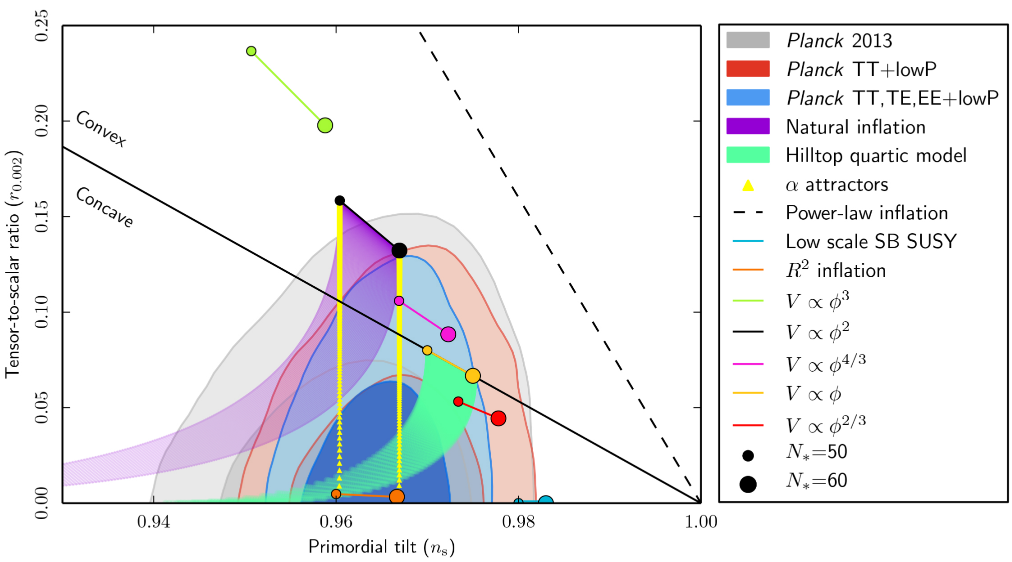

Planck 2015 results. XX
arXiv:1502.02114

Question

Can we modify only tensor modes without changing the scalar sector?

Outline

- Introduction
- Construction of quadratic curvature gravity
- How the tensor amplitude is modified ?
- Results with Planck 2015

Construction of theories

Action: $S = S_{\rm EH} + S_\phi + S_{\rm higher}$

$$S_{\rm EH} = \frac{1}{2\kappa}\int {\rm d}^4x\sqrt{-g}\mathcal{R}, \qquad \kappa = 8\pi G$$

$$S_\phi = \int {\rm d}^4x\sqrt{-g}P(\phi, \partial^\mu\phi\partial_\mu\phi),$$

$$S_{\rm higher} = \frac{1}{\kappa}\int {\rm d}^4x\sqrt{-g}\left(\frac{1}{M^2}\mathcal{R}_{\mu\nu\rho\sigma}\mathcal{R}^{\mu\nu\rho\sigma} + \cdots\right).$$

ghosts

Construction of theories

Theories we want have the properties as follows:

- No ghost degrees of freedom

- Changing the dynamics of tensor perturbations while the scalar perturbations is left unchanged

Construction of theories

Construction with

the unit normal to constant ϕ hypersurfaces

$$u_\mu := -\frac{\partial_\mu \phi}{\sqrt{-\partial^\nu \phi \partial_\nu \phi}},$$

the induced metric

$$\gamma_{\mu\nu} = g_{\mu\nu} + u_\mu u_\nu,$$

for example: $\mathcal{R}_{\mu\nu\rho\sigma}\mathcal{R}_{\mu'\nu'\rho'\sigma'}\gamma^{\mu\mu'}\gamma^{\nu\nu'}\gamma^{\rho\rho'}u^\sigma u^{\sigma'}$

Construction of theories

ADM decomposition

taking constant ϕ hypersurfaces
as constant time hypersurfaces,

$$\mathrm{d}s^2 = -N^2 \mathrm{d}t^2 + \gamma_{ij}\left(\mathrm{d}x^i + N^i \mathrm{d}t\right)\left(\mathrm{d}x^j + N^j \mathrm{d}t\right).$$

quadratic curvature terms

$$\sqrt{\gamma}N \;\times\; \{K^4,\ K_{ij}K^{ij}K^2,\ \cdots,\ R^2,\ R_{ij}R^{ij},$$
$$K^2R,\ KK^{ij}R_{ij},\ \cdots,\ D_iK_{jk}D^iK^{jk},\ \cdots\}$$

Cosmological perturbations

$$N = 1 + \delta N, \quad N_i = \partial_i \chi + \chi_i, \quad \gamma_{ij} = a^2 e^{2\zeta} \left(e^h\right)_{ij},$$

About scalar perturbations

$$K_i^{\ j} = H\delta_i^{\ j} + \frac{1}{3}\delta K \delta_i^{\ j} + \delta \widetilde{K}_i^{\ j},$$

where

$$\begin{aligned} \delta K &= \ -3H\delta N + 3\dot{\zeta} - \frac{1}{a^2}\partial^2\chi, \\ \delta \widetilde{K}_i^{\ j} &= \ -\frac{1}{a^2}\left(\partial_i\partial^j - \frac{1}{3}\delta_i^{\ j}\partial^2\right)\chi, \end{aligned}$$

and

$$\delta R_i^{\ j} = -\frac{1}{a^2}\left(\partial_i\partial^j + \delta_i^{\ j}\partial^2\right)\zeta.$$

Combinations for which the scalar variables are canceled out

$$2\partial_i \delta\widetilde{K}_{jk}\partial^i\delta\widetilde{K}^{jk} - 3\partial_i\delta\widetilde{K}^{ik}\partial^j\delta\widetilde{K}_{jk},$$

and

$$\delta R_{ij}\delta R^{ij} - \frac{3}{8}\delta R^2,$$

Including vector and tensor perturbations

$$\begin{aligned} &2\partial_i \delta\widetilde{K}_{jk}\partial^i\delta\widetilde{K}^{jk} - 3\partial_i\delta\widetilde{K}^{ik}\partial^j\delta\widetilde{K}_{jk} \\ &\qquad\qquad = \frac{1}{2a^2}\left(\partial_i \dot{h}_{jk}\right)^2 + \frac{1}{4a^6}\left(\partial^2\chi_i\right)^2, \end{aligned}$$

$$\delta R_{ij}\delta R^{ij} - \frac{3}{8}\delta R^2 = \frac{1}{4a^4}\left(\partial^2 h_{ij}\right)^2.$$

Construction of Lagrangian

$$\mathcal{L}_1' = \frac{\sqrt{\gamma}N}{M^2}\left(2D_i\widetilde{K}_{jk}D^i\widetilde{K}^{jk} - 3D_i\widetilde{K}^{ik}D^j\widetilde{K}_{jk}\right),$$
$$\mathcal{L}_2 = \frac{\sqrt{\gamma}N}{M^2}\left(R_{ij}R^{ij} - \frac{3}{8}R^2\right),$$

As alternated for $\mathcal{L}_1'$

$$\mathcal{L}_1 = \frac{\sqrt{\gamma}N}{M^2}\left(2D_i\widetilde{K}_{jk}D^i\widetilde{K}^{jk} - D_i\widetilde{K}^{ik}D^j\widetilde{K}_{jk} - 2D_i\widetilde{K}_{jk}D^j\widetilde{K}^{ik}\right)$$

this can be written as

$$\mathcal{L}_1 = \frac{\sqrt{\gamma}N}{M^2}W_{ijk}W^{ijk}, \qquad W_{ijk} = 2D_{[i}\widetilde{K}_{j]k} + D_l\widetilde{K}^l{}_{[i}\gamma_{j]k}.$$
$$= \frac{\sqrt{-g}}{M^2}C_{\mu\nu\rho\sigma}C_{\mu'\nu'\rho'\sigma'}\gamma^{\mu\mu'}\gamma^{\nu\nu'}\gamma^{\rho\rho'}u^\sigma u^{\sigma'}$$

N. Deruelle, M. Sasaki, Y. Sendouda and A. Youssef, JHEP **09**, 009 (2012)

Tensor amplitudes in $\mathcal{L}_1$ and $\mathcal{L}_2$ model

$\mathcal{L}_1$ model

$$S = S_{\mathrm{EH}} + S_\phi + S_{\mathrm{higher}}$$

$$S_{\mathrm{higher}} = \frac{1}{\kappa}\int \mathrm{d}^4 x \mathcal{L}_1$$

$$\mathcal{L}_1 = \frac{\sqrt{\gamma}N}{M^2}\left(2D_i\widetilde{K}_{jk}D^i\widetilde{K}^{jk} - D_i\widetilde{K}^{ik}D^j\widetilde{K}_{jk} - 2D_i\widetilde{K}_{jk}D^j\widetilde{K}^{ik}\right)$$

for tensor perturbations

$$S = \frac{1}{8\kappa}\int \mathrm{d}t\mathrm{d}^3x\, a^3\left[\dot{h}_{ij}^2 - \frac{1}{a^2}(\partial_k h_{ij})^2 + \frac{4}{M^2a^2}(\partial_k\dot{h}_{ij})^2\right]$$

$\mathcal{L}_1$ model

$$f_k^\lambda(t) = \left(\frac{1}{4\kappa}\right)^{1/2} a^{3/2}\left(1 + \frac{4k^2}{M^2a^2}\right)^{1/2} h_k^\lambda$$

$$\ddot{f}_k + \omega_k^2(t)f_k = 0$$

$$\omega_k^2 := -\frac{1}{4}\left(H^2 + 2\dot{H}\right) + \frac{k^2/a^2 - 2H^2 - \dot{H}}{1 + 4k^2/M^2a^2} - \frac{4H^2k^2/M^2a^2}{(1 + 4k^2/M^2a^2)^2}$$

WKB solution for $k^2/a^2 \gg H^2, M^2$

$$f_k \simeq \frac{1}{\sqrt{2\omega_k}}\exp\left[-\mathrm{i}\int^t \omega_k(t')\mathrm{d}t'\right]$$

$\mathcal{L}_1$ model

$$\mathcal{P}_T(k) = \frac{k^2}{\pi^2}\left|h_k\right|^2$$

N. Deruelle et al. JHEP **09**, 009 (2012)

$$\mathcal{P}_T = \frac{2\kappa H^2}{\pi^2}\Xi_1(H/M),$$

where

$$\Xi_1(x) := \frac{\cosh(\pi\nu/2)\coth(\pi\nu/2)|\Gamma(-1/4 + \mathrm{i}\nu/4)|^4}{128\pi^2 x^3},$$

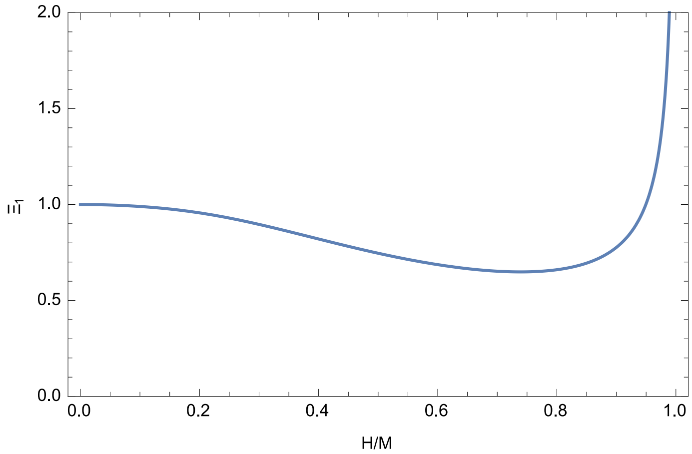

$$\nu := \sqrt{x^{-2} - 1}$$

$\mathcal{L}_1$ model

$$\mathcal{P}_T(k) = \frac{2\kappa H^2}{\pi^2}\Xi_1(H/M)\bigg|_{k=aH}$$

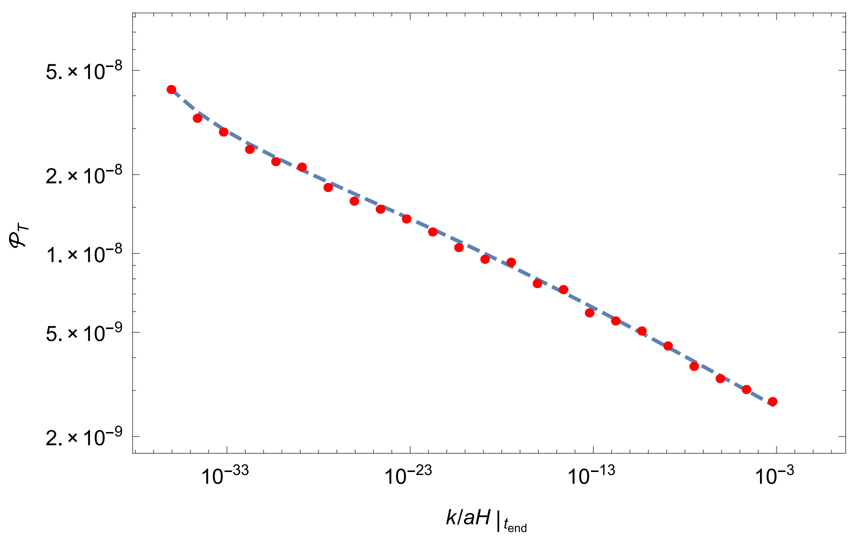

Blue dashed line: analytic
Red points: numerical

Tensor to scalar ratio $\quad r = 16\epsilon\Xi_1$

Tensor tilt $\quad n_T := \mathrm{d}\ln\mathcal{P}_T/\mathrm{d}\ln k$

$$n_T = -\frac{2\epsilon}{1-\epsilon}\left[1+\frac{1}{2}\frac{\mathrm{d}\ln\Xi_1}{\mathrm{d}\ln(H/M)}\right]\Bigg|_{k=aH} \quad < 0$$

Consistency relation

$$-8n_T/r \simeq \mathcal{D}|_{k=aH}$$

$$\mathcal{D} := \frac{1+(1/2)\mathrm{d}\ln\Xi_1/\mathrm{d}\ln x}{\Xi_1}\Bigg|_{x=H/M}$$

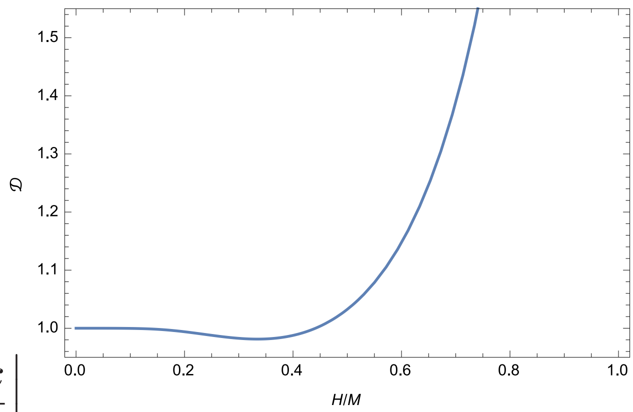

$\mathcal{L}_2$ model

$$S = S_{\mathrm{EH}} + S_\phi + S_{\mathrm{higher}}$$

$$S_{\mathrm{higher}} = -\frac{1}{2\kappa}\int \mathrm{d}^4x\mathcal{L}_2$$

$$\mathcal{L}_2 = \frac{\sqrt{\gamma}N}{M^2}\left(R_{ij}R^{ij} - \frac{3}{8}R^2\right),$$

for tensor perturbations

$$S = \frac{1}{8\kappa}\int \mathrm{d}t\mathrm{d}^3x\, a^3\left[\dot{h}_{ij}^2 - \frac{1}{a^2}(\partial_k h_{ij})^2 - \frac{1}{M^2a^4}(\partial^2 h_{ij})^2\right]$$

$\mathcal{L}_2$ model

$$v_k^\lambda := (4\kappa)^{-1/2} a h_k^\lambda$$

$$\frac{\mathrm{d}^2 v_k}{\mathrm{d}\eta^2} + \omega_k^2(\eta) v_k = 0$$

$$\omega_k^2 := k^2 + \frac{k^4}{M^2 a^2} - \frac{1}{a}\frac{\mathrm{d}^2 a}{\mathrm{d}\eta^2}$$

WKB solution

$$v_k \simeq \frac{1}{\sqrt{2\omega_k}} \exp\left[-\mathrm{i}\int^\eta \omega_k(\eta')\mathrm{d}\eta'\right]$$

solution at large k in de Sitter background

$$v_k = \frac{e^{-\pi/8x} W_{\mathrm{i}/4x,3/4}(-\mathrm{i}xk^2\eta^2)}{(-2xk^2\eta)^{1/2}}$$

$\mathcal{L}_2$ model

$$\mathcal{P}_T = \frac{2\kappa H^2}{\pi^2}\Xi_2(H/M)$$

$$\Xi_2(x) := \frac{\pi}{4}\left[e^{\pi/(4x)} x^{3/2} \left|\Gamma(5/4 + \mathrm{i}/(4x))\right|^2\right]^{-1}$$

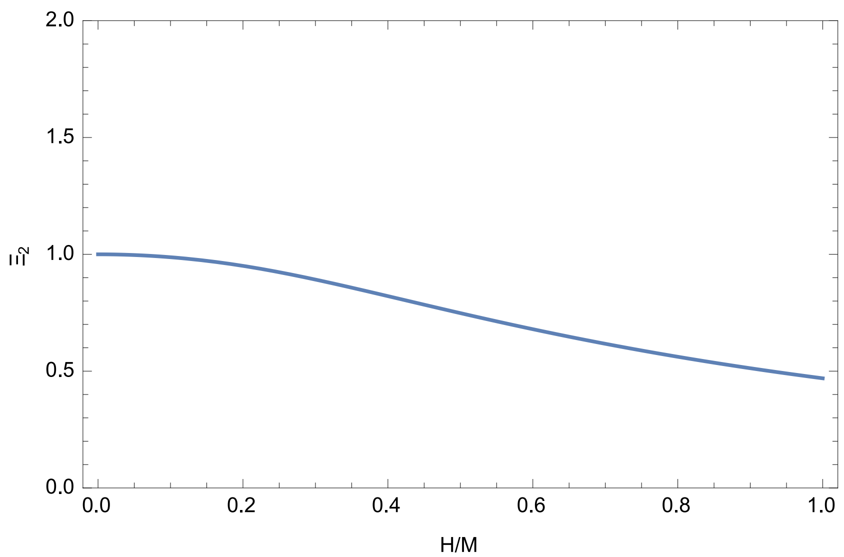

$\mathcal{L}_2$ model

$\mathcal{L}_2$ contains

$$\mathcal{L}_2 \sim \frac{1}{M^2}\zeta(\partial^2\zeta)^2$$

non-Gaussianity generated by this term

$$f_{NL} \sim \frac{H^2}{\epsilon M^2}$$

$f_{\rm NL} \lesssim 1$

$$\frac{H}{M} \lesssim \epsilon^{1/2} \ll 1$$

$\mathcal{L}_2$ model

$$\mathcal{P}_T = \frac{2\kappa H^2}{\pi^2}\Xi_2(H/M)$$

$$\Xi_2(x) := \frac{\pi}{4}\left[e^{\pi/(4x)}x^{3/2}\left|\Gamma(5/4+\mathrm{i}/(4x))\right|^2\right]^{-1}$$

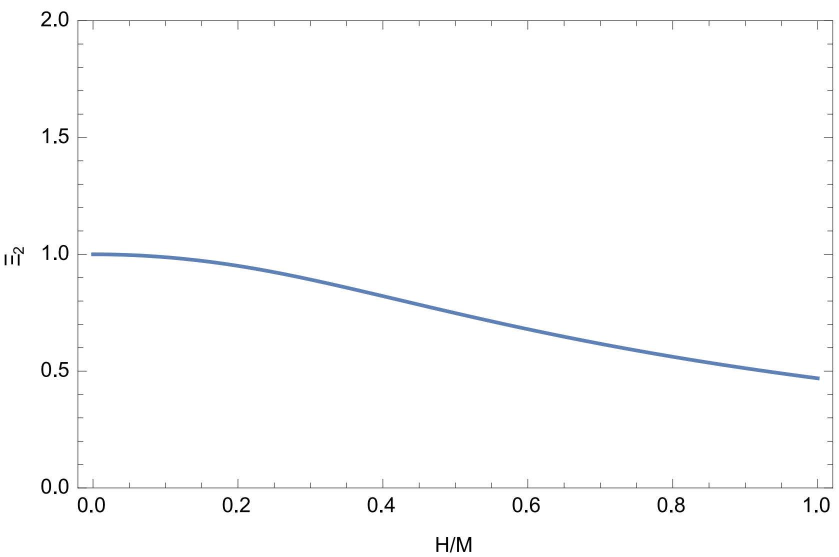

Results with Planck 2015

Suppression with $\mathcal{L}_1$ model

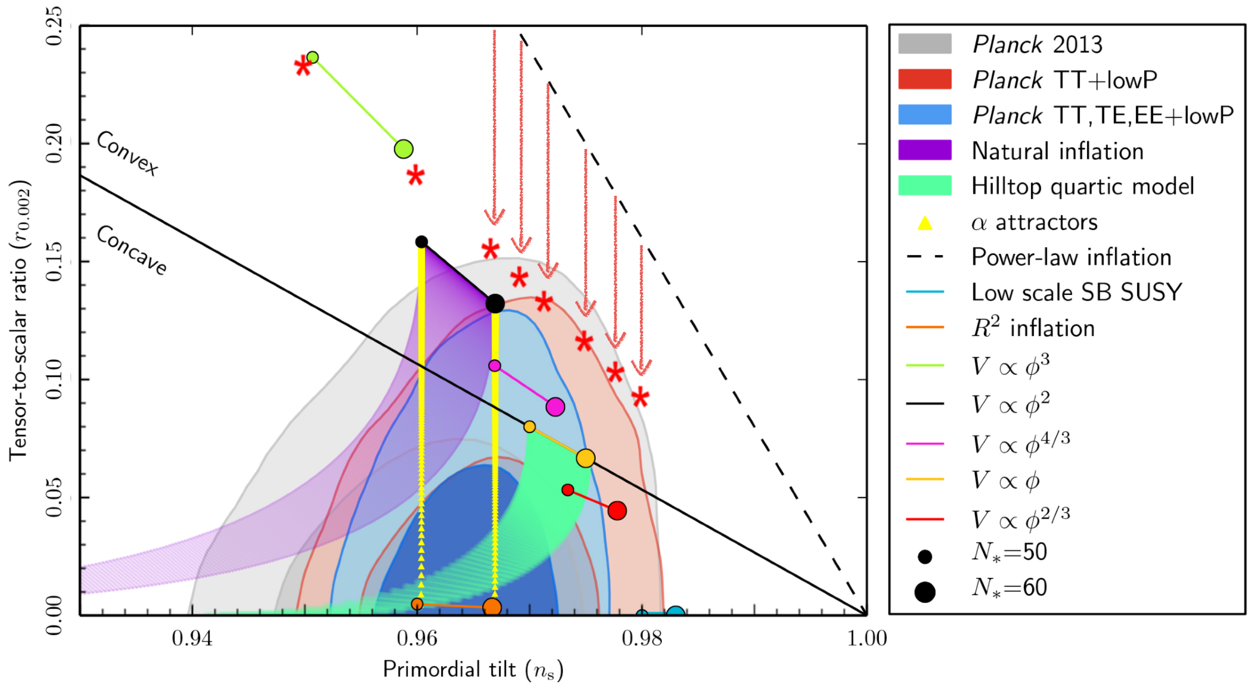

Summary

- We construct two possible theories which change only the dynamics of tensor perturbations without changing scalar sector.
- One of the theories, $\mathcal{L}_1$, can decrease the tensor amplitude up to 65%.
- We can put some inflation models which are out of the observational constraints into the 2σ contour with this suppression effect.

“Quasi-Normal Modes of Lovelock Black Hole”

by Daisuke Yoshida

[JGRG25(2015)4b6]

JGRG : 4b6 : Wednesday Morning Parallel Session B (at Masukawa Hall)

Quasi-Normal Modes of Lovelock Black Hole

Daisuke Yoshida
and
Jiro Soda

Kobe Univ.
Elementary Particle Physics and Cosmology Group

1

In this research,…

- We modified **the method of QNF-calculation with WKB-method in Lovelock Theory**.

- **This method enabled us to calculate QNF of Lovelock BH in arbitrary dimensions**, and we checked **the QNFs of this BH in 7 and 8 dimensions**.

2

Why did we choose Lovelock Black Hole?

- D-brane theory needs higher dimensions.
- Lovelock Theory (LT) is one of the most natural higher dimensional theories.
- LT has the BH solutions, so their stability is the significant problems.
- There is **the problem of QNF-calculation in Lovelock theory** with WKB-approximation.

Lovelock Theory

- LT has two important features.

1) **general coordinate covariance**
2) **no higher derivative terms in EoM**

In D-dims, its Lagrangian is given by

$$\mathcal{L}_{(q)} \equiv \delta^{\lambda_1\sigma_1\cdots\lambda_q\sigma_q}_{\rho_1\kappa_1\cdots\rho_q\kappa_q} R^{\rho_1\kappa_1}{}_{\lambda_1\sigma_1}\cdots R^{\rho_q\kappa_q}{}_{\lambda_q\sigma_q}$$

$$\mathcal{L}_D \equiv -2\Lambda + \sum_{q=1}^{\left[\frac{D-1}{2}\right]} \frac{a_q}{q\cdot 2^{q+1}}\mathcal{L}_{(q)}$$

a_q : coupling constant

$$= -2\Lambda + a_1 R + a_2 f_{\mathrm{GBE}}(R) + a_3 g(R) + \cdots$$

D=4→Einstein：GR

D=5,6→Gauss-Bonnet-Einstein Theory

(http://math.arizona.edu/~dsl/casie/lovelock.htm)

Master equation of Physical Fields

- physical fields

ex) Tensor field→**EoM of BH perturbation theory**
in Lovelock theory, T.Takahashi & J.Soda (2009), Phys.Rev.D.79.104025
Scalar field→**Klein-Gordon eq**

- physical fields **in the radial direction**

→ **master equation**

$$\frac{\mathrm{d}^2\Phi(x)}{\mathrm{d}x^2} = \left[\omega^2 - V_{\mathrm{eff}}(x)\right]\Phi(x)$$

$L \quad g_{\mu\nu} \quad m \quad \mathcal{M} \quad D$

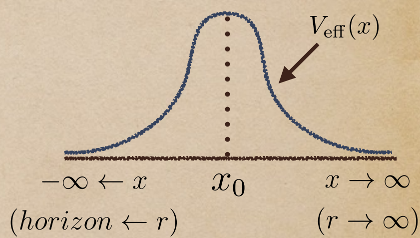

$$\frac{\mathrm{d}x}{\mathrm{d}r} = \frac{1}{f}$$

What is the Quasi-Normal Mode?

- QNM appear on the special boundary condition.

No wave comes from horizon.

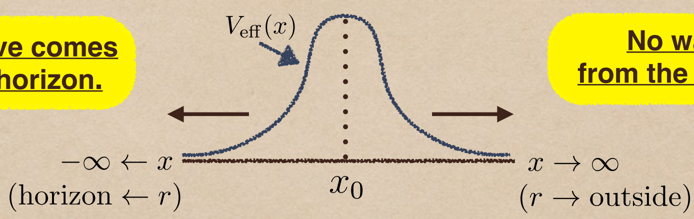

No wave comes from the outside of BH.

- These oscillations are **discrete complex numbers**.

→Quasi-Normal Frequency(**QNF**)

→So, these oscillations will damp.

ex) BH is stable. $\supset$ BH has QNMs.

- Of course, **QNM is characterized by physical conditions.**

How do we calculate the QNF?

T.Regge & J.A.Wheeler (1957), Phys.Rev.108.1063,
B.F.Schutz & C.M.Will (1985),Astrophys.J.291.L33-36
S.Iyer & C.M.Will (1987), Phys.Rev.D.35.3621)

- They defined the Nth-order WKB method.

$$V_{\rm eff}(x) \simeq V_0 + \underbrace{\sum_{q=2}^{2N} \frac{1}{q!} V_0^{(q)} (x-x_0)^q}_{\text{Taylor series}}$$

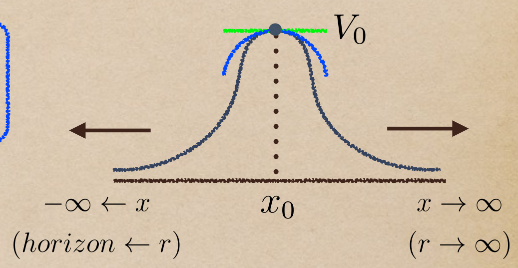

So, we got the formula of approximation,

$$\omega = \sqrt{V_0 + \sqrt{\frac{V_0^{(2)}}{2}} \left(n_{\rm tone} + \frac{1}{2} + \sum_{q=0}^{N-1} \Omega_q \right)}$$

tone number

collection term of approximation

So we need the analytical expression of the potential!!!

Difficulty of the static and spherical BH in Lovelock theory

- There is the static and spherical BH solution in LT.

$$ds^2 = \underbrace{-f(r)dt^2 + \frac{1}{f(r)}dr^2}_{\text{2-dim metric}} + \underbrace{r^2 \gamma_{ij} dx^i dx^j}_{n \equiv D-2\text{-dim metric}}$$

- Then, we got the EoM in Lovelock theory, $\psi(r) \equiv \dfrac{1-f}{r^2}$ $\qquad A_q \equiv \dfrac{a_q}{q} \prod_{p=1}^{2q-2} (n-p)$

$$\mathcal{P}(\psi) \equiv \sum_{q=2}^{\left[\frac{D-1}{2}\right]} A_q \psi^q + \psi - \frac{2\Lambda}{n(n+1)} = \frac{\mathcal{M}}{r^{n+1}}$$

$\mathcal{M}$ is the value related the ADM mass of BH.

A_q is coupling constant.

Ploblems :
1)In arbitrary dimensions, **we can't solve f for r.**
2)Using the formulas of solution is very complicated.

Solution!! : valuable transformation; $r \rightarrow \psi$

$$r = \sqrt[n+1]{\frac{\mathcal{M}}{\mathcal{P}(\psi)}}$$

With parameter ψ , f **is expressed analytically**.
→The analytical shape of potential is decided.

- To simplify this, we concentrate the case of

$A_q \geq 0 \ \ (q \geq 2)$ and $\Lambda = 0$ **: asymptotic flatness**

Under these condition, we got the transformation of parameter.

$$\begin{cases} r & : & r_{\text{horizon}} & \leftrightarrow & \infty \\ \psi & : & \psi_{\text{horizon}} & \leftrightarrow & 0 \end{cases}$$

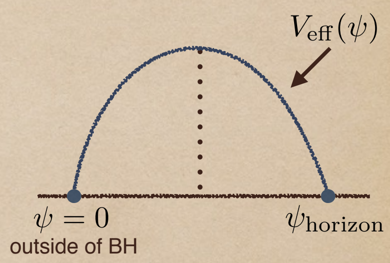

→We got **the analytical expression of potential** in finite region.

So, we can calculate the QNF.

Results

- We calculated **QNFs of the tensor field in 7 and 8 dimensions by 3rd-order WKB method.**

GBE theory : A_2 **from 0.00 to 1.50 by 0.05-digits,**

higher dimensional theory : A_3 **from 0.0 to 1.0 by 0.1-digits.**

- **Tone number was set to 0** (This condition is for the best approximation.).

QNF of tensor field by tensor perturbation D=7,M=50,L=2

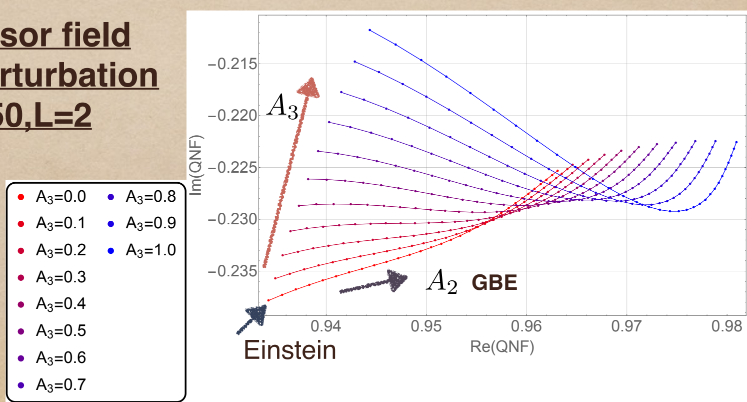

Results : QNF of Tensor Field in 7,8-dim by Tensor Perturbation

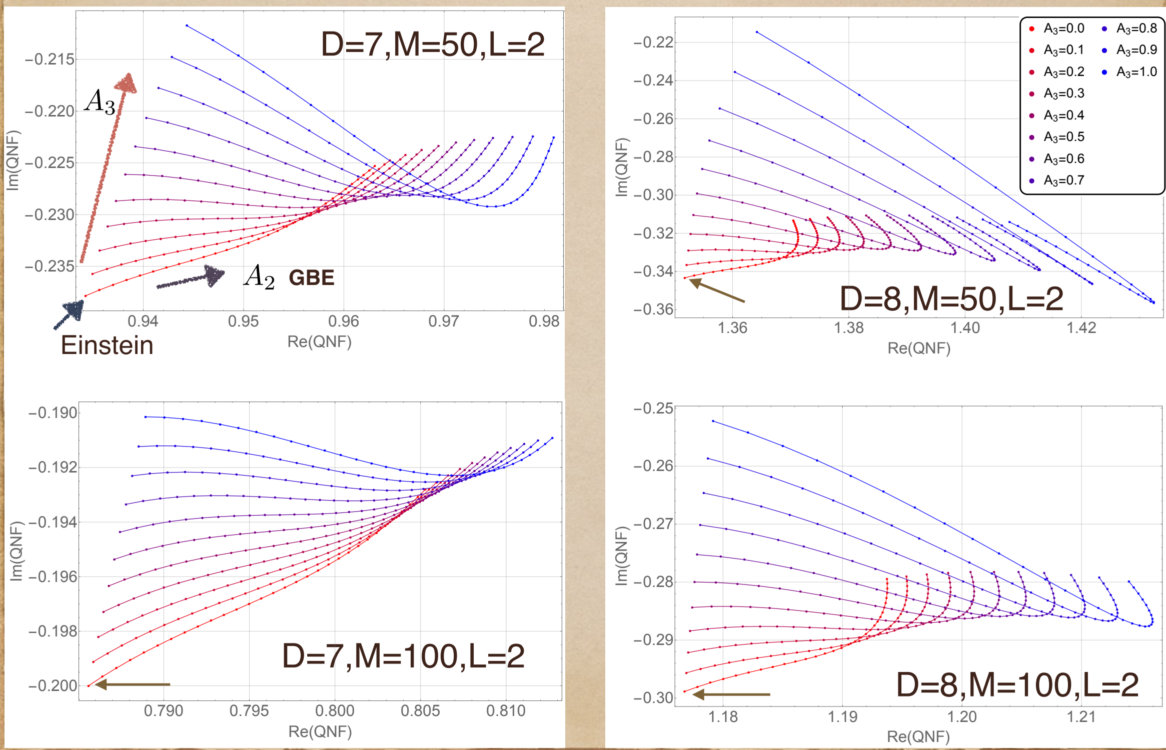

Summary

- We modified **the method of QNF-calculation with WKB-method in Lovelock Theory**.

- **This method enabled us to calculate QNF of Lovelock BH in arbitrary dimensions**, and we checked **the QNFs of this BH in 7 and 8 dimensions**.

Thank you for your attention!!!!!!!!!

“Holographic Reheating”

by Shinsuke Kawai

[JGRG25(2015)5a1]

Holographic Reheating

Shinsuke Kawai (Sungkyunkwan Univ.)
[arXiv:1509.04661] w/ Yu Nakayama

JGRG25 @ YITP, Kyoto
December 2015

Reheating of the Universe

Inflation
Reheating
Radiation dominant
Matter dominant
DE dominant

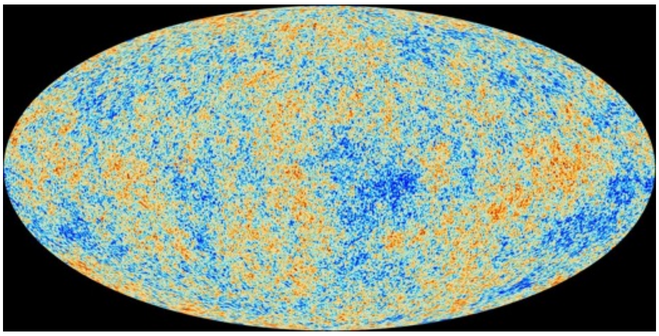

[Planck@ESA]

- Standard lore: out-of-equilibrium decay of inflaton
- Thermalisation of SM particles (hot Big Bang)

Reheating of the Universe

- Reheating temperature —> number of e-folds
  - Perturbative decay scenario $T_{\rm prh} \approx \left(\frac{90}{\pi^2 g_*}\right)^{\frac{1}{4}} (M_{\rm P}\Gamma)^{\frac{1}{2}}$.
  - Instant reheating scenario $T_{\rm irh} = \left(\frac{30\rho_*}{\pi^2 g_*}\right)^{\frac{1}{4}}$.
  - Evaporation of PBHs, Q-balls, nonmin coupling…

a few MeV < Trh < 10^9 GeV

BBN | QH ph. tr. | EW ph. tr. | gravitino prob.

Strongly coupled dynamics?

Parametric resonance

- Non-perturbative decay — explosive production of decay products, breakdown of the perturbative scenario ("preheating") [Dolgov Kirilova (1990)] [Traschen Brandenberger (1990)] [Kofman Linde Starobinsky (1994)] [Shtanov Traschen Brandenberger (1995)]

$\phi \to \chi \to$ SM particles

- Estimation of reheating temperature is generally difficult

AdS/CFT?

Holographic Thermalisation

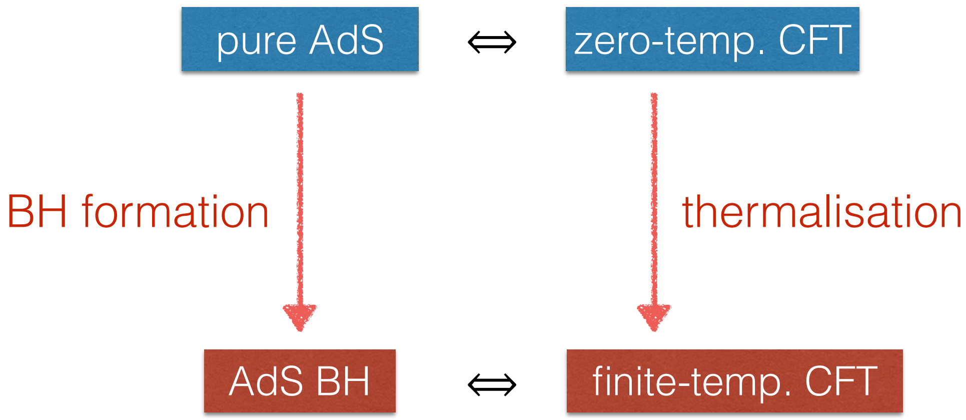

Holographic thermalisation:
thermalisation of CFT is dual to BH formation in AdS

[Witten (1998)] [Danielsson Keski-Vakkuri Kruczenski (1999)]

Holographic Reheating Scenario

Reheating of the Universe as holographic thermalisation?

assumptions:

1. The Universe = CFT on expanding S^3
2. Oscillating inflaton = external shock
3. Reheating temperature = Hawking temperature of 5d BH

1. The Universe = CFT on expanding S³

$$\mathcal{L} = \underbrace{-\frac{1}{2}(\partial\varphi)^2 - \frac{1}{2}m^2\varphi^2}_{\text{inflaton}} \underbrace{- \frac{1}{2}(\partial\chi)^2}_{\text{intermediate decay field}} \underbrace{- g^2\varphi^2\chi^2}_{\text{coupling}} + \cdots$$

$$S_{\rm bdry} = S_{\rm CFT} + \int d^4x \Phi_0(\tau)\mathcal{O}(\tau),$$

matter in the Universe (excluding inflaton)

oscillating inflaton (external shock)

Needs dynamical cutoff [Witten] [Gubser] [Savonije, Verlinde]

2. Oscillating inflaton = external shock

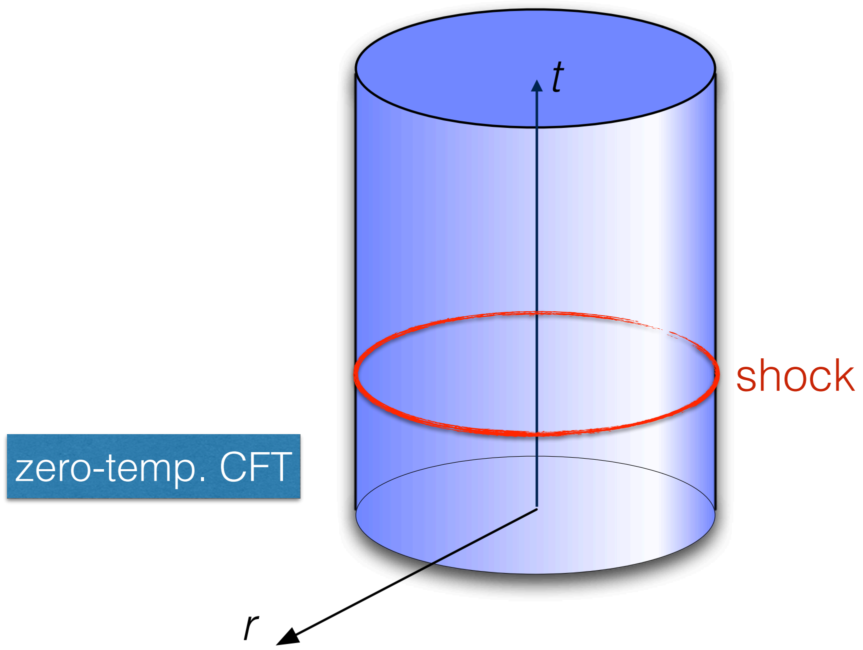

2. Oscillating inflaton = external shock

finite-temp. CFT

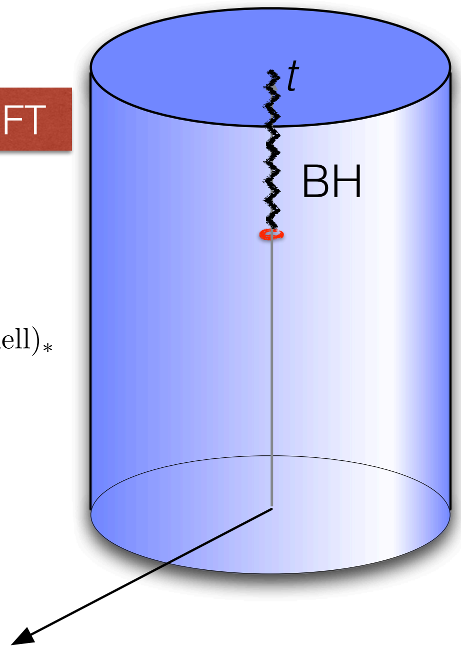

inflaton energy $\Longrightarrow$ BH mass

$$M_5 = \varepsilon \times (\text{area of shell})_* \times (\text{energy density of shell})_*$$

ε: efficiency of BH formation

3. Reheating temperature = Hawking temperature of 5d BH

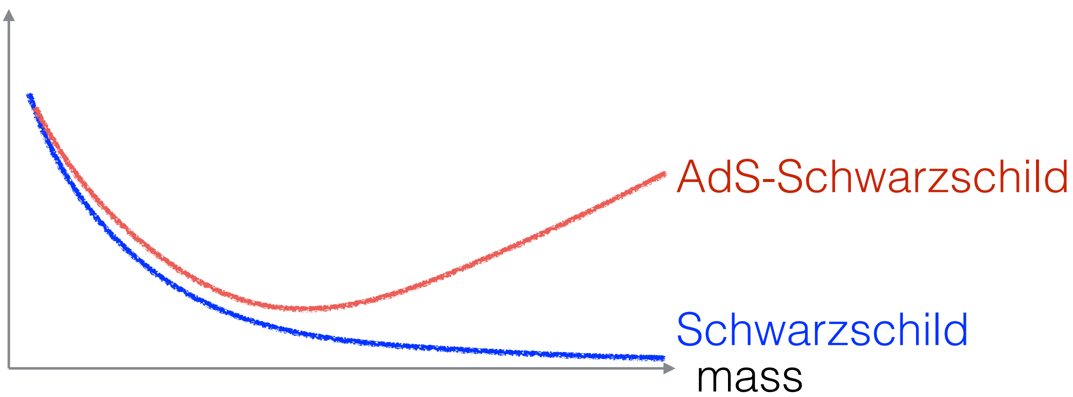

AdS-Schwarzschild: BH in a box

positive specific heat

Holographic Reheating Temperature

Holographic reheating temp.

$$T_{\rm hrh} = \left(\frac{\varepsilon\rho_*}{3M_{\rm P}^2 R_{\rm AdS}^2}\right)^{1/4} \frac{a_{\rm ini}}{\pi a_{\rm fin}} = \varepsilon^{1/4}\left(\frac{H_*}{R_{\rm AdS}}\right)^{1/2} \frac{a_{\rm ini}}{\pi a_{\rm fin}}.$$

cf.

perturbative reheating temp. $$T_{\rm prh} \approx \left(\frac{90}{\pi^2 g_*}\right)^{\frac{1}{4}} (M_{\rm P}\Gamma)^{\frac{1}{2}}.$$

instant reheating temp. $$T_{\rm irh} = \left(\frac{30\rho_*}{\pi^2 g_*}\right)^{\frac{1}{4}}.$$

Effective dof for the holographic model

$$g_*^{\rm eff} = \frac{90\pi^2 M_P^2 R_{\rm AdS}^2}{\varepsilon}\left(\frac{a_{\rm fin}}{a_{\rm ini}}\right)^4.$$

Example: chaotic inflation

$m^2\phi^2$ chaotic inflation with $m = 10^{13}$ GeV

$$\rho_* = 3M_{\rm P}^2 H_*^2 = \left[\frac{1}{2}(\partial_\tau\varphi)^2 + \frac{1}{2}m^2\varphi^2\right]_* \approx m^2\varphi_*^2,$$

yielding $\rho_* \approx 8\times 10^{-11} M_{\rm P}^4.$

Instant reheating with $g_*^{\rm SM} \sim 100$ gives $T_{\rm irh} \sim 3\times 10^{15}$ GeV

Recall $$g_*^{\rm eff} = \frac{90\pi^2 M_P^2 R_{\rm AdS}^2}{\varepsilon}\left(\frac{a_{\rm fin}}{a_{\rm ini}}\right)^4.$$

The holographic model gives lower reheating temperature than instant reheating

$$T_{\rm hrh} \lesssim 200\ {\rm MeV} \Rightarrow g_*^{\rm eff} \lesssim 5\times 10^{66}.$$

Example: holographic QCD reheating

Sakai-Sugimoto: three is large N

$g_*^{\rm eff} \sim 100 \sim g_*^{\rm SM}$

If the reheating temperature is in the QCD scale (~ 200 MeV), inflationary scale is ρ¼ ~ GeV-TeV

in this case, $R_{\rm AdS} \sim \ell_{\rm P}$

Summary

- Reheating as holographic thermalisation
- Reheating temperature evaluated as Hawking temperature of developed 5d BH
- Nonperturbative + strongly coupled dynamics

Open questions

— Turbulent instabilities [Bizon, Rostworowski] play any role?

— String/brane construction?

— Baryogenesis?

— Inhomogeneities?

Thank you for your attention.

"Unstable Mechanism of Low T/W Dynamical Instability"

by Motoyuki Saijo

[JGRG25(2015)5a2]

Unstable Mechanism of Low T/W Dynamical Instability

Motoyuki Saijo (Waseda U.)
Shin'ichirou Yoshida (U. Tokyo)

CONTENTS

1. Introduction

Low T/W dynamical instability

Common dynamical bar Features

- Bar structure appears throughout time evolution
- Generates quasi-periodic gravitational waves
- Considered as an outcome of binary neutron star merger or supernova explosion

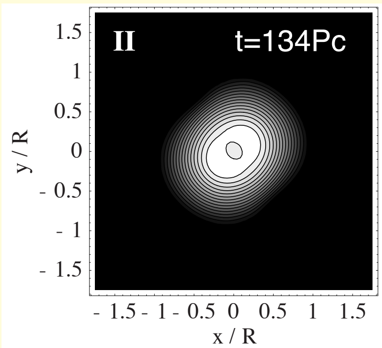

T/W=0.119, n=1, $\Omega_c/\Omega_{eq} = 26.0$

Significant Difference

- Instability occurs significantly lower T/W from the standard dynamical and secular (bar) instability
- Weak bar formation
- May occur in the realistic parameter range of binary neutron star merger or supernova explosion

Require "high" degree of differential rotation to trigger instability

Mechanism still not known

Corotation Resonance

(e.g. Kato 89; Shu 92)

Flow and the turbulence of the fluid has a resonance interaction at the corotation radius → Turbulence excites and absorbs by the resonance interaction

$$\boxed{\Omega = \omega/m}$$

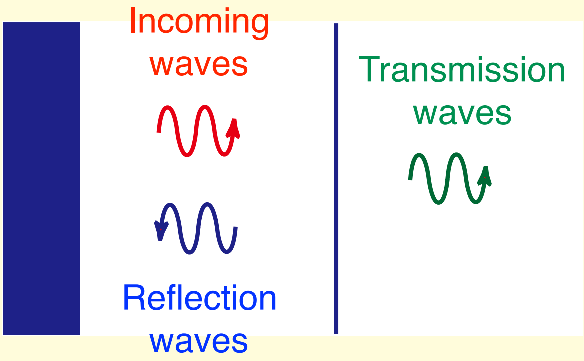

Reflection Wall

Corotation Plane

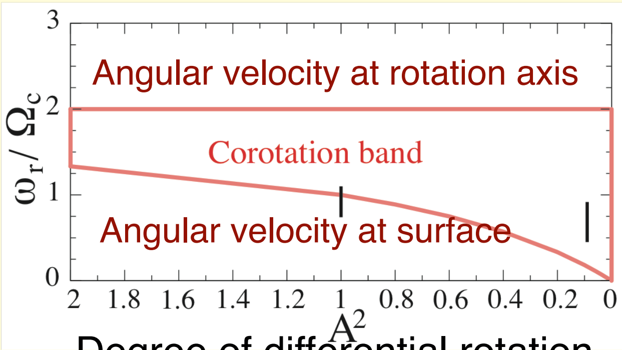

Degree of differential rotation

Cylindrical star, accretion disk system including coronation singularity

Cylindrical, differential rotating star

(Balbinski 85)

- Instability regime of T/W is significantly lower than the standard case
- Regarded as f^+, f^- mode

Dynamical stability of differentially rotating disks

(Papaloizou & Pringle 87)

- Investigate infinite cylindrical torus with differential rotation
- Analyses unstable features using WKB approximation (focus on high azimuthal wave numbers)

Super-reflection in fluid disks

(Tsang & Lai 08)

- Detailed analysis of Keplarian disk with differential rotation
- Incoming waves from infinity
- Matching the solutions using WKB approximation
- Corotation amplification/absorption can occur in their condition

Purpose

- Understand the mechanism of low T/W dynamical instability
- Understand the role of corotation radius
- Find the complex eigenfrequency of the system (Normal modes in differentially rotating stars)

2. Linear Perturbation in Differentially Rotating Stars

Non-axisymmetric Perturbations in Rapidly Rotating Stars

δh : perturbed enthalpy

$\delta\Phi$: perturbed gravitational potential

(e.g. Ipser & Lindblom 90)

$$\delta U \equiv \delta h + \delta\Phi$$

$$\delta q = \delta q(\varpi, z) e^{-i(\omega t - m\varphi)}$$

Continuity Eq + Euler Eq

$$\left[\partial_\varpi^2 - \left(\partial_\varpi \ln \frac{D}{\rho\varpi}\right)\partial_\varpi - \frac{2m\Omega}{\varpi\tilde{\omega}}\left(\partial_\varpi \ln \frac{\rho\Omega}{D}\right) - \frac{m^2}{\varpi^2} - \frac{D}{dp/d\rho} - \frac{D}{\tilde{\omega}^2}\left(\partial_z^2 + \frac{\partial_z\rho}{\rho}\partial_z\right)\right]\delta U = -\frac{D}{dp/d\rho}\delta\Phi$$

Poisson Eq

$$\left[\partial_\varpi^2 + \frac{1}{\varpi}\partial_\varpi - \frac{m^2}{\varpi^2} + \partial_z^2 + 4\pi\rho\frac{d\rho}{dp}\right]\delta\Phi = 4\pi\rho\frac{d\rho}{dp}\delta U$$

Further Approximation

Only equatorial motion is taken into account in the star

⬅ Characteristic wave propagation due to rotation should lie in the equatorial plane

Basic Equations

$$\left[\partial_\varpi^2 - \left(\partial_\varpi \ln \frac{D}{\rho\varpi}\right)\partial_\varpi - \frac{2m\Omega}{\varpi\tilde{\omega}}\left(\partial_\varpi \ln \frac{\rho\Omega}{D}\right) - \frac{m^2}{\varpi^2} - \frac{D}{dp/d\rho}\right]\delta U = -\frac{D}{dp/d\rho}\delta\Phi$$

$$\left[\partial_\varpi^2 + \frac{1}{\varpi}\partial_\varpi - \frac{m^2}{\varpi^2} + 4\pi\rho\frac{d\rho}{dp}\right]\delta\Phi = 4\pi\rho\frac{d\rho}{dp}\delta U$$

- Two 2nd order differential equations with source term
- Background object is taken as low T/W unstable star
- Singularity at corotation radius

$$\tilde{\omega} \equiv \omega - m\Omega = 0$$

- Removable singularity at Lindbald radius

$$D \equiv \kappa^2 - \tilde{\omega}^2 = 0$$

- Set frequency from the outcome of numerical simulations

Wave Propagation

(e.g. Tsang & Lai 08)

Translate the perturbed potential to formulate the wave-type basic equation

$$\left[\frac{d^2}{d\varpi^2} - V_{\rm eff}(\varpi)\right]\delta\eta(\varpi) = -\frac{D}{dp/d\rho}S^{-1/2}\delta\Phi(\varpi)$$

Regions and Bridging Technique

Effective Potential V_{eff}

- Classify into two regimes
- Directly solve two fundamental perturbative variables

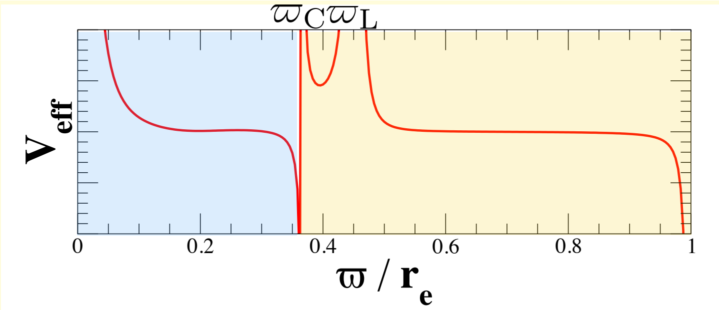

Region I

$$\delta U = C_1 \varpi^m$$
$$\delta\Phi = C_2 \varpi^m$$

- Regularity condition at origin
- Solve integral equation numerically
- Bridging the solution around corotation radius

$$\left[\frac{d^2}{d\varpi^2} - \frac{2m\Omega}{\varpi\tilde{\omega}}\left(\frac{d}{d\varpi}\ln\frac{\rho\Omega}{D}\right)\right]\delta U = 0$$

Solution

$$\delta U = A_1\varpi + A_2\left[1 + |\beta|\varpi(-1 + 2\gamma + \ln|\beta| + \ln\varpi)\right]$$

Bridging technique

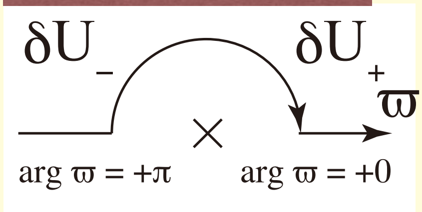

- Complex frequency
- Take the limit of imaginary part as +0

Region II

- Bridging solutions from Region I
- Solve integral equation numerically
- Extract "plane waves" around the surface

$$\delta\eta = Ie^{-ik\varpi} + Re^{ik\varpi}$$
$$k^2 \equiv -V_{\mathrm{eff}}(\varpi)$$

3. Scattering Problem in Differentially Rotating Stars

Setup

- Insert "incoming wave" from the surface
- Investigate the amplification rate of the "reflection wave"

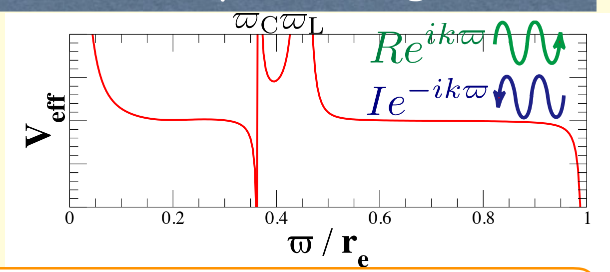

Results

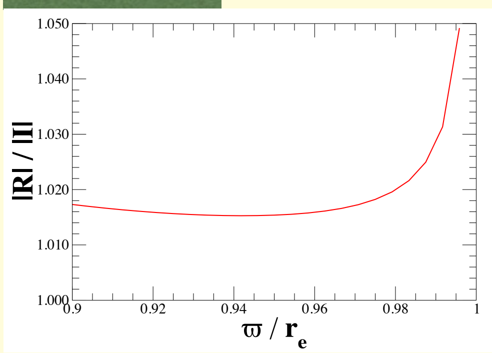

Exponential growth	$\delta\rho = \delta\rho_0 \exp\left[\frac{t}{\tau}\right]$
Amplification rate	$\frac{\lvert R\rvert}{\lvert I\rvert}$
Growth Timescale	$\tau = \frac{T}{\ln\lvert R\rvert - \ln\lvert I\rvert}$

- Amplification of the "reflection wave"

➡ Unstable system

- Growth rate of the amplification is dynamical

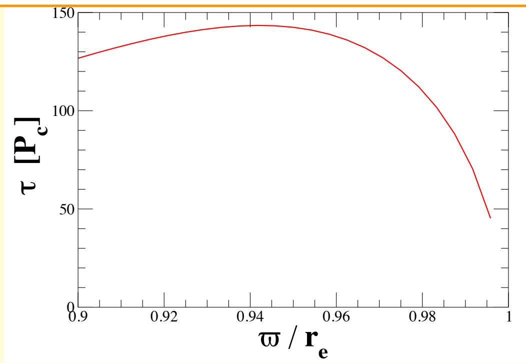

4. Unstable Normal Modes in Differentially Rotating Stars

Complex frequency removes the singularity! $\tilde{\omega} \equiv \omega - m\Omega \neq 0$

Boundary condition

- Regularity at origin
- Enthalpy vanishes at the perturbed surface of the star $\delta h + \xi^j \nabla_j h = 0$

Complex eigenfrequency

Cylindrical model

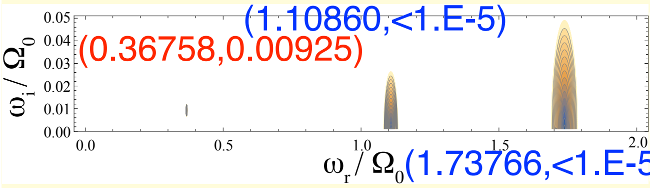

Spherical model

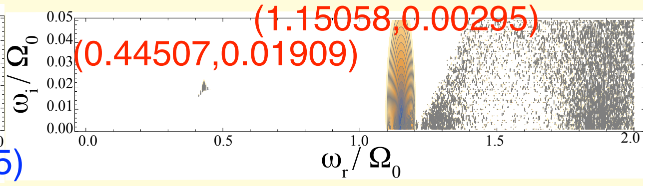

(1.87122,0.00852)

Growth Timescale is Dynamical !

$$\tau \equiv \frac{1}{\Im \omega} = 50 \sim 100[P_c]$$

Deformed configuration may accelerate the growth timescale

5. Comparison with Numerical Simulation

Diagnostics

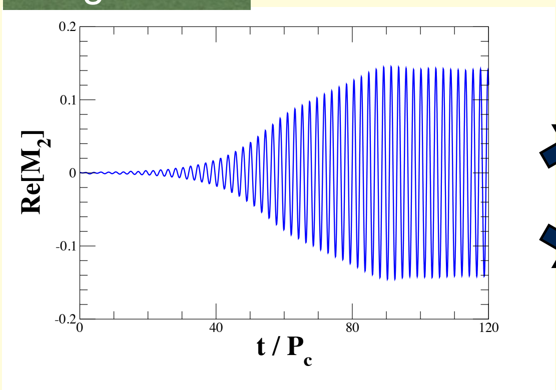

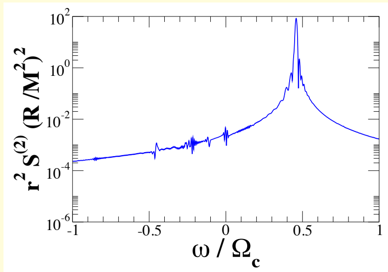

Resonant frequency

$\omega/\Omega_c = 0.459$

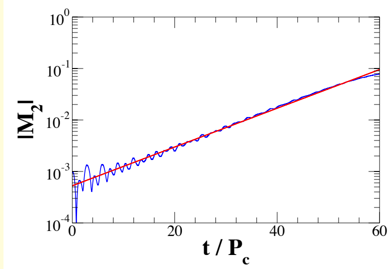

Growth timescale

$\tau/P_c = 11.5$

Compare between numerical simulation and spherical model

- Resonant frequency has a good agreement
- Growth timescale has some gap

(0.44507,0.01909)

Deformed configuration may accelerate the growth timescale

6. Summary

We have investigated the unstable mechanism of low T/W dynamical instability in differential rotating stars by means of linear perturbation in the equatorial plane

- The mechanism can be understood as amplification of the reflection waves due to the existence of corotation singularity
- Unstable normal mode is found in low T/W dynamically unstable star
- Fairly good agreement with the results from numerical simulation

“Oscillation spectra of neutron stars with highy tangled magnetic fields”

by Hajime Sotani

[JGRG25(2015)5a3]

Oscillation spectra of neutron stars with highly tangled magnetic fields

Hajime SOTANI (NAOJ)

contents

1. introduction
2. understanding of the magnetic oscillations of neutron stars with dipole (quadrupole) magnetic fields
3. magnetic oscillations with highly tangled magnetic fields
4. conclusion

neutron stars

- Structure of NS
  - solid layer (crust)
  - fluid core (uniform matter)

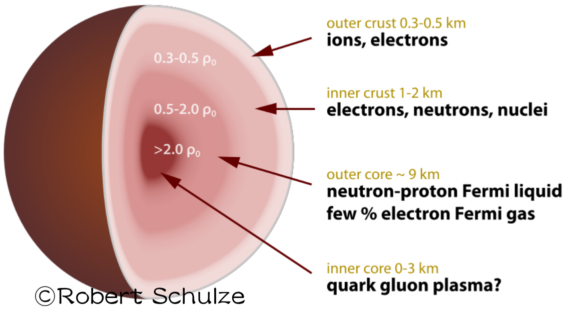

- Determination of EOS for high density (core) region could be quite difficult on the Earth
- Magnetic configuration and strength inside the star are also unknown
- To extract the stellar properties via observations of neutron stars
  - stellar mass and radius
  - stellar oscillations (& emitted GWs)

  "(GW) asteroseismology"

  This is a motivation why we consider the neutron star oscillations

Dec. 9. 2015 JGRG25@YITP 2

QPOs in giant flares

- Afterglow of giant flares → *quasi periodic oscillations (QPOs)*
  Barat et.al. (1983); Israel et.al. (2005); Strohmayer & Watts (2005, 2006)
  - SGR 0526-66 : 23ms (43Hz), B ~ 4 × 10^{14}G
  - SGR 1900+14 : B > 4 × 10^{14}G, **28, 54, 84, 155 Hz**
  - SGR 1806-20 : B ~ 8 × 10^{14}G, L ~ 10^{46} ergs/s
    18, 26, 30, 92.5, 150, 626.5, 1837 Hz + something ?
- Theoretical attempts to explain...
  - torsional oscillations in neutron star crust
  - magnetic oscillations (Alfven oscillations)
  c.f.) fundamental modes of NS is order of kHz

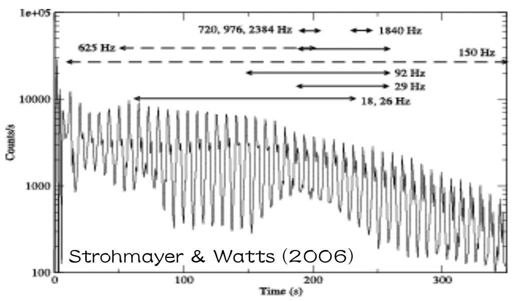

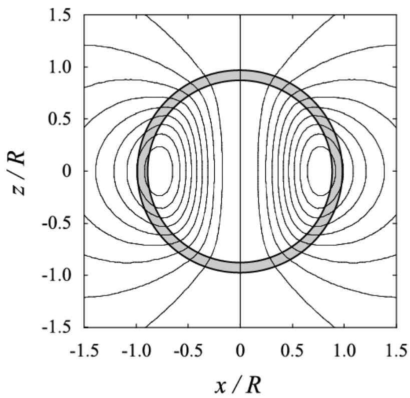

Dec. 9. 2015 JGRG25@YITP 3

axial Alfven oscillations

(HS+2008)

two families in Alfven oscillations

- continuum spectrum
- upper & lower QPOs
- $f_{Ln} \cong (n+1)\, f_{L0}$, $f_{Un} \cong (n+1)\, f_{U0}$
- $f_{Ln} / f_{Un} \cong 0.6$ independently of the stellar model
- f_{Ln} & $f_{Un} \propto$ the magnetic field strength

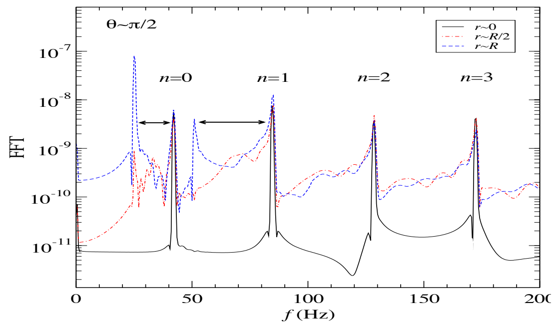

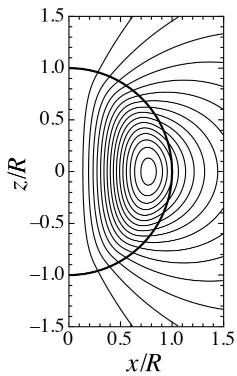

effective amplitude

(Cerda-Dulan+2010)

- Upper (lower) QPOs are associated with the open (closed) field liens

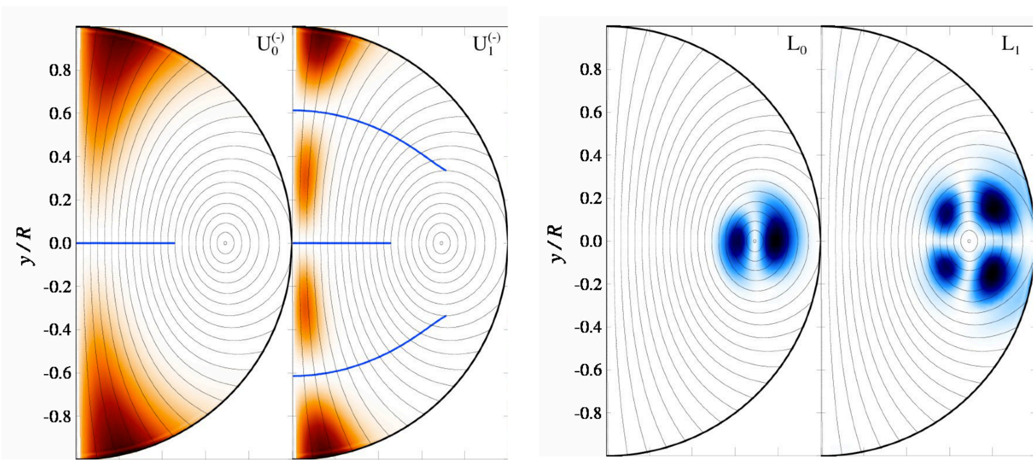

different type of magnetic distribution

(Gabler+2012)

Taking into account the quadruple component as well as dipole component, the Alfven oscillations are examined…

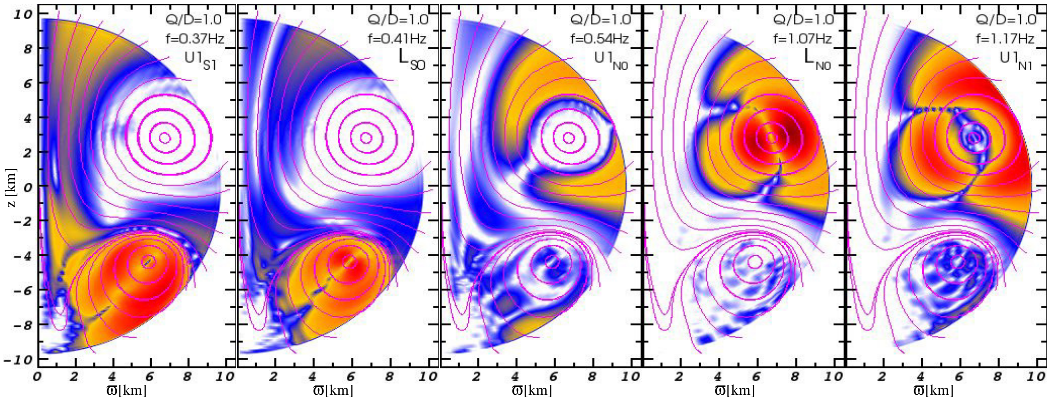

Magnetic oscillations strongly depend on the magnetic configuration !

effect of crust elasticity

(Colaiuda+2011, Gabler+2011, 2012)

- Strong magnetic field
  - no crust torsional oscillations
- Weak magnetic field
  - Alfven oscillations are confined in core region
  - surface oscillations become crust torsional oscillations

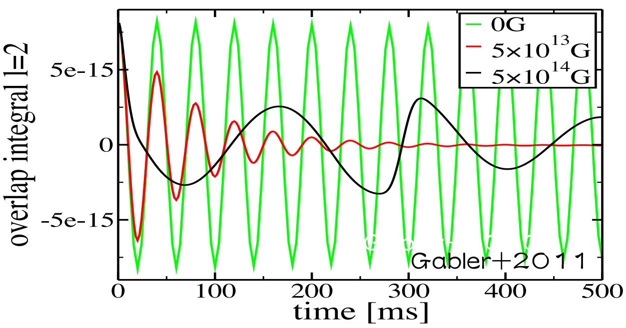

current understanding of axial Alfven oscillations

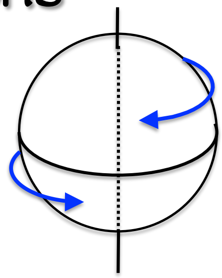

- Continuum spectrum
  - upper & lower QPOs
- Stronger magnetic field than ~10^{15} G
  - only Alfven oscillations can be excited
- Weaker magnetic field than ~10^{15} G
  - crust torsional oscillations can be excited near surface
  - Alfven oscillations are confined in the core region

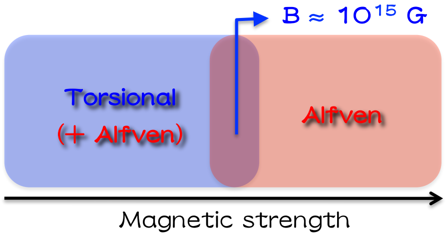

why continuum spectra

- frequency ~ (typical timescale)$^{-1}$
  ~ (Alfven velocity) / (length of field line)
  - global magnetic structure (dipole fields)
    → length of field line is changing continuously
  - frequency also becomes continuum

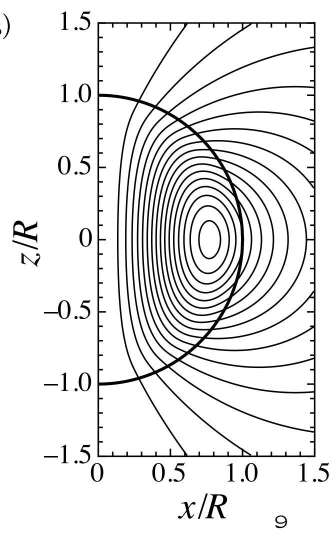

- how about the highly tangled fields?
  - proto neutron stars
  - NSs just after binary merger

tangled magnetic field

- B-field is decomposed as $B = B^{(G)} + B^{(T)}$
- assuming that $B^{(G)} \ll B^{(T)}$ and $\lambda \ll \lambda_A$
  - typical length scale of $B^{(T)}$: λ
  - wave length of Alfven oscillations : λ_A
- correlation between $B^{(T)}_i$ and $B^{(T)}_j$ is negligible
- magnetic oscillations are determined with the local magnetic strength
  - assuming the B-field with phenomenological strength distribution

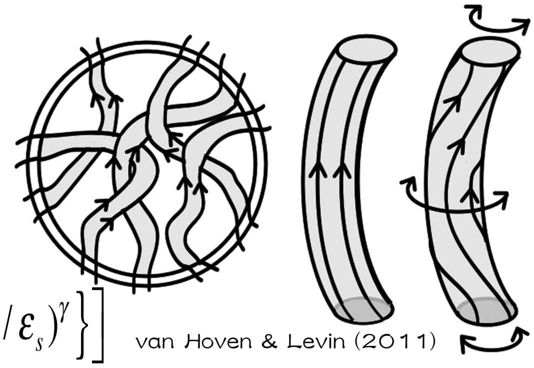

van Hoven & Levin (2011)

$$H(\varepsilon/\varepsilon_s) = H_{surf} + H_0\left[1 - \exp\left\{-\beta(\varepsilon/\varepsilon_s)^{\gamma}\right\}\right]$$

background stellar models

- EOS: proposed by Douchin & Haensel with SLy
- we adopt two parameter sets for field strength distribution
  - (β, γ) = (0.02, 3), (0.05, 2)

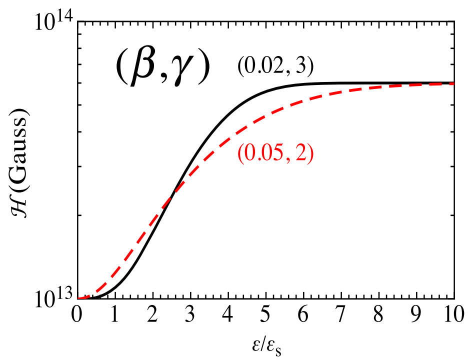

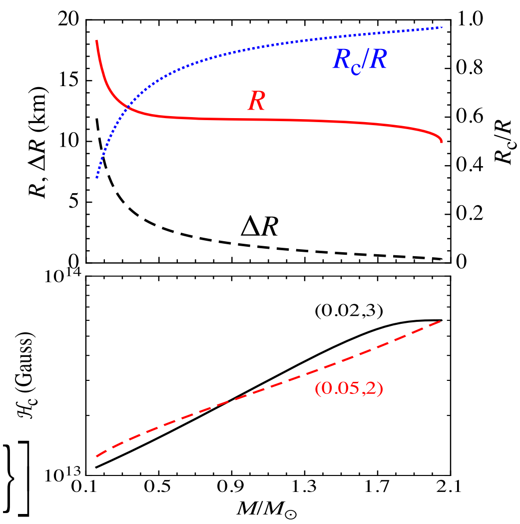

$$H(\varepsilon/\varepsilon_s) = H_{surf} + H_0\left[1 - \exp\left\{-\beta(\varepsilon/\varepsilon_s)^{\gamma}\right\}\right]$$

dependence of frequencies on field strength

- frequency of magnetic oscillations without crust elasticity
  - frequency is proportional to H_{surf}

$$ {}_\ell a_n = {}_\ell c_n \times \frac{\mathcal{H}_{surf}}{10^{13}\ \mathrm{Gauss}} $$

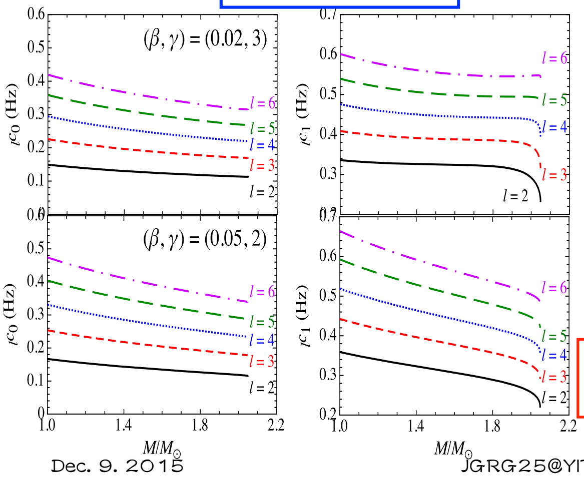

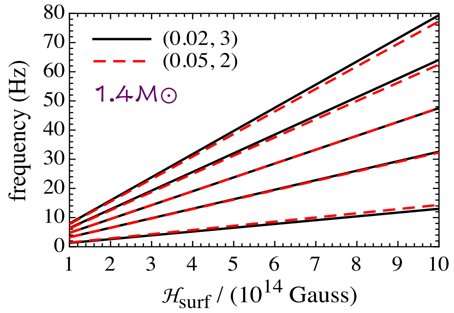

Different mass dependence of frequencies of magnetic oscillations.

oscillation spectra with crust elasticity

- discrete spectra
- even for weak magnetic field, frequencies are different from the crustal torsional oscillations

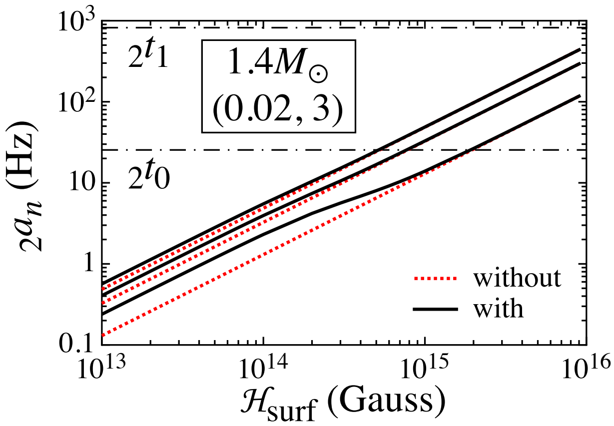

dependence on stellar mass

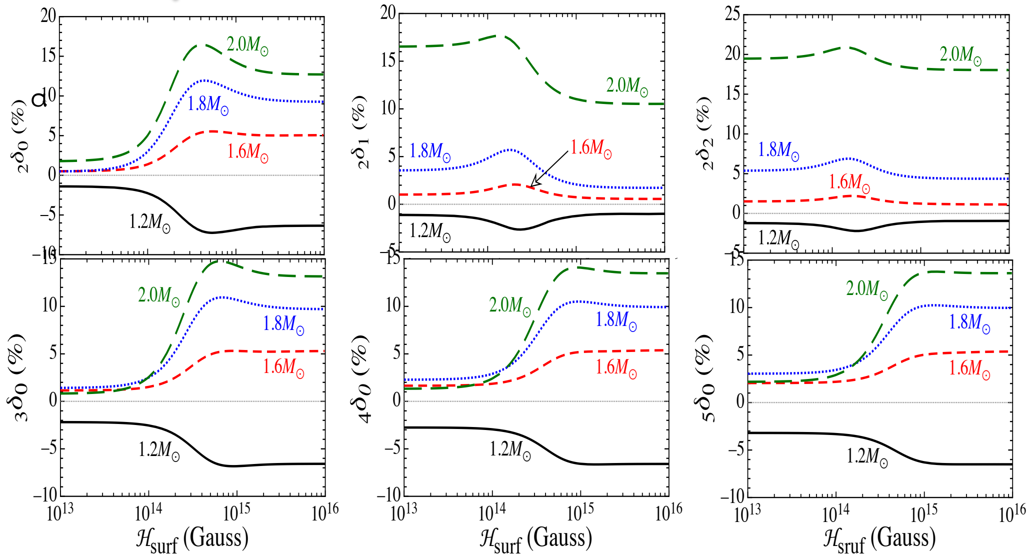

$$\boxed{{}_\ell\delta_n = \frac{{}_\ell a_n^{14} - {}_\ell a_n^{M}}{{}_\ell a_n^{14}}}$$

conclusion

- we consider the neutron star oscillations with highly tangled magnetic fields
- we find the oscillation spectra become discrete, unlike the Alfven continuum
- even for the weak magnetic field, the frequencies are completely different from the crustal torsional oscillations
- we should also
  - consider the effect of $B^{(G)}$
  - examine the dependence on EOS and the strength distribution of magnetic field
  - examine the polar oscillations, strongly associated with GWs

“Deformation of thin-shell gravastars”

by Nami Uchikata

[JGRG25(2015)5a4]

Deformation of thin-shell gravastars

Nami Uchikata (Rikkyo University, Japan)

Paolo Pani (Sapienza University of Rome, Italy & Instituto Superior Tecnico, Portugal)

Shijun Yoshida (Tohoku University, Japan)

Gravastars

- Mazur & Mottola (2004)

Gravitational Vacuum Stars

Compact object model alternative to black holes without the event horizon.

During the gravitational collapse, a quantum phase transition occurs before the event horizon is formed.

(e.g. Gliner 1966, Markov 1982)

cosmological constant (de Sitter) + thin shell

- Mazur & Mottola (2004)

Spherically symmetric, as compact as black holes.

$$ds^2 = -f(r)dt^2 + \frac{dr^2}{f(r)} + r^2\left(d\theta^2 + \sin\theta^2 d\phi^2\right)$$

$$f(r) = \begin{cases} 1 - \frac{r^2}{L^2}\left(= f^-(r)\right) & (r < R) \\ 1 - \frac{2M}{r}\left(= f^+(r)\right) & (r > R) \end{cases}$$

R : radius of the shell, L : de Sitter horizon radius

To prevent the formation of the event horizon,

$$2M < R < L$$

Deformation of gravastars

- Rotational deformation → quadrupole moment, Q
- Tidal deformation → tidal Love number, λ

  Ratio of the induced quadrupole moment to the perturbing tidal field.

- Moment of inertia, I

➡ I-Love-Q relations for gravastars

The universality of I-Love-Q relations

Yagi & Yunes (2013)
I-Love-Q relations do not depend sensitively on neutron star's inner structure, or the equation of state.

Our purpose

- To investigate the behaviour of I-Love-Q relations in the black hole limit.
- We use a thin-shell gravastar model, since it is more compact than neutron stars. (Pani 2015)
- Also, we know the solutions of slowly rotating thin-shell gravastars. (Uchikata & Yoshida 2015)

- Rotational deformation (quadrupole moment, Q)
  isolated and slowly rotating stars

- Tidal deformation (tidal Love number, λ)
  a static star in a static tidal field

Quadrupole deformation
The similar derivation is used.

$$\Delta\phi = 0 \quad \Rightarrow \quad \phi = \sum_l \left(A_l r^l + \frac{B_l}{r^{l+1}} \right) P_l(\cos\theta)$$

Newtonian potential

Legendre polynomial

quadrupole deformation → l=2

Perturbation

- Rotational quadrupole moment
  → Slow rotation approximation
  (rotational effect is perturbative)

- Tidal Love number
  (tidal effect is perturbative)

- Metric (Hartle 1967, Hartle & Thorne 1968)

$$ds^2 = \boxed{-f(r)(1+2\epsilon^2 h(r,\theta))dt^2} + \frac{1}{f(r)}\left(1+\frac{2\epsilon^2 m(r,\theta)}{rf(r)}\right)dr^2 + r^2(1+2\epsilon^2 k(r,\theta))(d\theta^2+\sin^2\theta(d\phi-\epsilon\omega(r)dt)^2).$$

$$\boxed{g_{tt}\approx -(1+2\phi)}$$

$$h(r,\theta) = h_0(r) + \boxed{h_2(r)}P_2(\cos\theta),$$
$$m(r,\theta) = m_0(r) + m_2(r)P_2(\cos\theta),$$
$$k(r,\theta) = k_2(r)P_2(\cos\theta).$$

$$f(r) = \begin{cases} 1-\dfrac{r^2}{L^2}(=f^-(r)) & (r<R) \\ 1-\dfrac{2M}{r}(=f^+(r)) & (r>R) \end{cases}$$

(+:outside the shell, -:inside the shell)

- inside the shell (Einstein eq. with $\Lambda>0$)

$$h_2^- = \frac{C_3}{8r^2}\left(\frac{-3L^2+5r^2}{L^2 f^-(r)} + \frac{3Lf^-(r)\mathrm{Arctanh}(r/L)}{r}\right), \qquad L=\sqrt{3/\Lambda}$$

integration constant

- outside the shell (vacuum Einstein eq.)

slowly rotating case (regular at infinity)

$$h_2^+ = J^2\left(\frac{1}{Mr^3}+\frac{1}{r^4}\right) + BQ_2^2\left(\frac{r}{M}-1\right), \quad \Rightarrow \quad \boxed{Q=\frac{J^2}{M}+\frac{8}{5}BM^3}$$

angular momentum   constant

tidal Love number case

$$h_2^+ = c_1 P_2^2\left(r/M-1\right) + c_2 Q_2^2\left(r/M-1\right)$$

associated Legendre functions (Hinderer 2008)

tidal field   induced quadrupole moment

$$\xrightarrow[(r\to\infty)]{} 3c_1\left(\frac{r}{M}\right)^2 + O(r) + \boxed{\frac{8}{5}c_2\left(\frac{M}{r}\right)^3} + O(r^{-4}) \quad \Rightarrow \quad \boxed{\lambda = \frac{8M^5}{45}\frac{c_2}{c_1}}$$

(c_1 and c_2 : integration constants)

shell

- Location of the shell $(x^{\pm})^{\mu} = (A^{\pm}T, R+\varepsilon^2\xi^{\pm}, \Theta, \Phi)$

  $A^+=1$, $A^-=$const.

- Stress energy tensor of the shell

  $$S_{ab} = ([[K_{ab}]] - h_{ab}[[K]]),$$

  h_{ab}:induced metric
  K_{ab}:extrinsic curvature
  $K=K_{ab}h^{ab}$

- Expansions

  $$\xi^{\pm} = \xi_0^{\pm} + \xi_2^{\pm} P_2(\cos\theta)$$

  energy density $\sigma = \sigma_0 + \varepsilon^2\{\delta\sigma_0 + \delta\sigma_2 P_2(\cos\theta)\}$

  pressure $p = p_0 + \varepsilon^2\{\delta p_0 + \delta p_2 P_2(\cos\theta)\}$

  $$\sigma_0 = \frac{\sqrt{f^-(R)} - \sqrt{f^+(R)}}{4\pi R}$$

  $$p_0 = -\frac{1}{8\pi}\left(\frac{M-R}{\sqrt{f^+(R)}} + R\frac{1-2R^2/L^2}{\sqrt{f^-(R)}}\right)$$

- Equation of state

  $$p = k\sigma^{1+\frac{1}{n}}$$

  (k,n : constants)

Results

Dimensionless quantities and the black hole limit

- moment of inertia

  $$I = \frac{J}{\Omega} \to aM\left(\frac{a}{r_+^2 + a^2}\right)^{-1} \approx 4M^3, \quad \bar{I} = \frac{I}{M^3} \to 4$$

- Love number

  $$\bar{\lambda} = \frac{\lambda}{M^5} \to 0$$

- Quadrupole moment

  $$\bar{Q} = \frac{QM}{J^2} = 1 + \frac{8BM^4}{J^2} \to 1$$

Solutions for n=1 (rescaled by L=1)

$\bar{\lambda}$

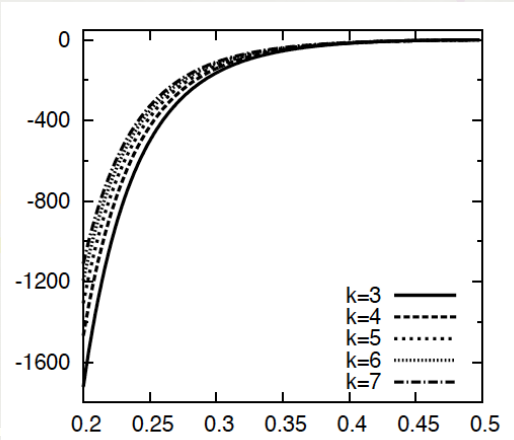

$p = k\sigma^{1+\frac{1}{n}}$

M/R → black hole

$\bar{I}$

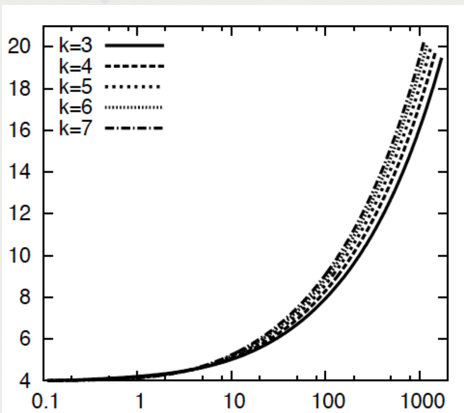

←black hole

$\bar{Q}$

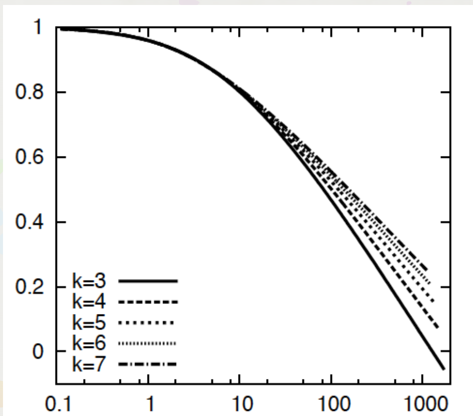

←black hole

$|\bar{\lambda}|$

- ellipticity due to the rotation $e^2/\varepsilon^2 \equiv -3\left(k_2^{\pm}(R) + \xi_2^{\pm}/R\right)$

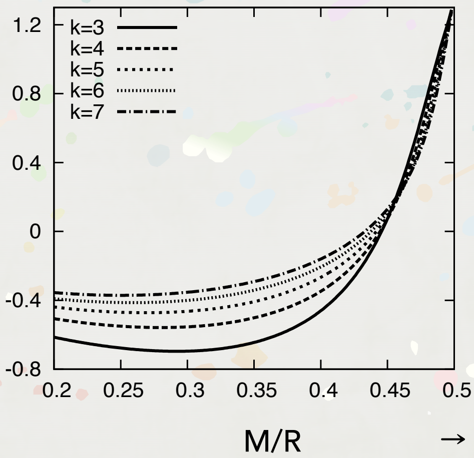

→ black hole

- Negative Love number and prolate shape shell
  → Pani (2015) also obtained similar results for $\sigma_0 = 0$.

- Slowly rotating prolate shell is obtained.

  (De la Cruz & Israel 1968, Pfister & Braun 1985, 1986)

Slowly rotating thin shell in a vacuum spacetime obtained by matching two spacetimes.
(The same formalism.)

Summary

- We have calculated the I-Love-Q relations for gravastars.
- Unlike neutron stars, most solutions have negative tidal Love number.
- The relations are almost independent of the equation of state in the black hole limit.

“Primordial non-Gaussianities of gravitational waves beyond Horndeski”

by Yuji Akita

[JGRG25(2015)5a5]

Primordial non-Gaussianities of gravitational waves beyond Horndeski

Yuji Akita (Rikkyo Univ.)

Collaborator: Tsutomu Kobayashi (Rikkyo)

arXiv: 1512.01380 [hep-th]

JGRG 2015 @YITP

Talk Plan

- 1. Introduction & Motivation
- 2. ADM decomposition of scalar-tensor theories
  —— General framework
- 3. The Lagrangians
  —— second and cubic order
- 4. Results

Talk Plan

- 1. Introduction & Motivation
- 2. ADM decomposition of scalar-tensor theories
  —— General framework
- 3. The Lagrangians
  —— second and cubic order
- 4. Results

Introduction & Motivation

- Inflation
  - Almost perfect standard scenario
    - scalar field ``inflaton''
    - gravitational waves
  - Power spectrum, non-Gaussianities

Focus on **Gravitational waves** h_{ij}

- Various models

  compute model by model…??

Introduction & Motivation

- Inflation

In general framework

  - Almost perfect standard scenario
    - scalar field ``inflaton"
    - gravitational waves
  - Power spectrum, non-Gaussianities

Focus on **Gravitational waves** h_{ij}

- Various models

compute model by model…??

Talk Plan

- 1. Introduction & Motivation
- 2. ADM decomposition of scalar-tensor theories
  —— General framework
- 3. The Lagrangians
  —— second and cubic order
- 4. Results

Horndeski theory

- The most general single-scalar-tensor theory with 2nd order e.o.m.

$$
\begin{aligned}
\frac{\mathcal{L}}{\sqrt{-g}} &= G_2(\phi, X) - G_3(\phi, X)\Box\phi + G_4(\phi, X)R \\
&+G_{4,X}\left[(\Box\phi)^2 - (\nabla_\mu\nabla_\nu\phi)^2\right] \\
&+G_5(\phi, X)G^{\mu\nu}\nabla_\mu\nabla_\nu\phi - \frac{1}{6}G_{5,X}\left[(\Box\phi)^3 + \dots\right]
\end{aligned}
$$

Horndeski (1974); Deffayet, *et al.* (2011); TK, Yamaguchi, Yokoyama (2011)

- 4-arbitrary functions of ϕ and $X = -\frac{1}{2}g^{\mu\nu}\partial_\mu\phi\partial_\nu\phi$.
- No k^4 term. $\boxed{\text{Further generalization?}}$

ADM decomposition

- Take $\phi = \mathrm{const}$ as constant time hypersurfaces

$$
\begin{aligned}
&G(\phi, X) = G(\phi(t), \dot{\phi}^2(t)/2N^2) = A(t, N) \\
&R = R^{(3)} + K_{ij}K^{ij} - K^2 + \cdots \\
&\nabla_\mu\nabla_\nu\phi \sim K_{ij}
\end{aligned}
$$

- ADM form of Horndeski

$$
\begin{aligned}
\frac{\mathcal{L}}{N\sqrt{\gamma}} &= A_2(t, N) + A_3(t, N)K + B_4(t, N)R^{(3)} \\
&- (B_4 + NB_{4,N})\left(K^2 - K_{ij}^2\right) + B_5(t, N)G_{ij}^{(3)}K^{ij} + \cdots
\end{aligned}
$$

  - 4-arbitrary functions of t and N.

ADM decomposition

Horndeski in ADM form

$$\frac{\mathcal{L}}{\sqrt{-g}} = A_2(t,N) + A_3(t,N)K + A_4(t,N)\left(K^2 - K_{ij}K^{ij}\right) + B_4(t,N)R$$
$$+ A_5(t,N)\left(K^3 - 3KK_{ij}K^{ij} + 2K_{ij}K^{jk}K^i_k\right) + B_5(t,N)K^{ij}\left(R_{ij} - \frac{1}{2}g_{ij}R\right),$$

with

$$A_4 = -B_4 - N\frac{\partial B_4}{\partial N}, \quad A_5 = \frac{N}{6}\frac{\partial B_5}{\partial N}$$

4 arbitrary functions

Extensions from Horndeski

- **GLPV** theory Gleyzes, *et al.* (2014)

Horndeski in ADM form

$$\frac{\mathcal{L}}{\sqrt{-g}} = A_2(t,N) + A_3(t,N)K + A_4(t,N)\left(K^2 - K_{ij}K^{ij}\right) + B_4(t,N)R$$
$$+ A_5(t,N)\left(K^3 - 3KK_{ij}K^{ij} + 2K_{ij}K^{jk}K^i_k\right) + B_5(t,N)K^{ij}\left(R_{ij} - \frac{1}{2}g_{ij}R\right),$$

with

$$A_4 = -B_4 - N\frac{\partial B_4}{\partial N}, \quad A_5 = \frac{N}{6}\frac{\partial B_5}{\partial N}$$

4 arbitrary functions

Extensions from Horndeski

- **GLPV** theory   Gleyzes, *et al.* (2014)

Horndeski in ADM form

$$\frac{\mathcal{L}}{\sqrt{-g}} = A_2(t,N) + A_3(t,N)K + A_4(t,N)\left(K^2 - K_{ij}K^{ij}\right) + B_4(t,N)R$$
$$+ A_5(t,N)\left(K^3 - 3KK_{ij}K^{ij} + 2K_{ij}K^{jk}K^i_k\right) + B_5(t,N)K^{ij}\left(R_{ij} - \frac{1}{2}g_{ij}R\right),$$

~~with~~

$$\cancel{A_4 = -B_4 - N\frac{\partial B_4}{\partial N}, \quad A_5 = \frac{N}{6}\frac{\partial B_5}{\partial N}}$$

4 arbitrary functions

Extensions from Horndeski

- **GLPV** theory   Gleyzes, *et al.* (2014)

Horndeski in ADM form

$$\frac{\mathcal{L}}{\sqrt{-g}} = A_2(t,N) + A_3(t,N)K + A_4(t,N)\left(K^2 - K_{ij}K^{ij}\right) + B_4(t,N)R$$
$$+ A_5(t,N)\left(K^3 - 3KK_{ij}K^{ij} + 2K_{ij}K^{jk}K^i_k\right) + B_5(t,N)K^{ij}\left(R_{ij} - \frac{1}{2}g_{ij}R\right),$$

~~with~~

$$\cancel{A_4 = -B_4 - N\frac{\partial B_4}{\partial N}, \quad A_5 = \frac{N}{6}\frac{\partial B_5}{\partial N}}$$

4 arbitrary functions

New 2 functions: A4 and A5

- Higher order derivatives remaining d.o.f

Extensions from Horndeski

- GLPV theory

$$\frac{\mathcal{L}}{\sqrt{-g}} = A_2(t,N) + A_3(t,N)K + A_4(t,N)\left(K^2 - K_{ij}K^{ij}\right) + B_4(t,N)R$$
$$+ A_5(t,N)\left(K^3 - 3KK_{ij}K^{ij} + 2K_{ij}K^{jk}K^i_k\right) + B_5(t,N)K^{ij}\left(R_{ij} - \frac{1}{2}g_{ij}R\right),$$

- Unifying framework Gao. (2014)

$$\frac{\mathcal{L}}{N\sqrt{\gamma}} = A_2(t,N) + A_3(t,N)K + B_4(t,N)R^{(3)}$$
$$+A_4(t,N)K^2 - \widetilde{A}_4(t,N)K_{ij}K^{ij} + \cdots$$

  - Retains same structure, yielding same d.o.f
  - Add new terms preserving spatial covariance

Talk Plan

- 1. Introduction & Motivation
- 2. ADM decomposition of scalar-tensor theories
  —— General framework
- 3. The Lagrangians
  —— second and cubic order
- 4. Results

The Lagrangians

- Start from Unifying framework: Gao. (2014)
  — including beyond Horndeski, k-essence, ghost condensate…
- Focus on gravitational waves
  — Power spectrum, non-Gaussianities
- Relevant terms to tensor perturbations:

$$\frac{\mathcal{L}}{\sqrt{-g}} = \widetilde{d}_1 R + \widetilde{d}_3 R_i^j R_j^i + d_7 R_i^j R_j^k R_k^i + \widetilde{b}_2 \delta K_i^j \delta K_j^i + c_3 \delta K_i^j \delta K_j^k \delta K_k^i$$
$$+\widetilde{a}_2 R_i^j \delta K_j^i + a_7 R_i^j R_j^k \delta K_k^i + b_6 R_i^j \delta K_j^k \delta K_k^i$$

8 terms.

- Subclass GLPV: $\widetilde{d}_1$, $\widetilde{b}_2$, c_3, and $\widetilde{a}_2$ **We have 4 new terms!**

The Lagrangians

- Start from Unifying framework: Gao. (2014)
  — including beyond Horndeski, k-essence, ghost condensate…
- Focus on gravitational waves
  — Power spectrum, non-Gaussianities
- Quadratic:

$$S = \frac{1}{8} \int \mathrm{d}t \mathrm{d}^3 x \, a^3 \left[\mathcal{G}_T \dot{h}_{ij}^2 - \frac{\mathcal{F}_T}{a^2} \left(\partial_k h_{ij}\right)^2 + 2 \frac{\tilde{d}_3}{a^4} \left(\partial^2 h_{ij}\right)^2 \right],$$

The Lagrangians

- Start from Unifying framework: Gao. (2014)
  - — including beyond Horndeski, k-essence, ghost condensate…
- Focus on gravitational waves
  - — Power spectrum, non-Gaussianities
- Quadratic:

$$S = \frac{1}{8}\int \mathrm{d}t\mathrm{d}^3x\, a^3 \left[\mathcal{G}_T \dot{h}_{ij}^2 - \frac{\mathcal{F}_T}{a^2}(\partial_k h_{ij})^2 + 2\frac{\tilde{d}_3}{a^4}(\partial^2 h_{ij})^2\right],$$

$$\delta K_{ij}\delta K^{ij} \qquad R \qquad R^i_j R^j_i$$

$$R^i_j \delta K^j_i$$

Linear order

- Quadratic:

$$S = \frac{1}{8}\int \mathrm{d}t\mathrm{d}^3x\, a^3 \left[\mathcal{G}_T \dot{h}_{ij}^2 - \frac{\mathcal{F}_T}{a^2}(\partial_k h_{ij})^2 + 2\frac{\tilde{d}_3}{a^4}(\partial^2 h_{ij})^2\right],$$

- Key feature:

$$\omega^2 = c_h^2 k^2 + \epsilon^2 k^4 \eta^2 \quad \text{with} \quad c_h^2 := \frac{\mathcal{F}_T}{\mathcal{G}_T}, \quad \epsilon^2 := -2H^2\frac{\tilde{d}_3}{\mathcal{G}_T}.$$

  - Exact solution: Whittaker function
- Power spectrum

$$\mathcal{P}_h(k) = 2\frac{H^2}{\pi^2}\frac{\mathcal{G}_T^{1/2}}{\mathcal{F}_T^{3/2}}|F(\epsilon/c_h^2)|^2$$

Coincide with Fujita *et al*

Methods

- In-in formalism Maldacena 2002

$$\langle \widetilde{h}_{i_1j_1}(\mathbf{k}_1)\widetilde{h}_{i_2j_2}(\mathbf{k}_2)\widetilde{h}_{i_3j_3}(\mathbf{k}_3)\rangle = -i\int_{t_0}^{t} \mathrm{d}t' \left\langle \left[\widetilde{h}_{i_1j_1}(t,\mathbf{k}_1)\widetilde{h}_{i_2j_2}(t,\mathbf{k}_2)\widetilde{h}_{i_3j_3}(t,\mathbf{k}_3),\ H_{\mathrm{int}}(t')\right]\right\rangle,$$

This cannot be integrated ! (due to Whittaker function)

- Approximation form of Whittaker function

$$\frac{a\sqrt{\mathcal{G}_T}}{2}\psi_{\mathbf{k}} = F(\delta)\frac{e^{-iy+i\delta y^2/2}}{\sqrt{2c_h k}}\left[-\frac{i}{y}+1-\frac{\delta}{2}(y+iy^2)-\delta^2\left(\frac{5}{12}y^2+\frac{i}{24}y^3+\frac{1}{8}y^4\right)+\mathcal{O}(\delta^3)\right]$$

where $y := c_h k\eta$ and $\delta := \epsilon/c_h^2$

Include ϵ perturbatively

Interaction terms

- Cubic action

$$\begin{aligned} S = \int \mathrm{d}t\mathrm{d}^3x\, a^3\Big\{ & \frac{c_3}{8}\dot{h}_i^j\dot{h}_j^k\dot{h}_k^i + \frac{\mathcal{F}_T}{4a^2}\left(h_{ik}h_{jl}-\frac{1}{2}h_{ij}h_{kl}\right)h_{ij,kl} \\ & +\frac{a_7}{8a^4}\dot{h}_k^i\partial^2 h_j^k\partial^2 h_i^j - \frac{b_6}{8a^2}\dot{h}_k^i\dot{h}_j^k\partial^2 h_i^j \\ & +\frac{\tilde{d}_3}{a^4}\partial^2 h_{ij}\left[\frac{1}{2}h_{ik,l}h_{jl,k}+h_{kl}\left(h_{ik,lj}-\frac{1}{4}h_{kl,ij}-\frac{1}{2}h_{ij,kl}\right)\right] \\ & -\frac{d_7}{8a^6}\partial^2 h_i^j\partial^2 h_j^k\partial^2 h_k^i\Big\}. \end{aligned}$$

- **6** interaction terms

$c_3,\ \mathcal{F}_T,\ a_7,\ b_6,\ d_7,\ \tilde{d}_3$

Interaction terms

- Cubic action

Horndeski case

$$S = \int \mathrm{d}t\mathrm{d}^3x\, a^3 \left\{ \frac{c_3}{8}\dot{h}_i^j \dot{h}_j^k \dot{h}_k^i + \frac{\mathcal{F}_T}{4a^2}\left(h_{ik}h_{jl} - \frac{1}{2}h_{ij}h_{kl}\right)h_{ij,kl} \right.$$
$$+ \frac{a_7}{8a^4}\dot{h}_k^i \partial^2 h_j^k \partial^2 h_i^j - \frac{b_6}{8a^2}\dot{h}_k^i \dot{h}_j^k \partial^2 h_i^j$$
$$+ \frac{\tilde{d}_3}{a^4}\partial^2 h_{ij}\left[\frac{1}{2}h_{ik,l}h_{jl,k} + h_{kl}\left(h_{ik,lj} - \frac{1}{4}h_{kl,ij} - \frac{1}{2}h_{ij,kl}\right)\right]$$
$$\left. - \frac{d_7}{8a^6}\partial^2 h_i^j \partial^2 h_j^k \partial^2 h_k^i \right\}.$$

- **6** interaction terms

$c_3,\ \mathcal{F}_T,\ a_7,\ b_6,\ d_7,\ \tilde{d}_3$

Interaction terms

- Cubic action

Horndeski case

$$S = \int \mathrm{d}t\mathrm{d}^3x\, a^3 \left\{ \frac{c_3}{8}\dot{h}_i^j \dot{h}_j^k \dot{h}_k^i + \frac{\mathcal{F}_T}{4a^2}\left(h_{ik}h_{jl} - \frac{1}{2}h_{ij}h_{kl}\right)h_{ij,kl} \right.$$
$$+ \frac{a_7}{8a^4}\dot{h}_k^i \partial^2 h_j^k \partial^2 h_i^j - \frac{b_6}{8a^2}\dot{h}_k^i \dot{h}_j^k \partial^2 h_i^j$$
$$+ \frac{\tilde{d}_3}{a^4}\partial^2 h_{ij}\left[\frac{1}{2}h_{ik,l}h_{jl,k} + h_{kl}\left(h_{ik,lj} - \frac{1}{4}h_{kl,ij} - \frac{1}{2}h_{ij,kl}\right)\right]$$
$$\left. - \frac{d_7}{8a^6}\partial^2 h_i^j \partial^2 h_j^k \partial^2 h_k^i \right\}.$$

- **6** interaction terms

$c_3,\ \mathcal{F}_T,\ a_7,\ b_6,\ d_7,\ \tilde{d}_3$

- GLPV subclass: $a_7 = b_6 = \tilde{d}_3 = d_7 = 0$

no new interactions when Horndeski → GLPV

Interaction terms

- Cubic action

Horndeski case

$$S = \int \mathrm{d}t\mathrm{d}^3x\, a^3 \Big\{ \frac{c_3}{8}\dot{h}_i^j \dot{h}_j^k \dot{h}_k^i + \frac{\mathcal{F}_T}{4a^2}\left(h_{ik}h_{jl} - \frac{1}{2}h_{ij}h_{kl}\right)h_{ij,kl}$$
$$+\frac{a_7}{8a^4}\dot{h}_k^i \partial^2 h_j^k \partial^2 h_i^j - \frac{b_6}{8a^2}\dot{h}_k^i \dot{h}_j^k \partial^2 h_i^j$$
$$+\frac{\tilde{d}_3}{a^4}\partial^2 h_{ij}\left[\frac{1}{2}h_{ik,l}h_{jl,k} + h_{kl}\left(h_{ik,lj} - \frac{1}{4}h_{kl,ij} - \frac{1}{2}h_{ij,kl}\right)\right]$$
$$-\frac{d_7}{8a^6}\partial^2 h_i^j \partial^2 h_j^k \partial^2 h_k^i \Big\}.$$

New terms in Gao's framework

- **6** interaction terms

$c_3,\ \mathcal{F}_T,\ a_7,\ b_6,\ d_7,\ \tilde{d}_3$

- GLPV subclass: $a_7 = b_6 = \tilde{d}_3 = d_7 = 0$

no new interactions when Horndeski → GLPV

non-Gaussianities

- Three point correlation function

$$\langle \tilde{h}_{i_1j_1}(\mathbf{k}_1)\tilde{h}_{i_2j_2}(\mathbf{k}_2)\tilde{h}_{i_3j_3}(\mathbf{k}_3)\rangle = (2\pi)^7\delta^{(3)}(\mathbf{k}_1+\mathbf{k}_2+\mathbf{k}_3)\frac{\mathcal{P}_h^2}{k_1^3k_2^3k_3^3}\mathcal{A}_{i_1j_1i_2j_2i_3j_3}$$

$$\mathcal{A}_{i_1j_1i_2j_2i_3j_3} = \sum_{\bullet=c_3,a_7,\cdots}\left(\mathcal{A}^{(\bullet)}_{i_1j_1i_2j_2i_3j_3} + \frac{\epsilon^2}{c_h^4}\mathcal{C}^{(\bullet)}_{i_1j_1i_2j_2i_3j_3}\right)$$

Leading + Correction

- For polarization modes $\xi^{(s)}(\mathbf{k}) = \tilde{h}_{ij}(\mathbf{k})e_{ij}^{*(s)}(\mathbf{k})$,

$$A^{s_1s_2s_3} = \sum_{\bullet=c_3,a_7,\cdots}\left(\mathcal{A}_{(\bullet)}^{s_1s_2s_3} + \frac{\epsilon^2}{c_h^4}\mathcal{C}_{(\bullet)}^{s_1s_2s_3}\right)$$

→ Show the pictures of $A_{(\bullet)}^{+++}$ and $C_{(\bullet)}^{+++}$

Talk Plan

- 1. Introduction & Motivation
- 2. ADM decomposition of scalar-tensor theories
  —— General framework
- 3. The Lagrangians
  —— second and cubic order
- 4. Results

The result 1: Local type

- Peaks in squeezed limit … $\mathcal{F}_T$ **(only term in GR)**

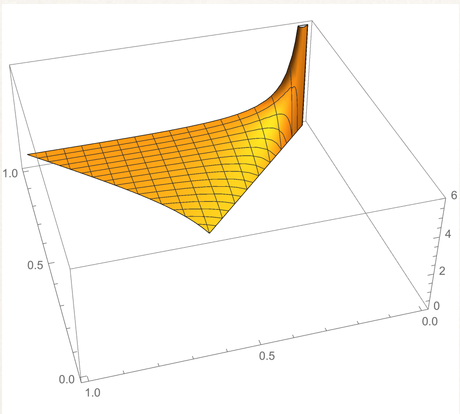

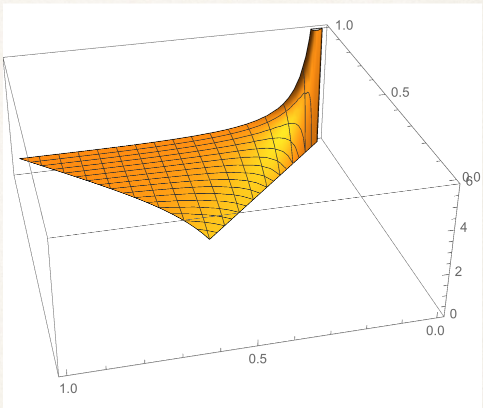

Leading order **Correction … also mild.**

$$\mathcal{A}^{+++}_{(\mathcal{F}_T)} = \frac{K_t}{16}\left(-1 + \frac{K_2}{K_t^2} + \frac{K_3}{K_t^3}\right) \times \frac{1}{128} \cdot \frac{K_t^8}{K_3^2}\left(1 - 4\frac{K_2}{K_t^2} + 8\frac{K_3}{K_t^3}\right)$$

The result 1: Local type

- Peaks in squeezed limit … $\mathcal{F}_T$ **(only term in GR)**

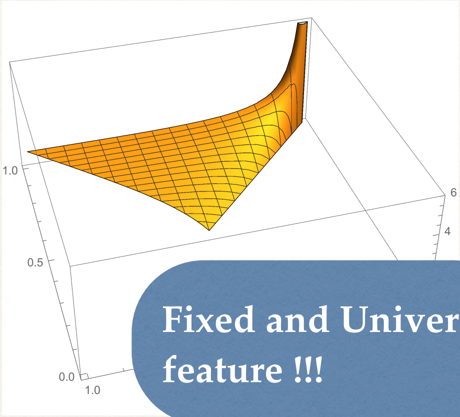

Fixed and Universal feature !!!

Leading order

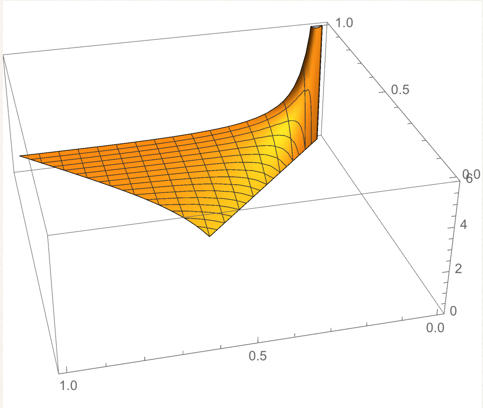

Correction … same peak.

$$\mathcal{A}^{+++}_{(\mathcal{F}_T)} = \frac{K_t}{16}\left(-1+\frac{K_2}{K_t^2}+\frac{K_3}{K_t^3}\right)\times\frac{1}{128}\cdot\frac{K_t^8}{K_3^2}\left(1-4\frac{K_2}{K_t^2}+8\frac{K_3}{K_t^3}\right)$$

The result 1: Local type

- Peaks in squeezed limit … $\mathcal{F}_T$ **(only term in GR)**

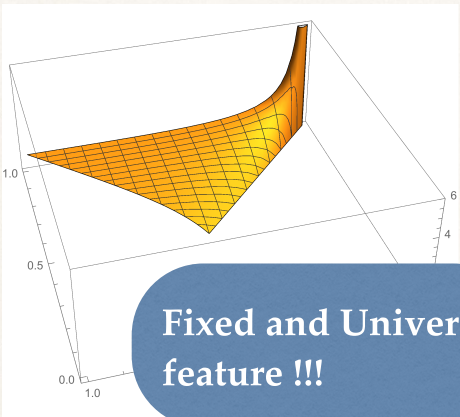

Fixed and Universal feature !!!

Leading order

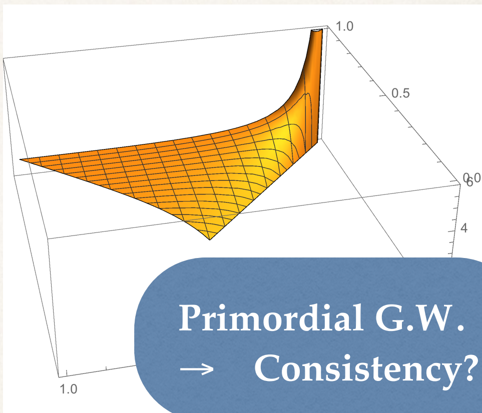

Primordial G.W. → Consistency?

Correction … same peak.

$$\mathcal{A}^{+++}_{(\mathcal{F}_T)} = \frac{K_t}{16}\left(-1+\frac{K_2}{K_t^2}+\frac{K_3}{K_t^3}\right)\times\frac{1}{128}\cdot\frac{K_t^8}{K_3^2}\left(1-4\frac{K_2}{K_t^2}+8\frac{K_3}{K_t^3}\right)$$

The result 1: Local type

- $\tilde{d}_3$ term also peaks in squeezed limit

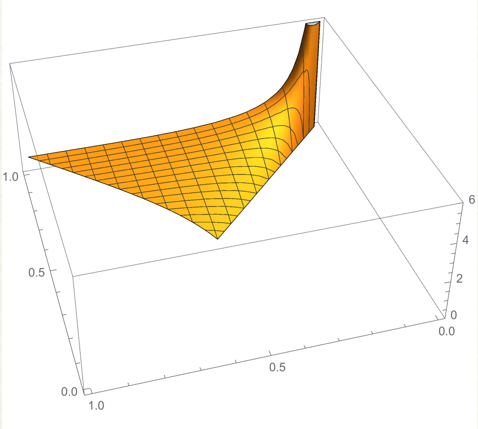

Only correction term exist.
since $\tilde{d}_3 \sim \epsilon^2$

The result 1: Local type

- $\tilde{d}_3$ term also peaks in squeezed limit

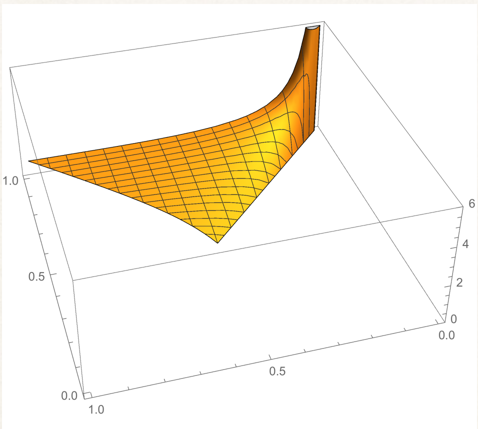

Small correction

$\mathcal{F}_T$ **contribution is**
....Fixed and Universal,
....only the term generating Local type

Only correction term exist.
since $\tilde{d}_3 \sim \epsilon^2$

The result 2: Equilateral type

- Equilateral type … $c_3,\ a_7,\ b_6,\ d_7$ **: 4 of 6 interactions**

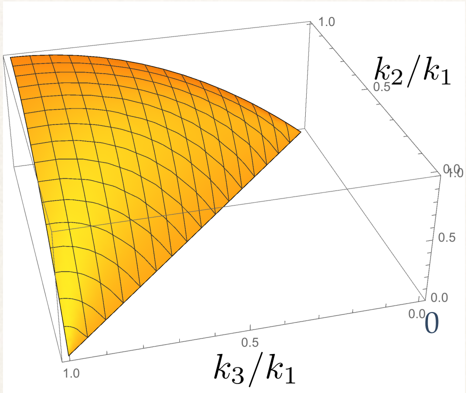

Leading order

$$\mathcal{A}^{s_1s_2s_3}_{(c_3)} = \frac{3c_3}{8}\frac{H}{\mathcal{G}_T}\cdot\frac{K_3^2}{K_t^3}F^{s_1s_2s_3}_{(\mathrm{H})},$$

$$F^{+++}_{(\mathrm{H})} := \frac{1}{64}\cdot\frac{K_t^6}{K_3^2}\left(1-4\frac{K_2}{K_t^2}+8\frac{K_3}{K_t^3}\right)$$

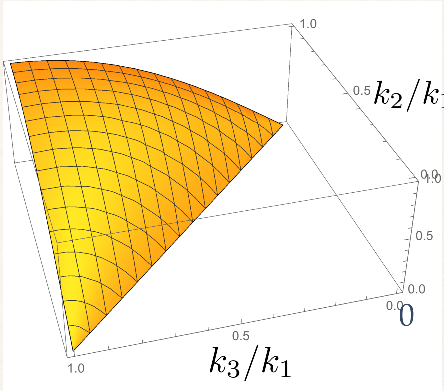

Correction

$$\mathcal{C}^{s_1s_2s_3}_{(c_3)} = \mathcal{A}^{s_1s_2s_3}_{(c_3)}\cdot 2\underbrace{\left(1-12\frac{K_2}{K_t^2}+15\frac{K_3}{K_t^3}\right)}_{\mathcal{O}(1)}$$

Similar momentum dependences !

The result 2: Equilateral type

Leading order / Correction

a_7

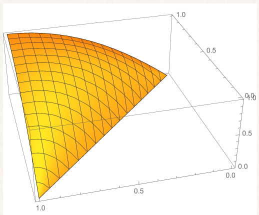

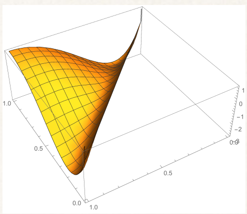

b_6

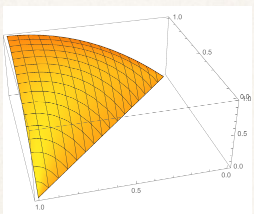

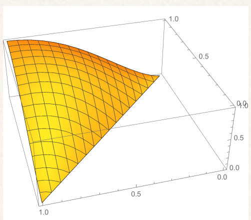

d_7

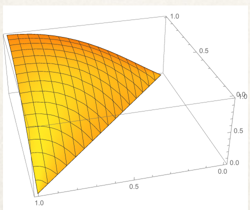

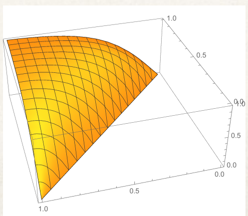

Also,
Corrections are mild.

The result 2: Equilateral type

	Leading order	Correction
a_7	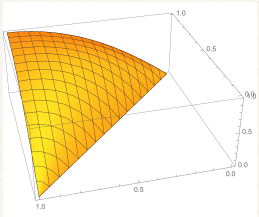	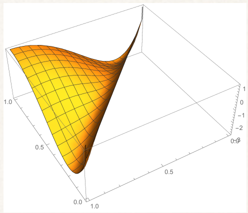
b_6	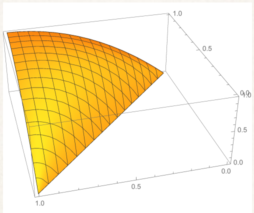	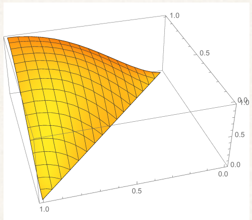
d_7	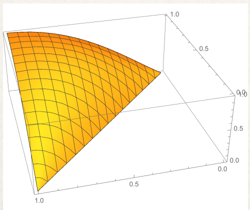	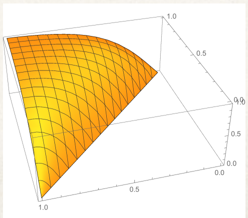

Non-standard modification

↓

Equilateral type non-Gaussianities

$c_3,\ a_7,\ b_6,\ d_7$

Also,
Corrections are mild.

Summary

- Unifying framework

  → **2+4 interaction terms,**
  modified dispersion relation. $\tilde{d}_3 \leftrightarrow \epsilon^2$ **Correction of amplitude**

- The peaks: Equilateral or Squeezed

  Equilateral: non-standard extensions

  Squeezed: Leading order of $\mathcal{F}_T$ has **Fixed** and **Universal** feature

  → There is only **one interaction term** generating squeezed N.G.
  only term present in GR

  (when the effect of modified dispersion relation is small)

- more details and discussions: **arXiv: 1512.01380 [hep-th]**

Approx:

Good for $\delta \times y^2 \lesssim 1$

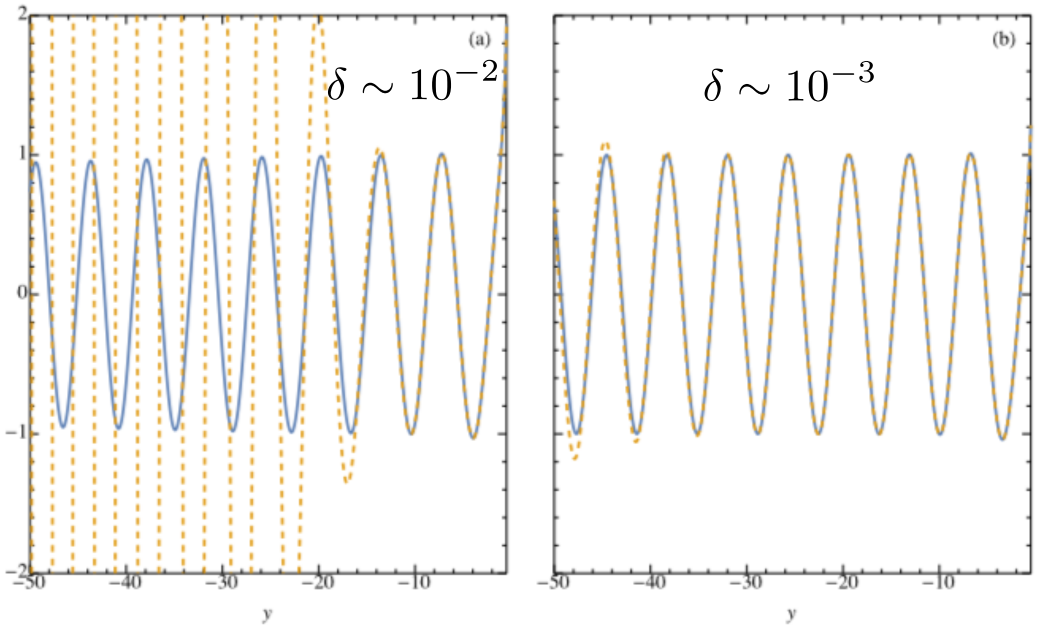

Dashed: approximation. Solid: exact solution.

“New definition of wormhole throat”

by Yoshimune Tomikawa

[JGRG25(2015)5a6]

JGRG25 Dec. 7-11（2015）

New definition of wormhole throat

Yoshimune Tomikawa

Department of Mathematics, Nagoya University

based on

Y.Tomikawa, K.Izumi, T.Shiromizu, PRD91, 104008 (2015)

Contents

1. Introduction

Wormhole

For example, M.S.Morris, K.S.Thorne (1988)

・"minimal surface"
(throat with flare-out condition)

・no event horizon

(・traversability)

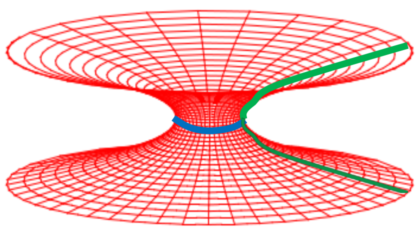

There are several definitions of throat

Exotic

M.S.Morris, K.S.Thorne (1988), D.Hochberg, M.Visser (1997, 1998)

▪It is well-known that exotic matter is required on wormhole throat ∼Violation of null energy condition (NEC)

Exception

H.Maeda, T.Harada, B.J.Carr (2009)

▪Cosmological wormhole with initial singularity

Several throat definition

1. M.S.Morris, K.S.Thorne (1988)

   ▪minimal surface on embedded time slice into 3D Euclid space

2. D.Hochberg, M.Visser (1998)

   ▪“minimal surface” on null hypersurface

3. H.Maeda, T.Harada, B.J.Carr (2009)

   ▪minimal surface on spacelike hypersurface

It is slightly hard to show general properties of wormhole throat…

→We propose new definition of wormhole throat

2. New definition

Our definition of throat

We define throat as "minimal surface" on "spacelike hypersurface"

that is

codimension-2 spacelike surface satisfying $k = 0$ and $r^a \nabla_a k > 0$

$$k = \theta_+ - \theta_-$$

$\theta_\pm$: null expansion rate of geodesic congruence

$$r^a = (\partial_{\lambda_+} - \partial_{\lambda_-})^a$$

$\lambda_\pm$: affine parameter of future directed ingoing/outgoing null geodesic

Traversable wormhole

$\lambda_\pm$: affine parameter of future directed ingoing/outgoing null geodesic

We define traversablity

Time sequence of throats

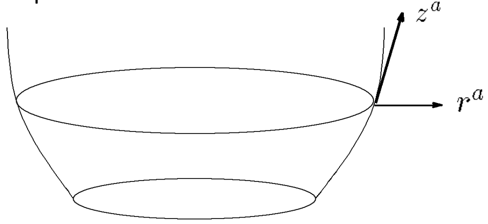

tangent vector of time sequence of throat

$$z^a = \alpha(\partial_{\lambda_+})^a + \beta(\partial_{\lambda_-})^a \qquad \alpha, \beta > 0$$

is timelike

$\Rightarrow$ $z^a \nabla_a k = 0$ along the time sequence

General properties

- non-exotic wormhole
- static wormhole

Non-exotic wormhole

- Raychaudhuri equation with null energy condition

  → $\partial_{\lambda_+}\theta_+ \leq 0$

- Flare-out condition and traversability

  → $\partial_{\lambda_+}\theta_+|_{\rm th} > \partial_{\lambda_+}\theta_-|_{\rm th}$

⇨ $\partial_{\lambda_+}\theta_-|_{\rm th} < 0$ is required at least for the presence of traversable wormhole

Static wormhole

$$r^a = (\partial_{\lambda_+} - \partial_{\lambda_-})^a$$

$$t^a = (\partial_{\lambda_+} + \partial_{\lambda_-})^a$$

$$k = \theta_+ - \theta_-$$

$$\bar{k} = \theta_+ + \theta_-$$

$$r^a \nabla_a k + t^a \nabla_a \bar{k} = 2(\partial_{\lambda_+}\theta_+ + \partial_{\lambda_-}\theta_-)$$

→Raychaudhuri equation with null energy condition (NEC) implies $r^a \nabla_a k + t^a \nabla_a \bar{k} \leq 0$

→If wormhole spacetime is static, $t^a \nabla_a \bar{k} = 0$

→ $r^a \nabla_a k \leq 0$ (violation of flare-out condition)

⇨ It is required that NEC does not hold for static wormhole

(It is simpler than D.Hochberg, M.Visser (1997))

3. Spherically symmetric cases

Non-wormhole

	$k = 0$	$r^a \nabla_a k > 0$	no event horizon
Schwarzschild	○	○	×
de Sitter	○	×	○

Wormhole

	$k = 0$	$r^a \nabla_a k > 0$	no event horizon
Morris-Throne	◎	◎	◎
dynamical Ellis (initial singularity)	◎	◎	◎

4. Summary

Summary

We gave new definition of wormhole throat and traversability

- Throat is “minimal surface” on “spacelike hypersurface” satisfying $k=0$ and $r^a \nabla_a k > 0$

- Traversability : tangent vector of time sequence of throats is “timelike”

Issues

- We have to examine more general spacetimes.

  Because we considered only spherically symmetric case.

“Observational constraints on variable equation of state parameters of dark energy”

by E. P. Berni Ann Thushari

[JGRG25(2015)5b1]

Observational constraints on variable equation of state parameters of dark energy

E.P. B. A.Thushari, R. Ichimasa & M. Hashimoto
Department of Physics,
Kyushu University

2015/12/09

Content….

- ✓ Motivation
- ✓ Objectives
- ✓ Theoretical explanation of the Model
- ✓ Observational constraints from the

  Type Ia Supernovae (SNe Ia)

  Gamma Ray Burst (GRB)
- ✓ Results and discussion

Motivation…

Journey beyond the standard model….

- Explain the observed late time acceleration

Cosmological term is one candidate to the dark energy

Early value $\rho_{vac} \sim 10^{74} GeV^4 \neq$ Present value $\rho_{\Lambda} \sim 10^{-47} \mathrm{GeV}^4$

121 orders of magnitude different

$\boxed{\text{Cosmological Constant Problem}}$ **[Weinberg 1989]**

- **Cosmological constant may not be a constant**
- **It decreases large value to the present value**
- **It may require some new functional form of matter(Dark Energy -DE)**
- **New modified theories beyond the standard model are needed**

(2)

Journey beyond the standard model….

Modifications to the cosmological term

✓ Several possibilities are suggested as a solution for cosmological constant problem

✓ Various functional forms to the cosmological term are introduced

As a time dependent function
[Silviera & Waga 1997]

In terms of scalar field
[Weinberg 1989, Huter &Turner 1999, Endo & Fukui 1977]

Decaying cosmological term with scale factor
[Kimura et al, 2001, Hashimoto et al. 2003, Wang et al, 2005]

The second question is whether the general relativity is applicable to describe the universe as a whole ?

(3)

Objectives….

- Construct a cosmological model where the equations of state (EOS) dark energy (DE) vary with time.
- How the evolving EOS for DE can modify the CDM paradigm
- Study the evolution of the energy densities with the parameters
- Constrain this model using SNe Ia and Gamma Ray Bursts observations for the present universe
- Constrain the model parameters using *Markov chain Monte Carlo* (*MCMC*) method

(4)

Field Equations ……..

Einstein's field equation

$$R_{\mu\nu} - \frac{1}{2} R g_{\mu\nu} + \Lambda g_{\mu\nu} = 8\pi G T_{\mu\nu}$$

For homogeneous and isotropic universe,

Robertson Walker metric $$ds^2 = dt^2 - a^2\left(\frac{dr^2}{1-kr^2} + r^2 d\theta^2 + r^2 \sin\theta d\phi\right)$$

Energy momentum tenor $$T_{\mu\nu} = diag(-\rho, p, p, p)$$

This leads two independent equations

(A)
$$\boxed{\begin{aligned} \frac{3\dot{a}^2}{a^2} + \frac{3k}{a^2} &= \rho = \sum_{i=1}^{N} \rho^{(i)}, \\ \frac{2\ddot{a}}{a} + \frac{\dot{a}^2}{a^2} + \frac{k}{a^2} &= -p = -\sum_{i=1}^{N} p^{(i)}, \end{aligned}}$$

H : Hubble parameter
a : Scale factor
G : Gravitational constant
k : Curvature constant
Λ : Cosmological constant
Ω : Density parameter

$\left.\begin{array}{ll} \rho^{(i)}; & \text{Energy density} \\ p^{(i)}; & \text{Pressure} \end{array}\right\}$ of the i^{th} component that fills the universe; sums are to N

components of the energy density $\rho = \rho_\gamma + \rho_\nu + \rho_m + \rho_\Lambda$

where γ, ν, m, Λ photons, neutrino, matter (baryon + cold dark matter) ,cosmological term

Field Equations ....

Above equations **(A)** can be combined to obtain

$$\dot{\rho} = -3(\rho + p)\frac{\dot{a}}{a} = 0$$ ➡ Continuity equation

Which is equivalent to the conservation equation $T^{\mu\nu}_{;\nu} = 0$

Here we use $8\pi G = c = 1$, 0 denotes the quantity given at the current epoch

General integration of the field equations ....

$$\rho = \rho^{(DE)} + \rho^{(M)},$$
$$p = p^{(DE)} + p^{(M)},$$

where $\rho^{(DE)}, p^{(DE)}$ Dark Energy contribution

$$\rho^{(M)} = \sum_i \rho^{(i)}, p^{(M)} = \sum_i p^{(i)}$$

Neglect any matter-DE interaction, $\rho^{(DE)}, \rho^{(M)}$ satisfy continuity equation separately

Simplest EOS $p/\rho = \omega$, where ω is in relativistic units- is a dimensionless constant.

(6)

In this work a direct generalization to this equation is to assume ϖ is not a constant but a function of the epoch.

We assume that both, matter and DE satisfy such type of EOS,

$$p^{(M)} = \varpi(a)\rho^{(M)},$$
$$p^{(DE)} = W(a)\rho^{(DE)}.$$

To explain the accelerated expansion, we accept that the DE component violates the strong energy condition

Thus we assume $W < -1/3$

Solving the field equations $\boxed{\Omega^{(M)} + \Omega^{(DE)} = 1 + \frac{k}{a^2H^2}}$

where $\Omega^{(M)} = \rho^{(M)}/3H^2$ and $\Omega^{(DE)} = \rho^{(DE)}/3H^2$

(7)

$$p^{(M)} = \varpi(a)\rho^{(M)},$$
$$p^{(DE)} = W(a)\rho^{(DE)}.$$

The continuity equation for $\rho^{(M)}$ and $\rho^{(DE)}$ can be formally integrated to obtain the evolution of the energy densities as

$$\rho^{(M)} = \frac{C_1}{a^3} e^{-3\int \frac{\omega(a)}{a} da}, \qquad p^{(DE)} = \frac{C_2}{a^3} e^{-3\int \frac{W(a)}{a} da,}.$$

$$\rho^{(M)}(a_*) = \rho^{(DE)}(a_*) \quad \Longrightarrow \quad x \equiv \frac{a}{a_*}$$

$$\rho^{(M)} = \frac{C}{x^3} e^{-3\int_1^x \frac{\varpi(u)}{u} du}, \qquad p^{(DE)} = \frac{C}{x^3} e^{-3\int_1^x \frac{W(u)}{u} du,}.$$

where C_1 and C_2 are constants of integration

C_2 represents the common value shared by the densities at $x = 1 (a = a_*)$

We denote

$$F(x) = e^{-3\int_1^x \frac{\omega(u)}{u} du}, \qquad G(x) = e^{-3\int_1^x \frac{W(u)}{u} du}.$$

Present universe is flat universe $\Longrightarrow$ $k = 0$ **[Dunckley et al., 2009]**

$$\Omega^{(M)} + \Omega^{(DE)} = 1 + \frac{k}{a^2H^2}$$

$$3H^2 = \frac{C}{x^3}\left[F(x) + G(x)\right]$$

$$\Omega^M = \frac{F(x)}{F(x) + G(x)}, \Omega^{(DE)} = \frac{G(x)}{F(x) + G(x)}$$

$F(1) = G(1) = 1 \Longrightarrow \Omega^{(M)} = \Omega^{(DE)} = 1/2$ at $x = 1$

Zero denotes the present epoch

(B) $$F(x_0) = \left[\frac{\Omega_0^{(M)}}{\Omega_0^{(DE)}}\right] G(x_0) \qquad 3H^2 = \frac{C}{x^3}\left[F(x) + G(x)\right]$$

$$a = \frac{a_0}{1+z} \Longrightarrow z = \frac{x_0}{x} - 1$$

$$C = \frac{3H_0^2 x_0^3 \Omega_0^{(M)}}{F(x_0)} = \frac{3H_0^2 x_0^3 \Omega_0^{(DE)}}{G(x_0)}$$

$$H = H_0\left(\frac{x_0}{x}\right)^{3/2}\left[\Omega_0^{(M)}\frac{F(x)}{F(x_0)} + \Omega_0^{(DE)}\frac{G(x)}{G(x_0)}\right]^{1/2}$$

J. Ponce de Leon (Class. Quantum, Grav. 29 (2012)

(9)

The Hubble and density parameters

Applying general formula to EoS

$$W = \frac{\omega x^\beta + \gamma}{x^\beta + 1} \qquad F(x) = 1, G(x) = \frac{2^{3(\omega-\gamma)/\beta}}{x^{3\omega}}\left[1+\frac{1}{x^\beta}\right]^{-3(\omega-\gamma)/\beta}$$

$$H(x) = H_0\left[\Omega_0^{(M)}\left(\frac{x_0}{x}\right)^3 + \Omega_0^{(DE)}\left(\frac{x_0}{x}\right)^{3(\omega+1)} g(x)\right]^{1/2}$$

$$g(x) = \left[\frac{K + \frac{1}{x_0^\beta}}{K + \frac{1}{x^\beta}}\right]^{3(\omega-\gamma)/\beta} \qquad \rho^{(M)} = \rho_0^{(M)}\left(\frac{x_0}{x}\right)^3,$$

$$\rho^{(DE)} = \rho_0^{(DE)}\left(\frac{x_0}{x}\right)^{3(1+\omega)} g(x).$$

From (B)

$$x_0^{3\omega}\left(K + \frac{1}{x_0^\alpha}\right)^{3n/\alpha}\left(1+\frac{1}{x_0^\beta}\right)^{3(\omega-\gamma)/\beta} = 2^{3(\omega-\gamma)/\beta}(K+1)^{3n/\alpha}\left[\frac{\Omega_0^{(M)}}{\Omega_0^{(DE)}}\right]$$

Cosmological model with variable equation of state

- ✓ **General Relativity**
- ✓ **Matter** (Cold dark matter + Baryonic matter)
  Non-relativistic particle
- ✓ **Dark Energy**
  Generalized EoS which has two convergence values

$$\boxed{W = \frac{\omega x^\beta + \gamma}{x^\beta + 1}}$$

S. Hannestad and E. Mortsell (2004)

- ✓ Flatness
  Curvature : $K = 0$
- ✓ Each component has no interaction (source) term

$$\frac{d\rho^{(i)}}{dt} + 3H\left(\rho^{(i)} + P^{(i)}\right) = 0$$

(10)

Method……

✓ At the present stage

- Present equation of state

$$W_{DE(a_0)} = \frac{\omega a_0^{\beta} + \gamma}{a_0^{\beta} + 1}$$

- Derivative at the present time

$$\left.\frac{\partial W_{DE}(a)}{\partial a}\right|_{a=a_0} = \frac{\beta(\omega-\gamma)a_0^{\beta-1}}{\left(a_0^{\beta}+1\right)^2}$$

- **Dark Energy density**

$$\rho^{DE}(a) = \rho_0^{DE} a^{-3(\omega-1)} \left(\frac{1+a_0^{-\beta}}{1+a^{-\beta}}\right)^{3(\omega-\gamma)/\beta}$$

✓ Observational constraints

MCMC method

Parameters : H_0, $\Omega_{m,}$, ω, γ, β

Observational data : 695 SNe Ia [Suzuki et al., ApJ (2011), *Union 2.1 Comp.*]

138 GRBs [J. Liu and J. Wei, astro-ph:1410.3960]

Constant cosmological term $(W = -1)$, For Variable EoS W?

13

(6)

✓ Density evolution

γ dependency

$$W_{DE(a)} = \frac{\omega a^{\beta} + \gamma}{a^{\beta} + 1}$$

H_0 = 70 $\mathrm{Kms^{-1}Mpc^{-1}}$

Ω_m = 0.27

β = 20

ω = -2

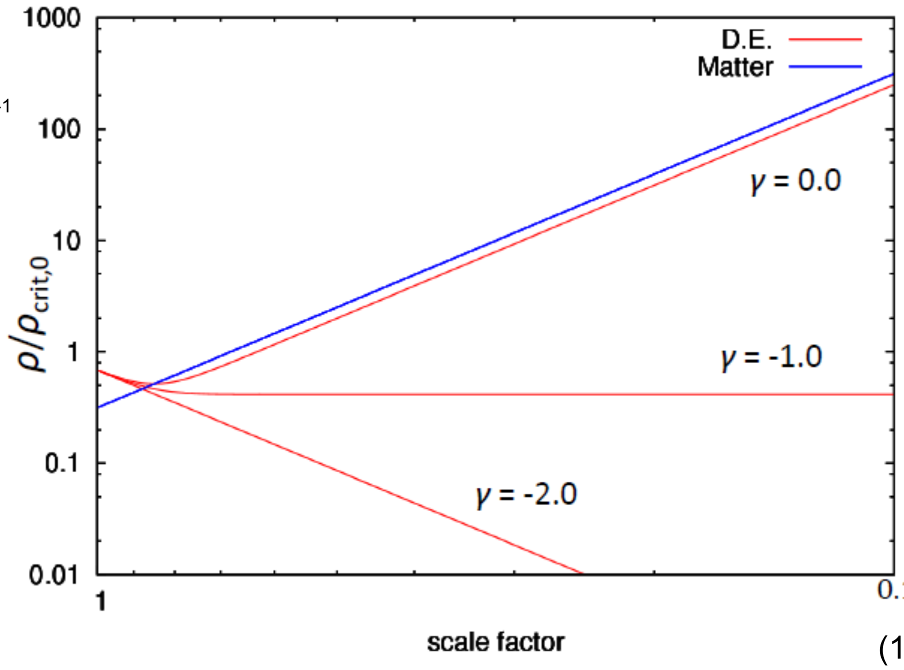

(11)

✓ Density evolution

✓ *ω*-dependencies

$$W_{DE(a)} = \frac{\omega a^{\beta} + \gamma}{a^{\beta} + 1}$$

H_0 = 70 $Kms^{-1}Mpc^{-1}$

Ω_m = 0.27

β = 20

γ = -1

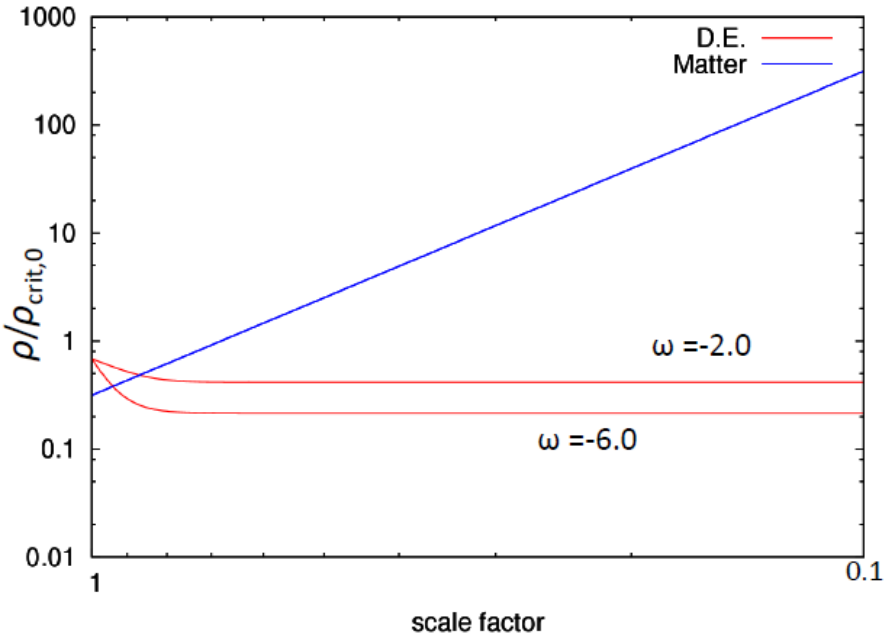

(12)

✓ Density evolution

✓ *β*-dependencies

$$W_{DE(a)} = \frac{\omega a^{\beta} + \gamma}{a^{\beta} + 1}$$

H_0 = 70 $Kms^{-1}Mpc^{-1}$

Ω_m = 0.27

ω = -6

γ = -1

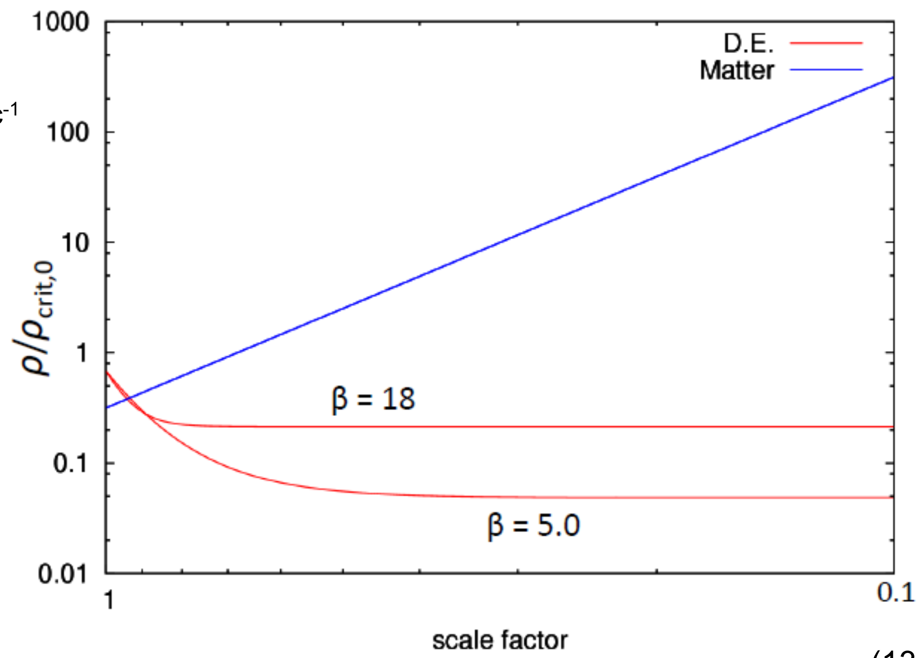

(13)

Magnitude Redshift relation in the modified EOS model

For Homogeneous Isotropic universe, Robetson Walker metric for photons;

$$\int_0^{t_0}\frac{dt}{a(t)}=\int_0^{r_p}\frac{dr}{\sqrt{(1-kr^2)}}\ \xrightarrow[H=\dot{a}/a]{a=1/(1+z)}\ \int_0^{z}\frac{dz}{H}=\int_0^{r_p}\frac{dr}{\sqrt{(1-kr^2)}}$$

$$\int_0^{z}\frac{dz}{H}=r_p, k=0$$

Flat universe [*Weinberg 2008*]

✓ Hubble Parameter

$$H^2=H_0^2\left[\Omega_0^{(M)}(1+z)^3+\Omega_0^{(DE)}(1+z)^{3(\omega+1)}\left[\frac{x_0^\beta+(1+z)^\beta}{x_0^\beta+1}\right]^{-3(\omega-\gamma)/\beta}\right]$$

The distance modulus μ_{th} of the source at the redshift z is,

$$\boxed{\mu_{th}=m-M=5\log_{10}(1+z)r_p+25} \tag{14}$$

Best Fit values for γ and ω

Variable EOS and ΛCDM

Best fit for

$H_0=70.6\pm3.3$ Kms^{-1}Mpc^{-1}

P.A.R.Ade al., 2015

$\Omega_0^M=0.271$

N.Suzuki et al.,2011

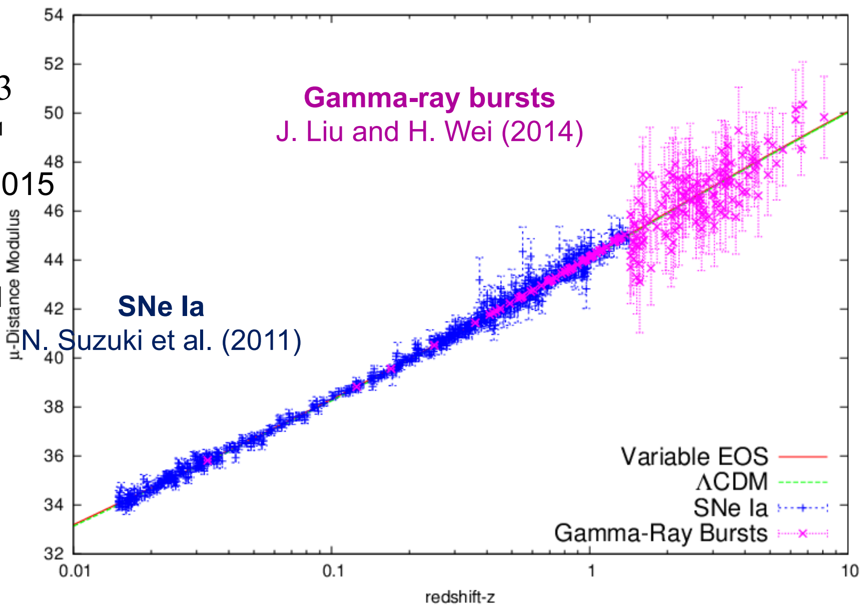

$$\boxed{\begin{aligned}\beta&=20\\ \gamma&=-0.88\\ \omega&=-1.04\end{aligned}}$$

$$\boxed{\chi_\gamma^2=\frac{\chi^2}{N}=\frac{729}{833}=0.87}\qquad\boxed{W_{DE,0}=-1.03} \tag{15}$$

MCMC method

Best Fit m-z relation for variable EoS

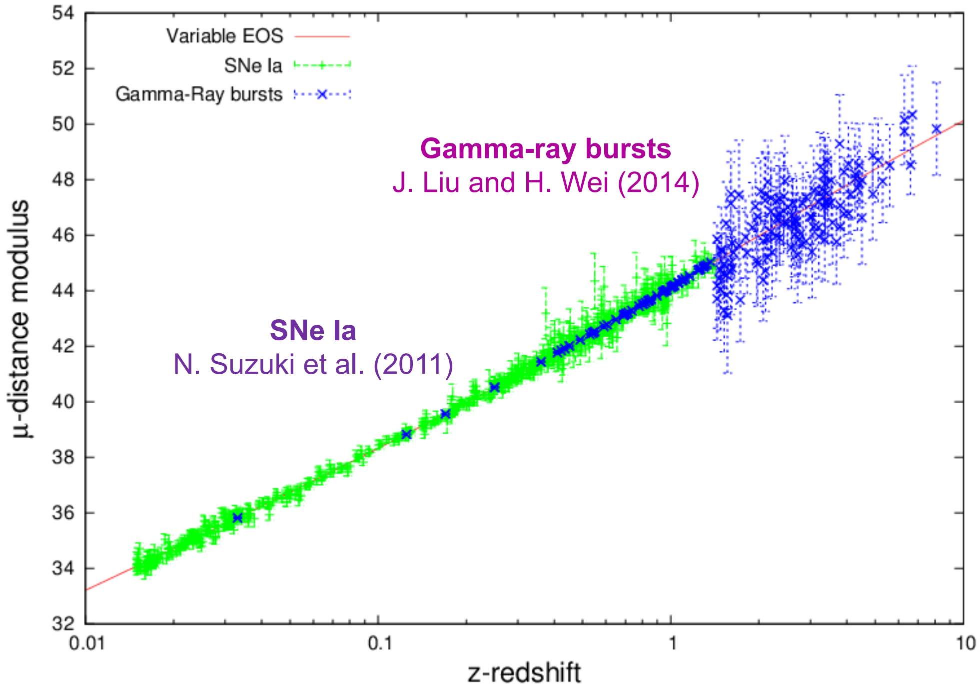

(13)

Results & Discussion

Model	ω	γ	H_0	Ω_m	$w_{DE,0}$	$\partial W_{DE} / \partial a$	χ^2 ($\Delta\chi^2$)
Variable EoS	**-1.01**	**-0.85**	**70.0**	**0.2755**	**-1.01**	**-8.12×10^{-3}**	**727.26 (0.00)**
Constant ω_{DE}	-1.03		69.9	0.2993	-1.03	0	728.85 (+1.59)
Fixed values	-1		69.8	0.2897	-1	0	729.35 (+2.09)

Model significance ..

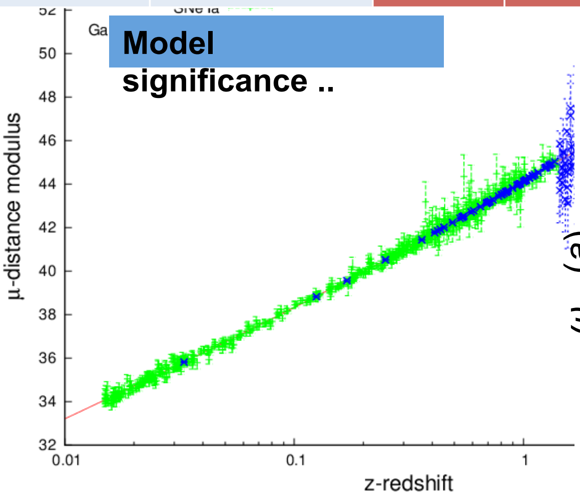

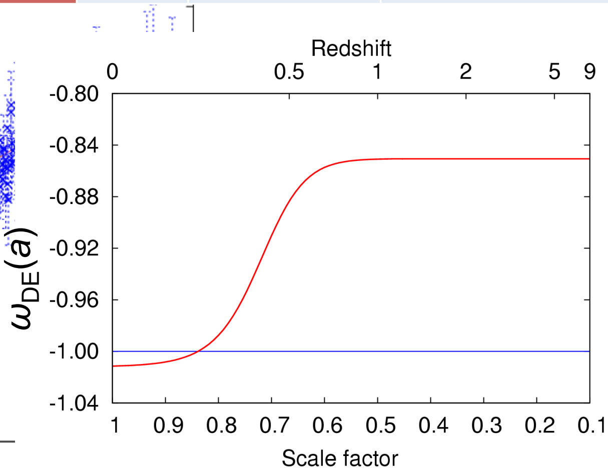

(16)

✓ MCMC results
Probability distributions

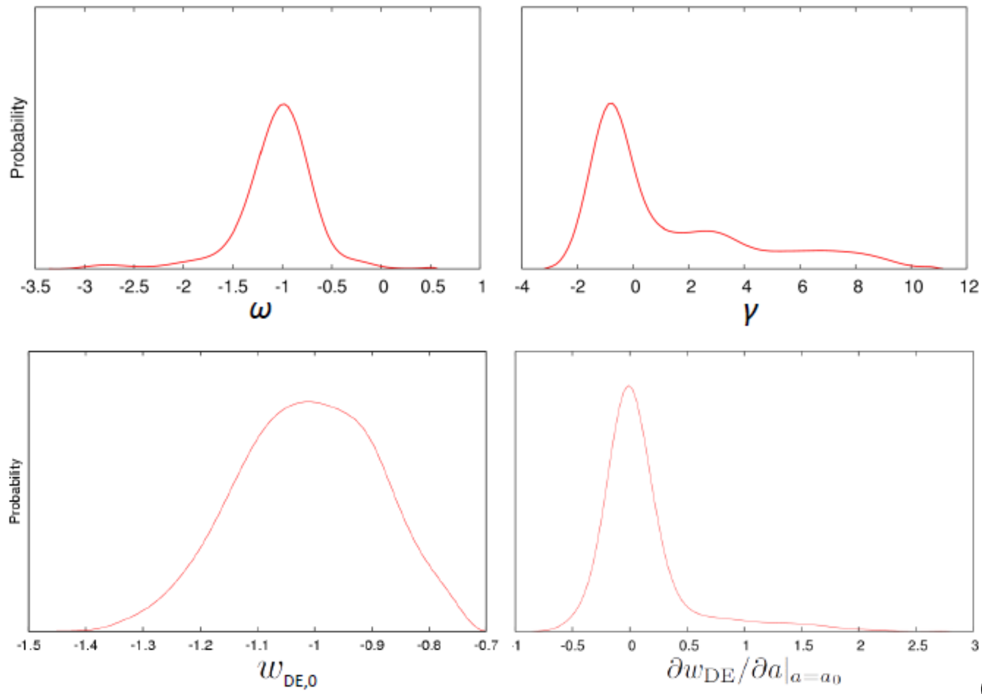

(17)

✓ MCMC results
Probability distributions

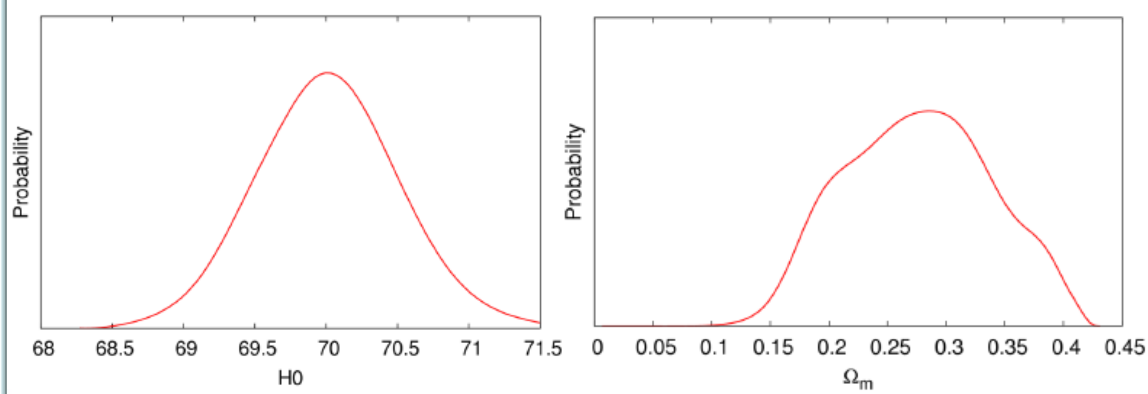

(18)

Summary….

✓ **Best fit parameters (1σ C.L.)**

SNe Ia + GRBs (N_{dof}= 833)

$w_{\mathrm{DE},0} = -1.01^{+0.12}_{-0.13}$

$\left.\frac{\partial w_{\mathrm{DE}}(a)}{\partial a}\right|_{a=a_0} = -8.12 \times 10^{-3}\,{}^{+0.161}_{-0.147}$

$\Omega_m = 0.275^{+0.066}_{-0.073}$

$H_0 = 70.04^{+0.43}_{-0.52}$

$\chi^2_{min} = 727.26$

Compatible with other results

This model moves to ΛCDM for low redshifts and $\gamma = \omega$

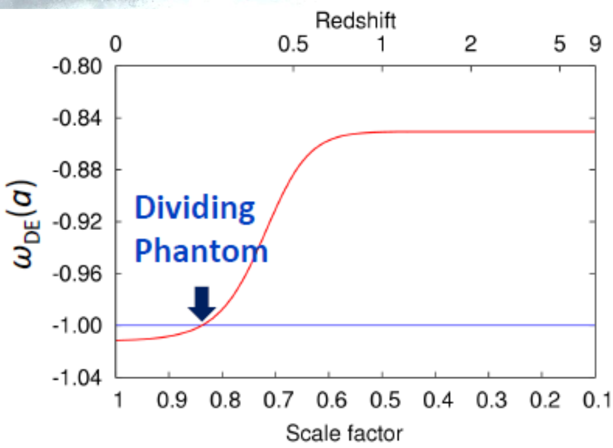

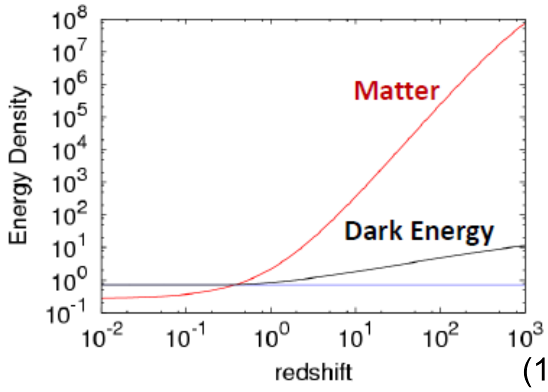

(19)

THANK YOU!

“Gravitational scalar-tensor theory”

by Atsushi Naruko

[JGRG25(2015)5b2]

Gravitational scalar-tensor theory

Atsushi NARUKO (TiTech = To-Ko-Dai)

with : Daisuke Yoshida (TiTech) Shinji Mukohyama (YITP)

arXiv : 1512.xxxxx (hopefully)

outline of my talk

1. Introduction
2. Model
3. Summary

Introduction

Accelerated expansion of the universe

- inflation (ancient) & dark energy (current)

$$\frac{\ddot{a}}{a} = -\frac{\rho + 3P}{6} \geq 0 \quad \Rightarrow \quad P \leq -\frac{\rho}{3} \quad \text{for} \quad \ddot{a} > 0$$

exotic matter ?? **change of gravity law ??**

- (canonical) scalar field :

$$\rho = \frac{1}{2}\dot{\phi}^2 + V(\phi)\,, \quad P = \frac{1}{2}\dot{\phi}^2 - V(\phi)\,, \quad \Rightarrow \quad P \approx -\rho$$

$$\text{if} \quad \dot{\phi}^2 \ll V$$

→ **scalar - tensor theory**

Einstein's General Relativity

- "**The classical theory of fields**" by Landau & Lifshitz,

  GR is a **unique theory of gravity** provided
  - composed by metric and its derivatives
  - covariant theory
  - 4D (Lovelock's theory in general)
  - EOM is (at most) 2nd order

- have to abandon one (or more) of assumptions above

  metric ? **covariance ?** **> 4D ?** **2nd order EOM ?**

f (R) theory

- The action is given by a **non-linear** function of **R**

- **EOM is 4th order** because $R \supset \ddot{g} + \dot{g}^2$

$$\int \mathrm{d}^4x \sqrt{-g}\, f(R) \sim \int \mathrm{d}^4x\, f(\ddot{g}) \;\rightarrow\; \ddot{f}(\ddot{g}) \supset \overset{\cdot\cdot\cdot\cdot}{g} \quad : \text{EOM}$$

- The evolution of the system is determined by
  initial position, velocity, acceleration & its derivative.

- **f (R) theory** is related with **a scalar-tensor theory**
  ➡ exotic matter = change of gravity law !!

f (R) = R + $\phi^{\text{canonical}}$

- Under a **Weyl (conformal) transformation**,

$$g_{\mu\nu} \to \Omega^2 g_{\mu\nu}$$

f (R) theory **=** Einstein + **canonical scalar**
(at classical level)

3 d.o.f.s **2 (GW) + 1 d.o.f.s**

Question

What if we introduce derivatives of R ?

What is the corresponding scalar-tensor theory ??

Model

The model

- The action is given by R and derivatives of R :

$$f\Big(R\,,\,(\nabla R)^2\,,\,\Box R\,,\cdots\Big) \qquad (\nabla R)^2 = g^{\mu\nu}\,\nabla_\mu R\,\nabla_\nu R$$

c.f. **f (Riemann)** theory
Deruelle et.al. (2009)

"Ostrogradsky's theorem"

- **A non-degenerate Lagrangian** $(\mathrm{d}^2L/\mathrm{d}\ddot{q}^2 \neq 0)$ dependent on time derivatives of higher than the first corresponds to a **linearly unstable Hamiltonian** associated with the Lagrangian via a Legendre tr. …

$$L = L(q\,,\dot{q}\,,\ddot{q})$$

$$H = P_1\,Q_2 + P_2\,f(Q_1\,,Q_2\,,P_2) - L(Q_1\,,Q_2\,,P_2)$$
$$(Q_1 = q\,,Q_2 = \dot{q})$$

→ **Hamiltonian is unbounded below**

- Although $f\Big(R\,,(\nabla R)^2\,,\Box R\,,\cdots\Big) \supset f\Big(g\,,\dot{g}\,,\ddot{g}\,,\cdots\Big)$ …

proof of healthiness

- replace **R** by **ϕ** introducing **λ** : $(\nabla R)^2 = g^{\mu\nu}\nabla_\mu R \nabla_\nu R$

$$f\Big(R\,,(\nabla R)^2\Big) = f\Big(\phi\,,(\nabla\phi)^2\Big) - \lambda(\phi - R)$$

- conformal transformation :

$$\widetilde{R} - (\widetilde{\nabla}\lambda)^2 - f\Big(\phi\,,2\lambda\,(\widetilde{\nabla}\phi)^2\Big) - \lambda\,\phi$$

- **ϕ** & **λ** are **healthy & dynamical d.o.f.s**

  ⇔ **R + k-essential multi-scalar fields**

- # of d.o.f.s : **2 (GW) + 2 (scalar)** (≠ **2 + 1** in f(R))

Genralisations

- KGB : $K\Big(R\,,(\nabla R)^2\Big) + G\Big(R\,,(\nabla R)^2\Big) \times \Box R$

- Horndeski, B-Horndeski terms can be included.
  (GAO will be also my friend)

$$Q\Big(R\,,(\nabla R)^2\Big)\,R + Q_X\Big(R\,,(\nabla R)^2\Big)\Big[(\Box R)^2 - (\nabla\nabla R)^2\Big]$$

  ⇔ equivalent to 2-field Horndeski

- Without specific combinations (e.g. $(\Box R)^2 - (\nabla\nabla R)^2$),
  non-linear term in □R is not allowed (induce ghost).

summary

summary

- We have considered a theory of gravity in which the action is given by R and derivatives of R.

- Despite the higher derivative nature of the action, the resultant system is healthy (if f is properly chosen) = no Ghost & no Ostrogradsky's instabilities

- # of d.o.f.s = 2(GW) + 2(scalar) ⇔ 2scalars-tensor theory

- Higher derivative terms (KGB, Horndeski, B-Horn) are also included.

Thank you
for your attention !!

“Compact stars in massive gravity”

by Taishi Katsuragawa

[JGRG25(2015)5b3]

JGRG25 @Kyoto Univ. 2015/12/9

Compact stars in massive gravity

Taishi Katsuragawa (Nagoya Univ.)

NAGOYA UNIVERSITY

In collaboration with
S. Nojiri (Nagoya Univ. & KMI), S.D. Odintsov (CSIC/IEEC-ICE, ICREA)
M. Yamazaki(Nagoya Univ.)

(Work in progress)

Alternative Theories to General Relativity

GR is simple but successful theory!

Planck (2013)

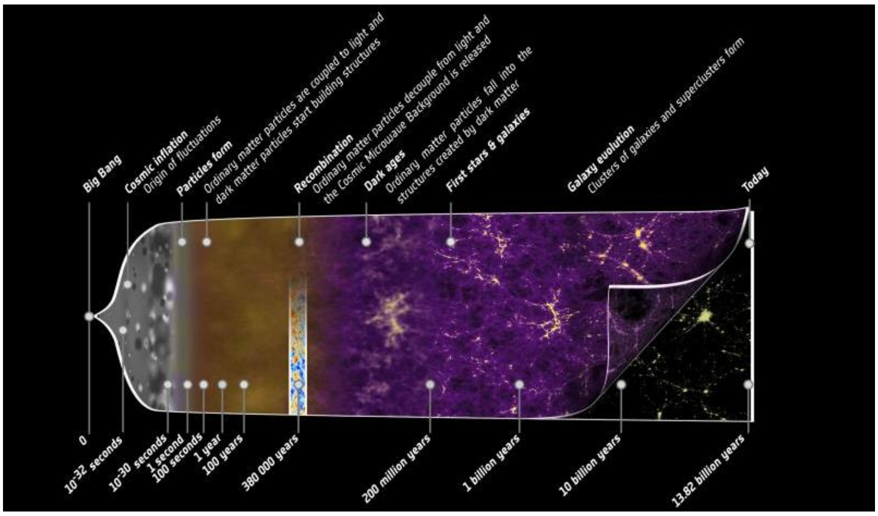

However, there are many reasons and motivations to consider alternative theories of gravity to GR.

Motivation for Modified Gravity

Low energy physics

The observations imply the existence of Dark energy and Dark matter.

- Cosmological constant problem $\Lambda_{theo} \sim 10^{120}\Lambda_{obs}$
- Origin of Cold Dark Matter etc.

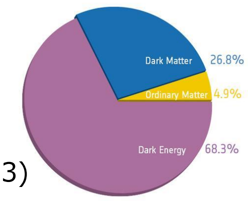

Planck (2013)

Strong-gravity regime

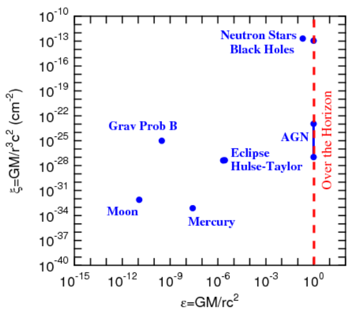

Psaltis (2008)

GR is well-tested in weak-gravity field (solar system w/ PPN) while it is **not in strong-gravity field.**

- Neutron Stars or Black Holes in modified gravity

Massive Neutron Stars

Recently, **Neutron Stars** whose mass is $M \sim 2M_{\odot}$ has been found. It could be hardly understood in the framework of GR with standard matter EoS...

Attractive force by gravity $\xleftrightarrow{\text{Balance}}$ Repulsive force by matter

→ We may need to modify matter EoS and/or Gravitational theory.

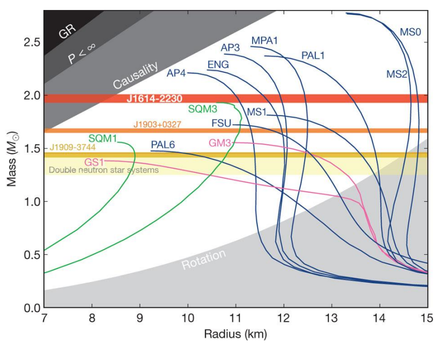

Demorest et al. (2010)

F(R) gravity can explain massive neutron star.

[Astashenok, Capozziello and Odintsov (2014)] etc.

Non-perturbative effects in strong-gravity regime depend on details of the theory.
→ we need **to study NS in other modified gravity.**

Massive graviton

If the graviton has a small mass, the gravitational force becomes weak at large scale because of Yukawa-type suppression, which may cause the accelerated expansion of Universe.

Theory of massive graviton without ghost problem
→ **de Rham-Gabadadze-Tolley (dRGT) massive gravity**

[de Rham, Gabadadze and Tolley (2011)]

The dRGT massive gravity is considered to be able to avoid the constraint from the experiments at short scale thanks to the Vainshtein mechanism.

→ What happens in strong-gravity field?

In this work, we study **relativistic stars**, quark star and neutron star, **in dRGT massive gravity**.

dRGT Massive Gravity

Action of dRGT massive gravity

$$S_{\mathrm{dRGT}} = \frac{1}{2\kappa^2}\int d^4x\sqrt{-\det(g)}\left[R - 2m_0^2\sum_{n=0}^{4}\beta_n e_n\left(\sqrt{g^{-1}f}\right)\right] + S_{\mathrm{matter}}$$

m_0 is graviton mass, and potential terms are

$$e_0(\mathbf{X}) = 1\,,\quad e_1(\mathbf{X}) = [\mathbf{X}]\,, e_2(\mathbf{X}) = \frac{1}{2}\left([\mathbf{X}]^2 - [\mathbf{X}^2]\right)\,,$$

$$e_3(\mathbf{X}) = \frac{1}{6}\left([\mathbf{X}]^3 - 3[\mathbf{X}][\mathbf{X}^2] + 2[\mathbf{X}^3]\right)\,, e_4(\mathbf{X}) = \det(\mathbf{X}) \quad [X] = X^{\mu}{}_{\mu}$$

Square-root of matrix $\left(\sqrt{g^{-1}f}\right)^{\mu}{}_{\rho}\left(\sqrt{g^{-1}f}\right)^{\rho}{}_{\nu} = g^{\mu\rho}f_{\rho\nu}$

$g_{\mu\nu}$ is dynamical metric, $f_{\mu\nu}$ is reference (non-dynamical) metric. We choose the reference metric by hand, which is corresponding to specifying a model of the massive gravity.

dRGT Massive Gravity

Equations of motion

$$
\begin{aligned}
0 =& R_{\mu\nu}(g) - \frac{1}{2}R(g)g_{\mu\nu} \\
&+ \frac{1}{2}m_0^2 \sum_{n=0}^{3}(-1)^n \beta_n \left[g_{\mu\lambda}Y^{\lambda}_{(n)\nu}(\sqrt{g^{-1}f}) + g_{\nu\lambda}Y^{\lambda}_{(n)\mu}(\sqrt{g^{-1}f})\right] - \kappa^2 T_{\mu\nu} \\
Y_0(\mathbf{X}) =& \mathbf{1}\,, \quad Y_1(\mathbf{X}) = \mathbf{X} - \mathbf{1}[\mathbf{X}]\,, \quad Y_2(\mathbf{X}) = \mathbf{X}^2 - \mathbf{X}[\mathbf{X}] + \frac{1}{2}\mathbf{1}\left([\mathbf{X}]^2 - [\mathbf{X}^2]\right)\,, \\
Y_3(\mathbf{X}) =& \mathbf{X}^3 - \mathbf{X}^2[\mathbf{X}] + \frac{1}{2}\mathbf{X}\left([\mathbf{X}]^2 - [\mathbf{X}^2]\right) - \frac{1}{6}\mathbf{1}\left([\mathbf{X}]^3 - 3[\mathbf{X}][\mathbf{X}^2] + 2[\mathbf{X}^3]\right)
\end{aligned}
$$

If $g_{\mu\nu}$ and $f_{\mu\nu}$ are diagonal, $\sqrt{g^{-1}f}$ is symmetric and EoMs are

$$
G_{\mu\nu} + m_0^2 I_{\mu\nu} = \kappa^2 T_{\mu\nu} \qquad I_{\mu\nu} = \sum_{n=0}^{3}(-1)^n \beta_n g_{\mu\lambda} Y^{\lambda}_{(n)\nu}(\sqrt{g^{-1}f})
$$

We assume minimal coupling with matter.

[de Rham, Heisenberg and Ribeiro (2014)] etc.

TOV equation

We study the static and spherical equations of motion with the perfect fluid in hydrostatic equilibrium, called the **Tolman-Oppenheimer-Volkoff (TOV) equation** in GR.
And, we use the Minkowski space-time for the reference metric.

$$
\begin{aligned}
g_{\mu\nu}dx^\mu dx^\nu &= -\mathrm{e}^{2\phi(r)}dt^2 + \mathrm{e}^{2\lambda(r)}dr^2 + r^2\left(d\theta^2 + \sin^2\theta d\varphi^2\right) \\
T_{\mu\nu} &= \mathrm{diag}\left(\mathrm{e}^{2\phi}\rho, \mathrm{e}^{2\lambda}P, r^2 P, r^2\sin^2\theta P\right) \\
f_{\mu\nu}dx^\mu dx^\nu &= -h(r)dt^2 + h^{-1}(r)dr^2 + r^2\left(d\theta^2 + \sin^2 d\varphi^2\right)\,, \quad h(r) = 1
\end{aligned}
$$

We fix the parameters β_n (minimal model).

$$
\beta_0 = 3\,, \quad \beta_1 = -1\,, \quad \beta_2 = 0\,, \quad \beta_3 = 0
$$

If we assume the conservation of energy-momentum, the potential terms have to be conserved, separately.

$$
\nabla_\mu\left(G^{\mu\nu} + m_o^2 I^{\mu\nu}\right) = \nabla_\mu T^{\mu\nu} \to \nabla_\mu I^{\mu\nu} = 0
$$

Fundamental equations

After introducing the dimensionless variables for numerical calculation, we find 2 EoMs + 1 constraint.

$$m'(r) = 4\pi\tilde{\rho}(r)r^2 + \underline{\frac{1}{2}\alpha^2 \left(r_g M_\odot\right)^2 r^2 \left[1 - \left(1 - \frac{2m(r)}{r}\right)^{1/2}\right]}$$

Corrections from mass term

$$8\pi p(r) = -\frac{2m(r)}{r^3} - \frac{2}{r}\left(1 - \frac{2m(r)}{r}\right)(p+\tilde{\rho})^{-1}p' + \underline{\alpha^2 \left(r_g M_\odot\right)^2 \left[1 - e^{\int (P+\tilde{\rho})^{-1}P' dr}\right]}$$

$$0 = \left(\frac{2}{r} - (p+\tilde{\rho})^{-1}p'\right)\left(1 - \frac{2m(r)}{r}\right)^{1/2} - \frac{2}{r} \qquad r_g = GM_\odot\,, \quad m_0 = \alpha M_\odot$$

$$\begin{aligned}
&8\pi p(r)q(r)r^3\left(1-\frac{1}{2}q(r)r\right)^3 \\
&= q(r)r\left(1-\frac{1}{2}q(r)r\right)(1-2q(r)r) - q(r)r\left(1-\frac{1}{2}q(r)r\right)^3 + \alpha^2\left(r_g M_\odot\right)^2 q(r)r^3\left(1-\frac{1}{2}q(r)r\right)^3 \\
&+ 8\pi p'(r)r^3\left(1-\frac{1}{2}q(r)r\right)^3 + 2\left(1-\frac{1}{2}q(r)r\right)(1-2q(r)r) - r\left(q'(r)r+q(r)\right)(1-2q(r)r) \\
&+ 2r\left(1-\frac{1}{2}q(r)r\right)\left(q'(r)r+q(r)\right) - 2\left(1-\frac{1}{2}q(r)r\right)^3 \qquad q = \frac{p'}{\tilde{\rho}+p'}
\end{aligned}$$

Space-time Outside the Star

Outside the stars, $\rho = p = 0$, we find

$$m'(r) = \frac{1}{2}\alpha^2 \left(r_g M_\odot\right)^2 r^2 \left[1 - \left(1 - \frac{2m(r)}{r}\right)^{1/2}\right]$$

α^2 is very small and $m'(r) \sim 0$ when r is smaller than the cosmological scale but larger than solar scale.
→ **$m(r)$ is almost constant**, and external geometry around relativistic star is approximately described by **Schwarzschild metric.**

When r becomes larger, $\frac{2m(r)}{r}$ becomes larger unboundedly, and $m(r)$ becomes **complex at finite value of** $r = r_{max}$.
→ **There is no geometry if $r > r_{max}$?**

For the cosmological scales, we cannot assume spherically symmetric space-time because there exist other stars and galaxies in the observable Universe.

Assumptions for Numerical Calculation

We study quark star and neutron star with 2 types of EoS.

Quark star : MIT Bag model

$$p = c(\rho - 4B) \qquad \text{c=0.28 B=60[MeV/fm}^3\text{]}$$

Neutron star : SLy model

$$\xi = \log(\rho/\mathrm{g\,cm^{-3}})\,, \quad \zeta = \log(P/\mathrm{dyn\,cm^{-2}})\,, \quad f_0(x) = \frac{1}{e^x + 1}$$

$$\begin{aligned}\zeta =& \frac{6.22 + 6.121\,\xi + 0.006004\,\xi^3}{1 + 0.16345\,\xi} f_0(6.50\,(\xi - 11.8440)) \\ &+ (17.24 + 1.065\,\xi) f_0(6.54\,(11.8421 - \xi)) \\ &+ (-22.003 + 1.5552\,\xi) f_0(9.3\,(14.19 - \xi)) \\ &+ (23.73 - 1.508\,\xi) f_0(1.79\,(15.13 - \xi))\end{aligned}$$

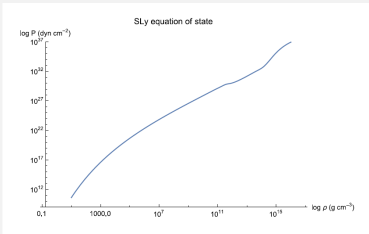

And, we assume $m_0 = \Lambda^{1/2}$ for accelerated expansion of Universe.

Quark Star

We solve ODE as initial value problem at $r = 0$.
Initial value of $p''(r = 0)$ is chosen so that the radius of star becomes identical with that in GR (Boundary condition).
We plot $m - \rho$ and $m - r$ in GR and massive gravity.

Mass-Central density

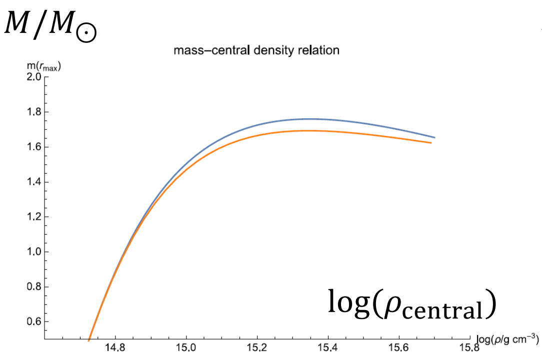

Mass-Radius

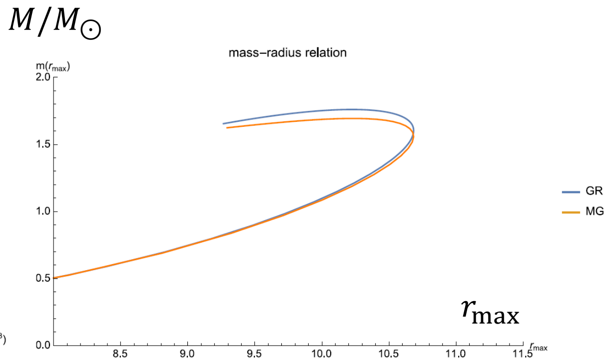

Neutron Star

For neutron star, the region of total mass is narrow compared with the case in GR.

Mass-Central density

Mass-Radius

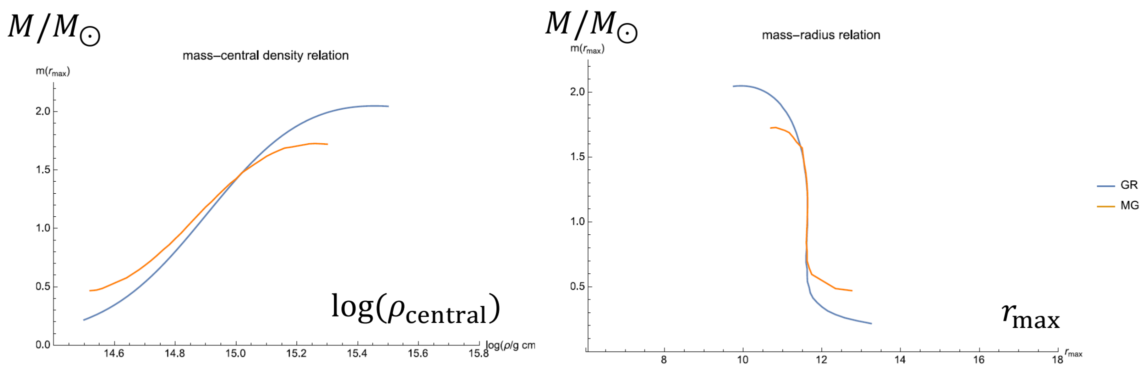

Consistency Check

We found the deviation from GR. However, we need to check the consistency...

2 EoMs + 1 constraint + 1 EoS = 4 equations
$m(r)$ + $p(r)$ + $\tilde{\rho}(r)$ = 3 variables

From the constraint, we find another differential equation

$$
\begin{aligned}
&8\pi\tilde{\rho}(r)q(r)r^3\left(1-\frac{1}{2}q(r)r\right)^3 \\
&= q(r)r\left(1-\frac{1}{2}q(r)r\right)^3 - q(r)r\left(1-\frac{1}{2}q(r)r\right) - q(r)r^2(q'(r)r+q(r)) \\
&\quad - \alpha^2\left(r_g M_\odot\right)^2 q(r)r^3\left(1-\frac{1}{2}q(r)r\right)^3 + \alpha^2\left(r_g M_\odot\right)^2 q(r)r^3\left(1-\frac{1}{2}q(r)r\right)^2
\end{aligned}
$$

We are checking the consistency now... If it is inconsistent, we need to change assumptions on $g_{\mu\nu}$ and $f_{\mu\nu}$.

Summary and Future Work

- Relativistic star with standard matter EoS in the dRGT massive gravity was investigated.
- TOV equation is corrected by the term proportional to the graviton mass, and one constraint appears.
- The mass-central density and mass-radius relation for quark star and neutron star were computed in numerical calculation.

✓ For quark star, the maximal mass gets smaller.
✓ For neutron star, the maximal mass gets smaller and the minimal mass gets larger.
✓ Theoretical structure is completely different from that in GR.
✓ Deviation from GR may derive from the constraint, which relates ρ and p with $m(r)$ inside star.

- [ ] Consistency check (Change the form of metric-ansatz?)
- [ ] Generalization to bigravity?

“Matter Creation in Generalized Galilean Genesis”

by Sakine Nishi

[JGRG25(2015)5b4]

Matter Creation in Generalized Galilean Genesis

Sakine Nishi (Rikkyo, D1)

in collaboration with Tsutomu Kobayashi (Rikkyo)
in preparation. [arXiv:1512.nnnnn]

JGRG25@Kyoto

Introduction

Introduction

- There are many kinds of models which explain the early universe.
- Inflation explains the observational result well.
- Galilean Genesis is an alternative to Inflation.

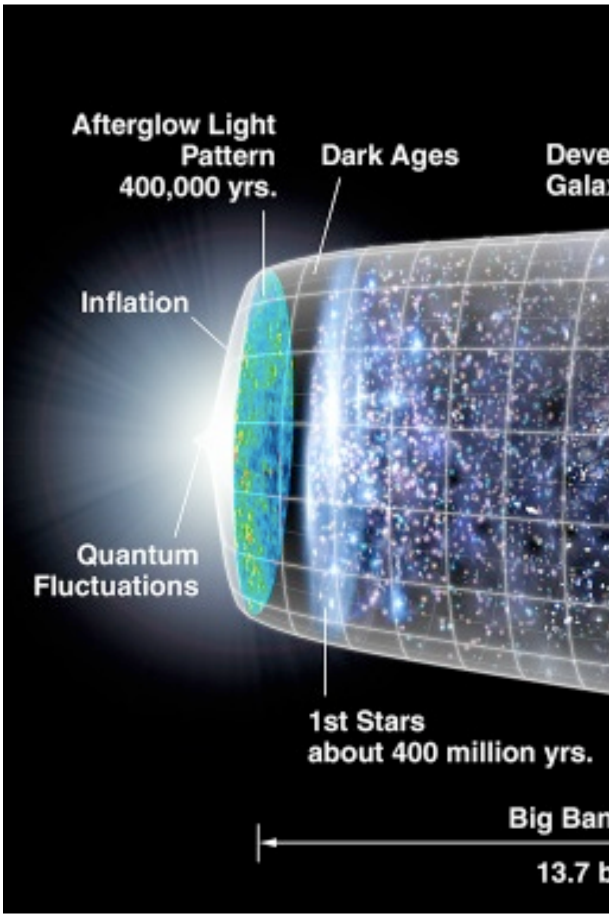

Introduction - motivation

- **Only inflation can explain the early universe?**
  compare genesis to the other inflation models and discuss observational implications.

In the previous study…

- Background evolution
- Perturbations
  - Scalar, Tensor

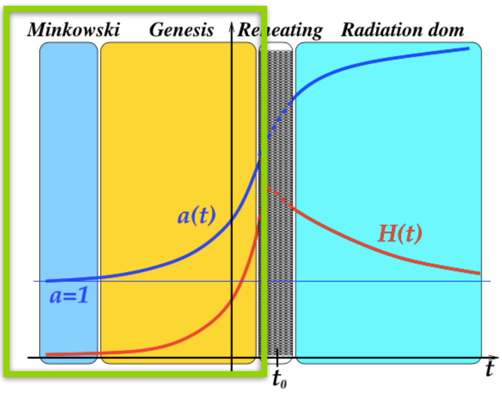

[P. Creminelli, A. Nicolis and E. Trincherini (2010)]

Introduction - motivation

- **Only inflation can explain the early universe?**
  compare genesis to the other inflation models and discuss observational implications.

In this talk…

- Matter creation
- Gravitational Waves

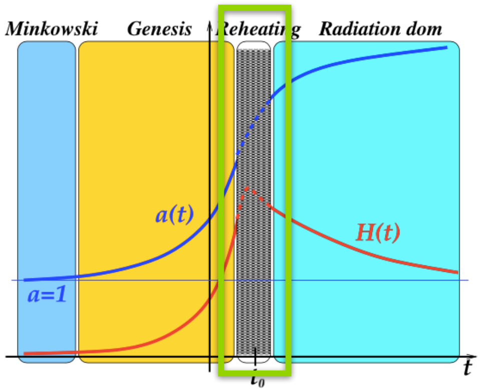

[P. Creminelli, A. Nicolis and E. Trincherini (2010)]

Outline

- Introduction
- Genesis
- Matter Creation
- Gravitational Waves
- Conclustion

Galilean Genesis

- Horndeski theory
- Original model
- Generalized model

Galilean Genesis - Horndeski theory

- The most general scalar-tensor theory
- Field eqs. have no 3rd and higher derivative terms
- Generalized Galilean Genesis is subclass of this theory.

$$
\begin{aligned}
S_{\rm Hor} = \int \mathrm{d}^4x\sqrt{-g}\Big\{ & G_2(\phi,X) - G_3(\phi,X)\Box\phi + G_4(\phi,X)R \\
& + G_{4X}\left[(\Box\phi)^2 - (\nabla_\mu\nabla_\nu\phi)^2\right] + G_5(\phi,X)G^{\mu\nu}\nabla_\mu\nabla_\nu\phi \\
& - \frac{1}{6}G_{5X}\left[(\Box\phi)^3 - 3\Box\phi(\nabla_\mu\nabla_\nu\phi)^2 + 2(\nabla_\mu\nabla_\nu\phi)^3\right]\Big\}
\end{aligned}
$$

$$X := -g^{\mu\nu}\partial_\mu\phi\partial_\nu\phi/2$$

[G. W. Horndeski (1974)]
[T. Kobayashi, M. Yamaguchi and J. Yokoyama (2011)]

Galilean Genesis - Original model

- Null energy condition is violated stably
- Original model is constructed in Galilean theory

$$\mathcal{S} = \int \mathrm{d}x^4 \sqrt{-g}\left[f^2 e^{2\phi}(\partial\phi)^2 + \frac{f^3}{\Lambda^3}(\partial\phi)^2\Box\phi + \frac{f^3}{2\Lambda^3}(\partial\phi)^4\right]$$

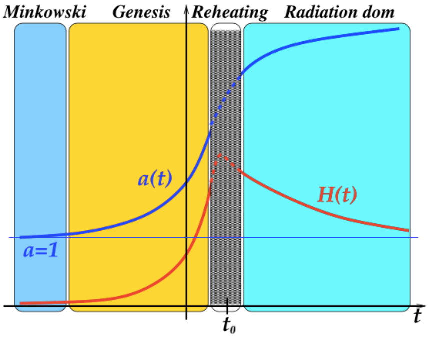

Solutions $\boxed{t \to -\infty}$

$$e^{\lambda\phi} \propto (-t)^{-1}$$

$$H(t) \simeq -\frac{f^2}{3M_{Pl}^2}\frac{1}{H_0^2 t^3}$$

$a(t) \simeq 1$ → Minkowski space-time

[P. Creminelli, A. Nicolis and E. Trincherini (2010)]

Galilean Genesis - Original model

- Null energy condition is violated stably
- Original model is constructed in Galilean theory

$$\mathcal{S} = \int \mathrm{d}x^4 \sqrt{-g}\left[f^2 e^{2\phi}(\partial\phi)^2 + \frac{f^3}{\Lambda^3}(\partial\phi)^2\Box\phi + \frac{f^3}{2\Lambda^3}(\partial\phi)^4\right]$$

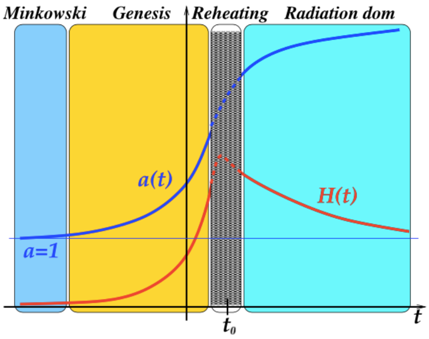

Solutions $\boxed{t \to t_0}$

$$a(t) = \exp\left[\frac{8f^2}{3H_0^2 M_{Pl}^2}\frac{1}{(t_0 - t)^2}\right]$$

$$H(t) \simeq \frac{16 f^2}{3M_{Pl}^2}\frac{1}{H_0^2(t_0 - t)^3}$$

[P. Creminelli, A. Nicolis and E. Trincherini (2010)]

Galilean Genesis - Generalized model

- include the various models of Genesis
- parameter α
  arbitrary function $g_i(Y)$

$$G_2 = e^{2(\alpha+1)\lambda\phi} g_2(Y), \quad G_3 = e^{2\alpha\lambda\phi} g_3(Y),$$

$$G_4 = \frac{M_{\rm Pl}^2}{2} + e^{2\alpha\lambda\phi} g_4(Y), \quad G_5 = e^{-2\lambda\phi} g_5(Y). \quad Y := e^{-2\lambda\phi} X$$

- Example - Original model

$$g_2 = 2f^2 Y + 2\frac{f^3}{\Lambda^3} Y^2, \quad g_3 = 2\frac{f^3}{\Lambda^3} Y, \quad g_4 = g_5 = 0, \quad \alpha = \lambda = 1$$

[S. Nishi, T. Kobayashi, (2015)]

Galilean Genesis

- Solutions
- $t \to -\infty$ $\quad a(t) \to a_G$
  Minkowski
- $t \to 0$ $\quad a(t) \to \infty$
  diverge

$$e^{\lambda\phi} \simeq \frac{1}{\lambda\sqrt{2Y_0}} \frac{1}{(-t)}$$

$$H \simeq \frac{h_0}{(-t)^{2\alpha+1}}$$

$$a \simeq a_G \left[1 + \frac{1}{2\alpha} \frac{h_0}{(-t)^{2\alpha}}\right]$$

de-Sitter inflation $\quad H_{inf} = \text{const.}$

Genesis $\quad H$ decrease

$$(-\infty < t < 0)$$

[S. Nishi, T. Kobayashi, (2015)]

Matter Creation

- scenario
- gravitational particle production
- conditions

Matter Creation - scenario

- Massless scalar field matter χ is generated.

$$\mathcal{L}_\chi = -\frac{1}{2} g^{\mu\nu}\partial_\mu\chi\partial_\nu\chi$$

- Genesis $\downarrow$ Kination

at the end of genesis

$$a \simeq a_G \left[1 + \underbrace{\frac{1}{2\alpha}\frac{h_0}{(-t)^{2\alpha}}}_{= \delta_* \ll 1}\right]$$

$$\mathcal{L} \simeq \frac{M_{Pl}^2}{2} R + X$$ (X : Kinetic term)

Matter Creation - scenario

- Massless scalar field matter χ is generated.

$$\mathcal{L}_\chi = -\frac{1}{2} g^{\mu\nu} \partial_\mu \chi \partial_\nu \chi$$

- Genesis at the end of genes

$\downarrow$

Kination

$$\mathcal{L} \simeq \frac{M_{Pl}^2}{2} R + X \quad (\qquad \lesssim 1$$

× potential
× oscillation

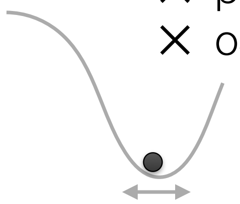

Matter Creation - scenario

- Massless scalar field matter χ is generated.

$$\mathcal{L}_\chi = -\frac{1}{2} g^{\mu\nu} \partial_\mu \chi \partial_\nu \chi$$

- Genesis at the end of genes

$\downarrow$

Kination

$$\mathcal{L} \simeq \frac{M_{Pl}^2}{2} R + X \quad (\qquad \lesssim 1$$

interaction

$$\phi \longleftrightarrow g_{\mu\nu} \longleftrightarrow \chi$$

Matter Creation - scenario

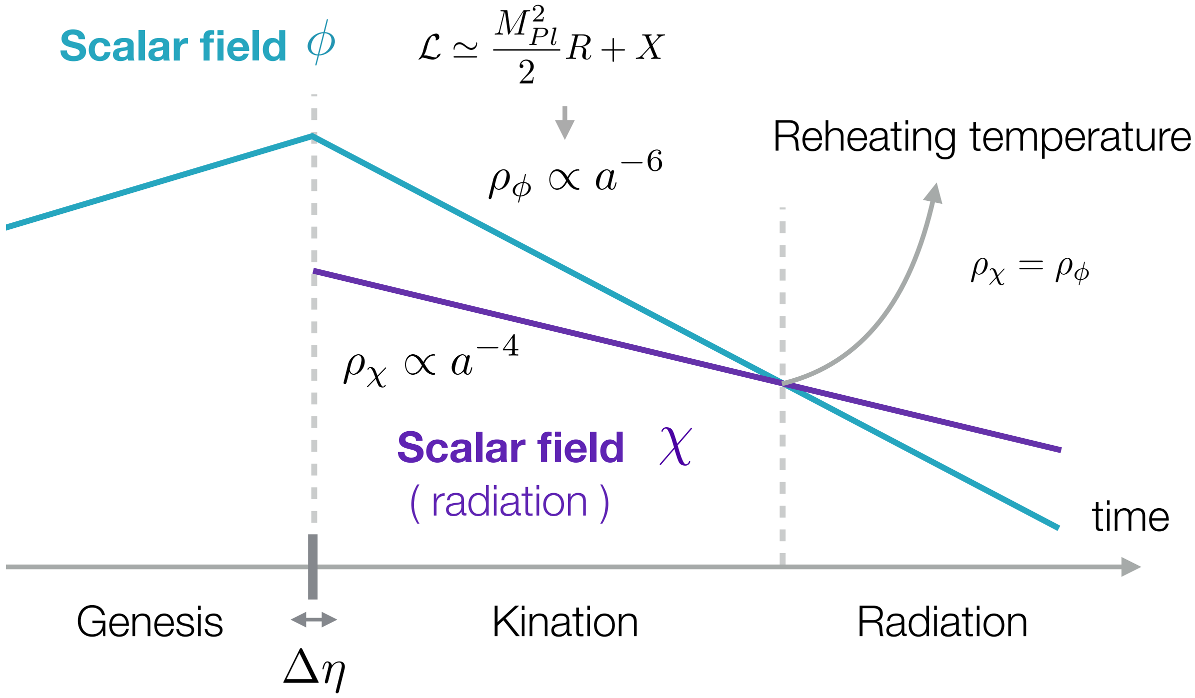

Matter Creation

- Solution of χ

$$a(\eta)\chi_k(\eta) = \frac{\alpha_k(\eta)}{\sqrt{2k}} e^{ik\eta} + \frac{\beta_k(\eta)}{\sqrt{2k}} e^{-ik\eta}$$

- Definition of β_k and energy density

$$\beta_k(\eta) = -\frac{i}{2k} \int_{-\infty}^{\eta} e^{-2iks} \frac{a''}{a} \mathrm{d}s \qquad \rho_\chi = \frac{1}{2\pi^2 a^4} \int_0^\infty k^3 \left|\beta_k(\infty)\right|^2 \mathrm{d}k$$

$$\downarrow$$

$$\rho_\chi = -\frac{1}{128\pi^2 a^4} \int_{-\infty}^{\infty} \mathrm{d}\eta_1 \int_{-\infty}^{\infty} \mathrm{d}\eta_2 \ln(|\eta_1 - \eta_2|) V'(\eta_1) V'(\eta_2)$$

[L. Ford (1987)] [T. Kunimitsu, J. Yokoyama (2012)]

Matter Creation

We do not have the analytical solution.

$$\rho_\chi = -\frac{1}{128\pi^2 a^4}\int_{-\infty}^{\infty} \mathrm{d}\eta_1 \int_{-\infty}^{\infty} \mathrm{d}\eta_2 \ln(|\eta_1 - \eta_2|)V'(\eta_1)V'(\eta_2)$$

$$V(\eta) = \frac{f''f - (f')^2/2}{f^2}$$

$$f(\eta) := a^2(\eta)$$

- set
  genesis ends at $\eta = \eta_*$
  kination starts at $\eta = \eta_* + \Delta\eta$
- seek
  $V(\eta)$ in $\Delta\eta$

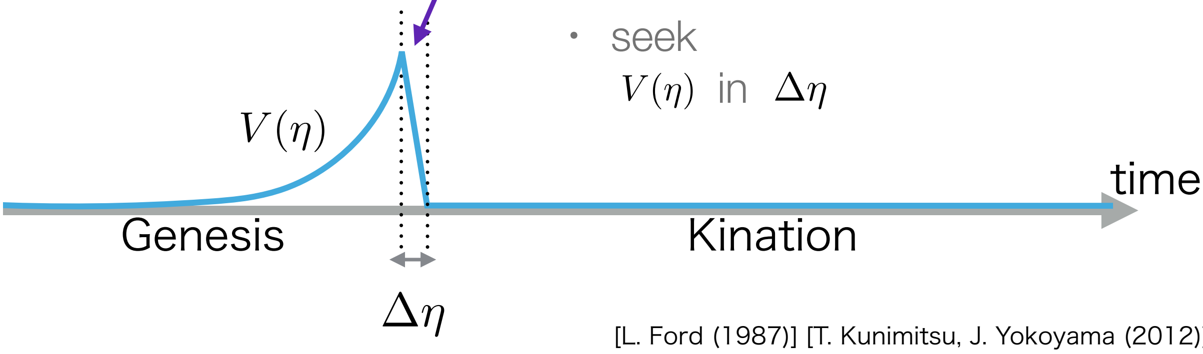

[L. Ford (1987)] [T. Kunimitsu, J. Yokoyama (2012)]

Matter Creation

$V(\eta)$ is approximately a straight line.

$$\rho_\chi = -\frac{1}{128\pi^2 a^4}\int_{-\infty}^{\infty} \mathrm{d}\eta_1 \int_{-\infty}^{\infty} \mathrm{d}\eta_2 \ln(|\eta_1 - \eta_2|)V'(\eta_1)V'(\eta_2)$$

$$V(\eta) = \frac{f''f - (f')^2/2}{f^2}$$

$$f(\eta) := a^2(\eta)$$

- assume
  $f(\eta) = b_0 + b_1\eta + b_2\eta^2 + b_3\eta^3$

$$f(\eta) = c_0\frac{\eta}{(-\eta_*)} + c_1$$

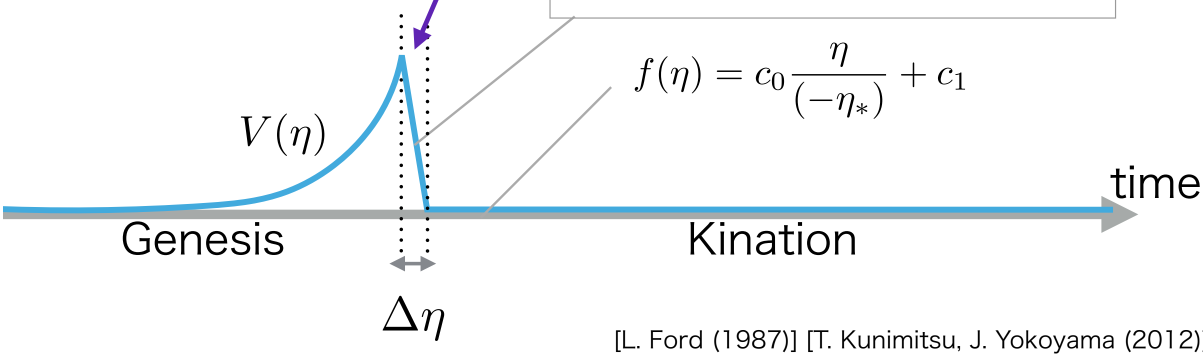

[L. Ford (1987)] [T. Kunimitsu, J. Yokoyama (2012)]

Matter Creation

- Therefore…

Matter χ is generated in $\Delta\eta$

$$\rho_\chi = \frac{(2\alpha+1)^2}{32\pi^2}\left[\frac{3}{2} + \underbrace{\ln\left(\frac{1}{\Delta\eta}\right)}_{\text{assume } \mathcal{O}(1)}\right]\frac{h_0^2}{(-t_*)^{4(\alpha+1)}}\left(\frac{a_G}{a}\right)^4$$

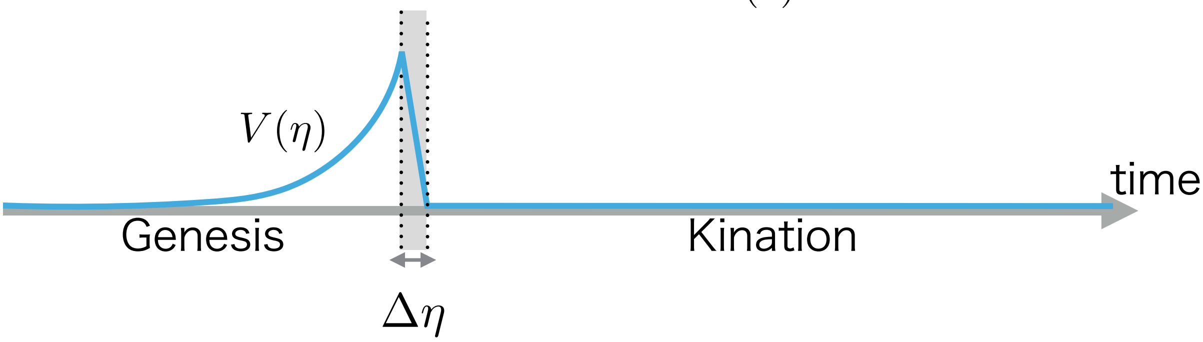

Matter Creation

in inflation $T_R \sim \frac{H_{inf}^2}{M_{Pl}}$

Reheating temperature

$$T_R = \left(\frac{30}{\pi^2 g_*}\right)^{1/4}\frac{A^{3/4}}{\sqrt{3}(32\pi^2)^{3/4}(2\alpha)^{3/2}}\frac{H_*^2}{M_{Pl}\delta_*^{3/2}}$$

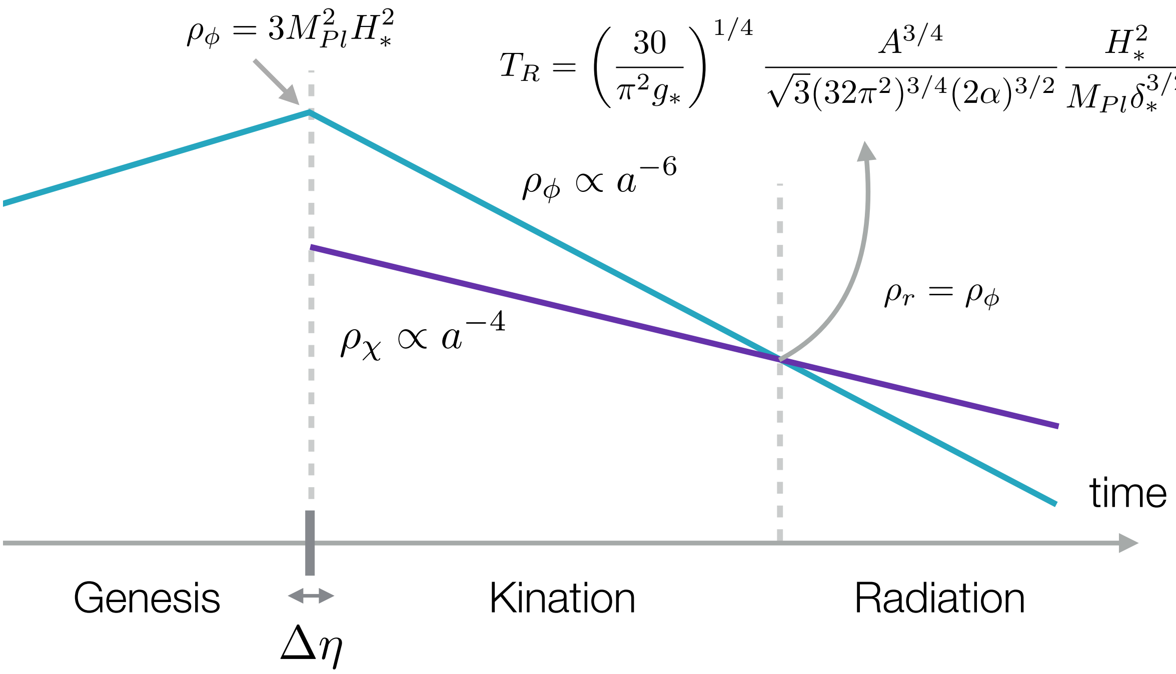

Gravitational Waves

- spectrum
- Examples

Gravitational Waves

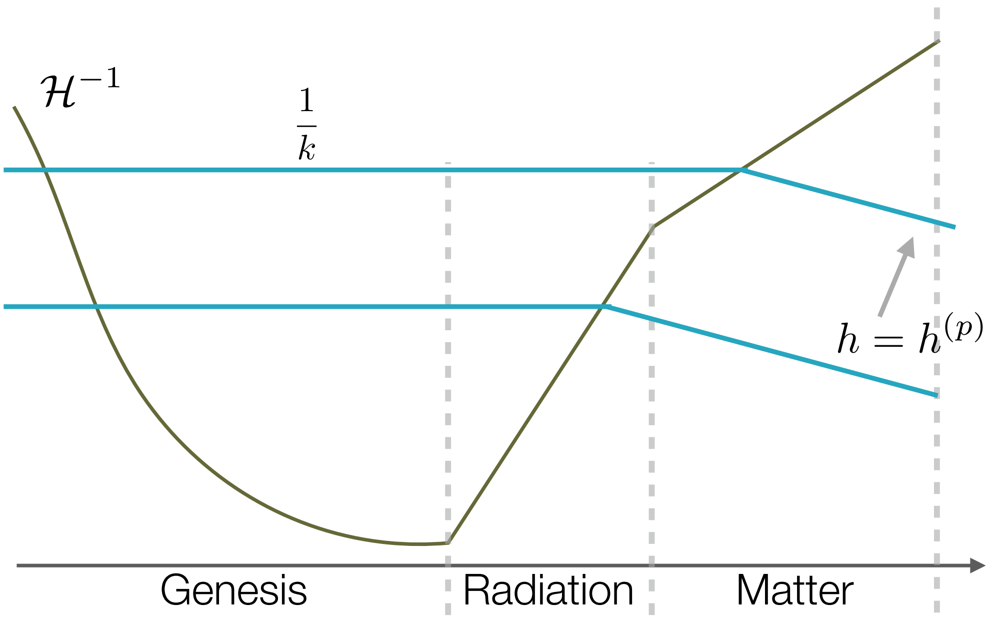

Gravitational Waves

$$\Omega_{\rm gw} = \Omega_{\rm gw}^{(p)}(k) \times \begin{cases} \frac{k_R}{k}\frac{k_{\rm eq}^2}{k_R^2}\frac{k_0^4}{k_{\rm eq}^4} & (k_R < k < k_*) \\ \frac{k_{\rm eq}^2}{k^2}\frac{k_0^4}{k_{\rm eq}^4} & (k_{\rm eq} < k < k_R) \\ \frac{k_0^4}{k^4} & (k_0 < k < k_{\rm eq}) \end{cases}$$

Kination

Radiation

Matter

- h_k do not grow in genesis.

$$h_k = \frac{1}{a}\sqrt{\frac{2}{\mathcal{G}c_t k}}e^{-ic_t k\eta}$$

- $|h_k|$ do not change at the horizoncross.

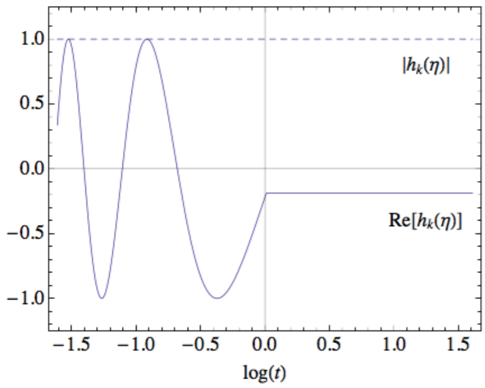

Gravitational Waves

$$\Omega_{\rm gw} = \begin{cases} \propto k^3 & (k_R < k < k_*) \\ \propto k^2 & (k_{\rm eq} < k < k_R) \\ \text{const.} & (k_0 < k < k_{\rm eq}) \end{cases}$$

$$\downarrow$$

$$\Omega_{gw}(k_R) \simeq \left(\frac{H_*}{M_{Pl}}\right)^2\left(\frac{a_R}{a_G}\right)^{-4} \times 10^{-5}$$

$$\Omega_{gw}(k_*) \simeq \left(\frac{H_*}{M_{Pl}}\right)^2\left(\frac{a_R}{a_G}\right)^{2} \times 10^{-5}$$

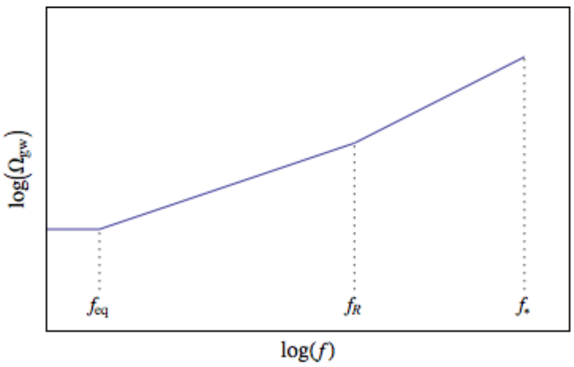

Gravitational Waves

- Inflation
- Genesis

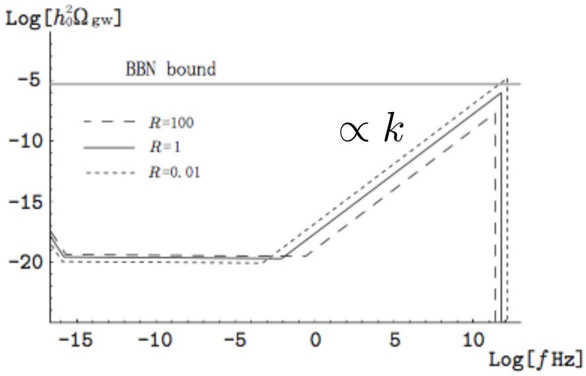

[H. Tashiro, T. Chiba, M. Sasaki, (2012)]

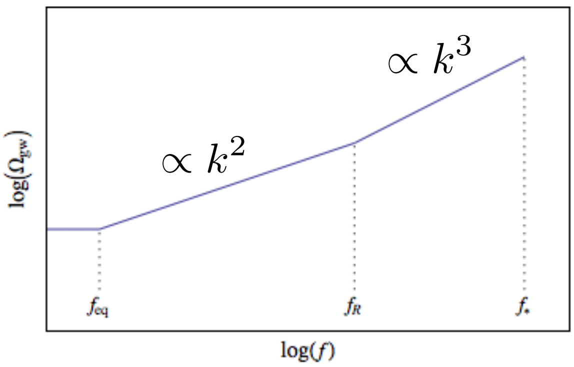

Gravitational Waves

- genesis

$$\boxed{\Omega_{gw}(k_R) \simeq \left(\frac{H_*}{M_{Pl}}\right)^2 \left(\frac{a_R}{a_G}\right)^{-4} \times 10^{-5}}$$

$$\Omega_{gw}(k_*) \simeq \left(\frac{H_*}{M_{Pl}}\right)^2 \left(\frac{a_R}{a_G}\right)^2 \times 10^{-5}$$

- inflation

$$\boxed{\Omega_{gw}^{inf} \simeq \left(\frac{H_{inf}}{M_{Pl}}\right)^2 \times 10^{-5}}$$

Ω_{gw}^{gen} can not be larger than Ω_{gw}^{inf}

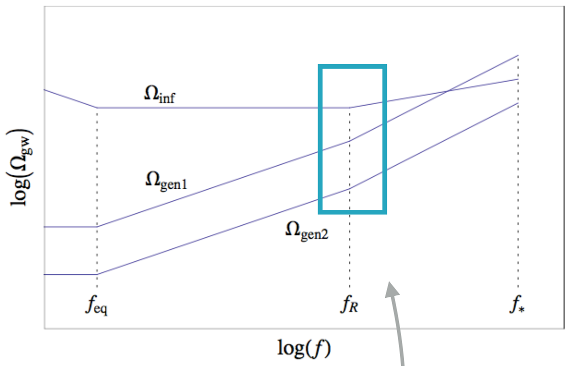

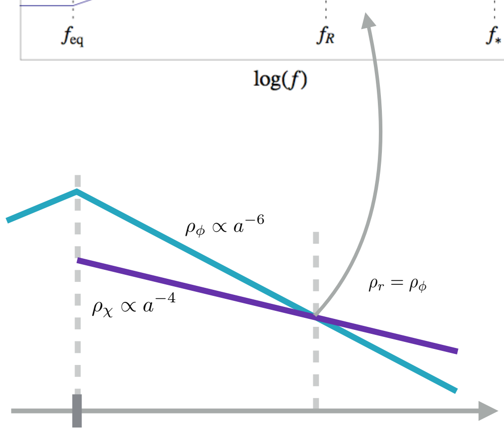

Gravitational Waves - example 1

- Original model

$$g_2 = -2f^2 Y + \frac{2f^3}{\Lambda^3} Y^2, \quad g_3 = \frac{2f^3}{\Lambda^3} Y,$$
$$g_4 = g_5 = 0, \quad \lambda = 1, \quad \alpha = 1,$$

↓

$$\Omega_{\rm gw}(k_R) \simeq 10^{-31} \left(\frac{g_*}{106.75}\right)^{5/6} \left(\frac{f}{\Lambda}\right) \left(\frac{T_R}{10^{10}\,\mathrm{GeV}}\right)^{10/3}$$
$$\Omega_{\rm gw}(k_*) \simeq 10^{-10} \left(\frac{g_*}{106.75}\right)^{1/3} \left(\frac{f}{\Lambda}\right)^4 \left(\frac{T_R}{10^{10}\,\mathrm{GeV}}\right)^{4/3}$$

frequency

$$f_* = 10^9 \left(\frac{g_*}{106.75}\right)^{1/6} \left(\frac{f}{\Lambda}\right) \left(\frac{T_R}{10^{10}\,\mathrm{GeV}}\right)^{2/3} \ \mathrm{Hz}$$

Gravitational Waves - example 2

- $\alpha = 2$ (the scale invariant curvature perturbation)

$$g_2 = 2f^2 Y + \frac{2f^3}{\Lambda^3} Y^2, \quad g_3 = \frac{2f^3}{\Lambda^3} Y,$$
$$g_4 = g_5 = 0, \quad \lambda = 1,$$

↓

$$\Omega_{\rm gw}(k_R) \simeq 10^{-32} \left(\frac{g_*}{106.75}\right)^{7/8} \left(\frac{M_{Pl} f^2}{\Lambda^3}\right)^{1/2} \left(\frac{T_R}{10^{10}\,\mathrm{GeV}}\right)^{7/2}$$
$$\Omega_{\rm gw}(k_*) \simeq 10^{-17} \left(\frac{g_*}{106.75}\right)^{1/2} \left(\frac{M_{Pl} f^2}{\Lambda^3}\right)^2 \left(\frac{T_R}{10^{10}\,\mathrm{GeV}}\right)^2$$

frequency

$$f_* = 10^8 \left(\frac{g_*}{106.75}\right)^{1/24} \left(\frac{M_{Pl} f^2}{\Lambda^3}\right)^{1/2} \left(\frac{T_R}{10^{10}\,\mathrm{GeV}}\right)^{1/2} \ \mathrm{Hz}$$

Gravitational Waves - example 3

- dependence of α

  assume the energy scales $\mu \sim \Lambda \sim f, \quad \lambda = \dfrac{1}{\mu}$

$$\downarrow$$

$$\Omega_{gw}(k_R) \propto \left(\frac{T_R}{M_{Pl}}\right)^{\frac{4\alpha+6}{\alpha+2}} \left(\frac{\mu}{M_{Pl}}\right)^{\frac{2(1-\alpha)}{\alpha+2}}$$

$$\Omega_{gw}(k_*) \propto \left(\frac{T_R}{M_{Pl}}\right)^{\frac{4\alpha+1}{\alpha+2}} \left(\frac{\mu}{M_{Pl}}\right)^{\frac{7(1-\alpha)}{\alpha+2}}$$

Conclusion

Conclusion

- H_* of genesis can be smaller than that of inflation.
- Ω_{gw}^{gen} in Genesis is smaller than that of inflation in $k < k_R$.
- How we set the energy scale and the parameter α is important for the detection of GWs in $k_R < k < k_*$.

Matter Creation scenario

- Massless
- Genesis

↓

Kination

How $\mathcal{L}$ changes ?

In Genesis

$$S_{\mathrm{Hor}} = \int \mathrm{d}^4x\sqrt{-g}\Big\{G_2(\phi,X) - G_3(\phi,X)\Box\phi + G_4(\phi,X)R + G_{4X}\left[(\Box\phi)^2 - (\nabla_\mu\nabla_\nu\phi)^2\right] + G_5(\phi,X)G^{\mu\nu}\nabla_\mu\nabla_\nu\phi - \frac{1}{6}G_{5X}\left[(\Box\phi)^3 - 3\Box\phi(\nabla_\mu\nabla_\nu\phi)^2 + 2(\nabla_\mu\nabla_\nu\phi)^3\right]\Big\}$$

$$G_2 = e^{2(\alpha+1)\lambda\phi}g_2(Y), \quad G_3 = e^{2\alpha\lambda\phi}g_3(Y),$$

$$G_4 = \frac{M_{\mathrm{Pl}}^2}{2} + e^{2\alpha\lambda\phi}g_4(Y), \quad G_5 = e^{-2\lambda\phi}g_5(Y). \quad Y := e^{-2\lambda\phi}X$$

$= \delta_* \ll 1$

$$\mathcal{L} \simeq \frac{M_{Pl}^2}{2}R + X \quad (\text{X : Kinetic term})$$

Matter Creation scenario

- Massless
- Genesis

↓

Kination

How $\mathcal{L}$ changes ?

introduce ↓ in $g_2(Y)$

$$S = \int d^4x\,\sqrt{-g}\left[\frac{1}{2}M_{\mathrm{Pl}}^2R + f^2\boxed{\frac{e^{2\pi}}{1+\beta e^{2\pi}}}(\partial\pi)^2 + \frac{f^3}{\Lambda^3}(\partial\pi)^2\Box\pi + \frac{f^3}{2\Lambda^3}(\partial\pi)^4\right]$$

[D. Pirtskhalava, L. Santoni, E. Trincherini, P. Uttayarat (2014)]

$= \delta_* \ll 1$

$$\mathcal{L} \simeq \frac{M_{Pl}^2}{2}R + X \quad (\text{X : Kinetic term})$$

“Instability of hairy black holes in shift-symmetric Horndeski theories”

by Hiromu Ogawa

[JGRG25(2015)5b5]

Instability of Hairy Black Holes in shift-symmetric Horndeski theories

arXiv:1510.07100

JGRG25
Dec. 7th-11th@ **Kyoto Univ.**

Hiromu Ogawa
Tsutomu Kobayashi
Rikkyo Univ.

Teruaki Suyama
RESCEU

Introduction&Motivation

Hairy BH in shift-symmetric scalar-tensor theory

Introduction

BH hair in scalar tensor (ST) theory

No-hair theorem holds in many ST theories

BH hair
mass, charge, angular momentum

Brans-Dicke theory

$$\mathcal{L} = \frac{R}{2} - \frac{1}{2}(\partial\phi)^2 - U(\phi)$$ (in Einstein frame)

Hawking (1972); Bekenstein (1996)……

Covariant Galileon

$$\mathcal{L} \supset (\partial\phi)^2\Box\phi, \cdots$$ (spherically symmetric BHs)

Hui, Nicolis (2013)

and more…

However…

One consider shift-symmetric ST theory **with time-dependent scalar field**

$\longrightarrow$ BH solutions are found with non-trivial **scalar hair**

Bavichev, Charmousis(2014)

Bavichev, Charmousis(2014)

Dressing BH in shift-symmetric ST theory

Shift & reflection symmetry: $\phi \to \phi + \text{const.}, \quad \phi \to -\phi$

$$\mathcal{L} = [\zeta R - \eta(\partial\phi)^2 + \beta G^{\mu\nu}\partial_\mu\phi\partial_\nu\phi - 2\Lambda]$$

$\zeta > 0, \eta, \beta : \text{const}$
$\Lambda :$ cosmological constant

Shift symmetry

$\phi \to \phi + \text{const.}$ $\longrightarrow$

EOM for scalar

$$\nabla_\mu J^\mu = 0$$

$$J^\mu = (\eta g^{\mu\nu} - \beta G^{\mu\nu})\partial_\nu\phi$$

Assumptions in Bavichev and Charmousis paper

$ds^2 = -A(r)dt^2 + \frac{1}{B(r)}dr^2 + r^2 d\Omega^2$ static and spherical symmetric

$J^r = 0$ $\longrightarrow$ Current $J^2 = J_\mu J^\mu$ regular at the horizon

$\phi(t,r) = qt + \psi(r)$ $\longrightarrow$ **Space-time is static in shift-symmetric theory**

Bavichev, Charmousis(2014)

Dressing BH in **shift-symmetric ST theory**

Shift & reflection symmetry: $\phi \to \phi + \text{const.}, \quad \phi \to -\phi$

$$\mathcal{L} = [\zeta R - \eta(\partial\phi)^2 + \beta G^{\mu\nu}\partial_\mu\phi\partial_\nu\phi - 2\Lambda]$$

$\zeta > 0, \eta, \beta : \text{const}$

$\Lambda :$ cosmological constant

does not contain bare ϕ

contain derivative term $\partial_\mu\phi$

→ Time dependence term dose not appear in the theory.

(* We are not afraid that value of scalar field is unbound.)

$ds^2 = -A(r)dt^2 + \frac{1}{B(r)}dr^2 + r^2 d\Omega^2$ static and spherical symmetric

$J^r = 0$ → Current $J^2 = J_\mu J^\mu$ regular at the horizon

$\phi(t,r) = qt + \psi(r)$ → **Space-time is static in shift-symmetric theory**

Bavichev, Charmousis(2014)

Dressing BH in **shift-symmetric ST theory**

$$\mathcal{L} = [\zeta R - \eta(\partial\phi)^2 + \beta G^{\mu\nu}\partial_\mu\phi\partial_\nu\phi - 2\Lambda] \qquad \phi(t,r) = qt + \psi(r)$$

$$ds^2 = -A(r)dt^2 + \frac{1}{B(r)}dr^2 + r^2 d\Omega^2$$

Stealth Schwarzschild

$$A(r) = B(r) = 1 - \frac{\mu}{r} \qquad \mu : \text{const.}$$

$$\phi_\pm = qt \pm q\mu\left[2\sqrt{\frac{r}{\mu}} + \log\frac{\sqrt{r}-\sqrt{\mu}}{\sqrt{r}+\sqrt{\mu}}\right] + \phi_0$$

Self-tuned Schwarzschild-de-sitter

$$A(r) = B(r) = 1 - \frac{\mu}{r} + \frac{\eta}{3\beta}r^2 \longrightarrow \Lambda_{\text{eff}} = -\frac{\zeta\eta}{\beta} \neq \Lambda$$

This metric represent Schwarzschild BH in the presence of cosmological constant.

We do not conceive huge bare Λ through the metric.

Hairy BH solutions in the generalized theory

$$\mathcal{L} = [\zeta R - \eta(\partial\phi)^2 + \beta G^{\mu\nu}\partial_\mu\phi\partial_\nu\phi - 2\Lambda] \qquad \phi(t,r) = qt + \psi(r)$$

Stealth Schwarzschild

Many of found BHs are X *constant solutions*

$$A(r) = B(r) = 1 - \frac{\mu}{r} \qquad \mu : \text{const.}$$

$$\phi_\pm = qt \pm q\mu\left[2\sqrt{\frac{r}{\mu}} + \log\frac{\sqrt{r}-\sqrt{\mu}}{\sqrt{r}+\sqrt{\mu}}\right] + \phi_0$$

Self-tuned Schwarzschild-de-sitter

$$A(r) = B(r) = 1 - \frac{\mu}{r} + \frac{\eta}{3\beta}r^2 \rightarrow \Lambda_{\text{eff}} = -\frac{\zeta\eta}{\beta} \neq \Lambda$$

Babichev, Charmousis(2014) can be generalized

$$\mathcal{L} = G_2(X) + G_4(X)R + G_{4X}\left[(\Box\phi)^2 - (\nabla_\mu\nabla_\nu\phi)^2\right]$$

$$G_{4X} := \frac{\partial G_4}{\partial X} \qquad X := -\frac{1}{2}(\partial\phi)^2$$ Kobayashi, Tanahashi(2014)

The most general 2nd-order theory with shift & reflection symmetries

Motivation

Stealth Schwarzschild sol and
Self-tuned Schwarzschild-de-sitter sol
are very interesting solutions.

How about stability of BHs?

Instability of Hairy BH in shift symmetric Horndeski theories

HO, T. Kobayashi, T. Suyama

arXiv:1510.07100

BH perturbations with time-dependent scalar

$$\mathcal{L} = G_2(X) + G_4(X)R + G_{4X}\left[(\Box\phi)^2 - (\nabla_\mu\nabla_\nu\phi)^2\right] \qquad ds^2 = -A(r)dt^2 + \frac{1}{B(r)}dr^2 + r^2 d\Omega^2$$

$$\phi(t,r) = qt + \psi(r)$$

Basic Procedure

action 2nd-order in perturbations

↓ **Hamiltonian analysis**

stability conditions

Set up

The most general 2nd-order theory with shift & reflection symmetries

$$\mathcal{L} = G_2(X) + G_4(X)R + G_{4X}\left[(\Box\phi)^2 - (\nabla_\mu\nabla_\nu\phi)^2\right]$$
$$\phi(t,r) = qt + \psi(r)\ , \ G_{4X} := \frac{\partial G_4}{\partial X}$$

Perturbations can be written as following eqs (odd-parity)

$$g_{\mu\nu} = g^{(0)}_{\mu\nu} + h_{\mu\nu}$$

$$ds^2 = -A(r)dt^2 + \frac{1}{B(r)}dr^2 + r^2 d\Omega^2$$

$$h_{tt} = 0, \quad h_{tr} = 0, \quad h_{rr} = 0$$

$$E_{ab} = \sqrt{\det\gamma}\,\epsilon_{ab}$$

$$h_{ta} = \sum_{l,m} h_{0,lm}(t,r)E_{ab}\partial^b Y_{lm}(\theta,\varphi)$$

γ_{ab} two-dim metric on the sphere

ϵ_{ab} Levi-Civita symbol

$$h_{ra} = \sum_{l,m} h_{1,lm}(t,r)E_{ab}\partial^b Y_{lm}(\theta,\varphi)$$

$$h_{ab} = \sum_{l,m} \cancel{h_{2,lm}}(t,r)[E_a{}^c\nabla_c\nabla_b Y_{lm}(\theta,\varphi) + E_b{}^c\nabla_c\nabla_a Y_{lm}(\theta,\varphi)]$$

gauge fixed (Regge-Wheeler gauge)

BH perturbations with time-dependent scalar

$$\mathcal{L} = G_2(X) + G_4(X)R + G_{4X}\left[(\Box\phi)^2 - (\nabla_\mu\nabla_\nu\phi)^2\right] \quad ds^2 = -A(r)dt^2 + \frac{1}{B(r)}dr^2 + r^2 d\Omega^2$$
$$\phi(t,r) = qt + \psi(r),\ X := -\frac{1}{2}(\partial\phi)^2$$

action 2nd-order in perturbations

Quadratic Lagrangian

$$\frac{2l+1}{2\pi}\mathcal{L}^{(2)} = A_1 h_0^2 + A_2 h_1^2 + A_4 h_0 h_1 + A_3\left(\dot{h}_1^2 - 2h_0'\dot{h}_1 + h_0'^2 + \frac{4}{r}h_0\dot{h}_1\right)$$

$$\dot{h}_i := \frac{\partial h_i}{\partial t}, \quad h_i' := \frac{\partial h_i}{\partial r}$$

$$A_1 = -\frac{l(l+1)(r^2A^2BA'G_4 - 2q^2r^2ABA'G_{4X} + \cdots}{A^{5/2}B^{1/2}}$$

$$A_1, A_2, A_3, A_4 \supset A(r), B(r), G_2, G_4, \cdots$$

BH perturbations with time-dependent scalar

$\mathcal{L} = G_2(X) + G_4(X)R + G_{4X}\left[(\Box\phi)^2 - (\nabla_\mu\nabla_\nu\phi)^2\right]$ $\quad ds^2 = -A(r)dt^2 + \frac{1}{B(r)}dr^2 + r^2 d\Omega^2$

$\phi(t,r) = qt + \psi(r)$, $X := -\frac{1}{2}(\partial\phi)^2$

action 2nd-order in perturbations

Time-dependent scalar(our result) **new term**

$$\frac{2l+1}{2\pi}\mathcal{L}^{(2)} = A_1 h_0^2 + A_2 h_1^2 + A_4 h_0 h_1 + A_3\left(\dot{h}_1^2 - 2h_0'\dot{h}_1 + h_0'^2 + \frac{4}{r}h_0\dot{h}_1\right)$$

$$\dot{h}_i := \frac{\partial h_i}{\partial t}, \quad h_i' := \frac{\partial h_i}{\partial r}$$

In the previous work (static scalar), quadratic action was obtained

$$\frac{2l+1}{2\pi}\mathcal{L}^{(2)} = a_1 h_0^2 + a_2 h_1^2 + a_3\left(\dot{h}_1^2 - 2\dot{h}_1 h_0' + {h_0'}^2 + \frac{4}{r}\dot{h}_1 h_0\right)$$

Kobayashi, Motohashi, Suyama(2012)

BH perturbations with time-dependent scalar

$\mathcal{L} = G_2(X) + G_4(X)R + G_{4X}\left[(\Box\phi)^2 - (\nabla_\mu\nabla_\nu\phi)^2\right]$ $\quad ds^2 = -A(r)dt^2 + \frac{1}{B(r)}dr^2 + r^2 d\Omega^2$

$\phi(t,r) = qt + \psi(r)$, $X := -\frac{1}{2}(\partial\phi)^2$

field redefinition

$$\frac{2l+1}{2\pi}\mathcal{L}^{(2)} = A_1 h_0^2 + A_2 h_1^2 + A_4 h_0 h_1 + A_3\left(\dot{h}_1^2 - 2h_0'\dot{h}_1 + h_0'^2 + \frac{4}{r}h_0\dot{h}_1\right)$$

To remove non-dynamical h_0 we introduce a new field χ

$$\frac{2l+1}{2\pi}\mathcal{L}^{(2)} = \left(A_1 - \frac{2(rA_3)'}{r^2}\right)h_0^2 + A_2 h_1^2 + A_3\left[-\chi^2 + 2\chi\left(\dot{h}_1 - h_0' + \frac{2}{r}h_0\right)\right] + A_4 h_0 h_1$$

BH perturbations with **time-dependent scalar**

$\mathcal{L} = G_2(X) + G_4(X)R + G_{4X}\left[(\Box\phi)^2 - (\nabla_\mu\nabla_\nu\phi)^2\right]$ $\quad ds^2 = -A(r)dt^2 + \frac{1}{B(r)}dr^2 + r^2 d\Omega^2$

$\phi(t,r) = qt + \psi(r)$, $X := -\frac{1}{2}(\partial\phi)^2$

field redefinition

$$\frac{2l+1}{2\pi}\mathcal{L}^{(2)} = \left(A_1 - \frac{2(rA_3)'}{r^2}\right)h_0^2 + A_2 h_1^2 + A_3\left[-\chi^2 + 2\chi\left(\dot{h}_1 - h_0' + \frac{2}{r}h_0\right)\right] + A_4 h_0 h_1$$

$$h_0 = -\frac{2r\left\{2a_2\left[r(\chi a_3)' + 2\chi a_3\right] + r\dot{\chi}a_3 a_4\right\}}{4a_2[r^2 a_1 - 2\,(ra_3)'] - r^2 {a_4}^2},$$

$$h_1 = \frac{4a_3\dot{\chi}[r^2 a_1 - 2(ra_3)'] + 2ra_4[r(\chi a_3)' + 2a_3\chi]}{4a_2[r^2 a_1 - 2(ra_3)'] - r^2 {a_4}^2}.$$

$$\boxed{\frac{2l+1}{2\pi}\mathcal{L}^{(2)} = \frac{l(l+1)}{(l-1)(l+2)}\sqrt{\frac{B}{A}}\left(b_1\dot{\chi}^2 - b_2\chi'^2 + b_3\dot{\chi}\chi' - l(l+1)b_4\chi^2 - V(r)\chi^2\right)}$$

BH perturbations with **time-dependent scalar**

$\mathcal{L} = G_2(X) + G_4(X)R + G_{4X}\left[(\Box\phi)^2 - (\nabla_\mu\nabla_\nu\phi)^2\right]$, $\quad ds^2 = -A(r)dt^2 + \frac{1}{B(r)}dr^2 + r^2 d\Omega^2$

$\phi(t,r) = qt + \psi(r)$

stability conditions

no-ghost instability condition

no-gradient instability condition (radial,angular)

$$\mathcal{F} = 2\left[G_4 - \frac{q^2}{A}G_{4X}\right] > 0,$$

$$\mathcal{G} = 2\left[G_4 - 2XG_{4X} + \frac{q^2}{A}G_{4X}\right] > 0,$$

$$\mathcal{H} = 2\left(G_4 - 2XG_{4X}\right) > 0$$

Application to sample solution

ST theory: $\mathcal{L} = G_2(X) + G_4(X)R + G_{4X}\left[(\Box\phi)^2 - (\nabla_\mu\nabla_\nu\phi)^2\right]$

$\phi(t,r) = qt + \psi(r)$, $X := -\frac{1}{2}(\partial\phi)^2$, $G_{4X} := \frac{\partial G_4}{\partial X}$, $ds^2 = -A(r)dt^2 + \frac{1}{B(r)}dr^2 + r^2 d\Omega^2$

Stealth sol, self-tuned de-sitter sol: $X = \text{const.}$

$$\mathcal{F} = 2\Big[\underbrace{G_4}_{\text{const}} - \frac{q^2}{A}G_{4X}\Big] > 0,$$

these terms are of opposite sign

$$\mathcal{G} = 2\Big[\underbrace{G_4 - 2XG_{4X}}_{\text{const}} + \frac{q^2}{A}G_{4X}\Big] > 0,$$

$$\mathcal{H} = 2\underbrace{(G_4 - 2XG_{4X})}_{\text{const}} > 0$$

$\xrightarrow{\text{near the horizon}}$ $\mathcal{F}\mathcal{G} \simeq -4\left(\frac{q^2}{A}G_{4X}\right)^2 < 0$

X=const solutions are unstable

Summary

Hairy BH solutions in shift-symmetric ST theory

Very interesting solutions are found

BH stability conditions

We obtain stability conditions (Hamiltonian analysis)

$$\mathcal{F} > 0, \mathcal{G} > 0, \mathcal{H} > 0$$

Hairy BH are unstable **due to time-dependent scalar**

$X := -\frac{1}{2}(\partial\phi)^2$ *=const. BH solutions are unstable*

"Effects of Vainstein Screening on LSB Galaxies and Milky Way"

by Sirachak Panpanich

[JGRG25(2015)5b6]

The 25th Workshop on General Relativity and Gravitation in Japan

Effects of Vainshtein screening on LSB galaxies and Milky Way

Sirachak Panpanich

Waseda University
(Supervisor: Prof. Kei-ichi Maeda)

December 9, 2015

Outline

Motivation

Can modified gravity models which have Vainshtein mechanism explain the rotation curve problem?.

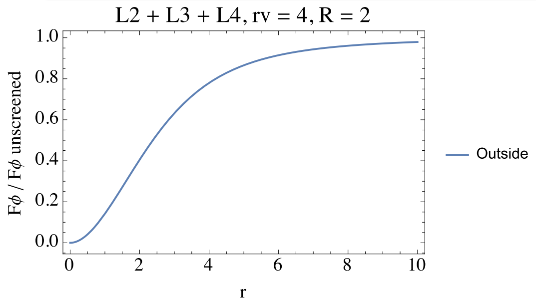

Vainshtein $\Rightarrow$ Dark Matter ?

Tested models

- Galileon in flat space
- DBIonic

Galileon in flat space

Action

$$S = \int d^4x\sqrt{-g}\left[-\frac{1}{2}\mathcal{L}_2 - \frac{1}{2\Lambda^3}\mathcal{L}_3 - \frac{\lambda_4}{2\Lambda^6}\mathcal{L}_4 - \frac{\lambda_5}{2\Lambda^9}\mathcal{L}_5 + \frac{g\phi}{M_{pl}}T\right]$$

where

$$\mathcal{L}_2 = (\nabla\phi)^2$$
$$\mathcal{L}_3 = \Box\phi(\nabla\phi)^2$$
$$\mathcal{L}_4 = (\nabla\phi)^2[(\Box\phi)^2 - (\nabla_\mu\nabla_\nu\phi)^2]$$
$$\mathcal{L}_5 = (\nabla\phi)^2[(\Box\phi)^3 - 3\Box\phi(\nabla_\mu\nabla_\nu\phi)^2 + 2(\nabla_\mu\nabla_\nu\phi)^3]$$

When the nonlinear terms dominate, the fifth force is screened.

DBIonic

DBI-like action (C. Burrage, J. Khoury, 2014)

$$S = \int d^4x\sqrt{-g}\left[+\Lambda^4\sqrt{1-\Lambda^{-4}(\partial\phi)^2}+\frac{g\phi}{M_{pl}}T\right]$$

Flip sign $\rightarrow$ screening mechanism + no ghost

EOM

$$\nabla_\mu\left(\frac{\nabla^\mu\phi}{\sqrt{1-\Lambda^{-4}(\partial\phi)^2}}\right) = -\frac{g}{M_{pl}}T$$

This model gives analogous Vainshtein screening mechanism.

Vainshtein Galileon VS Vainshtein DBIonic

Galileon L2 + L3

$$r_v = \frac{1}{\Lambda}\left(\frac{8gM_0}{4\pi M_{pl}}\right)^{1/3}$$

DBIonic

$$r_v = \frac{1}{\Lambda}\left(\frac{gM_0}{4\pi M_{pl}}\right)^{1/2}$$

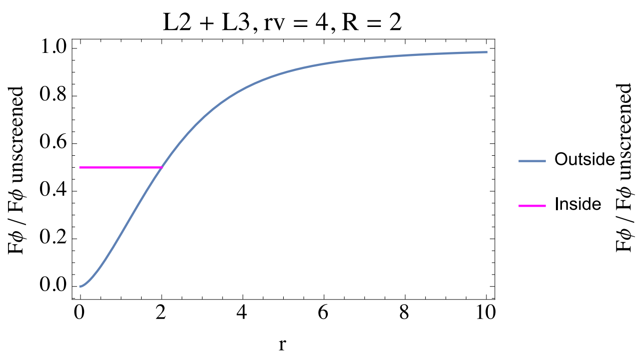

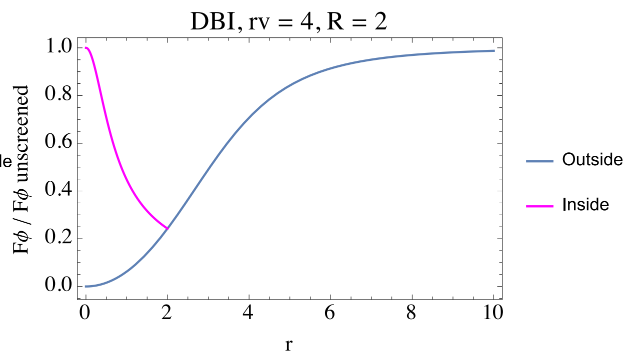

Outline

Galaxies

Observational data

Milky Way : Sofue, Y. et al. Publ.Astron.Soc.Jap. 61 (2009) 227
LSB galaxies : de Blok, W.J.G. et al. Astron.Astrophys. 385 (2002) 816

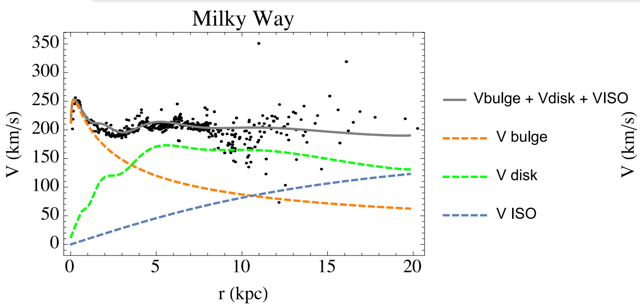

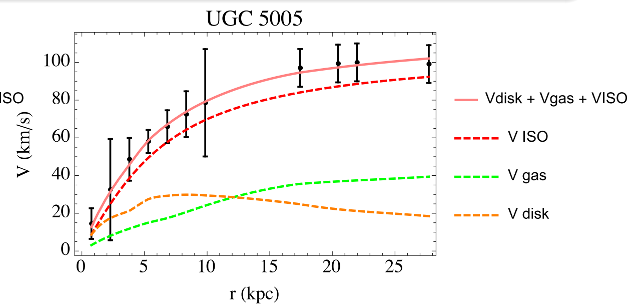

Bulge : de Vaucouleurs law $\Sigma(r) = \Sigma_e \exp\left(-\kappa\left[\left(\frac{r}{R_e}\right)^{1/4} - 1\right]\right)$

Disk : Exponential disk $\sigma(r) = \sigma_0 \exp(-r/R_d)$

Galileon in spherical coordinates

EOM in spherical coordinates

$$\frac{g}{M_{pl}}\rho(r) = \phi'' + \frac{2\phi'}{r} + \frac{2\phi'^2}{r^2\Lambda^3} + \frac{4\phi'\phi''}{r\Lambda^3} + \frac{6\lambda_4\phi'^2\phi''}{r^2\Lambda^6} + 0$$

Fifth force on a non-relativistic object (spherical symmetry)

$$\vec{F}_\phi = -\frac{g}{M_{pl}} m \frac{d\phi}{dr}\hat{r}$$

Circular velocity

$$F_N + F_\phi = \frac{GMm}{r^2} + \frac{g}{M_{pl}} m \frac{d\phi}{dr} = \frac{mv^2}{r}$$

$$v_{total}^2(r) = \frac{GM_{bul}(r)}{r} + v_5^2(r) \quad ; \quad v_5^2(r) = \frac{g}{M_{pl}} r \frac{d\phi}{dr}$$

Galileon in spherical coordinates

Solution : $\rho \neq$ const., $\mathcal{L}_2 + \mathcal{L}_3$

$$\phi'(r<R) = \frac{\Lambda^3 r}{4}\left(\sqrt{1+\alpha(r)\frac{r_{v23}^3}{r^3}} - 1\right)$$

Solution : $\rho \neq$ const., $\mathcal{L}_2 + \mathcal{L}_3 + \mathcal{L}_4$, $\lambda_4 = 2/3$

$$\phi'(r<R) = \frac{\Lambda^3 r}{2}\left[\left(1+\alpha(r)\frac{r_{v234}^3}{r^3}\right)^{1/3} - 1\right]$$

where

$$r_{v23} = \frac{1}{\Lambda}\left(\frac{8gM_0}{4\pi M_{pl}}\right)^{\frac{1}{3}}, r_{v234} = \left(\frac{3}{4}\right)^{\frac{1}{3}}\frac{1}{\Lambda}\left(\frac{8gM_0}{4\pi M_{pl}}\right)^{\frac{1}{3}}, \alpha(r) = \frac{M(r)}{M_0}$$

DBIonic in spherical coordinates

EOM in spherical coordinates

$$\frac{1}{r^2}\partial_r\left(\frac{r^2\phi'}{\sqrt{1-\Lambda^{-4}\phi'^2}}\right)=\frac{g}{M_{pl}}\rho(r)$$

Solution : $\rho \neq$ const.,

$$\phi'(r<R)=\frac{\Lambda^2}{\sqrt{1+\frac{1}{\alpha^2(r)}\frac{r^4}{r_v^4}}},\quad r_v=\frac{1}{\Lambda}\left(\frac{gM_0}{4\pi M_{pl}}\right)^{1/2},\alpha(r)=\frac{M(r)}{M_0}$$

v_5 by spherical bulge (of DBIonic)

$$v_5^2(r)=2g^2\frac{GM_{bul}(r)}{r}\frac{1}{\sqrt{1+\alpha^2(r)\frac{r_v^4}{r^4}}}$$

$\therefore v_5$ depends on mass distribution and total mass of bulge.

Outline

1. Introduction
2. Effects on galaxies
   - by a spherical bulge
   - by a disk
3. Results
4. Summary

Circular velocity of an exponential disk

Newtonian gravity :

$$\nabla^2\Phi = 4\pi G\rho \quad \rightarrow \Phi(R,z) = J(R)Z(z)$$

$$v_c^2(R) = R\left(\frac{\partial\Phi}{\partial R}\right)_{z=0} = 4\pi G\sigma_0 R_d y^2[I_0(y)K_0(y) - I_1(y)K_1(y)]$$

(I, K are modified Bessel functions)

Galileon : $\frac{g}{M_{pl}}\rho(r) = \Box\phi + \frac{1}{\Lambda^3}[(\Box\phi)^2 - (\nabla_\mu\nabla_\nu\phi)^2] + \ldots \rightarrow ?$

DBIonic : $\frac{g}{M_{pl}}\rho(r) = \nabla_\mu\left(\frac{\nabla^\mu\phi}{\sqrt{1-\Lambda^{-4}(\partial\phi)^2}}\right) \rightarrow ?$

Circular velocity of an exponential disk

Exponential disk : $\sigma(r) = \sigma_0 \exp(-r/R_d)$

Equivalent spherical distribution

$$M_{sphere}(r) = 2\pi\sigma_0 R_d^2\left[1 - \exp(-r/R_d)\left(1 + \frac{r}{R_d}\right)\right]$$

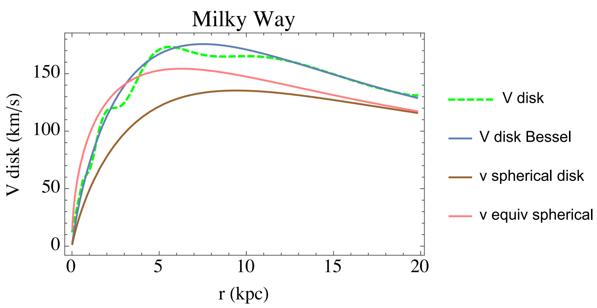

$v5$ by equivalent spherical distribution (of $\mathcal{L}_2 + \mathcal{L}_3 + \mathcal{L}_4$)

$\Downarrow$

$$v_{5disk}^2(r) = 6g^2\frac{GM_s(r)}{r}\left(\frac{r}{r_{v234}}\right)^3\frac{1}{\alpha(r)}\left(\left(1+\alpha(r)\frac{r_{v234}^3}{r^3}\right)^{1/3} - 1\right)$$

Milky Way (v5 by spherical bulge only)

$$v_{total}^2(r) = v_{bulge}^2(r) + v_{disk}^2(r) + v_5^2(r)$$

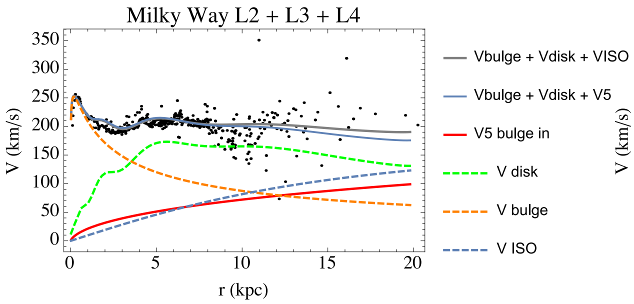

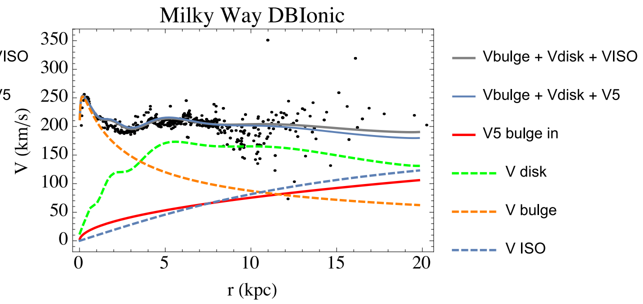

$$g = 6.5, \quad \Lambda = 10^{-12}\text{eV} \qquad g = 4.4, \quad \Lambda = 1.5 \times 10^{-4}\text{eV}$$

$$F_\phi/F_N(8.4\text{kpc}) = 0.49 \qquad F_\phi/F_N(8.4\text{kpc}) = 0.53$$

Milky Way (v5 by spherical bulge and disk)

$$v_{total}^2(r) = v_{bulge}^2(r) + v_{disk}^2(r) + v_{5bul}^2(r) + v_{5disk}^2(r)$$

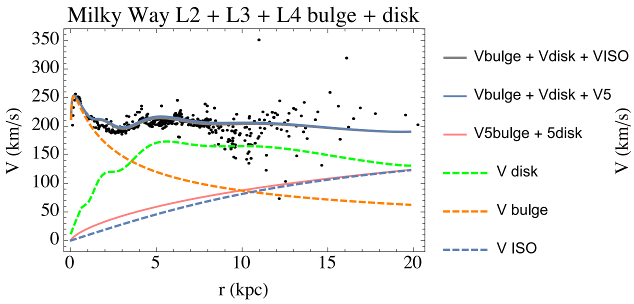

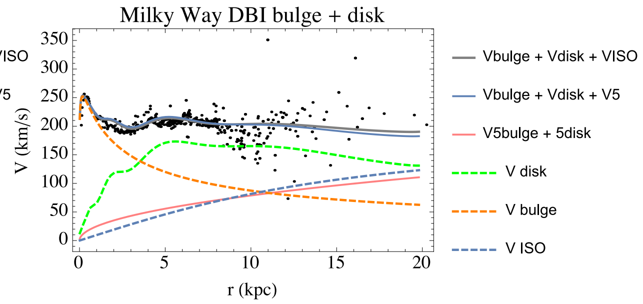

$$g = 4.5, \quad \Lambda = 10^{-12}\text{eV} \qquad g = 2.4, \quad \Lambda = 1.5 \times 10^{-4}\text{eV}$$

$$F_\phi/F_N(8.4\text{kpc}) = 0.46 \qquad F_\phi/F_N(8.4\text{kpc}) = 0.40$$

LSB galaxy (UGC5005, v5 by disk)

$$v_{total}^2(r) = v_{disk}^2(r) + v_{gas}^2(r) + v_{5disk}^2(r)$$

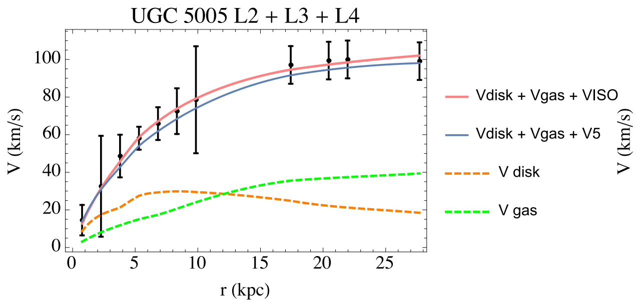

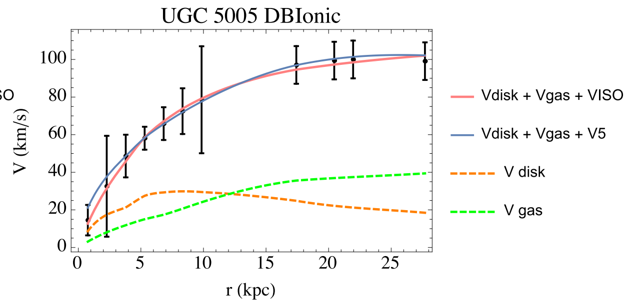

$g = 4, \quad \Lambda = 2 \times 10^{-12}\text{eV}$ $\qquad$ $g = 3.5, \quad \Lambda = 2 \times 10^{-4}\text{eV}$

Vainshtein screening inside Milky Way

Galileon

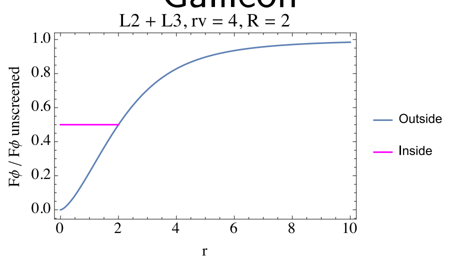

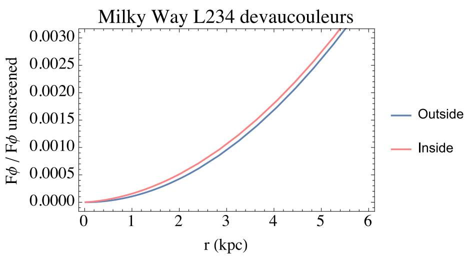

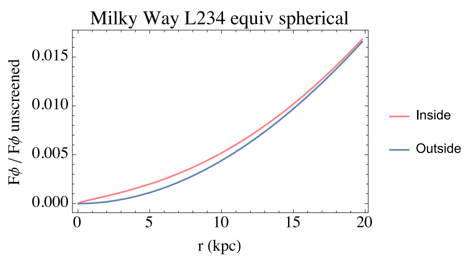

DBIonic

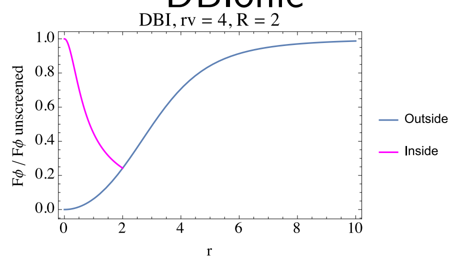

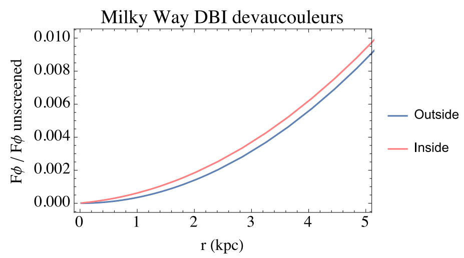

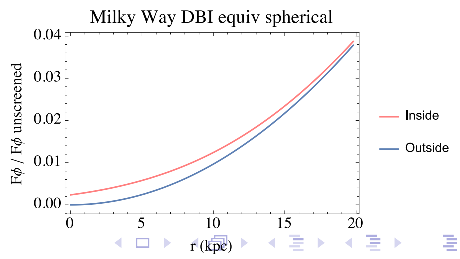

Summary

- We reproduced rotation curves by using the fifth force instead of dark matter halo.

Introduction Effects on galaxies Results Summary

Summary

- We reproduced rotation curves by using the fifth force instead of dark matter halo.
- In order to satisfy the observation, the fifth force at solar distance must be around half of the Newtonian force.

Summary

- We reproduced rotation curves by using the fifth force instead of dark matter halo.
- In order to satisfy the observation, the fifth force at solar distance must be around half of the Newtonian force.
- It is difficult to distinguish the effects of Galileon and DBIonic.

Summary

- We reproduced rotation curves by using the fifth force instead of dark matter halo.
- In order to satisfy the observation, the fifth force at solar distance must be around half of the Newtonian force.
- It is difficult to distinguish the effects of Galileon and DBIonic.
- The character of screening inside an spherical object depends on density profile of the object.

Summary

- We reproduced rotation curves by using the fifth force instead of dark matter halo.
- In order to satisfy the observation, the fifth force at solar distance must be around half of the Newtonian force.
- It is difficult to distinguish the effects of Galileon and DBIonic.
- The character of screening inside an spherical object depends on density profile of the object.

Thank you for your attention

Milky Way (v5 by spherical bulge only)

$$v_{total}^2(r) = v_{bulge}^2(r) + v_{disk}^2(r) + v_5^2(r)$$

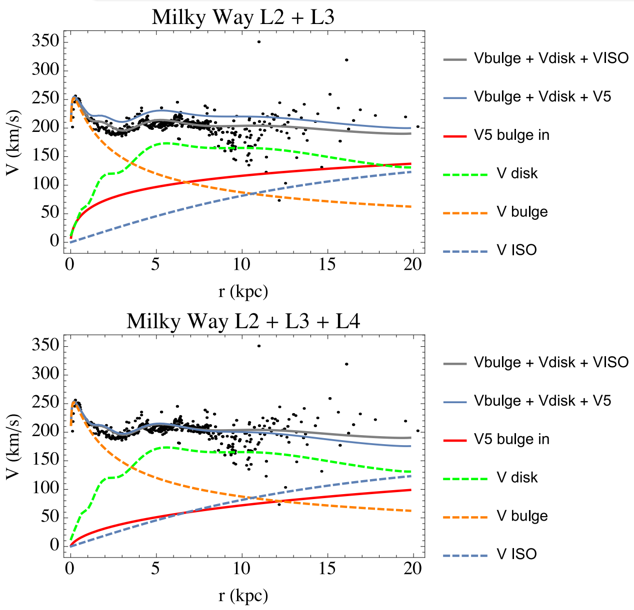

$$r_{v234} = \left(\frac{3}{4}\right)^{1/3} r_{v23}$$

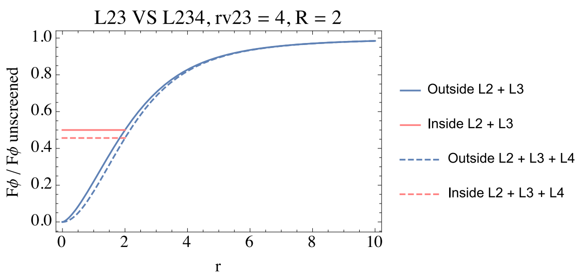

$$g = 6.5, \quad \Lambda = 10^{-12}\text{eV}$$

LSB galaxy (DDO189, v5 by disk)

$$v^2_{total}(r) = v^2_{disk}(r) + v^2_{gas}(r) + v^2_{5disk}(r)$$

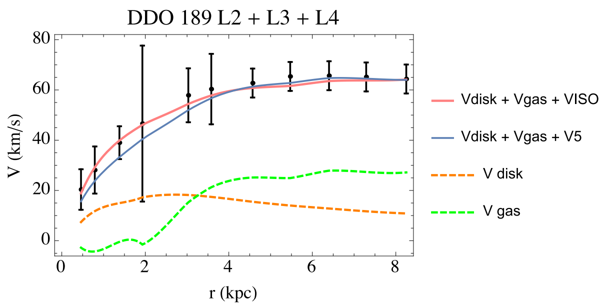

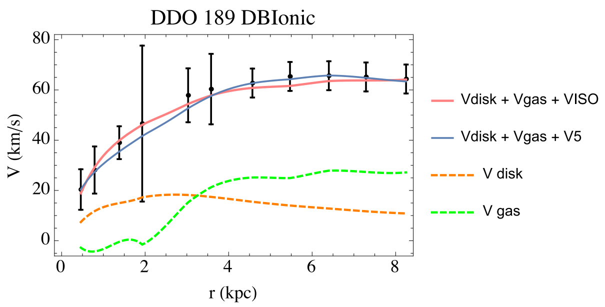

$g = 4, \quad \Lambda = 4 \times 10^{-12}\text{eV}$ $\qquad g = 3.5, \quad \Lambda = 2 \times 10^{-4}\text{eV}$

Vainshtein screening inside a non uniform object

$$\alpha(r) = \frac{M(r)}{M_0} = \left(\frac{r}{R}\right)^n$$

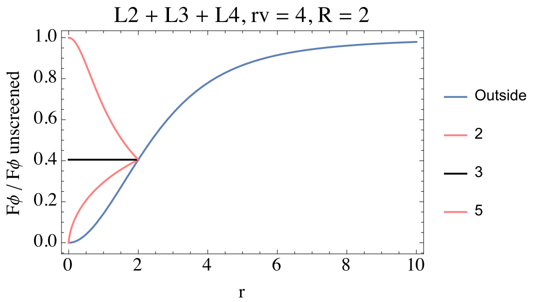

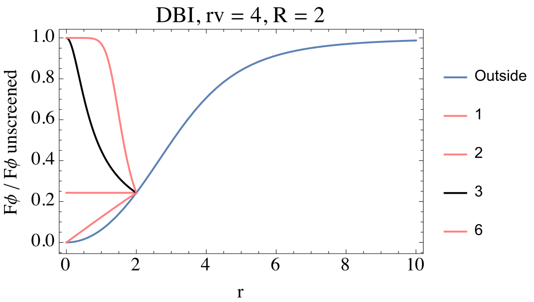

Circular velocity of an exponential disk

Exponential disk : $\sigma(r) = \sigma_0 \exp(-r/R_d)$

1) Relation between 2D profile and 3D profile

$$\rho(r) = -\frac{1}{\pi}\int_r^\infty \frac{d\sigma(R)}{dR}\frac{1}{\sqrt{R^2-r^2}}dR \quad \to \rho(r) = \frac{\sigma_0}{\pi R_d}K_0(\frac{r}{R_d})$$

2) Equivalent spherical distribution

$$M_{sphere}(r) = 2\pi\sigma_0 R_d^2\left[1-\exp(-r/R_d)\left(1+\frac{r}{R_d}\right)\right]$$

Calculating by spherical systems equations.

Circular velocity of an exponential disk

The effects by 2) is closer to the observational data than 1).

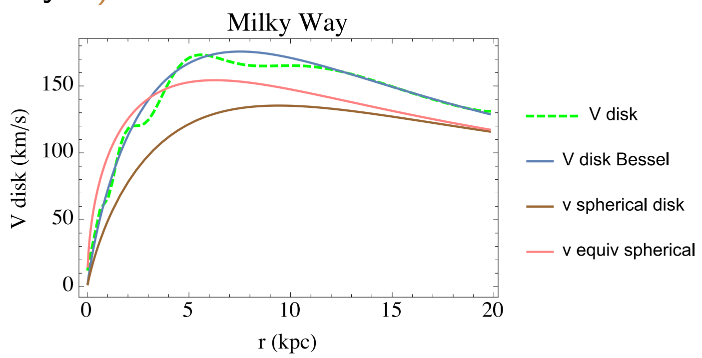

$v5$ by equivalent spherical distribution (of $\mathcal{L}_2 + \mathcal{L}_3 + \mathcal{L}_4$)

$$v_{5disk}^2(r) = 6g^2\frac{GM_s(r)}{r}\left(\frac{r}{r_{v234}}\right)^3\frac{1}{\alpha(r)}\left(\left(1+\alpha(r)\frac{r_{v234}^3}{r^3}\right)^{1/3}-1\right)$$

“Some Topics of Sources of Gravitational Waves and available Physics from them”

by Takashi Nakamura (invited)

[JGRG25(2015)I08]

Some Topics of Sources of Gravitational Waves and available Physics from them

2015.12.9
JGRG25

Kyoto University
Takashi Nakamura

- My talk is based on my recent papers :
- SGRB rate with Yonetoku, Sawano,Takahashi & Toyanago (2014)ApJ. 789:65
- Detectability of X-ray counter part of SGRB with Kisaka & Ioka (2015) ApJ. 809:L8
- Pop Synthesis of PopIII BH-BH binary with Kinugawa, Inayoshi, Hotokezaka & Nakauchi (2014) MNRAS 442 2963-2922
- QNM mode of PopIII binary BH-BH with Kinugawa, Miyamoto, & Kanda (2015) MNRAS in press
- Golden Event of QNM with Nakano & Tanaka (2015) PRD 92.064003
- Measuring speed of GW with Nishizawa (2014) PRD90 044048
- Graviton Oscillation with De Felice & Tanaka (2014) PTEP 043E01
- Detectability of Graviton Oscillation with Narikawa, Ueno, Tagoshi, Tanaka &Kanda (2015) PRD91.062007

References missed in my talk can be found in these papers.

GW and EM Counterparts / Followups got Grant Support in Japan !

科研費 KAKENHI

"New development in astrophysics through multimessenger observations of gravitational wave sources"

Grant-in-Aid for Scientific Research on Innovative Areas by MEXT, Japan

Head : Takashi Nakamura

Term of Project : Fiscal year 2012-2016 (until end of March 2017)

Budget : ~800 milion yen (~7.7 USD)

Consists of five groups :

1) **X & Gamma Ray**
2) **Optical & Infrared & Radio**
3) **Neutrino** anti ν
4) **GW data analysis** OOhara
5) **Theory** (PI Tanaka)

1) & 2) exchange MOU with LIGO

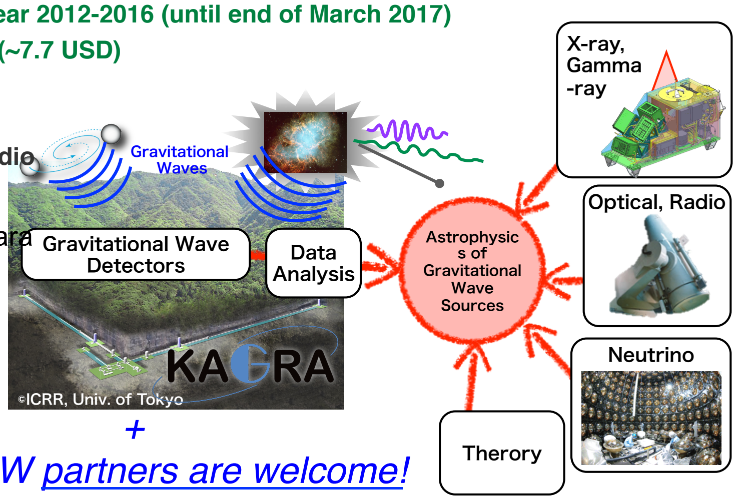

+

global GW partners are welcome!

I need some good results related to this Innovative Area before 2017 June when the final hearing will be took place at MEXT (Ministry of Education, Culture, Sports, Science and Technology-Japan).

In 2011, JGWC (Japan Gravitational Wave Community) was established. JGWC consists of JGRG +KAGRA + DECIGO+ Innovative Area with about 300 participants. Innovative area will support JGRG up to 2016 fiscal year.

Members of JGWC consists of GW experimentalists, Theorists, space scientists, radio , optical, X-ray, gamma ray astronomers and neutrino experimentalists.

Strategy of JGWC is KAGRA first and DECIGO next.

Section 1: Gravitational waves from coalescing binary neutron stars

Density contour
In the equator

Numerical Relativity simulation (zoom-in)

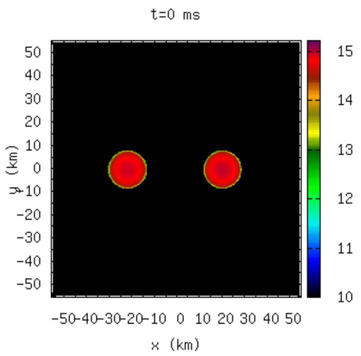

GW profile

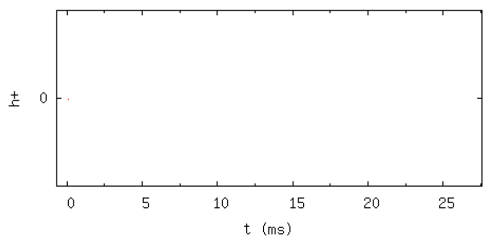

Hotokezaka et al. 2014

While this is the first numerical simulation of formation of the axially symmetric rotating black hole using 28x28 grid in 1981 by Nakamura.

Main results: If $J/M^2 <1$ then black hole is formed.

If $J/M^2 > 1$ outer part expand and BH with $Jc/Mc^2 <1$ inside

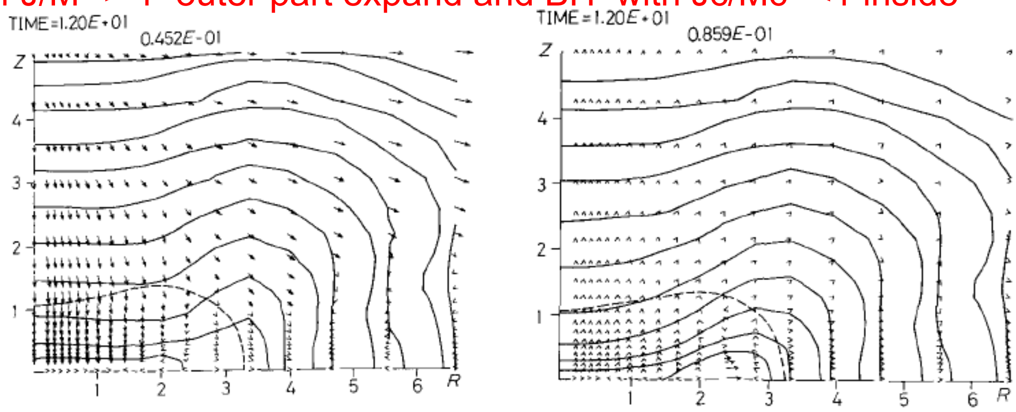

Fig. 3. (a) Contour lines of Q_b for M80 at $t=12.0$. Each line corresponds to $Q_b=(Q_b)_{max}\cdot 10^{-n/2}$ where $(Q_b)_{max}=4.52\cdot 10^{-2}$ for $n=1, 2, \cdots, 11$. Arrows show vectors (J_A/Q_b). The apparent horizon is shown by the dashed line.

(b) Contour lines of proper density (ρ) for M80 at $t=12.0$. Each line corresponds to $\rho=\rho_{max}\cdot 10^{-n/2}$ where $\rho_{max}=8.59\cdot 10^{-2}$ for $n=1, 2, \cdots, 11$. The apparent horizon is shown by the dashed line. Arrows show vectors E^A.

NS-NS and NS-BH merger rates

List of observed binary NS

Table 1
Properties of PSR–NS Binaries Considered in this Work

PSR Name	P_s (ms)	$\dot{P}_s$ 10^{-18} (ss^{-1})	M_{psr} ($M_\odot$)	M_c ($M_\odot$)	P_{orb} (hr)	e	$f_{b,obs}$	$f_{b,eff}$	τ_{age}^a (Gyr)	τ_{mgr} (Gyr)	τ_d (Gyr)	N_{psr}	C (kyr)	Ref[b]
Tight binaries														
B1913+16	59.	8.63	1.44	1.39	7.75	0.617	5.72	2.26	0.0653	0.301	4.31	576	111	1,2
B1534+12	37.9	2.43	1.33	1.35	10.1	0.274	6.04	1.89	0.200	2.73	9.48	429	1130	3,4
J0737-3039A	22.7	1.74	1.34	1.25	2.45	0.088		1.55	0.142	0.086	14.2	1403	105	5
J0737−3039B	2770.	892.			2.45	0.088		14.	0.0493		0.039			6
J1756−2251	28.5	1.02	1.4	1.18	7.67	0.181		1.68	0.382	1.65	16.1	664	1821	7
J1906+0746	144.	20300.	1.25	1.37	3.98	0.085		3.37	0.000112	0.308	0.082	192	126	8,9
Wide binaries														
J1518+4904	40.94	0.028	1.56	1.05	206.4	0.249		1.94	29.2	$>\tau_H$	51.0	276	18,700	10,11
J1811−1736	104.18	0.901	1.60	1.00	451.2	0.828		2.92	1.75	$>\tau_H$	7.9	584	5860	12,13
J1829+2456	41.01	0.053	1.14	1.36	28.3	0.139		1.94	12.3	$>\tau_H$	43.0	271	19,000	14
J1753−2240[c]	95.14	0.97	*1.25*	*1.25*	327.3	0.303		2.80	1.4	$>\tau_H$	8.2	270	13,900	15

The Astrophysical Journal, 715:230–241, 2010 May 20

Richard O'Shaughnessy[1] and Chunglee Kim[2]

Estimates of NS-NS merger rate

- Kim, Kalogera & Lorimer (2003)
- 1）input pulsar search with sensitivity level
- 2）Assume distribution function in galaxy

$$f(R, Z) \propto \exp\left(-\frac{R^2}{2R_0^2} - \frac{|Z|}{Z_0}\right);$$

- R_0, Z_0 are parameters
- 3）assume Pulsar Luminosity Function

$$\phi(L) = (p-1)L_{\rm min}^{p-1}L^{-p},$$

- p, L_{min} are parameters

SIMULATED PULSAR SURVEYS

Year	Telescope	ν^a (MHz)	$\Delta\nu^b$ (MHz)	$t_{obs}{}^c$ (s)	$t_{samp}{}^d$ (ms)	$S_{min}{}^e$ (mJy)	Detected[f]	References
1972	Lovell 76 m	408	4	660	40	10	51/31	1, 2
1974	Arecibo 305 m	430	8	137	17	1	50/40	3, 4
1977	Molonglo	408	4	45	20	10	224/155	5
1977	Green Bank 300 inch	400	16	138	17	10	50/23	6, 7
1982	Green Bank 300 inch	390	16	138	17	2	83/34	8
1983	Green Bank 300 inch	390	8	132	2	5	87/20	9
	Lovell 76 m	1400	40	524	2	1	61/40	10
1984	Arecibo 305 m	430	1	40	0.3	3	24/5	9
1985	Molonglo	843	3	132	0.5	8	10/1	11
1987	Arecibo 305 m	430	10	68	0.5	1	61/24	12
1988	Parkes 64 m	1520	320	150	0.3	1	100/46	13
1990	Arecibo 305 m	430	10	40	0.5	2	2/2	14
1992	Parkes 64 m	430	32	168	0.3	3	298/101	15, 16
1993	Arecibo 305 m	430	10	40	0.5	1	56/90	17–20
1994	Lovell 76 m	411	8	315	0.3	5	5/1	21
1995	Green Bank 140 inch	370	40	134	0.3	8	84/8	22
1998	Parkes 64 m	1374	288	265	0.1	0.5	69/170	23
	Parkes 64 m	1374	288	2100	0.3	0.2	~900/600	24, 25

[a] Center frequency.
[b] Bandwidth.
[c] Integration time.
[d] Sampling time.
[e] Sensitivity limit at the survey frequency for long-period pulsars (calculated for each trial in the simulations).
[f] Total number of detections and new pulsars.

REFERENCES.—(1) Davies, Lyne, & Seiradakis 1972. (2) Davies, Lyne, & Seiradakis 1973. (3) Hulse & Taylor 1974. (4) Hulse & Taylor 1975. (5) Manchester et al. 1978. (6) Damashek, Taylor, & Hulse 1978. (7) Damashek et al. 1982. (8) Dewey et al. 1985. (9) Stokes et al. 1986. (10) Clifton et al. 1992. (11) D'Amico et al. 1988. (12) Nice, Fruchter, & Taylor 1995. (13) Johnston et al. 1992. (14) Wolszczan 1991. (15) Manchester et al. 1996. (16) Lyne et al. 1998. (17) Ray et al. 1996. (18) Camilo et al. 1996. (19) Foster et al. 1995. (20) Lundgren, Zepka, & Cordes 1995. (21) Nicastro et al. 1995. (22) Sayer et al. 1997. (23) Edwards et al. 2001. (24) Lyne et al. 2000. (25) Manchester et al. 2001.

- Mont Carlo Simulations
- How many BNS in our galaxy as a whole？
- DM(Dispersion Measure) is not isotropic

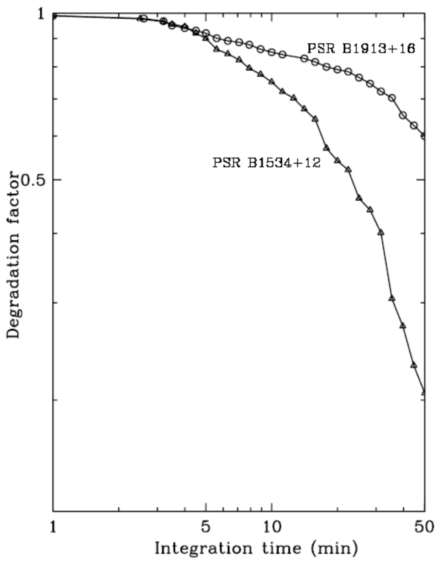

FIG. 1.—Average signal-to-noise degradation factor in pulsar search code vs. survey integration time for PSR B1913+16 and PSR B1534+12.

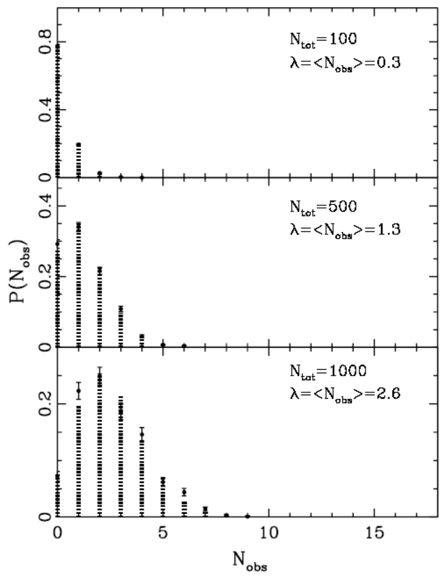

FIG. 2.—Poisson distribution fits of $P(N_{obs})$ for three values of the total number N_{tot} of PSR B1913+16–like pulsars in the Galaxy (results shown for model 1). Points and error bars represent the counts of model samples in our calculation. Dotted lines represent the theoretical Poisson distribution.

11

TABLE 2

MODEL PARAMETERS AND ESTIMATES FOR $\mathscr{R}_{tot}$ AND $\mathscr{R}_{det}$ AT VARIOUS STATISTICAL CONFIDENCE LEVELS FOR DIFFERENT POPULATION MODELS

	PARAMETERS				$\mathscr{R}_{tot}$ (Myr^{-1})			$\mathscr{R}_{det}$ OF LIGO (yr^{-1}) INITIAL ($\times 10^{-3}$)		ADVANCED	
MODEL[a]	L_{min}[b] (mJy kpc^2)	p[c]	R_0[d] (kpc)	Z_0[e] (kpc)	Peak[g]	68%[h]	95%[h]	Peak[g]	68%[h]	Peak[g]	68%[h]
1	1.0	2.0	4.0 (G[f])	1.5 (E[f])	8.0	$^{+9.3}_{-4.7}$	$^{+23.3}_{-6.7}$	3.3	$^{+3.9}_{-2.0}$	17.9	$^{+21.0}_{-10.6}$
2	1.0	2.0	4.0 (G)	0.5 (E)	7.1	$^{+8.3}_{-4.2}$	$^{+20.8}_{-5.9}$	3.0	$^{+3.5}_{-1.7}$	15.9	$^{+18.7}_{-9.4}$
3	1.0	2.0	4.0 (G)	2.0 (E)	8.4	$^{+9.9}_{-5.0}$	$^{+24.7}_{-7.1}$	3.5	$^{+4.1}_{-2.1}$	19.0	$^{+22.2}_{-11.2}$
4	1.0	2.0	4.0 (E)	1.5 (E)	8.7	$^{+10.2}_{-5.1}$	$^{+25.6}_{-7.3}$	3.6	$^{+4.3}_{-2.2}$	19.5	$^{+23.0}_{-11.6}$
5	1.0	2.0	4.0 (G)	1.5 (G)	7.9	$^{+9.2}_{-4.6}$	$^{+23.0}_{-6.6}$	3.3	$^{+3.9}_{-1.9}$	17.7	$^{+20.7}_{-10.}$
6	0.3	2.0	4.0 (G)	1.5 (E)	26.9	$^{+32.0}_{-16.1}$	$^{+80.3}_{-22.7}$	11.3	$^{+13.4}_{-6.7}$	60.5	$^{+72.1}_{-36.2}$
7	0.7	2.0	4.0 (G)	1.5 (E)	11.5	$^{+13.5}_{-6.8}$	$^{+33.9}_{-9.7}$	4.8	$^{+5.7}_{-2.9}$	25.9	$^{+30.5}_{-15.3}$
8	1.5	2.0	4.0 (G)	1.5 (E)	5.5	$^{+6.3}_{-3.2}$	$^{+15.9}_{-4.6}$	2.3	$^{+2.7}_{-1.3}$	12.3	$^{+14.3}_{-7.2}$
9	3.0	2.0	4.0 (G)	1.5 (E)	2.9	$^{+3.3}_{-1.7}$	$^{+8.3}_{-2.4}$	1.2	$^{+1.4}_{-0.7}$	6.4	$^{+7.4}_{-3.8}$
10	0.3	1.8	4.0 (G)	1.5 (E)	9.4	$^{+10.8}_{-5.5}$	$^{+27.1}_{-7.9}$	3.9	$^{+4.5}_{-2.3}$	21.2	$^{+24.3}_{-12.4}$
11	0.7	1.8	4.0 (G)	1.5 (E)	4.8	$^{+5.4}_{-2.8}$	$^{+13.5}_{-4.0}$	2.0	$^{+2.3}_{-1.2}$	10.7	$^{+12.2}_{-6.2}$
12	1.0	1.8	4.0 (G)	1.5 (E)	3.6	$^{+4.1}_{-2.1}$	$^{+10.3}_{-3.0}$	1.5	$^{+1.7}_{-0.9}$	8.2	$^{+9.3}_{-4.7}$
13	1.5	1.8	4.0 (G)	1.5 (E)	2.7	$^{+3.0}_{-1.5}$	$^{+7.6}_{-2.2}$	1.1	$^{+1.3}_{-0.6}$	6.0	$^{+6.8}_{-3.5}$
14	3.0	1.8	4.0 (G)	1.5 (E)	1.6	$^{+1.8}_{-0.9}$	$^{+4.4}_{-1.3}$	0.7	$^{+0.7}_{-0.4}$	3.5	$^{+4.0}_{-2.0}$
15	0.3	2.2	4.0 (G)	1.5 (E)	61.2	$^{+75.8}_{-37.5}$	$^{+190.3}_{-52.1}$	25.6	$^{+31.7}_{-15.7}$	137.6	$^{+170.5}_{-84.4}$
16	0.7	2.2	4.0 (G)	1.5 (E)	22.1	$^{+27.0}_{-13.4}$	$^{+67.8}_{-18.7}$	9.2	$^{+11.3}_{-5.6}$	49.7	$^{+60.8}_{-30.2}$
17	1.0	2.2	4.0 (G)	1.5 (E)	14.9	$^{+18.0}_{-9.0}$	$^{+45.2}_{-12.6}$	6.2	$^{+7.5}_{-3.8}$	33.5	$^{+40.5}_{-20.2}$
18	1.5	2.2	4.0 (G)	1.5 (E)	9.8	$^{+11.7}_{-5.9}$	$^{+29.4}_{-8.2}$	4.1	$^{+4.9}_{-2.5}$	22.0	$^{+26.4}_{-13.2}$
19	3.0	2.2	4.0 (G)	1.5 (E)	4.7	$^{+5.5}_{-2.8}$	$^{+13.8}_{-3.9}$	2.0	$^{+2.3}_{-1.2}$	10.5	$^{+12.4}_{-6.2}$
20	1.0	2.5	4.0 (G)	1.5 (E)	28.3	$^{+35.6}_{-17.5}$	$^{+89.4}_{-24.2}$	11.8	$^{+14.9}_{-7.3}$	63.6	$^{+80.0}_{-39.4}$
21	1.0	2.0	2.0 (G)	1.5 (E)	26.1	$^{+29.7}_{-15.2}$	$^{+74.2}_{-21.7}$	10.9	$^{+12.4}_{-6.3}$	58.6	$^{+66.7}_{-34.1}$
22	1.0	2.0	3.0 (G)	1.5 (E)	12.8	$^{+14.6}_{-7.4}$	$^{+36.4}_{-10.7}$	5.4	$^{+6.1}_{-3.1}$	28.9	$^{+32.8}_{-16.8}$
23	1.0	2.0	5.0 (G)	1.5 (E)	6.7	$^{+7.9}_{-4.0}$	$^{+19.8}_{-5.6}$	2.8	$^{+3.3}_{-1.7}$	15.1	$^{+17.8}_{-8.9}$
24	1.0	2.0	6.0 (G)	1.5 (E)	6.6	$^{+7.8}_{-3.9}$	$^{+19.5}_{-5.5}$	2.7	$^{+3.3}_{-1.6}$	14.8	$^{+17.5}_{-8.8}$
25	1.0	2.0	7.0 (G)	1.5 (E)	6.9	$^{+8.2}_{-4.1}$	$^{+20.5}_{-5.8}$	2.9	$^{+3.4}_{-1.7}$	15.5	$^{+18.4}_{-9.2}$
26	1.0	2.0	8.0 (G)	1.5 (E)	7.4	$^{+8.8}_{-4.4}$	$^{+22.2}_{-6.3}$	3.1	$^{+3.7}_{-1.9}$	16.8	$^{+19.9}_{-10.0}$
27	1.0	2.0	9.0 (G)	1.5 (E)	8.4	$^{+10.0}_{-5.0}$	$^{+25.1}_{-7.1}$	3.5	$^{+4.2}_{-2.1}$	18.9	$^{+22.6}_{-11.3}$

[a] Model number.
[b] Minimum luminosity L_{min}.
[c] Power index of the luminosity function p.
[d] Radial scale length R_0.
[e] Vertical scale height Z_0.
[f] Gaussian (G), and exponential (E) functions for spatial distributions.
[g] Peak value from $P(\mathscr{R}_{tot})$.
[h] Confidence level.

12

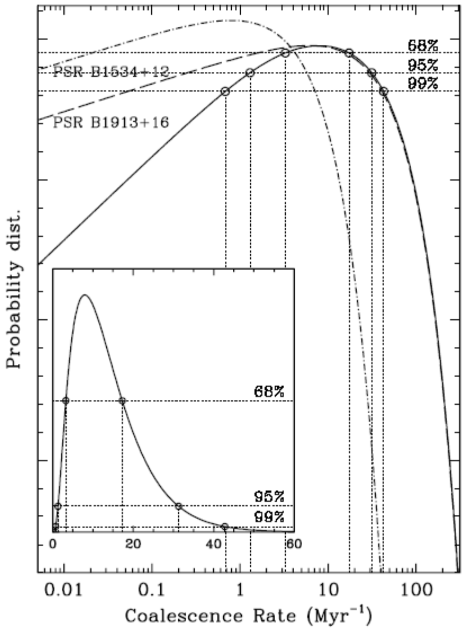

FIG. 4.—Probability distribution function of coalescence rates in both a ogarithmic and a linear scale (*inset*) for model 1. The solid line represents $P(\mathcal{R}_{tot})$ and the long- and short-dashed lines represent $P(\mathcal{R})$ for PSR B1913+16–like and PSR B1534+12–like populations, respectively. We also ndicate the confidence levels for $P(\mathcal{R}_{tot})$ by dotted lines.

$R \sim 10^{-5}$/y/galaxy

~2.5event/y

by adv LIGO, Virgo and KAGRA

Their model 1

Rates depend on parameters especially p and L_{min}

See 7 times difference Between model 1 and 15

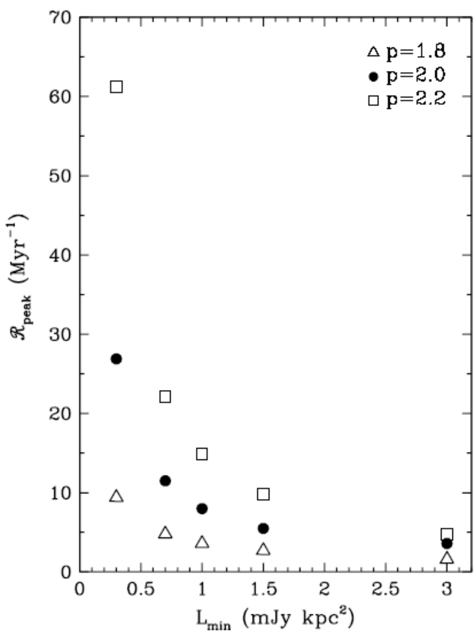

FIG. 5.—Correlation between $\mathcal{R}_{peak}$ and the cut-off luminosity L_{min} with different power indices p of the luminosity distribution function.

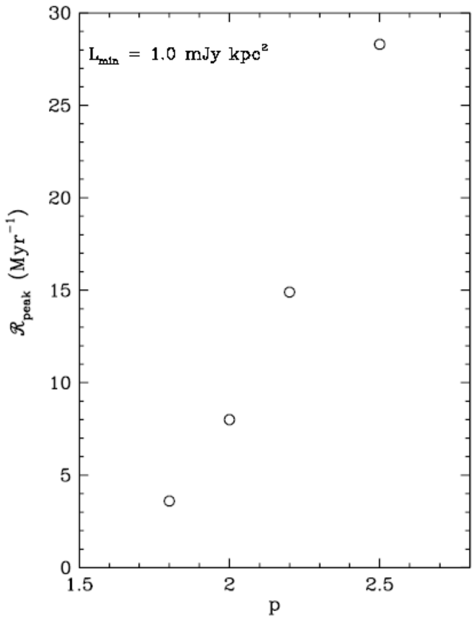

FIG. 6.—Correlation between $\mathcal{R}_{peak}$ and the power index of the luminosity distribution function p.

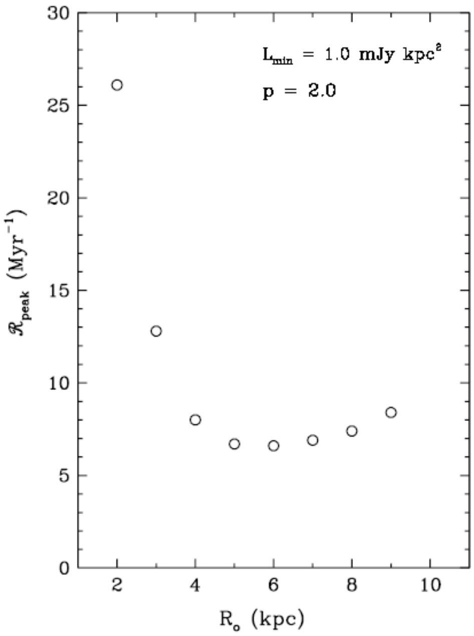

FIG. 7.—Correlation between $\mathcal{R}_{peak}$ and the radial scale length R_0. $\mathcal{R}_{peak}$, not sensitive to R_0 in the range between 4 and 9 kpc.

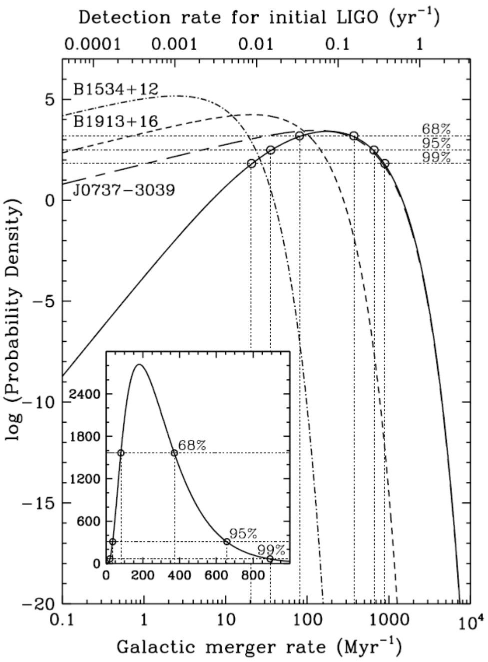

FIG. 1.— The probability density function of the DNS binary merger rate in the Galaxy (bottom axis) and the predicted initial LIGO rate (top axis) for our reference model. The solid line shows the total probability density along with those obtained for each of the three binary systems (dashed lines). Inset: The total probability density, and corresponding 68%, 95% and 99% confidence limits, shown in a linear scale.

Kalogera et al (2004)

New PSRJ0737-3039

Increased the rate as

(2-90)x10^{-5}event /y/galaxy

10 – 225 event/y
by adv LIGO, Virgo and KAGRA

Adopted model 6 but not Model 1

TABLE 1. ESTIMATES FOR GALACTIC INSPIRAL RATES AND PREDICTED LIGO TECTION RATES (AT 95% CONFIDENCE) FOR DIFFERENT POPULATION MODELS

Model[1]	$\mathcal{R}_{tot}$	IRF[2]	$\mathcal{R}_{det}$ of LIGO	
			initial	advanced
	Myr^{-1}		kyr^{-1}	yr^{-1}
1	56^{+148}_{-45}	7.0	23^{+62}_{-19}	125^{+334}_{-100}
6	180^{+477}_{-144}	6.7	75^{+200}_{-60}	405^{+1073}_{-325}
9	20^{+53}_{-16}	6.9	8^{+22}_{-7}	45^{+120}_{-36}
10	63^{+167}_{-51}	6.7	27^{+70}_{-21}	143^{+377}_{-114}
12	24^{+64}_{-19}	6.7	10^{+27}_{-8}	54^{+144}_{-43}
14	10^{+27}_{-8}	6.3	4^{+11}_{-3}	23^{+61}_{-18}
15	449^{+1183}_{-361}	7.3	188^{+495}_{-151}	1010^{+2661}_{-813}
17	102^{+268}_{-82}	6.8	43^{+112}_{-34}	229^{+602}_{-184}
19	32^{+85}_{-26}	6.8	13^{+36}_{-11}	72^{+191}_{-58}
20	195^{+506}_{-157}	6.9	82^{+212}_{-66}	439^{+1138}_{-352}

[1]Model numbers correspond to KKL. Model 1 was used as a reference model in KKL. Model 6 is our reference model in this study (see text).

[2]Increase rate factor compared to previous rates reported in KKL. IRF$\equiv \mathcal{R}_{peak,new}/\mathcal{R}_{peak,KKL}$.

Kalogera 2004b corrected the errors

TABLE 1

ESTIMATES FOR GALACTIC IN-SPIRAL RATES AND PREDICTED LIGO DETECTION RATES (AT 95% CONFIDENCE) FOR DIFFERENT POPULATION MODELS

MODEL[a]	$\mathcal{R}_{tot}$ (Myr^{-1})	IRF	$\mathcal{R}_{det}$ of LIGO[b] Initial (kyr^{-1})	$\mathcal{R}_{det}$ of LIGO[b] Advanced (yr^{-1})
1	$23.2^{+59.4}_{-18.5}$	6.4	$9.7^{+24.9}_{-7.7}$	$52.2^{+133.6}_{-41.6}$
6	$83.0^{+209.1}_{-66.1}$	6.3	$34.8^{+87.6}_{-27.7}$	$186.8^{+470.5}_{-148.7}$
9	$7.9^{+20.2}_{-6.3}$	6.6	$3.3^{+8.4}_{-2.6}$	$17.7^{+45.4}_{-14.1}$
10	$23.3^{+57.0}_{-18.4}$	5.8	$9.8^{+23.9}_{-7.7}$	$52.4^{+128.2}_{-41.3}$
12	$9.0^{+21.9}_{-7.1}$	6.0	$3.8^{+9.2}_{-3.0}$	$20.2^{+49.4}_{-15.9}$
14	$3.8^{+9.4}_{-2.8}$	5.8	$1.6^{+3.9}_{-1.2}$	$8.5^{+21.1}_{-6.2}$
15	$223.7^{+593.8}_{-180.6}$	7.1	$93.7^{+248.6}_{-75.6}$	$503.2^{+1336.0}_{-406.3}$
17	$51.6^{+135.3}_{-41.5}$	6.9	$21.6^{+56.7}_{-17.4}$	$116.1^{+304.4}_{-93.4}$
19	$14.6^{+38.2}_{-11.7}$	7.0	$6.1^{+16.0}_{-4.9}$	$32.8^{+86.0}_{-26.3}$
20	$89.0^{+217.9}_{-70.8}$	6.2	$37.3^{+91.2}_{-29.6}$	$200.3^{+490.3}_{-159.3}$

[a] Model numbers correspond to KKL. Model 1 was used as a reference model in KKL. Model 6 is our reference model in this study.

[b] Increase rate factor compared to previous rates reported in KKL. IRF $\equiv \mathcal{R}_{peak,new}/\mathcal{R}_{peak,KKL}$.

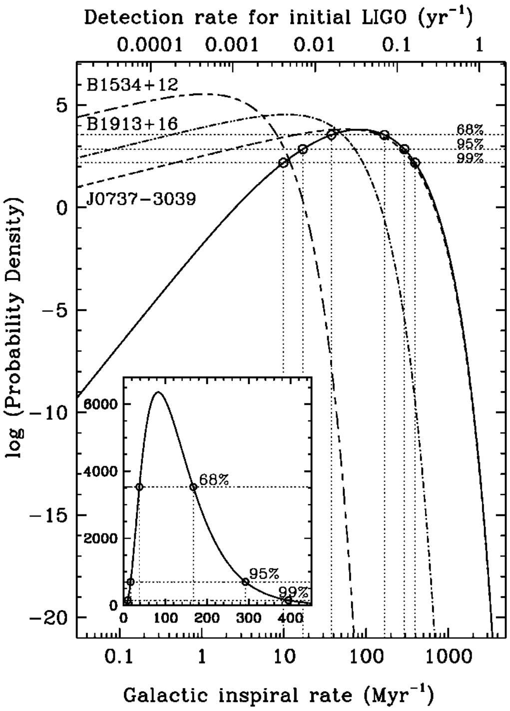

(1 – 40) x10^{-5} event/y/galaxy

2.5- 100 event /y

Central value 25 event/y

by adv LIGO, Virgo and KAGRA

Implications of PSR J0737−3039B for the Galactic NS−NS Binary Merger Rate

Chunglee Kim[1,2*], Benetge Bhakthi Pranama Perera[2,3], & Maura A. McLaughlin[2]

arXiv:1308.4676v3 [astro-ph.SR] 18 Mar 2015

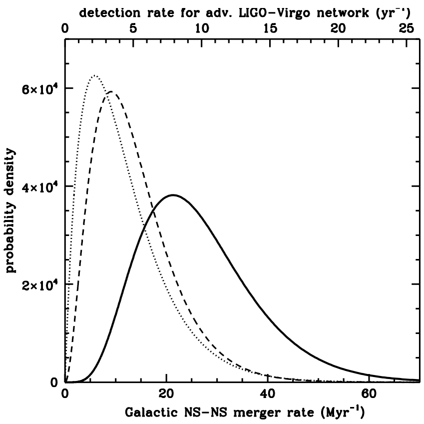

Figure 7. $\mathcal{P}_g(\mathcal{R}_g)$ (solid) is overlaid with individual $\mathcal{P}(\mathcal{R})$ obtained from PSR B1916+13 (dotted) and the Double Pulsar (short dashed). Based on our reference model, the Galactic NS−NS merger rate is most likely to be 21 Myr^{-1}. The corresponding GW detection rate for the advanced ground-based GW detectors is ~ 8 yr^{-1}.

R= 21^{+28}_{-14} Myr^{-1} at 95 per cent confidence

2015 (0.7 – 5.2)x10^{-5}/y/galaxy

while 2004 (2-30)x10^{-5}/y/galaxy
by adv LIGO, Virgo and KAGRA
Their rate now is
8^{+10}_{-5} yr^{-1} at 95 per cent confidence

2015 (3-18) event/y

2004 （5-75) event/y

SGRB=NS-NS merger ?

- This is just an assumption without smoking gun.
- Before 1997, almost every GRB scientists believed that GRB is the local event at most in our galaxy or its halo except for Pacynski.
- Many people believed that the compactness problem is denying the cosmological origin of GRBs although Γ>100 relativistic jet solved the problem.
- There are at least two Long GRBs without Super Nova so that no supernova in SGRBs so far is not a smoking gun.

I have ever proposed unified model of GRBs with Yamazaki et al. 2004

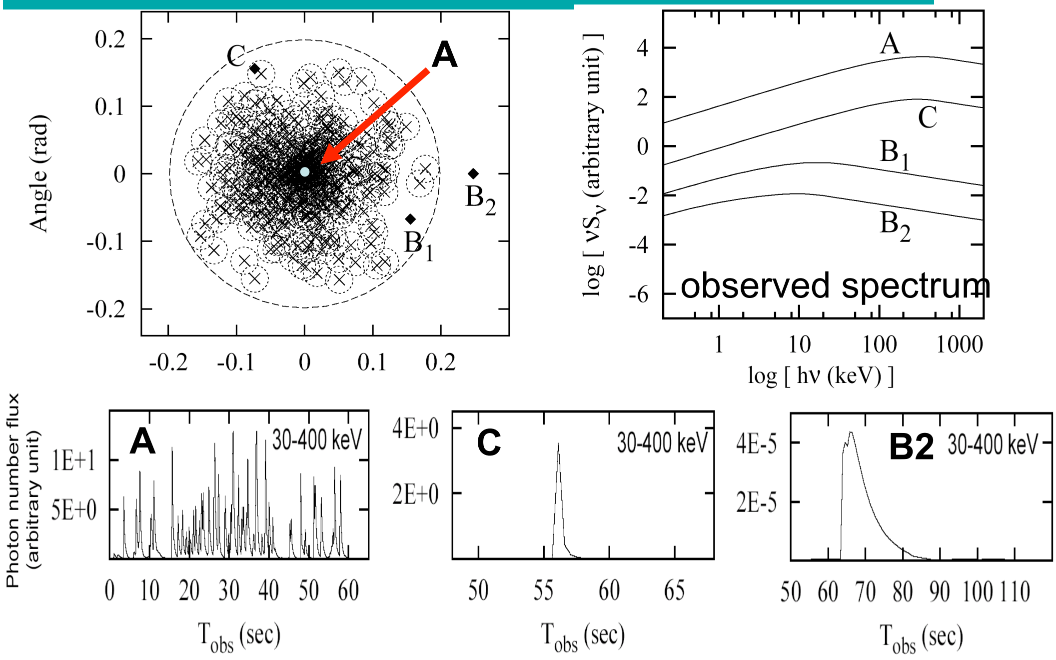

Long GRB **Short GRB** **XRF/XRR**

What is GRB(Gamma Ray Burst)

- Burst of photons with energy ~250keV coming from the cosmological distance with duration 10^{-2}sec – 10^{4}sec、event rate per year is about 1000.
- Arrival directions are isotropic.
- Spectrum is the empirical Band Spectrum
- At least two classes exist.
- Short GRBs, Long GRBs

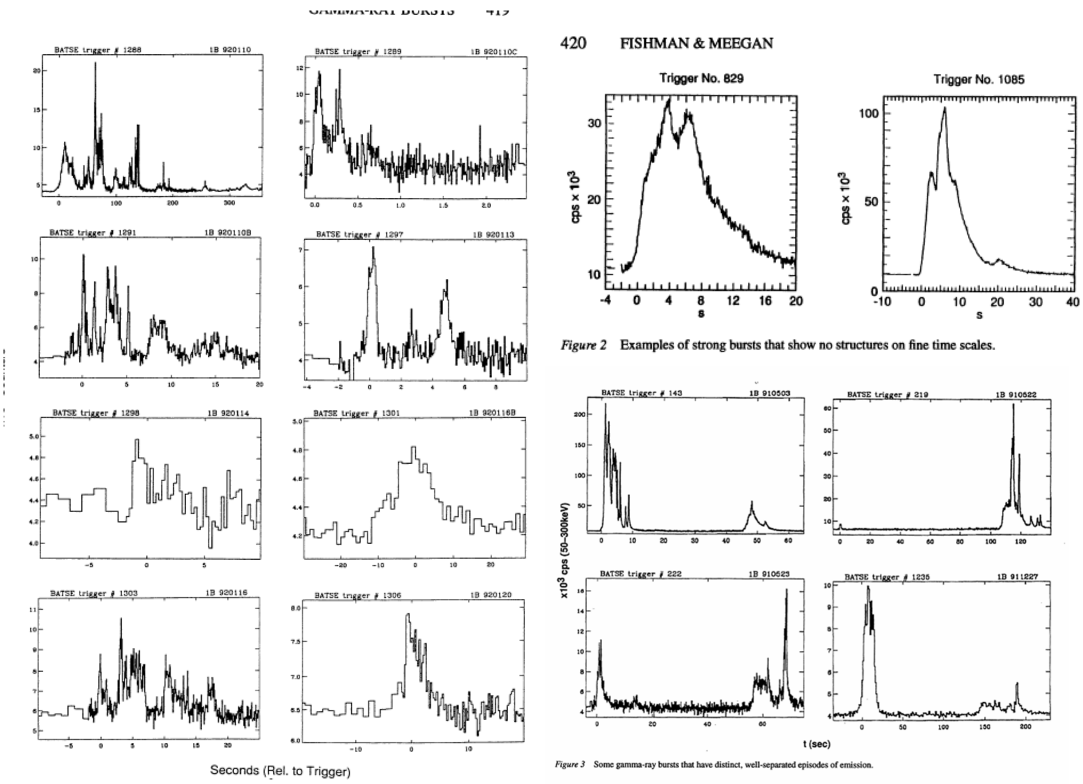

Figure 2 Examples of strong bursts that show no structures on fine time scales.

Figure 3 Some gamma-ray bursts that have distinct, well-separated episodes of emission.

Figure 1 Sample page from the *First BATSE Catalog of Gamma Ray Bursts* (Fishman et al 1994b), indicating the diversity in the time profiles, intensities, and durations of gamma-ray bursts.

Spectrum

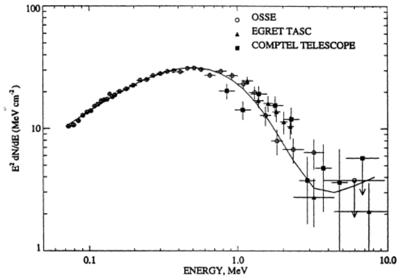

Figure 9 The spectrum of GB 910601 observed over a wide energy range, as measured by three experiments on *CGRO* (Share et al 1994). A typical broad spectrum with a peak power at about 600 keV is seen. (The fitted spectral up-turn above 4 MeV is not significant.)

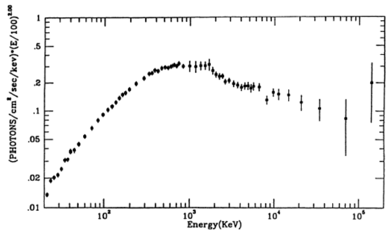

Figure 10 The spectrum of GB 910503, measured by all four experiments on the *Compton Gamma Ray Observatory* (Schaefer et al 1994d).

- Band spectrum(photon number)

$$N(E)dE =$$

$$AE^{\alpha}\exp(-\frac{E}{E_0}) \quad (\alpha-\beta)E_0 > E$$

$$BE^{\beta} \quad (\alpha-\beta)E_0 < E$$

$$F(E) = EN(E)$$

Energy/log interval

$$EF(E)d\ln E$$

- Peak energy (Max of EF(E))

$$E_p = (\alpha+2)E_0$$

$$\alpha \sim -1, \beta \sim -2$$

Ep distribution

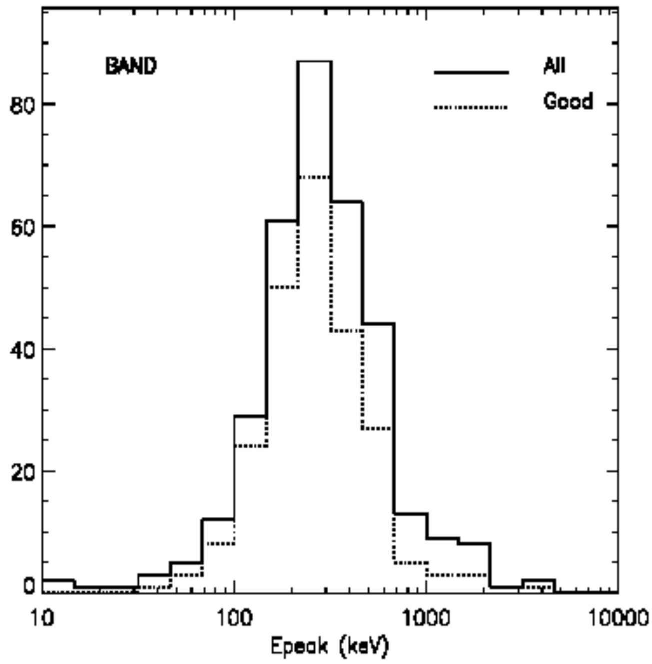

Kaneko et al. 2006

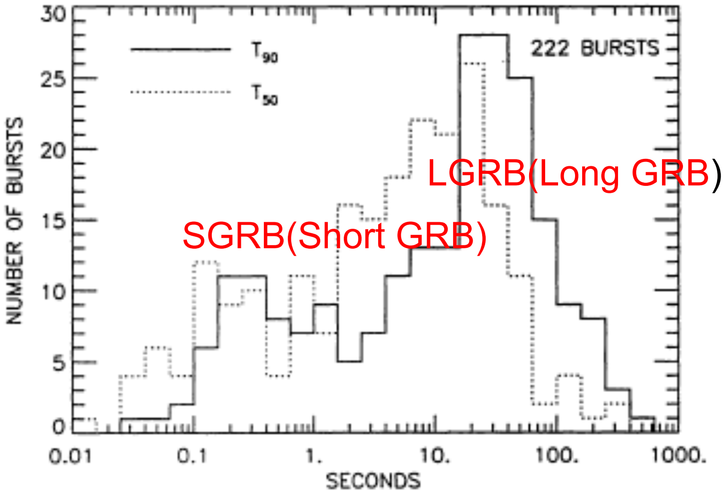

Figure 6 The duration distribution of 222 gamma-ray bursts from the BATSE catalog. Two separate measures are shown, representing 50% and 90% of the total burst fluence. A bimodal distribution is seen, with a separation near 2 s. (From Fishman et al 1994b.)

27

BATSE was launched in 1990 and observed ～2700GRBs.
Redshift z is unknown. Interestingly ～900 are SGRBs.

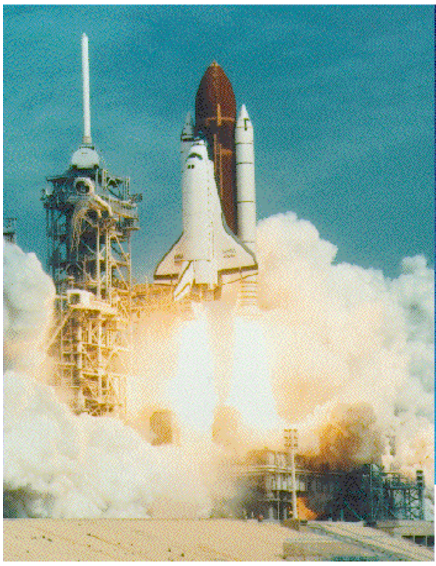

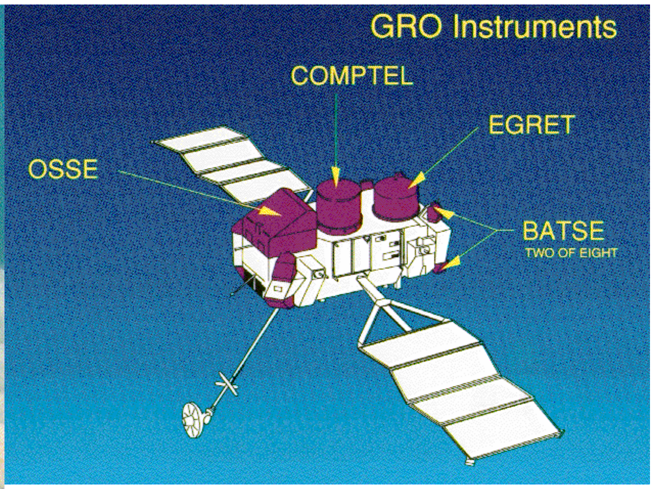

28

Arrival directions of

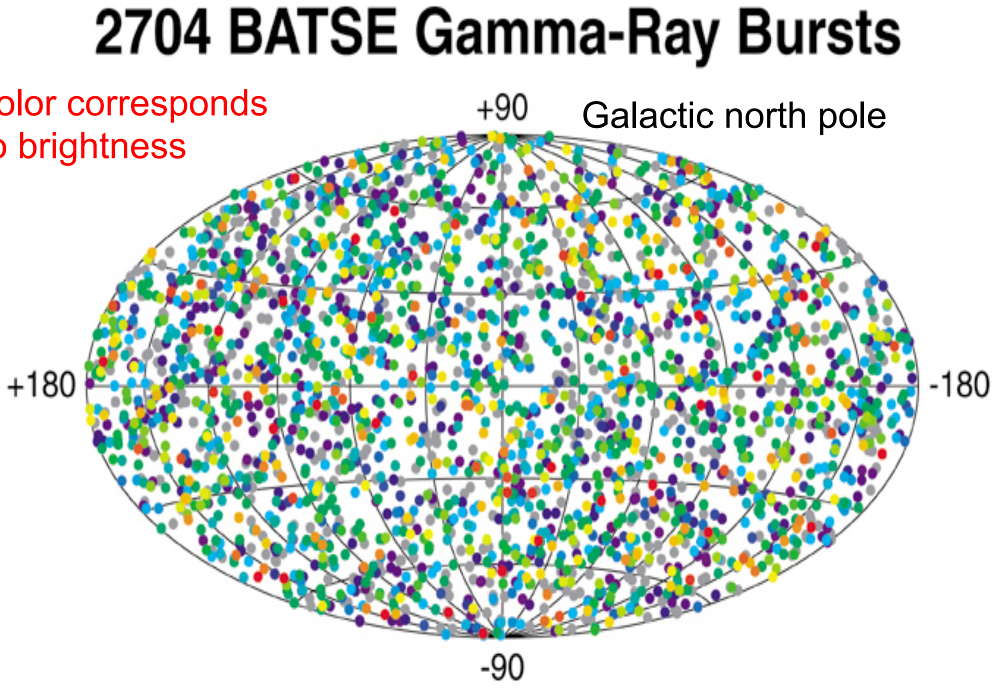

Color corresponds
To brightness

Galactic north pole

Galactic south pole

29

Example of SGRB

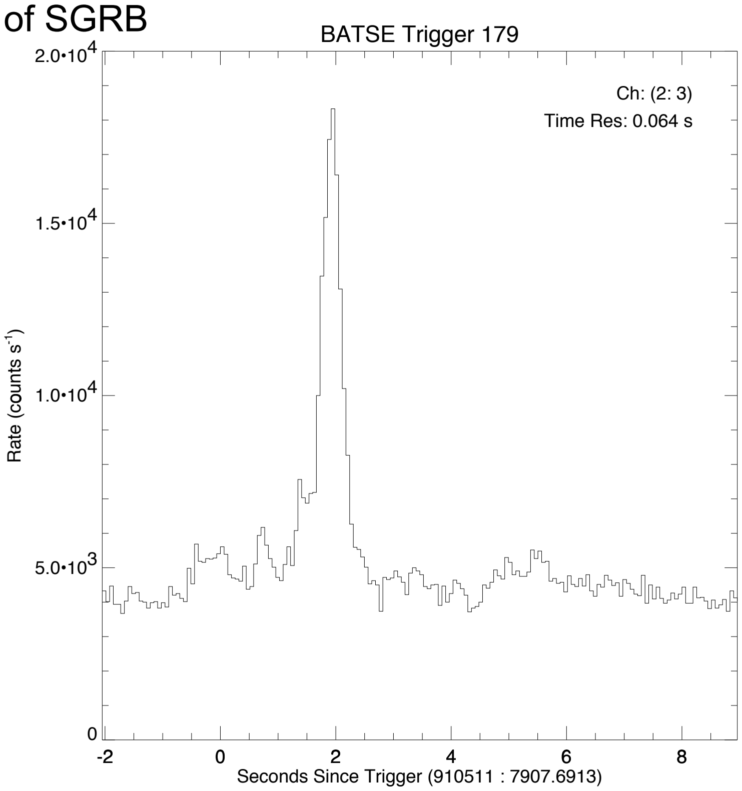

30

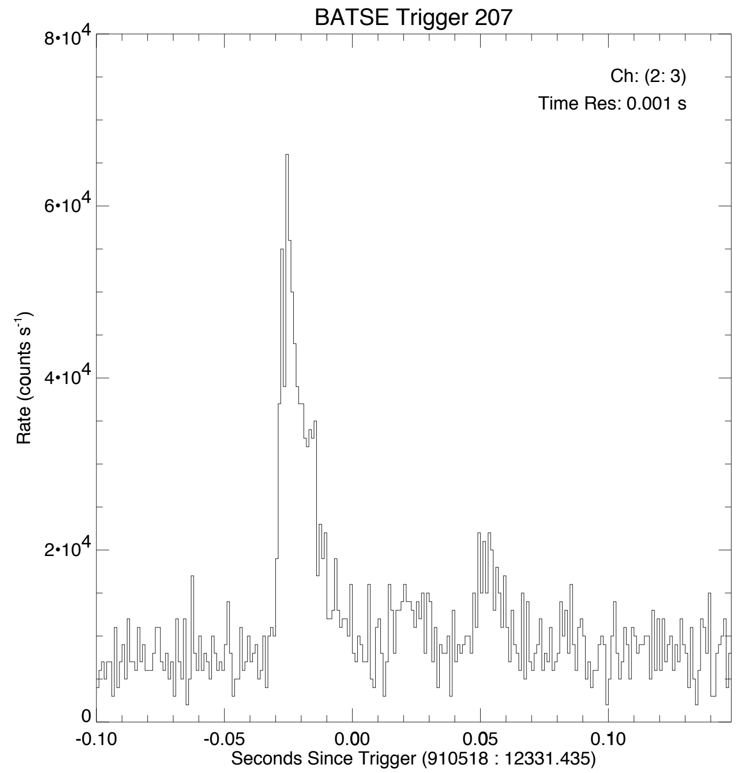
BATSE Trigger 207
Ch: (2: 3)
Time Res: 0.001 s
Rate (counts s-1)
Seconds Since Trigger (910518 : 12331.435)

31

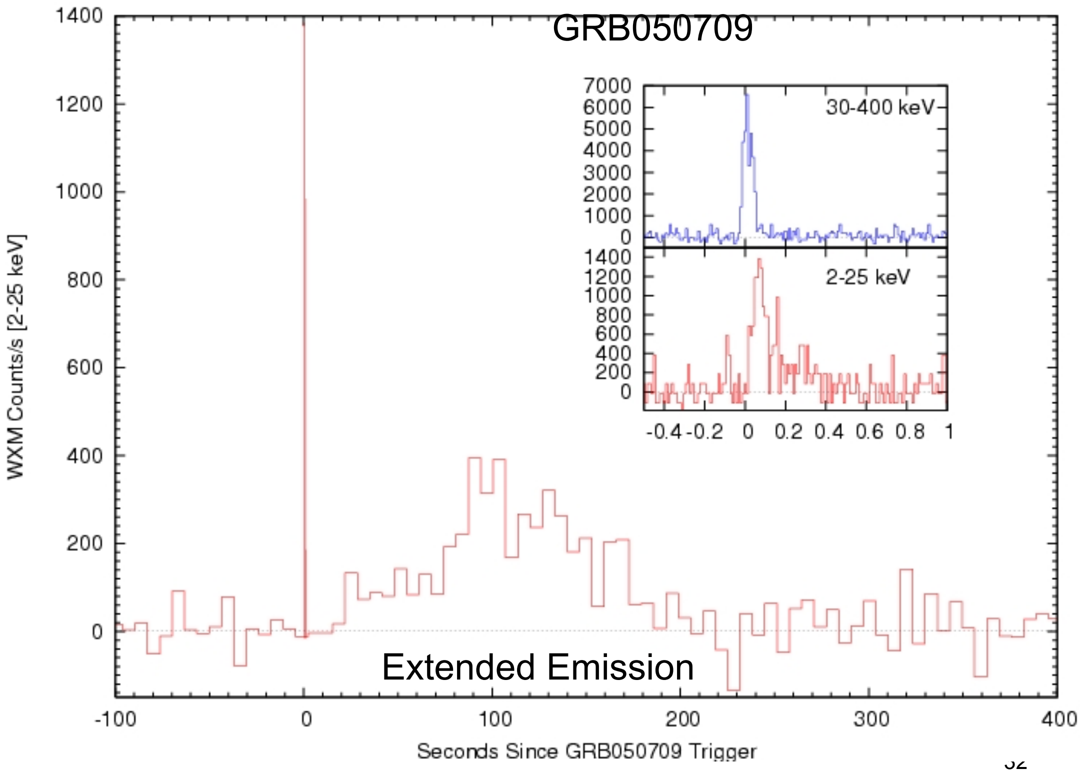
GRB050709
30-400 keV
2-25 keV
WXM Counts/s [2-25 keV]
Extended Emission
Seconds Since GRB050709 Trigger

32

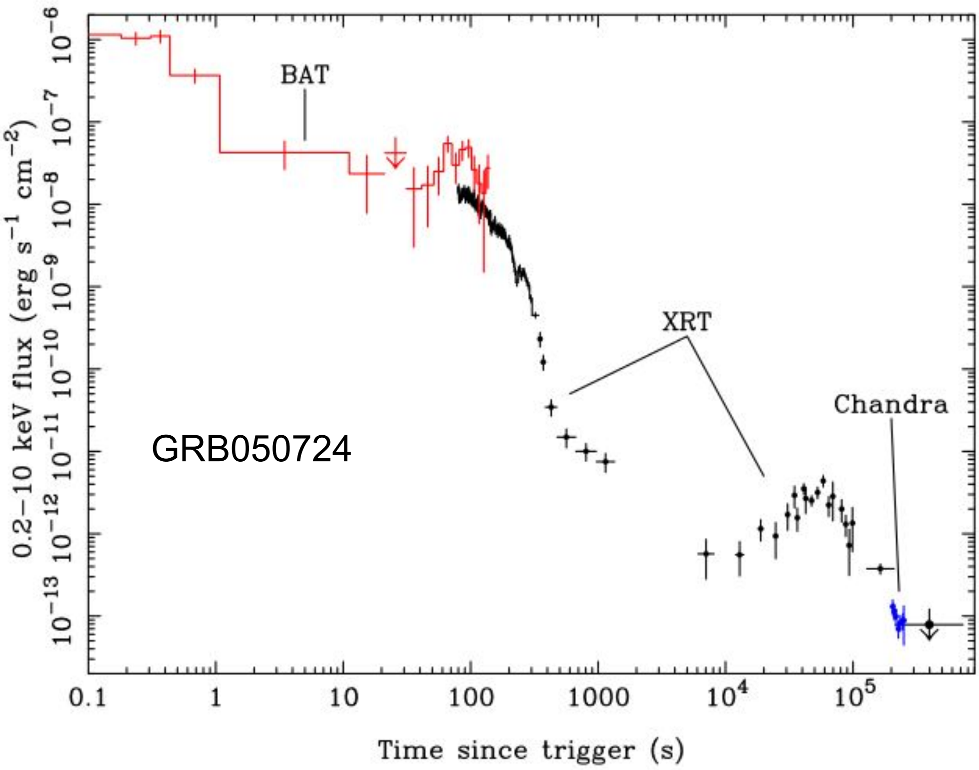

33

3 important variables

- E_{iso}= total energy if the emission is isotropic
- Lp= peak value of the luminosity
- Ep= peak energy of the photon
- for dim GRBs Ep is difficult to determine.
- It is impossible to determine these three values without redshift.
- Are there relations among Ep, Lp and Eiso? There are at least two empirical relations.

34

Yonetoku relation for（Ep-Lp）

- Yonetoku, Murakami, Nakamura et al. in 2004. We only had 11 LGRBs with z, Ep and Lp.

TABLE 1

SPECTRAL PARAMETERS FOR 11 KNOWN-REDSHIFT GRBs OF BATSE

GRB	Redshift	α	β	$E_p(1+z)$ (keV)	Peak Flux (10^{-6} ergs cm^{-2} s^{-1})	Peak Luminosity 10^{52} ergs s^{-1}	χ^2/dof	k_c
970508............	0.835	$-1.03^{+1.51}_{-0.06}$	$-2.20^{+0.10}_{-0.11}$	$89.8^{+37.8}_{-29.7}$	0.45 ± 0.10	0.14 ± 0.01	43.8/40	1.6
970828............	0.9578	$-0.45^{+0.06}_{-0.06}$	$-2.06^{+0.08}_{-0.10}$	$742.6^{+29.4}_{-32.1}$	5.93 ± 0.34	3.67 ± 0.15	96.0/82	1.5
971214............	3.418	$-0.36^{+0.14}_{-0.14}$	$-3.10^{+0.52}_{-6.90}$	$806.7^{+48.6}_{-63.2}$	1.25 ± 0.28	19.51 ± 0.17	68.9/66	1.2
980326............	0.9–1.1	$-0.93^{+0.09}_{-0.08}$	$-2.96^{+0.21}_{-0.51}$	35.0–100.0	0.65 ± 0.15	0.24–0.40	55.7/48	1.4
980329............	2.0–3.9	$-0.79^{+0.03}_{-0.03}$	$-2.27^{+0.04}_{-0.05}$	785.0–1085.0	5.79 ± 4.17	12.49–72.38	121.1/112	1.3
980703............	0.966	$-0.80^{+0.22}_{-0.16}$	$-1.60^{+0.06}_{-0.09}$	>150.0	2.64 ± 0.51	1.76 ± 0.05	89.6/91	1.3
990123............	1.600	$-0.18^{+0.08}_{-0.07}$	$-2.33^{+0.08}_{-0.09}$	$1333.7^{+49.8}_{-56.9}$	19.6 ± 0.16	31.22 ± 0.23	134.1/112	1.2
990506............	1.30	$-0.90^{+0.19}_{-0.13}$	$-2.08^{+0.08}_{-0.10}$	$737.6^{+69.2}_{-87.8}$	9.36 ± 0.20	13.28 ± 0.10	108.3/103	1.3
990510............	1.619	$-0.71^{+0.12}_{-0.12}$	$-3.79^{+0.51}_{-6.21}$	$538.4^{+22.3}_{-32.1}$	2.98 ± 0.18	6.19 ± 0.06	89.9/111	1.4
991216............	1.020	$-0.66^{+0.04}_{-0.04}$	$-2.44^{+0.12}_{-0.17}$	$1083.7^{+37.3}_{-41.3}$	61.4 ± 1.21	32.36 ± 0.11	125.8/102	1.2
000131............	4.5	$-0.91^{+0.20}_{-0.15}$	$-2.02^{+0.18}_{-0.32}$	$926.0^{+97.5}_{-83.1}$	2.67 ± 0.41	51.35 ± 7.88	115.1/97	1.4

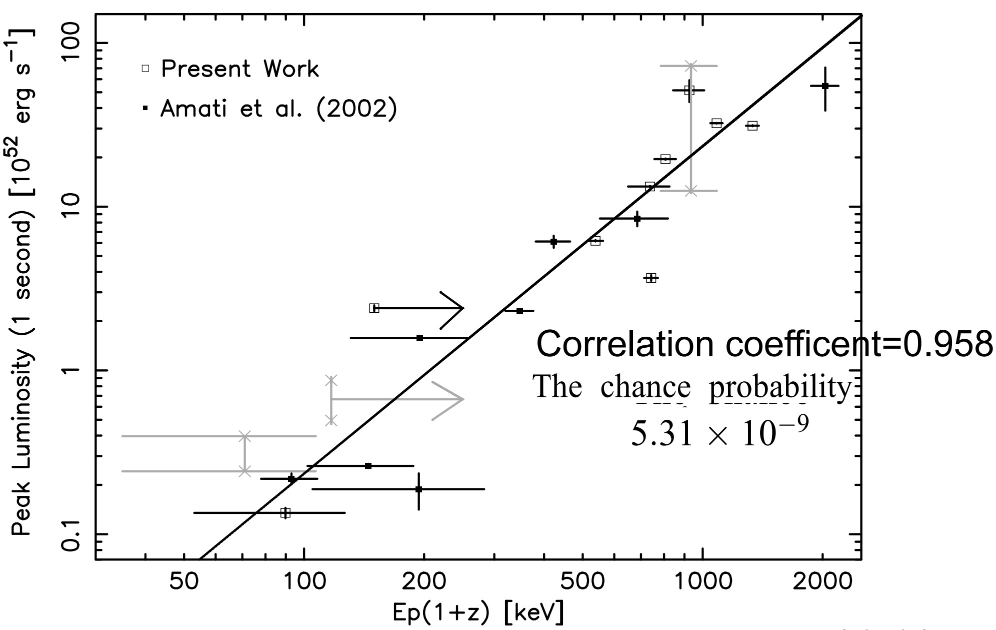

$$\frac{L}{10^{52}\ \mathrm{ergs\ s^{-1}}} = (2.34^{+2.29}_{-1.76}) \times 10^{-5} \left[\frac{E_p(1+z)}{1\ \mathrm{keV}}\right]^{2.0\mp0.2},$$

This relation can be used to determine the redshift of LGRBs.

That is, using the observed flux fp and the peak photon energy Ep with $d_L(z)$ being the luminosity distance to lead $L=4\pi d_L(z)^2 fp$. Inserting this luminosity, only z is unkown.

$$\frac{L}{10^{52}\ \mathrm{ergs\ s^{-1}}} = (2.34^{+2.29}_{-1.76}) \times 10^{-5} \left[\frac{E_p(1+z)}{1\ \mathrm{keV}} \right]^{2.0\mp0.2},$$

Therefore z is determined if you believe in Yonetoku Relation.

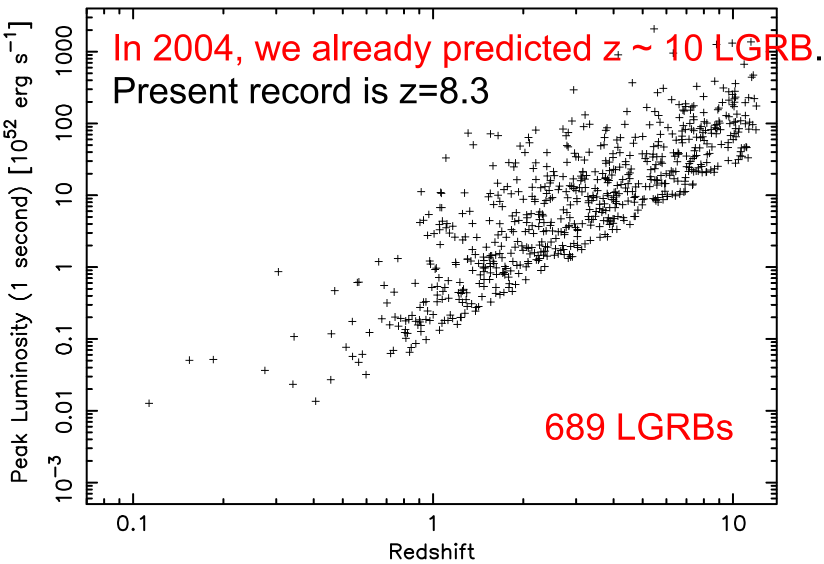

FIG. 2.—Distribution of the peak luminosity vs. redshift derived from the E_p-luminosity relation. The truncation of the lower end of the luminosity is caused by the flux limit of $F_{\mathrm{limit}} = 2 \times 10^{-7}$ ergs cm^{-2} s^{-1}.

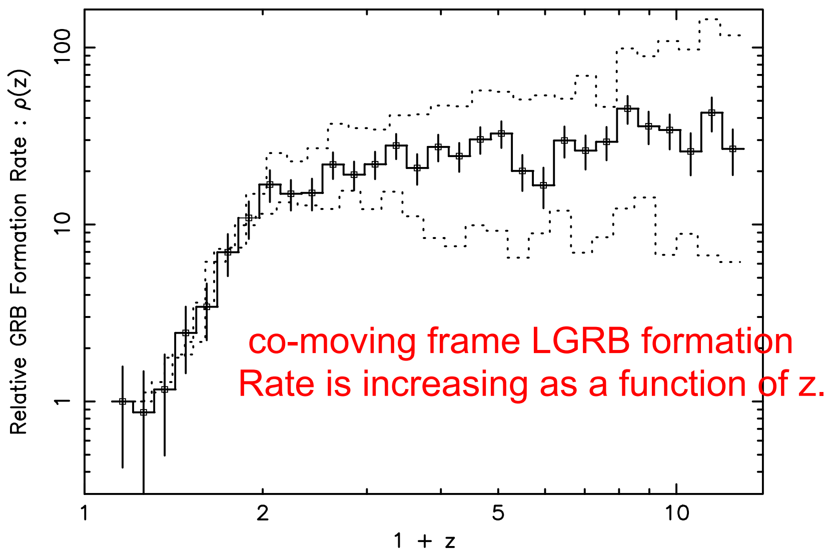

FIG. 8.—Relative GRB formation rate normalized at the first point. The solid line is the result based on the best fit of the E_p-luminosity relation. Two dotted lines indicate the upper and lower bounds caused by the uncertainty of the E_p-luminosity relation, and they are also normalized at the first point. The error bars accompanying the open squares represent the 1 σ statistical uncertainty of each point.

How about Ep-Lp relation for SGRBs？

- Many difficulties existed.
- Since the duration of SGRB is short, the number of photon is small. Therefore the determination of Ep is difficult.
- Many SGRBs have no or dim afterglow, so that it is difficult to determine redshift z.
- Host galaxies are far from SGRBs in many cases so that determination of z from host galaxy is also difficult.
- As a whole the number of SGRBs with z and Ep has been increasing very slowly.

Tsutsui, Yonetoku and Nakamura et al. succeeded to determine Ep--Lp relation in (MNRAS 2013 431, 1398).

13 SGRB candidates. However 5 belong to LGRB. We have only 8 SGRBs.

z, the rest-frame duration $T_{90}^{\rm rest} = T_{90}/(1+z)$, the spectral peak energy $E_{\rm p}$, the peak luminosity $L_{\rm p}$ in 64 ms of the observer frame time bin, the isotropic energy $E_{\rm iso}$, class of SGRB candidates and the reference, respectively. For details see the text.

GRB	Redshift	$T_{90}^{\rm rest}$ (s)	$E_{\rm p}$ (keV)	$L_{\rm p}$ (erg s^{-1})	$E_{\rm iso}$ (erg)	Class	Ref.[a]
040924	0.86	0.81	$124.55^{+11.15}_{-11.15}$	$(2.28^{+0.25}_{-0.24}) \times 10^{52}$	$(1.01^{+0.05}_{-0.05}) \times 10^{52}$	Misguided	(1)
050709[b]	0.16	0.60	$97.32^{+7.76}_{-0.58}$	$(7.51^{+0.76}_{-0.81}) \times 10^{50}$	$(4.33^{+0.29}_{-0.30}) \times 10^{49}$	Secure	(2)
051221	0.55	0.91	$621.69^{+87.42}_{-67.69}$	$(2.77^{+0.29}_{-0.29}) \times 10^{52}$	$(3.53^{+0.43}_{0.31}) \times 10^{51}$	Secure	(3)
061006	0.44	0.35	$954.63^{+198.39}_{-125.86}$	$(2.06^{+0.15}_{-0.31}) \times 10^{52}$	$(9.83^{+0.20}_{-0.94}) \times 10^{51}$	Secure	(4)
070714B	0.92	1.04	$2150.40^{+910.39}_{-443.52}$	$(6.56^{+0.79}_{-1.36}) \times 10^{52}$	$(1.61^{+0.18}_{-0.24}) \times 10^{52}$	Secure	(5)
071020	2.15	1.11	$1012.69^{+152.94}_{-101.33}$	$(3.06^{+0.35}_{-1.04}) \times 10^{53}$	$(1.24^{+0.04}_{-0.47}) \times 10^{53}$	Misguided	(6)
080913	6.70	1.04	$1008.05^{+1052.52}_{-224.54}$	$(3.18^{+0.28}_{-0.50}) \times 10^{53}$	$(1.09^{+0.11}_{-0.08}) \times 10^{53}$	Misguided	(7)
090423	8.26	1.30	$612.36^{+193.53}_{-193.53}$	$(4.63^{+9.95}_{-1.48}) \times 10^{53}$	$(1.17^{+1.45}_{-0.38}) \times 10^{53}$	Misguided	(8)
090510	0.90	0.16	$8679.58^{+947.69}_{-947.69}$	$(1.04^{+0.24}_{-0.14}) \times 10^{54}$	$(4.54^{+1.05}_{-0.61}) \times 10^{52}$	Secure	(8)
100117A	0.92	0.16	$936.96^{+297.60}_{-297.60}$	$(1.89^{+0.21}_{-0.35}) \times 10^{52}$	$(1.87^{+0.23}_{-0.23}) \times 10^{51}$	Secure	(8)
100206	0.41	0.09	$638.98^{+131.21}_{-131.21}$	$(9.98^{+11.50}_{-3.25}) \times 10^{51}$	$(7.63^{+7.89}_{-2.29}) \times 10^{50}$	Secure	(8)
100816A	0.81	1.11	$235.36^{+15.74}_{-15.74}$	$(9.69^{+1.95}_{-1.28}) \times 10^{51}$	$(9.03^{+1.52}_{-1.04}) \times 10^{51}$	Misguided	(8)
101219A	0.72	0.35	$841.82^{+107.56}_{-82.50}$	$(1.56^{+0.24}_{-0.23}) \times 10^{52}$	$(8.81^{+1.00}_{-1.05}) \times 10^{51}$	Secure	(9)

[a]References for spectral parameters, peak fluxes and fluences: (1) Golenetskii et al. (2004); (2) Villasenor et al. (2005); (3) Golenetskii et al. (2005); Norris et al. (2005); (4) Golenetskii et al. (2006); (5) Ohno et al. (2007); Kodaka et al. (2007); (6)

41

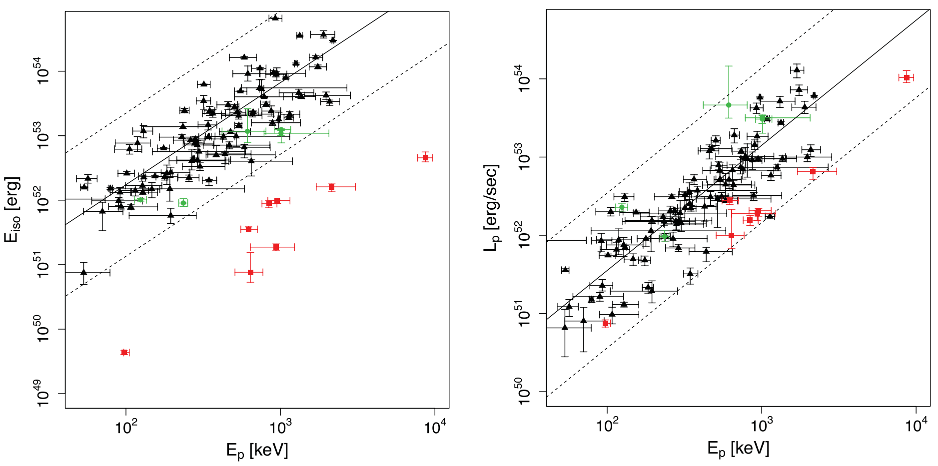

Figure 1. The $E_{\rm p}$–$E_{\rm iso}$ (left) and $E_{\rm p}$–$L_{\rm p}$ (right) diagrams. The LGRBs from Yonetoku et al. (2010) are marked with the black filled triangles, misguided SGRBs with the green filled circles and secure SGRBs with the red filled squares. The best-fitting function and $3\sigma_{\rm int}$ dispersion of the correlations of LGRBs from Yonetoku et al. (2010) are indicated with the black solid and dotted lines, respectively. The peak luminosities of LGRBs are defined by 1024 ms bin in the observer frame, while those of SGRBs by 64 ms bin in the observer frame.

Left Ep-Eiso relation
Black triangles→ LGRBs
Green → not SGRB but LGRB
Red squares → Secure SGRB

Right
black solid line → Ep-Lp for LGRBs with dotted 3σ dotted lines
All secure SGRBs are below Black solid line

42

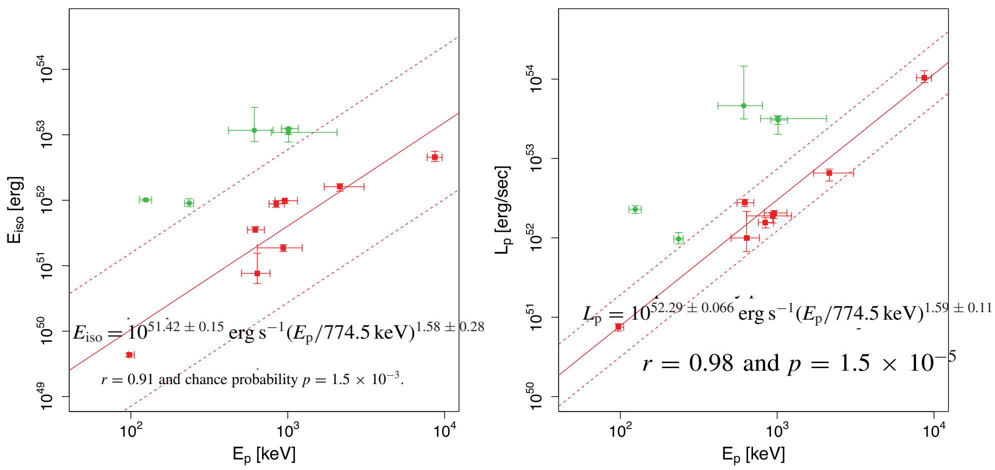

Figure 2. Left: the $E_{\rm p}-E_{\rm iso}$ diagram for SGRBs. Right: the $E_{\rm p}-L_{\rm p}$ diagram for SGRBs. In each figure, misguided SGRBs are marked with green filled circles, and secure SGRBs with red filled squares. The best-fitting function and $3\sigma_{\rm int}$ dispersion are indicated with the red solid and dotted lines, respectively.

Left
Ep-Eiso relation for SGRB
is 100 times dimmer than that
of LGRB

Right
Ep-Lp relation for SGRB
is 5 times dimmer than that
of LGRB

BATSE Bright SGRB Ghirlanda, Nava Ghisellini at al. 2009 with no z information

Table 6. The sample of 79 short BATSE GRBs.

Trig.	T_{90} s	P phot/(cm^2 s)	α	E_0 keV	χ^2(dof)	Fluence erg/cm^2	Peak flux erg/(cm^{2}s)
6293	0.192±0.091	88.53±1.00	-1.27±0.02		1.216(109)	4.56E-6	>5.74E-5
298	0.455±0.065	56.13±1.27	-0.57±0.92	85.38± 64.90	1.113(102)	1.99E-7	1.43E-5
3412	0.068±0.006	54.82±0.76	-1.31±0.52	110.20± 80.98	0.892(103)	2.62E-7	1.91E-5
6668	0.116±0.006	39.12±0.61	-0.39±0.49	126.80± 62.57	1.184(107)	4.99E-7	1.18E-5
444	0.256±0.091	28.55±0.76	-0.87±0.23	113.50± 28.39	1.132(102)	5.07E-7	8.04E-6
2514	0.200±0.094	28.40±0.74	-0.81±0.14	163.30± 25.95	1.129(100)	1.12E-6	8.99E-6
3152	1.793±0.066	25.34±0.72	-0.40±0.09	683.70±116.50	1.175(107)	6.55E-6	4.64E-5
5561	0.104±0.011	19.28±0.45	-1.20±1.48	48.51± 25.00	0.956(108)	1.65E-7	8.69E-6
3087	1.152±0.091	18.68±0.58	-1.19±0.15	273.10± 74.50	1.103(76)	2.89E-6	7.02E-6
2273	0.224±0.066	18.59±0.55	-0.18±0.45	132.70± 49.46	0.886(100)	3.88E-7	6.26E-6
7281	1.664±0.143	16.83±0.42	-0.83±0.15	123.30± 18.60	1.296(107)	2.21E-6	4.80E-6
2068	0.591±0.060	15.63±0.59	-0.22±0.26	97.07± 22.85	1.210(107)	3.91E-7	4.19E-6
2125	0.223±0.013	15.42±0.56	-0.48±0.30	240.50± 90.00	0.844(102)	4.57E-7	7.43E-6
3173	0.208±0.025	14.90±0.58	-1.00±0.18	559.60±281.65	1.356(105)	6.69E-7	9.52E-6
2679	0.256±0.091	13.73±0.51	-0.32±0.13	650.20±149.25	1.363(107)	3.14E-6	2.72E-5
1553	0.960±0.143	13.70±0.52	-0.87±0.11	764.00±183.60	1.173(96)	6.62E-6	1.35E-5
6123	0.186±0.042	12.83±0.42	-0.23±1.64	76.66± 49.00	1.107(108)	1.11E-7	3.10E-6
6635	1.152±0.143	12.05±0.39	-1.74±0.15	129.50± 32.70	1.014(91)	2.76E-6	6.57E-6
1088	0.192±0.091	11.92±0.55	0.10±2.11	68.08± 61.79	1.186(104)	7.41E-8	2.80E-6
1453	0.192±0.453	11.89±0.51	-0.16±0.65	94.20± 48.00	0.812(108)	1.80E-7	3.17E-6
6535	1.664±0.143	11.88±0.38	-0.97±0.08	1175.60±384.27	1.391(108)	7.36E-6	1.47E-5
2320	0.608±0.041	11.03±0.47	-0.58±0.19	129.00± 26.10	0.794(103)	7.57E-7	3.23E-6
2933	0.320±0.091	10.77±0.44	0.22±0.62	130.20± 55.94	1.429(107)	3.42E-6	4.33E-6
7939	1.039±0.072	10.77±0.38	-0.41±0.15	99.73± 12.96	1.193(82)	2.53E-6	2.86E-6
2614	0.296±0.057	10.49±0.52	-1.00±0.18	469.60±222.80	0.836(108)	6.08E-7	5.84E-6
2715	0.384±0.091	10.47±0.50	0.08±0.11	562.80± 85.20	1.049(108)	7.69E-6	3.30E-5
2896	0.456±0.033	10.44±0.48	-0.87±0.26	79.94± 18.19	1.072(106)	7.53E-7	2.89E-6
7784	1.918±1.995	10.29±0.34	-0.83±0.35	140.20± 54.30	1.432(108)	5.63E-7	3.05E-6
2317	0.896±0.091	9.73±0.46	-0.53±0.25	73.46± 13.12	1.249(65)	1.04E-6	2.41E-6
2834	0.680±0.011	8.79±0.44	-0.54±0.24	407.60±168.80	1.165(85)	1.36E-6	6.90E-6
6679	1.408±0.091	8.62±0.35	-0.61±0.27	318.90±141.60	1.409(107)	9.39E-7	4.91E-6
6527	1.856±0.516	8.47±0.38	-1.32±0.21	80.36± 15.60	1.090(95)	3.33E-6	3.25E-6
7353	0.249±0.004	8.47±0.38	0.00±0.22	615.80±197.40	1.181(107)	4.19E-6	2.72E-5
5277	0.496±0.023	8.14±0.33	0.29±0.24	208.40± 30.81	0.885(106)	1.54E-6	6.46E-6
8104	0.384±0.091	8.13±0.30	0.42±1.35	110.60± 70.37	0.774(107)	2.20E-7	3.04E-6
2330	0.804±0.009	8.03±0.39	-0.86±0.29	616.90±491.30	0.961(75)	1.02E-6	6.54E-6
6263	1.984±0.181	7.99±0.31	-0.36±0.64	69.14± 30.59	1.054(107)	3.78E-7	1.91E-6
5339	0.832±0.091	7.77±0.33	-0.40±0.10	567.90± 99.64	0.732(93)	4.95E-6	1.12E-5
603	1.472±0.272	7.50±0.56	-0.71±0.63	155.30± 93.62	1.004(85)	3.78E-7	2.36E-6
6368	0.896±0.326	7.24±0.34	-1.37±0.18		0.997(108)	3.21E-7	>4.26E-6
6606	0.704±0.389	7.16±0.29	-1.77±0.20		0.973(108)	5.02E-7	>3.04E-6
3642	0.704±0.091	6.83±0.31	0.21±0.88	89.97± 58.42	1.262(107)	2.92E-7	1.93E-6
6671	0.256±0.091	6.71±0.31	-1.39±0.13		0.937(100)	5.36E-7	>3.84E-6
5647	1.088±0.326	6.50±0.32	-0.06±0.80	108.50±115.16	1.366(107)	1.74E-7	1.95E-6
7375	0.311±0.073	6.40±0.31	-0.47±0.87	267.90±200.05	1.039(101)	3.19E-7	3.46E-6
677	0.055±0.008	6.21±0.44	0.65±1.29	127.20±168.26	0.751(105)	1.22E-7	3.18E-6
1076	0.161±0.016	6.18±0.44	-2.46±0.33		1.417(89)	1.20E-7	>2.16E-6
936	1.438±0.065	5.85±0.44	-0.84±0.26	341.50±179.45	1.069(104)	7.03E-7	2.91E-6
5607	1.088±0.091	5.85±0.30	-0.71±0.23	426.20±199.45	1.150(82)	1.19E-6	3.97E-6
7142	0.969±0.064	5.81±0.28	0.94±0.33	124.10± 12.79	0.953(107)	1.42E-6	3.50E-6
4955	0.464±0.036	5.73±0.31	-1.04±0.45	298.20±371.80	1.176(107)	2.71E-7	2.33E-6
4776	0.448±0.091	5.54±0.28	-0.19±0.32	232.70± 88.45	1.152(107)	6.90E-8	3.27E-6
7813	0.564±0.164	5.37±0.29	-2.68±0.17		1.053(108)	5.59E-7	>1.94E-6
1760	0.576±0.143	5.27±0.35	-0.25±0.28	188.70± 56.95	1.027(105)	6.18E-7	2.37E-6
7378	1.247±0.077	5.25±0.33	-0.52±0.16	536.20±153.35	1.465(107)	2.60E-6	5.87E-6
4660	1.168±0.080	5.15±0.29	0.56±0.21	161.70± 23.80	0.919(87)	1.92E-6	3.53E-6
5533	0.768±0.091	5.12±0.30	0.02±0.15	335.20± 60.15	0.971(87)	2.91E-7	6.26E-6
7078	0.448±0.091	5.11±0.42	-3.60±0.45		0.920(108)	1.73E-7	>2.90E-6

Table 6. continue....

Trig.	T_{90} s	P phot/(cm^2 s)	α	E_0 keV	χ^2(dof)	Fluence erg/cm^2	Peak flux erg/(cm^{2}s)
5527	0.820±0.008	5.04±0.26	-0.34±0.11	489.30± 88.30	0.760(90)	3.73E-6	6.41E-6
3735	1.301±0.091	4.83±0.29	0.00±0.18	301.70± 55.05	1.286(107)	2.60E-6	4.91E-6
3297	0.272±0.023	4.45±0.33	-0.83±0.37	496.80±501.70	1.198(106)	4.90E-7	3.07E-6
2952	0.680±0.018	4.37±0.34	-0.69±0.25	570.20±312.15	0.791(107)	8.76E-7	4.13E-6
5599	0.598±0.043	4.24±0.26	-0.79±0.30	664.70±637.40	1.234(106)	8.25E-7	4.07E-6
5529	1.015±0.129	4.23±0.29	1.37±0.96	65.65± 22.09	1.015(106)	2.95E-7	1.31E-6
7133	1.079±0.37	4.08±0.26	-0.14±0.29	135.80± 36.25	1.115(107)	6.01E-7	1.43E-6
7793	1.093±0.04	3.99±0.27	-0.05±0.22	470.90±126.35	1.054(106)	4.34E-6	7.56E-6
2377	0.496±0.011	3.98±0.33	0.06±0.26	229.30± 55.10	0.875(100)	6.90E-7	2.91E-6
3606	1.824±0.066	3.95±0.26	0.19±0.35	175.90± 49.60	1.216(102)	1.72E-6	2.26E-6
3113	0.976±0.023	3.90±0.35	-0.78±0.16	690.00±316.25	1.145(90)	1.54E-6	3.95E-6
6715	0.452±0.027	3.71±0.26	-0.25±0.78	206.20±187.77	1.178(107)	4.34E-7	1.83E-6
575	0.413±0.022	3.70±0.46	0.17±0.87	121.40± 63.56	0.890(106)	1.71E-7	1.35E-6
2217	0.656±0.029	3.56±0.31	0.36±0.27	281.00± 93.35	1.234(73)	1.46E-6	4.97E-6
3921	0.464±0.161	3.52±0.24	0.36±0.48	179.90± 66.60	1.086(106)	5.42E-7	2.39E-6
5206	0.304±0.023	3.46±0.28	-1.23±0.09		1.219(107)	3.81E-7	>2.34E-6
2918	0.448±0.091	3.44±0.34	-0.60±0.63	252.50±195.90	1.085(100)	1.77E-7	1.59E-6
3940	0.576±0.091	3.19±0.22	-0.33±0.44	101.80± 40.67	1.187(97)	2.50E-7	8.64E-7
7912	1.856±0.707	3.10±0.25	-0.28±0.26	150.90± 47.65	1.236(107)	8.05E-7	1.11E-6
6341	1.920±0.707	3.05±0.28	-0.25±0.29	332.00±143.20	0.878(107)	1.34E-6	2.64E-6
3359	0.344±0.025	3.01±0.25	0.67±0.90	121.00± 74.79	1.037(104)	2.35E-7	1.46E-6

The list of SGRBs with the observed or limit of z
Fong, Bergers and Chornock et al. 2013

Short GRB Host Galaxy Morphologies

GRB	T_{90}[a] (s)	z[b]	Type[c]	90% XRT Uncert.[d] (arcsec)	$P_{cc}(<\delta R)$	References
			Subarcsecond localized			
050709	0.07/130	0.161	L		3×10^{-3}	1–3
050724A	3	0.257	E		2×10^{-5}	4–5
051221A	1.4	0.546	L		5×10^{-5}	6–7
060121	2.0	<4.1	?		2×10^{-3}	8–9
060313	0.7	<1.7	?		3×10^{-3}	10–11
061006	0.4/130	0.4377	L		4×10^{-4}	12–15
061201	0.8	0.111	H/L		··· /0.08	9, 16–17
070429B	0.5	0.9023	L		3×10^{-3}	18–19
070707	1.1	<3.6	?		7×10^{-3}	20–21
070714B	2.0/64	0.9224	L		5×10^{-3}	19, 22–23
070724A	0.4	0.457	L		8×10^{-4}	24–25
070809	1.3	0.473	H/E		··· /0.03	9, 26
071227	1.8[e]	0.381	L		0.01	27–29
080503	0.3/170	<4.2	H/?		··· /0.1	9, 30–31
080905A	1.0	0.1218	L		0.01	32–33
081226A	0.4	<4.1	?		0.01	34–35
090305	0.4	<4.1	H/?		··· /0.06	9, 36
090426A	1.3	2.609	L		1.5×10^{-4}	37–38
090510	0.3	0.903	L		8×10^{-3}	39–40
090515	0.04	0.403	H/E		··· /0.15	9, 41
091109B	0.3	<4.4	?		...	42–43
100117A	0.3	0.915	E		7×10^{-5}	44–45
110112A	0.5	<5.3	H/?		0.43	46, This work
111020A[f]	0.4	...	?		0.01	47–48
111117A[f g]	0.5	1.3	L		0.02	49–50
			XRT only			
050509B	0.04	0.225	E	3.8	5×10^{-3}	51–52
050813[h]	0.6	0.72/1.8	E/?	2.9	...	53–57
051210	1.3	>1.4	?	1.6	0.04	14, 58
060502B	0.09	0.287	E	5.2	0.03	59–60
060801	0.5	1.130	L	1.5	0.02	61–62
061210	0.2/85	0.4095	L	3.9	0.02	14, 63
061217	0.2	0.827	L	5.5	0.24[i]	14, 64
070729[g]	0.9	0.8	E	2.5	0.05	65–66
080123	0.4/115	0.495	L	1.7	0.004	67–68
100206A	0.1	0.4075	L	3.3	0.02	69–70
100625A	0.3	0.452	E	1.8	0.04	71, This work
101219A	0.6	0.718	L	1.7	0.06	72, This work

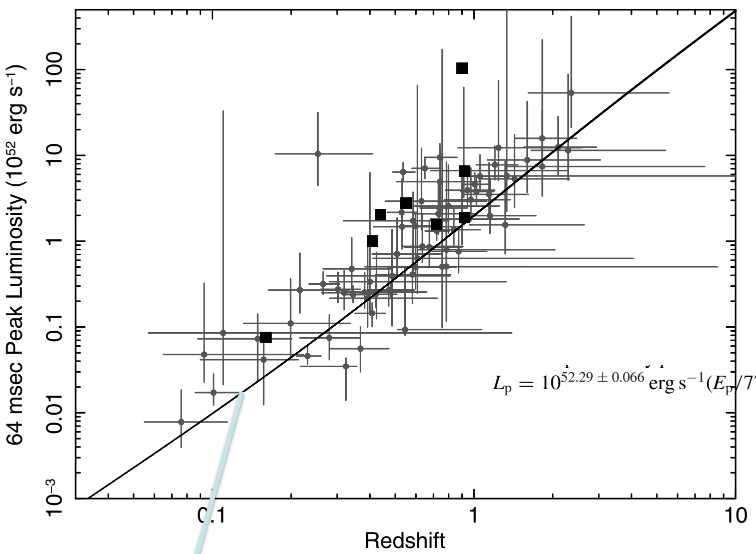

$$L_p = 10^{52.29 \pm 0.066}\,\mathrm{erg\,s^{-1}}(E_p/774.5\,\mathrm{keV})^{1.59 \pm 0.11}$$

Yonetoku, Nakamura, Sawano, et al. MNRAS 789 (2014)

Figure 1. Redshift distribution of SGRBs estimated by the E_p–luminosity correlation by Tsutsui et al. (2013). The solid squares are the known redshift samples, and the solid circles are those of pseudo-redshifts. The solid line is the flux limit of 4×10^{-6} erg cm^{-2} s^{-1}.

72 bright BATSE SGRBs with Ep. Using Ep-Lp relation of SGRB we determined z.
To derive the luminosity function and the event rate we used 45 SGRBs above the solid line of fp= 4×10^{-6}erg cm^{-2} s^{-1} so that we determined the lower limit of the event rate.
Squares are 8 SGRBs to determine Ep-Lp relation for SGRB.

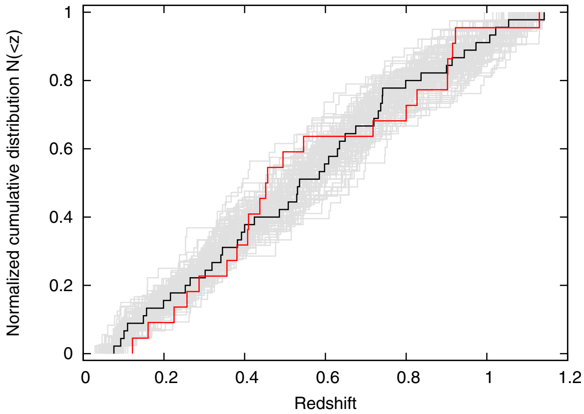

Figure 3. Cumulative redshift distribution of SGRBs up to $z = 1.14$. The black and the red solid lines are for 45 BATSE SGRBs in this paper and 22 known redshift samples observed by HETE-2 and *Swift*/BAT, respectively. The gray solid lines behind them show possible error regions estimated by the 100 Monte Carlo simulations. We can see the good agreement of red, black, and gray lines in the entire region. The Kolmogorv–Smirnov test between the black and red lines shows that the probability that the two curves arise from different distribution is 79.4%, and the error region shown in gray lines covers the red line. This strongly suggests that the E_p–L_p correlation for SGRB (Tsutsui et al. 2013) is a good distance indicator.

Black lines : cumulative redshift distribution of 45 BATSE SGRBs

Red lines : cumulative redshift distribution of 22 SGRBs by HETE-2 and Swift.

Grey : 100 Mont Carlo Simulations taking into Account of error in Ep and Lp

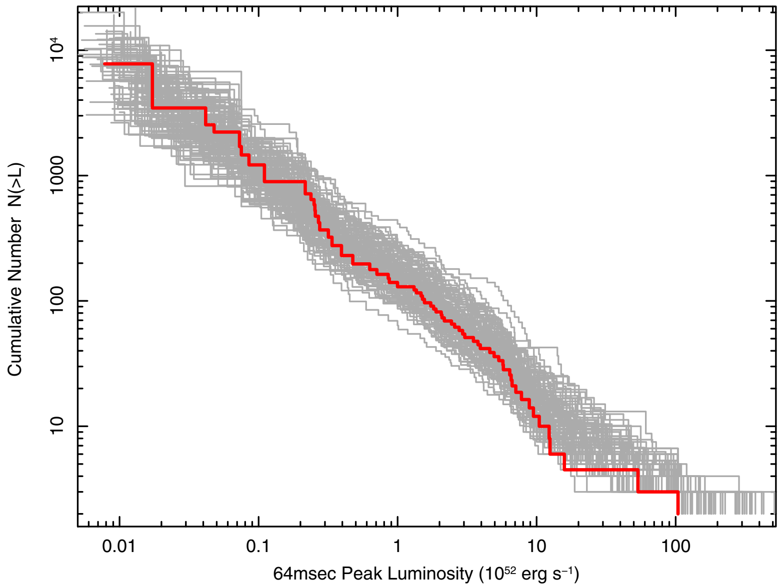

Figure 4. Luminosity function of SGRBs estimated from the data distribution of Figure 1. The red solid line shows one of the best estimations, and the 100 gray lines are the possible error region estimated by the Monte Carlo simulations. We can approximately describe it as a simple power-law function with an index of −1, and no obvious break has been found.

Red line : the cumulative luminosity function $\propto L^{-1}$

Grey lines: 100 Mont Carlo simulations

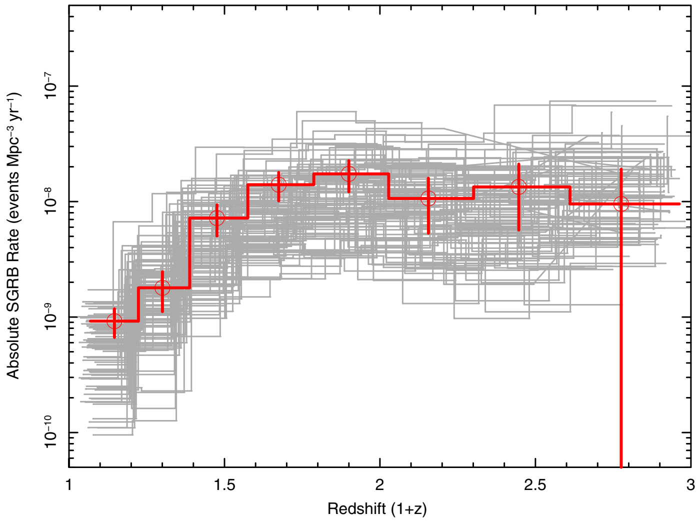

Figure 5. Absolute formation rate of SGRBs estimated from the data distribution of Figure 1. Again, the red line is the best estimation and the 100 gray lines are those from Monte Carlo simulations. The local event rate at $z = 0$ is $\rho_{\mathrm{SGRB}}(0) = 6.3^{+3.1}_{-3.9} \times 10^{-10}$ events Mpc^{-3} yr^{-1}.

Red line: SGRB formation rate

Grey lines: 100 Mont Carlo simulations.

$$R^{\mathrm{min}}_{\mathrm{on-axis}} = 6.3^{+3.1}_{-3.9} \times 10^{-10}\ \mathrm{events\ Mpc^{-3}\ yr^{-1}}$$

Number of SGRB with the determination of jet opening angle is only 4: SGRB130603B 4°-8°, SGRB11020A 3°-8°、SGRB090426 ~ 4.4°, SGRB051221 5.7°-7.3°

Taking a simple mean of 6°, we have off-axis SGRBs with the rate

$$\rho^{\mathrm{min}}_{\mathrm{SGRB,all}}(0) = 1.15^{+0.57}_{-0.71} \times 10^{-7}\ \mathrm{event\ Mpc^{-3}\ yr^{-1}}$$

If NS-NS is SGRB adv LIGO, Virgo. KAGRA will observe at least $3.9^{+1.9}_{-2.4}$ events yr^{-1}

If NS-BH(10Msun) is SGRB, the range is 3.4 times larger so that the expected event rate is

$$152^{+75}_{-94}\ \mathrm{events\ yr^{-1}}$$

If we include dimmer SGRBs below the flux limit
in the analysis, the rate would be 4 times larger.

What is happening in Adv LIGO O1 from 9/15-12/15?

Assuming that the range for NS-NS is 60Mpc and 100%
Duty cycle

If all SGRBs are NS-NS, expected number of event is
0.1 in O1.

If all SGRBs are NS-BH, expected event is 4.1 in O1.

If 10% of SGRB is NS-BH, expected event is 0.5 in O1.

We might see the paper like "The evidence for the detection
of GW from SGRB…………

Adv LIGO& Virgo

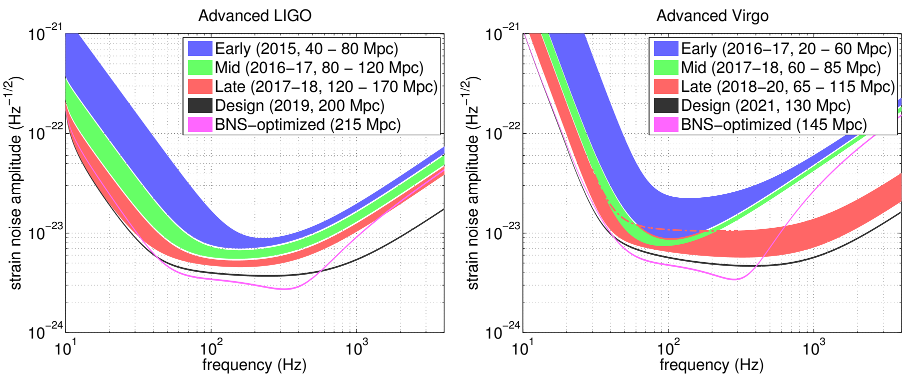

Figure 1: aLIGO (left) and AdV (right) target strain sensitivity as a function of frequency. The average distance to which binary neutron star (BNS) signals could be seen is given in Mpc. Current notions of the progression of sensitivity are given for early, middle, and late commissioning phases, as well as the final design sensitivity target and the BNS-optimized sensitivity. While both dates and sensitivity curves are subject to change, the overall progression represents our best current estimates.

Aasi et al. arXiv:1304.0670v1 [gr-qc] 2 Apr 2013

Extended Emission of SGRBs
Kisaka & Ioka 2015

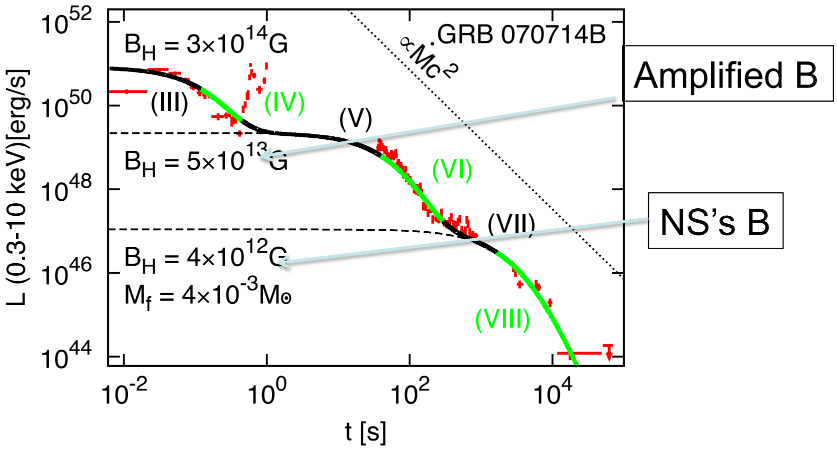

FIG. 2.— A representative light curve for prompt, extended and plateau emission in our BH model. Observational data of GRB 070714B is obtained from UK *Swift* Science Data Centre. Time shown in the horizontal axis denotes the rest-frame time since *Swift*/BAT triggers. For the redshift value, we follow Gompertz et al. (2013). The number III – VIII corresponds to the phase in Figure 1. For the rebrightening component at ~ 1 s, we consider flaring activities discussed in Section 4. 53

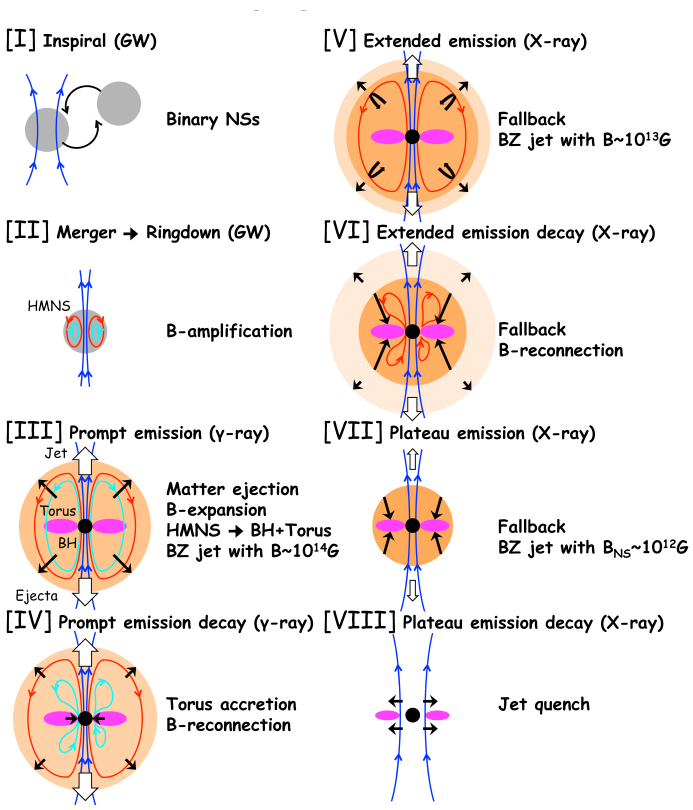

54

FIG. 1.— Schematic pictures of our BH model for short GRBs. See Section 2 for details.

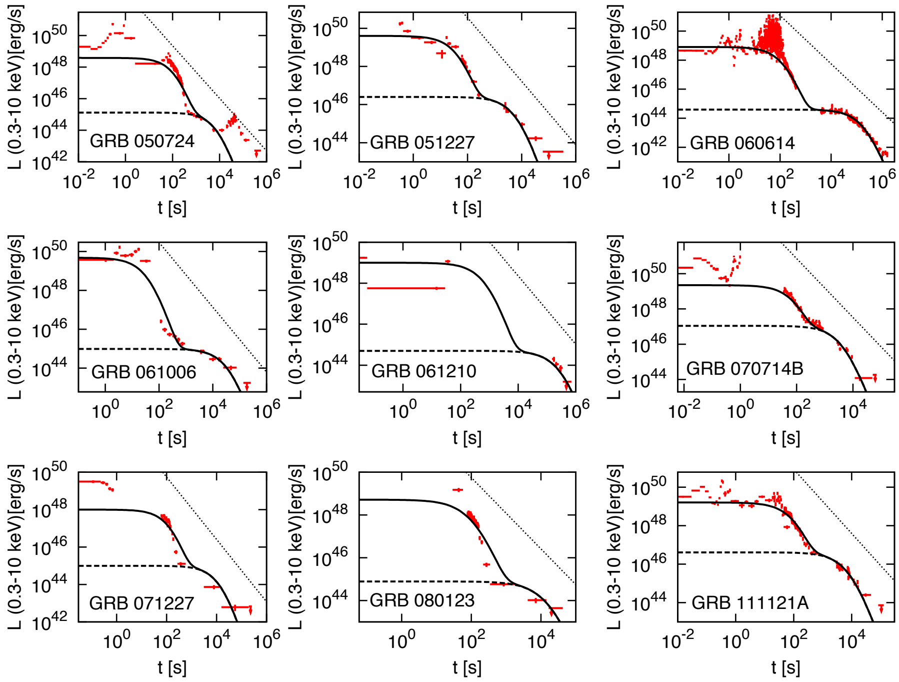

55

Kisaka, Ioka & Nakamura 2015

Scattered X- ray can be seen from every direction.

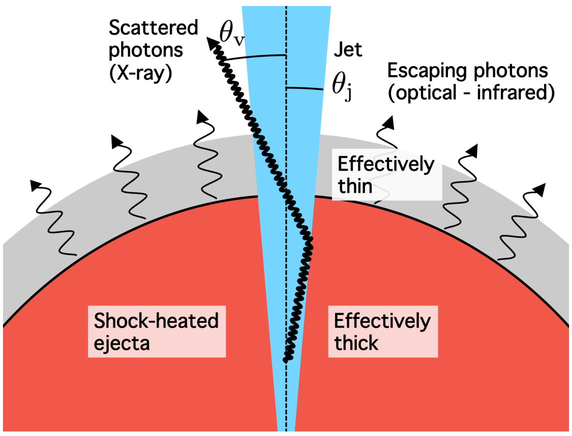

FIG. 1.— Schematic picture for the scattering of plateau emission and the engine-powered macronova. X-ray photons emitted from the inside of the jet (light blue region) are scattered by the optically thick ejecta (thick arrow). The grey region is effectively thin and the red region is effectively thick.

56

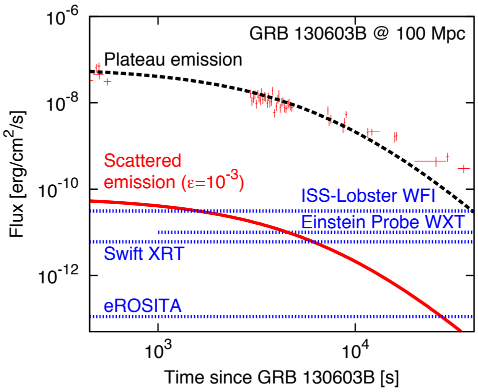

FIG. 2.— Light curves of the plateau (the black dashed curve) and its scattered emissions ($\epsilon = 10^{-3}$; the red solid curve). Red crosses are the plateau emission of GRB 130603B with the distance changed from the original redshift $z = 0.356$ to 100 Mpc. Observational data are obtained from UK *Swift* Science Data Centre. Blue dotted lines show the sensitivity limits for the soft X-ray detectors of *ISS-Lobster*/WTI (integration time 450 s), *Einstein Probe*/WXT (integration time 1000 s), *Swift*/XRT (integration time 100 s) and *eROSITA* (integration time corresponding to a single survey pass). The scattered emission is detectable for these X-ray detectors.

Polarization degree is

$$\Pi = (1 - \cos^2\theta)/(1 + \cos^2\theta)$$

Scattered X-ray is polarized.

θ is the inclination angle of the binary.

Direction of the polarization is the same as the Ascending node

These two values can be determined by GW also.

Section 2: Coalescence of stellar mass size Binary Black Hole(BBH)

- No definite candidates are observed .
- No EM radiation unless gas around BH exists
- Population Synthesis is the unique method.
- PopIII BBH with Kinugawa et al. 2014, 2015
- The code is the PopIII version of Hurley, Tout &Pols(2002)'s open code for Pop I.
- PopIII star is the zero metal star formed first in our Universe. Radius is small and no mass loss since it has no metals.

Evolution of PopIII star by Marigo et al.2001

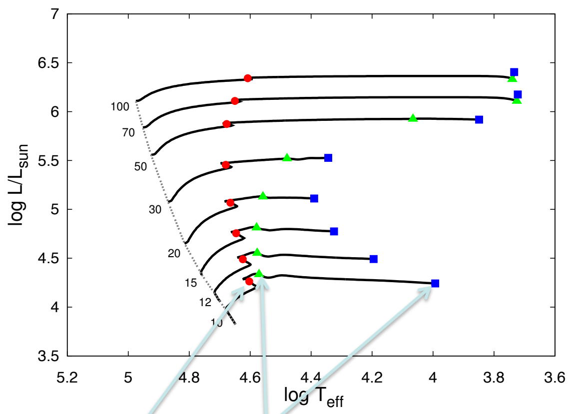

Figure 1. The Hertzsprung–Russell (HR) diagram for the Pop III stars of mass $10\ \mathrm{M}_\odot \leqslant M \leqslant 100\ \mathrm{M}_\odot$ using the data taken from Marigo et al. (2001). The number attached to each solid curve is the mass of each star in unit of $\mathrm{M}_\odot$. The dashed line shows the ZAMS (Zero Age Main Sequence) stars. Red circles, green triangles and blue squares correspond to the beginning of He-burning, the end of the He-burning and the beginning of the C-burning, respectively.

59

We make the fitting formula of the evolution of the radius of the star to save the time.

As shown in Fig. 1, we divide the life of Pop III stars into the four characteristic phases: (1) H-burning phase (from the ZAMS to red circle), (2) the He-burning phase (from red circle to green triangle), (3) the He-shell burning phase (blue square), and (4) after the C-ignition. In the followings, we show the fitting formulae in each phase. We use the subscripts H, He, HeS and C to each physical variables such as the radius and the mass to show the H-burning phase, the He-burning phase, the He-shell burning phase and the C-burning phase, respectively. The superscripts b and e denote the beginning and the end of each phase, respectively.

(1) H-burning phase

$$(R_{\mathrm{ZAMS}}/\mathrm{R}_\odot) = 1.22095 + 2.70041 \times 10^{-2}(M/10\ \mathrm{M}_\odot) + 0.135427(M/10\ \mathrm{M}_\odot)^2 - 1.95541 \times 10^{-2}(M/10\ \mathrm{M}_\odot)^3 + 8.7585 \times 10^{-4}(M/10\ \mathrm{M}_\odot)^4, \quad (1)$$

$$(R^{\mathrm{e}}_{\mathrm{H}}/\mathrm{R}_\odot) = 0.581309 + 2.27745(M/10\ \mathrm{M}_\odot) + 6.63321 \times 10^{-3}(M/10\ \mathrm{M}_\odot)^3, \quad (2)$$

and

$$(t_{\mathrm{H}}/\mathrm{Myr}) = 1.78652 + 10.4323(M/10\ \mathrm{M}_\odot)^{-1} + 3.70946(M/10\ \mathrm{M}_\odot)^{-2} + 2.04264(M/10\ \mathrm{M}_\odot)^{-3}, \quad (3)$$

$$\tau_{\mathrm{H}} = t/t_{\mathrm{H}}$$

$$\log(R_{\mathrm{H}}/\mathrm{R}_\odot) = \log(R_{\mathrm{ZAMS}}/\mathrm{R}_\odot) + a_{\mathrm{H}}\tau_{\mathrm{H}} + b_{\mathrm{H}}\tau_{\mathrm{H}}^{10} + c_{\mathrm{H}}\tau_{\mathrm{H}}^{500} + d_{\mathrm{H}}\tau_{\mathrm{H}}^{3}, \quad (4)$$

$$a_{\mathrm{H}} = \begin{cases} -0.430873 + 0.520408(M/10\ \mathrm{M}_\odot) \\ -7.99762 \times 10^{-2}(M/10\ \mathrm{M}_\odot)^2 \\ -3.55095 \times 10^{-3}(M/10\ \mathrm{M}_\odot)^3 \\ \qquad (10\ \mathrm{M}_\odot \leqslant M < 30\ \mathrm{M}_\odot), \\ 0.476498 - 9.07537 \times 10^{-2}(M/10\ \mathrm{M}_\odot) \\ +1.43538 \times 10^{-2}(M/10\ \mathrm{M}_\odot)^2 \\ -6.89108 \times 10^{-4}(M/10\ \mathrm{M}_\odot)^3 \\ \qquad (30\ \mathrm{M}_\odot \leqslant M \leqslant 100\ \mathrm{M}_\odot), \end{cases} \quad (5)$$

$$b_{\mathrm{H}} = \begin{cases} 0.669345 - 1.5518(M/10\ \mathrm{M}_\odot) + 1.15116(M/10\ \mathrm{M}_\odot)^2 \\ -0.254811(M/10\ \mathrm{M}_\odot)^3 \\ \qquad (10\ \mathrm{M}_\odot \leqslant M < 20\ \mathrm{M}_\odot), \\ 3.02801 \times 10^{-2} + 6.48197 \times 10^{-2}(M/10\ \mathrm{M}_\odot) \\ -6.64582 \times 10^{-3}(M/10\ \mathrm{M}_\odot)^2 \\ +3.37205 \times 10^{-4}(M/10\ \mathrm{M}_\odot)^3 \\ \qquad (20\ \mathrm{M}_\odot \leqslant M \leqslant 100\ \mathrm{M}_\odot), \end{cases} \quad (6)$$

$$c_{\mathrm{H}} = \begin{cases} 5.63328 \times 10^{-2} - 9.88927 \times 10^{-2}(M/10\ \mathrm{M}_\odot) \\ +2.00071 \times 10^{-2}(M/10\ \mathrm{M}_\odot)^2 \\ \qquad (10\ \mathrm{M}_\odot \leqslant M < 30\ \mathrm{M}_\odot), \\ -0.128025 + 3.63928 \times 10^{-2}(M/10\ \mathrm{M}_\odot) \\ -5.43719 \times 10^{-3}(M/10\ \mathrm{M}_\odot)^2 \\ +2.75137 \times 10^{-4}(M/10\ \mathrm{M}_\odot)^3 \\ \qquad (30\ \mathrm{M}_\odot \leqslant M \leqslant 100\ \mathrm{M}_\odot), \end{cases} \quad (7)$$

and

$$d_{\mathrm{H}} = \log(R^{\mathrm{e}}_{\mathrm{H}}/R_{\mathrm{ZAMS}}) - a_{\mathrm{H}} - b_{\mathrm{H}} - c_{\mathrm{H}}. \quad (8)$$

60

Comparison of the fitting formula with numerically computed evolution data

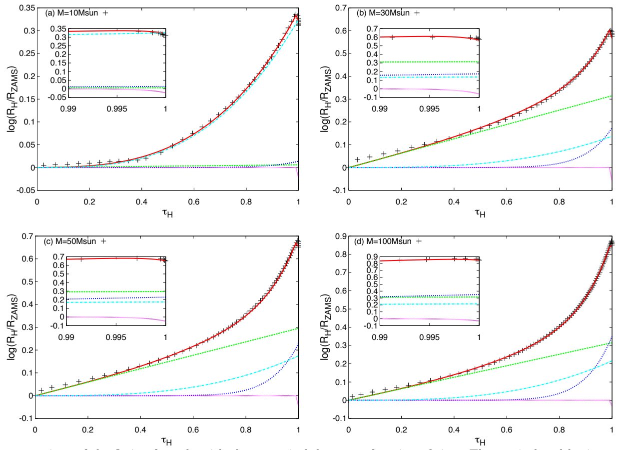

Figure 2. The comparison of the fitting formula with the numerical data as a function of time. The vertical and horizontal axises are $\log(R_{\rm H}/R_{\rm ZAMS})$ and $\tau_{\rm H} \equiv t/t_{\rm H}$ with $t_{\rm H}$ being the H-burning time, respectively. The red line is the fitting formula of stellar radius (Eq. 4) and the crosses are computed data given by Marigo et al. (2001). The green, blue, pink and light blue lines, represent the contributions from the second, third, fourth and fifth term of the fitting formula (Eq. 4), respectively. Each panel refers to the stellar mass (a) 10 $M_\odot$, (b) 30 $M_\odot$, (c) 50 $M_\odot$ and (d) 100 $M_\odot$, respectively. For the low mass case, the stellar radius can be expressed mainly by the fifth term of $d_{\rm H}\tau_{\rm H}^3$ (light blue line), whereas for high mass case they are mainly expressed by the terms of $a_{\rm H}\tau_{\rm H}$ (green line) and $b_{\rm H}\tau_{\rm H}^{10}$ ($\tau_{\rm H} \gtrsim 0.5$, blue line). Around the end of the main sequence lifetime ($\tau_{\rm H} \gtrsim 0.99$), the stellar radii dramatically shrink, because H has been exhausted in the central core. This prominent feature is called as the *main sequence hook* (see also Fig. 1) and is well described by the term of $c_{\rm H}\tau_{\rm H}^{500}$ (pink line) in Eq. (4). The inset in each figure is the magnification of the contribution from each term for $0.99 \leqslant \tau_{\rm H} \leqslant 1$ to show the effect of this term.

How much error？ Time averaged error of the radius of the star.

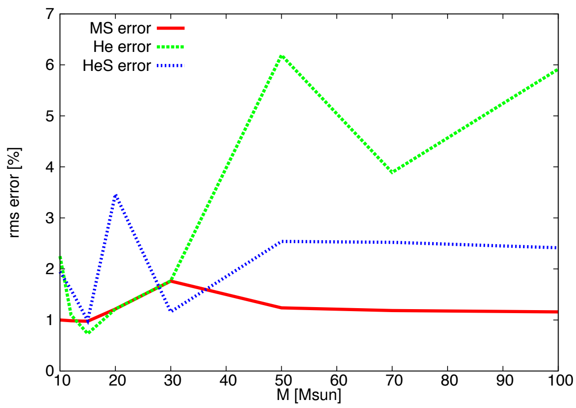

Figure 3. The time averaged root mean square (rms) errors of our fitting formulae relative to the numerical results given in Marigo et al. (2001), as a function of stellar mass. The red, green and blue lines correspond to those fitting formulae during the H-burning phase (Eq. 4), He-burning phase (Eq. 12) and He-shell burning phase (Eq. 25), respectively. We can see that our fitting formulae have relative accuracy within 2 %, 6 % and 3.5 % of numerical calculations by Marigo et al. (2001) for the H-burning, He-burning and He-shell burning phase, respectively.

(2) He-burning phase

$$\log(R^{\rm e}_{\rm He}/{\rm R}_\odot) = \begin{cases} -7.23005\times10^{-2} + 0.814329(M/10\ {\rm M}_\odot) \\ -0.252995(M/10\ {\rm M}_\odot)^2 \\ +5.88465\times10^{-2}(M/10\ {\rm M}_\odot)^3 \\ -4.28501\times10^{-3}(M/10\ {\rm M}_\odot)^4 \\ \qquad (10\ {\rm M}_\odot \leqslant M < 50\ {\rm M}_\odot), \\ -2.40224 + 1.32865\times(M/10\ {\rm M}_\odot) \\ -7.65293\times10^{(}-2)(M/10\ {\rm M}_\odot)^2 \\ \qquad (50\ {\rm M}_\odot \leqslant M \leqslant 100\ {\rm M}_\odot), \end{cases} \quad (9)$$

and

$$\log(t_{\rm He}/{\rm Myr}) = \begin{cases} 6.95516 - 1.17529(M/10\ {\rm M}_\odot) \\ +0.264783(M/10\ {\rm M}_\odot)^2 \\ \qquad (10\ {\rm M}_\odot \leqslant M < 20\ {\rm M}_\odot), \\ 6.13 - 0.331059(M/10\ {\rm M}_\odot) \\ +5.16053\times10^{-2}(M/10\ {\rm M}_\odot)^2 \\ -2.8\times10^{-3}(M/10\ {\rm M}_\odot)^3 \\ \qquad (20\ {\rm M}_\odot \leqslant M \leqslant 100\ {\rm M}_\odot), \end{cases} \quad (10)$$

$$\tau_{\rm He} \equiv \frac{t - t_{\rm H}}{t_{\rm He}}. \quad (11)$$

$$\log(R_{\rm He}/{\rm R}_\odot) = \log(R^{\rm e}_{\rm H}/{\rm R}_\odot) + a_{\rm He}\tau_{\rm He} + b_{\rm He}\tau^2_{\rm He} + c_{\rm He}\tau^3_{\rm He} + d_{\rm He}\tau^4_{\rm He} + \left(\log(R^{\rm e}_{\rm He}/R^{\rm e}_{\rm H}) - a_{\rm He} - b_{\rm He} - c_{\rm He} - d_{\rm He}\right)\tau^5_{\rm He}, \quad (12)$$

$$a_{\rm He} = \begin{cases} -0.891114 + 0.992291(M/10\ {\rm M}_\odot) \\ -0.500532(M/10\ {\rm M}_\odot)^2 + 7.46275\times10^{-2}(M/10\ {\rm M}_\odot)^3 \\ \qquad (10\ {\rm M}_\odot \leqslant M < 20\ {\rm M}_\odot), \\ 3.08883 - 3.85847(M/10\ {\rm M}_\odot) + 1.40618(M/10\ {\rm M}_\odot)^2 \\ -0.178175(M/10\ {\rm M}_\odot)^3 + 7.32187\times10^{-3}(M/10\ {\rm M}_\odot)^4 \\ \qquad (20\ {\rm M}_\odot \leqslant M \leqslant 100\ {\rm M}_\odot), \end{cases} \quad (13)$$

$$b_{\rm He} = \begin{cases} -0.433454 + 0.768418(M/10\ {\rm M}_\odot) \\ \qquad (10\ {\rm M}_\odot \leqslant M < 15\ {\rm M}_\odot), \\ -2.10737 + 1.88553(M/10\ {\rm M}_\odot) \\ \qquad (15\ {\rm M}_\odot \leqslant M < 20\ {\rm M}_\odot), \\ -28.3697 + 33.7648(M/10\ {\rm M}_\odot) - 12.2469(M/10\ {\rm M}_\odot)^2 \\ +1.56514(M/10\ {\rm M}_\odot)^3 - 6.4361\times10^{-2}(M/10\ {\rm M}_\odot)^4 \\ \qquad (20\ {\rm M}_\odot \leqslant M \leqslant 100\ {\rm M}_\odot), \end{cases} \quad (14)$$

$$c_{\rm He} = \begin{cases} 45.8092 - 114.873(M/10\ {\rm M}_\odot) + 110.156(M/10\ {\rm M}_\odot)^2 \\ -46.1519(M/10\ {\rm M}_\odot)^3 + 6.88478(M/10\ {\rm M}_\odot)^4 \\ \qquad (10\ {\rm M}_\odot \leqslant M < 20\ {\rm M}_\odot), \\ 85.996 - 100.37(M/10\ {\rm M}_\odot) + 36.7017(M/10\ {\rm M}_\odot)^2 \\ -4.68789(M/10\ {\rm M}_\odot)^3 + 0.191704(M/10\ {\rm M}_\odot)^4 \\ \qquad (20\ {\rm M}_\odot \leqslant M \leqslant 100\ {\rm M}_\odot), \end{cases} \quad (15)$$

and

$$d_{\rm He} = \begin{cases} -51.6917 + 125.87(M/10\ {\rm M}_\odot) - 121.373(M/10\ {\rm M}_\odot)^2 \\ +51.3681(M/10\ {\rm M}_\odot)^3 - 7.74452(M/10\ {\rm M}_\odot)^4 \\ \qquad (10\ {\rm M}_\odot \leqslant M < 20\ {\rm M}_\odot), \\ -103.871 + 120.228(M/10\ {\rm M}_\odot) - 44.0198(M/10\ {\rm M}_\odot)^2 \\ +5.58876(M/10\ {\rm M}_\odot)^3 - 0.226361(M/10\ {\rm M}_\odot)^4 \\ \qquad (20\ {\rm M}_\odot \leqslant M \leqslant 100\ {\rm M}_\odot). \end{cases} \quad (16)$$

He core mass evolution

$$(M^{\rm b}_{\rm He}/{\rm M}_\odot) = \begin{cases} -0.47466 + 2.49981(M/10\ {\rm M}_\odot)^{1.13274} \\ \qquad (10\ {\rm M}_\odot \leqslant M < 15\ {\rm M}_\odot), \\ -2.3546 + 3.61261(M/10\ {\rm M}_\odot)^{1.12392} \\ \qquad (15\ {\rm M}_\odot \leqslant M \leqslant 100\ {\rm M}_\odot), \end{cases} \quad (17)$$

and

$$(M^{\rm e}_{\rm He}/{\rm M}_\odot) = 1.31569(M/10\ {\rm M}_\odot) + 0.993475(M/10\ {\rm M}_\odot)^2 - 0.112405(M/10\ {\rm M}_\odot)^3 + 4.60669\times10^{-3}(M/10\ {\rm M}_\odot)^4. \quad (18)$$

mass and time can be given by

$$(M_{\rm He}/{\rm M}_\odot) = (M^{\rm b}_{\rm He}/{\rm M}_\odot) + A_{\rm He}\tau_{\rm He} + B_{\rm He}\tau^2_{\rm He} + ((M^{\rm e}_{\rm He}/{\rm M}_\odot) - (M^{\rm b}_{\rm He}/{\rm M}_\odot) - A_{\rm He} - B_{\rm He})\tau^3_{\rm He}, \quad (19)$$

$$A_{\rm He} = \begin{cases} -301.285 + 1210.26(M/10\ {\rm M}_\odot) - 1808.76(M/10\ {\rm M}_\odot)^2 \\ +1191.99(M/10\ {\rm M}_\odot)^3 - 292.114(M/10\ {\rm M}_\odot)^4 \\ \qquad (10\ {\rm M}_\odot \leqslant M < 12\ {\rm M}_\odot), \\ -1.27007 + 2.97787(M/10\ {\rm M}_\odot) - 1.66077(M/10\ {\rm M}_\odot)^2 \\ +0.307506(M/10\ {\rm M}_\odot)^3 \\ \qquad (12\ {\rm M}_\odot \leqslant M < 30\ {\rm M}_\odot), \\ 5.55735\times10^{-2} - 4.91742\times10^{-2}(M/10\ {\rm M}_\odot) \\ +9.62294\times10^{-2}(M/10\ {\rm M}_\odot)^2 \\ -9.4471\times10^{-3}(M/10\ {\rm M}_\odot)^3 \\ \qquad (30\ {\rm M}_\odot \leqslant M \leqslant 100\ {\rm M}_\odot), \end{cases} \quad (20)$$

and

$$B_{\rm He} = \begin{cases} 20.771 - 47.8361(M/10\ {\rm M}_\odot) + 38.9548(M/10\ {\rm M}_\odot)^2 \\ -13.6227(M/10\ {\rm M}_\odot)^3 + 1.70524(M/10\ {\rm M}_\odot)^4 \\ \qquad (10\ {\rm M}_\odot \leqslant M < 30\ {\rm M}_\odot), \\ -9.30219 + 4.79562(M/10\ {\rm M}_\odot) \\ -0.937401(M/10\ {\rm M}_\odot)^2 \\ +5.62695\times10^{-2}(M/10\ {\rm M}_\odot)^3 \\ \qquad (30\ {\rm M}_\odot \leqslant M \leqslant 100\ {\rm M}_\odot). \end{cases} \quad (21)$$

He-shell burning phase

$$\log(R^{\rm b}_{\rm C}/{\rm R}_\odot) = \begin{cases} 5.4491 - 5.78767(M/10\ {\rm M}_\odot) \\ +1.99667(M/10\ {\rm M}_\odot)^2 \\ \qquad (10\ {\rm M}_\odot \leqslant M < 15\ {\rm M}_\odot), \\ 1.39753 - 0.254317(M/10\ {\rm M}_\odot) \\ +0.106221(M/10\ {\rm M}_\odot)^2 \\ \qquad (15\ {\rm M}_\odot \leqslant M \leqslant 50\ {\rm M}_\odot) \\ 0.51943 + 0.621622(M/10\ {\rm M}_\odot) \\ -3.48026\times10^{-2}(M/10\ {\rm M}_\odot)^2 \\ \qquad (50\ {\rm M}_\odot \leqslant M \leqslant 100\ {\rm M}_\odot), \end{cases} \quad (22)$$

and

$$(t^{\rm b}_{\rm C}/{\rm Myr}) = 2.09464 + \frac{106.25}{10(M/10\ {\rm M}_\odot) - 3.90499}, \quad (23)$$

respectively. Then, using the normalized time which is defined by

$$\tau_{\rm HeS} \equiv \frac{t - t_{\rm H} - t_{\rm He}}{t^{\rm b}_{\rm C} - t_{\rm H} - t_{\rm He}}, \quad (24)$$

$$\log(R_{\rm HeS}/{\rm R}_\odot) = \begin{cases} \log(R^{\rm e}_{\rm He}/{\rm R}_\odot) + a_{\rm HeS}\tau_{\rm HeS} + b_{\rm HeS}\tau^2_{\rm HeS} \\ +c_{\rm HeS}\tau^3_{\rm HeS} + (\log(R^{\rm b}_{\rm C}/R^{\rm e}_{\rm He}) \\ -a_{\rm HeS} - b_{\rm HeS} - c_{\rm HeS})\tau^{15}_{\rm HeS} \\ \quad (10\ {\rm M}_\odot \leqslant {\rm M} \leqslant 50\ {\rm M}_\odot), \\ \log(R^{\rm e}_{\rm He}/{\rm R}_\odot) + \log(R^{\rm b}_{\rm C}/R^{\rm e}_{\rm He})\tau_{\rm HeS} \\ \quad (50\ {\rm M}_\odot < {\rm M} \leqslant 100\ {\rm M}_\odot), \end{cases} \tag{25}$$

where

$$a_{\rm HeS} = \begin{cases} 0.198773 - 8.62031 \times 10^{-2}(M/10\ {\rm M}_\odot) \\ -6.9987 \times 10^{-2}(M/10\ {\rm M}_\odot)^2 \\ \quad (10\ {\rm M}_\odot \leqslant M < 15\ {\rm M}_\odot), \\ -2.17094 + 2.46127(M/10\ {\rm M}_\odot) \\ -0.866681(M/10\ {\rm M}_\odot)^2 \\ +9.41554 \times 10^{-2}(M/10\ {\rm M}_\odot)^3 \\ \quad (15\ {\rm M}_\odot \leqslant M \leqslant 50\ {\rm M}_\odot), \end{cases} \tag{26}$$

$$b_{\rm HeS} = \begin{cases} 0.45 \quad (10\ {\rm M}_\odot \leqslant M < 15\ {\rm M}_\odot), \\ 5.85223 - 5.9911(M/10\ {\rm M}_\odot) + 2.05449(M/10\ {\rm M}_\odot)^2 \\ -0.217241(M/10\ {\rm M}_\odot)^3 \\ \quad (15\ {\rm M}_\odot \leqslant M \leqslant 50\ {\rm M}_\odot), \end{cases} \tag{27}$$

and

$$c_{\rm HeS} = \begin{cases} 0.15 \quad (10\ {\rm M}_\odot \leqslant M < 15\ {\rm M}_\odot), \\ -2.34416 + 2.5736(M/10\ {\rm M}_\odot) - 0.920019(M/10\ {\rm M}_\odot)^2 \\ +0.100612(M/10\ {\rm M}_\odot)^3 \\ \quad (15\ {\rm M}_\odot \leqslant M \leqslant 50\ {\rm M}_\odot), \end{cases} \tag{28}$$

$$\log\left(\frac{L}{{\rm L}_\odot}\right) = 6.74298 - 4.72995/(M/10\ {\rm M}_\odot) + 3.59526/(M/10\ {\rm M}_\odot)^2 - 1.27068/(M/10\ {\rm M}_\odot)^3 \tag{29}$$

Treatment of Compact Remnant

$$(M_{\rm CO}/{\rm M}_\odot) = 0.618397 - 0.57395(M/10\ {\rm M}_\odot) + 1.73053(M/10\ {\rm M}_\odot)^2 - 0.312008(M/10\ {\rm M}_\odot)^3 + 2.99858 \times 10^{-2}(M/10\ {\rm M}_\odot)^4 - 1.12942 \times 10^{-3}(M/10\ {\rm M}_\odot)^5. \tag{30}$$

$$M_{\rm FeNi} = \begin{cases} 0.161767 M_{\rm CO} + 1.067055\ {\rm M}_\odot & (M_{\rm CO} \leqslant 2.5\ {\rm M}_\odot), \\ 0.314154 M_{\rm CO} + 0.686088\ {\rm M}_\odot & (2.5\ {\rm M}_\odot \leqslant M_{\rm CO}). \end{cases} \tag{31}$$

$$M_{\rm rem} = \begin{cases} M_{\rm FeNi} & (M_{\rm CO} \leqslant 5\ {\rm M}_\odot), \\ M_{\rm FeNi} + \frac{M_{\rm CO}-5{\rm M}_\odot}{2.6{\rm M}_\odot}(M - M_{\rm FeNi}), & \\ & (5\ {\rm M}_\odot < M_{\rm CO} < 7.6\ {\rm M}_\odot), \\ M & (7.6\ {\rm M}_\odot \leqslant M_{\rm CO}). \end{cases} \tag{32}$$

BH is formed if $M_{\rm rem} > 3M_{\rm sun}$
If not , NS is formed.

Binary Evolution

1) Tidal evolution

$$\frac{\dot a}{a} = \frac{2e\dot e}{1-e^2} + 2\frac{\dot J_{\rm orb}}{J_{\rm orb}}$$

$$J_{\rm orb} + J_{\rm spin,1} + J_{\rm spin,2} = \text{const}$$

$$\dot J_{\rm orb} = -(\dot J_{\rm spin,1} + \dot J_{\rm spin,2})$$

$$\dot J_{\rm spin,i} = \dot I_i \Omega_{\rm spin,i} + I_i \dot\Omega_{\rm spin,i}$$

$$\dot\Omega_{\rm spin,1} = 3\frac{k}{T}\frac{q_2^2}{r_g^2}\left(\frac{R_1}{a}\right)^6 \frac{\Omega_{\rm orb}}{(1-e^2)^6} \times \left[f_1(e^2) - (1-e^2)^{\frac{3}{2}} f_2(e^2)\frac{\Omega_{\rm spin,1}}{\Omega_{\rm orb}}\right], \tag{35}$$

$$f_1(e^2) = 1 + \tfrac{15}{2}e^2 + \tfrac{45}{8}e^4 + \tfrac{5}{16}e^6, \tag{36}$$

$$f_2(e^2) = 1 + 3e^2 + \tfrac{3}{8}e^4, \tag{37}$$

$$q_2 \equiv M_2/M_1, \tag{38}$$

where T, k, $r_{\rm g}$ and $\Omega_{\rm orb}$ are the tidal timescale, the apsidal motion constant of the primary star, the gyration radius which is defined by $\sqrt{I_1/M_1/R_1^2}$ and the orbital angular velocity, respectively. T, k, and $r_{\rm g}$ depend on the properties of the internal structure of the primary star and their specific forms are given later. The time evolution of $\dot\Omega_{\rm spin,2}$ is given by changing 1 to 2 and 2 to 1 in the above equations.

Hut (1981) also gave the equations for $\dot e$ as

$$\dot e = -27\frac{k}{T}q_2(1+q_2)\left(\frac{R_1}{a}\right)^8 \frac{e}{(1-e^2)^{\frac{13}{2}}} \times \left[f_3(e^2) - \frac{11}{18}(1-e^2)^{\frac{3}{2}} f_4(e^2)\frac{\Omega_{\rm spin,1}}{\Omega_{\rm orb}}\right]$$

$$f_3(e^2) = 1 + \frac{15}{4}e^2 + \frac{15}{8}e^4 + \frac{5}{64}e^6, \tag{40}$$

$$f_4(e^2) = 1 + \frac{3}{2}e^2 + \frac{1}{8}e^4. \tag{41}$$

Moment of inertia depends on the structure of Pop III star.

$$I_i = k_{\rm env}(M_i - M_{{\rm c},i})R_i^2 + k_{\rm core}M_{{\rm c},i}R_{{\rm c},i}^2$$

$$\frac{R_{{\rm c},i}}{{\rm R}_\odot} = 0.9334\left(\frac{M_{{\rm c},i}}{10\ {\rm M}_\odot}\right)^{0.62}, \tag{42}$$

$$\Omega_{{\rm spin},i} = 45.35\left(\frac{v_{\rm rot}}{1\ {\rm km\ s^{-1}}}\right)\left(\frac{R_{\rm ZAMS}}{{\rm R}_\odot}\right)^{-1} {\rm yr}^{-1}, \tag{43}$$

$$v_{\rm rot}(M_i) = \frac{658437(M_i/10\ {\rm M}_\odot)^{3.3}}{15 + 2818(M_i/10\ {\rm M}_\odot)^{3.45}}\ {\rm km\ s^{-1}}. \tag{44}$$

Convective case

$$\frac{k}{T} = \frac{2}{21}\frac{f_{\rm con}}{\tau_{\rm con}}\frac{M_{\rm env,1}}{M_1}, \tag{45}$$

where $M_{\rm env,1} \equiv M_1 - M_{\rm c,1}$ is the primary envelope mass

$$\tau_{\rm con} = \left[\frac{M_{\rm env,1}R_{\rm env,1}\left(R_1 - \frac{1}{2}R_{\rm env,1}\right)}{3L_1}\right]^{1/3}, \tag{46}$$

where L_1 and $R_{\rm env,1} \equiv R_1 - R_{\rm c,1}$ are the stellar luminosity

$$f_{\rm con} = \min\left[1, \left(\frac{P_{\rm tid}}{2\tau_{\rm con}}\right)^2\right]. \qquad (47)$$

Radiative case

$$\frac{k}{T} = 4.3118\times10^{-8}\left(\frac{M_1}{\rm M_\odot}\right)\left(\frac{R_1}{\rm R_\odot}\right)^2 \times\left(\frac{a}{1\ \rm AU}\right)^{-5}(1+q_2)^{5/6}E\ {\rm yr}^{-1}, \qquad (48)$$

vhere the tidal coefficient E is described by Zahn (1975) as

$$E = 1.101\times10^{-6}\left(\frac{M_1}{10\ \rm M_\odot}\right)^{2.84}. \qquad (49)$$

Usually dynamical time is shorter than the Kelvin-Helmholtz time so that dynamical equilibriun holds first with

the adiabatic radius $R_{\rm ad,1}$

Then, thermal equilibrium holds very slowly witl

the thermal equilibrium radius $R_{\rm th,1}$

2） Roche lobe over flow

$$\frac{R_{\rm L,1}}{a} \approx \frac{0.49q_1^{2/3}}{0.6q_1^{2/3}+\ln(1+q_1^{1/3})}, \qquad (50)$$

$$q_1 \equiv M_1/M_2$$

$$\tau_{\rm dyn,1} = \frac{\pi}{2}\left(\frac{R_1^3}{2GM_1}\right)^{1/2} \qquad (51)$$

$$\tau_{\rm KH,1} = \frac{GM_1(M_1-M_{\rm c,1})}{L_1R_1}, \qquad (52)$$

$$\zeta_{\rm L} = \frac{d\log R_{\rm L,1}}{d\log M_1}, \qquad (53)$$

$$\zeta_{\rm ad} = \frac{d\log R_{\rm ad,1}}{d\log M_1}. \qquad (54)$$

In case that the total mass is conserved：

$$\zeta_{\rm L} \approx 2.13q_1 - 1.67 \quad (0 < q_1 < 50), \qquad (55)$$

the polytropic index of 1.5 so that $\zeta_{\rm ad}$ is given by

$$\zeta_{\rm ad} \approx -1 + \frac{2}{3}\frac{M_1}{M_1 - M_{\rm c1}}, \qquad (56)$$

If $\zeta_{\rm ad} < \zeta_{\rm L}$, $d\log M_1 < 0.$

$d\log R_{\rm ad,1} > d\log R_{\rm L,1}$

Mass transfer proceeds in the dynamical tim
1)If the companion has giant envelope
two stars become Common Envelope
phase which looks like single star from out
2)If the companion is the main sequence sta
or He star, two stars merge to be a single star.

If $\zeta_{\rm ad} > \zeta_{\rm L}$

$R_{\rm ad,1} < R_{\rm L,1}$

Companion star is inside Roche lobe so that Roche lobe overflow stops.
In Kelvin Helmholtz time、the radius become large again. If Roche lobe overflow condition is fulfilled again, mass transfer proceeds again.

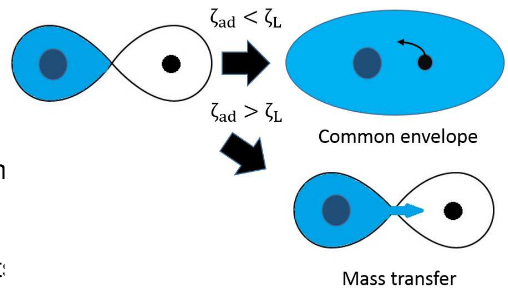

Figure 4. Schematic diagram of the mass transfer when the primary becomes a giant star. Let us define $\zeta_{\rm L} = d\log R_{\rm L,1}/d\log M_1$ and $\zeta_{\rm ad} = d\log R_{\rm ad,1}/d\log M_1$. When the primary star fulfills the Roche lobe as in the upper left of the figure, there are two destinies. 1) If $\zeta_{\rm ad} < \zeta_{\rm L}$, then $d\log R_{\rm ad,1} > d\log R_{\rm L,1}$ since $d\log M_1 < 0$ so that the mass transfer is dynamically unstable. The secondary star is swallowed by the primary envelope to be the common envelope phase as the upper right of the figure. 2) If $\zeta_{\rm ad} > \zeta_{\rm L}$, the mass transfer is dynamically stable so that the radius of the primary star becomes smaller than the Roche lobe radius on the dynamical timescale after losing the small fraction of the envelope mass. However in the thermal time scale (Kelvin-Helmholz time), the radius increases again and fulfills the Roche lobe so that the stable mass transfer from the primary star to the secondary star occurs like in the lower right of the figure.

$$\dot{M}_1 = F(M_1)\left[\ln\left(\frac{R_{\rm th,1}}{R_{\rm L,1}}\right)\right]^3 \ {\rm M_\odot\ yr^{-1}} \tag{57}$$

and

$$F(M_1) = 3\times 10^{-6}\left\{\min\left[\left(10\frac{M_1}{10\ {\rm M_\odot}}\right), 5.0\right]\right\}^2, \tag{58}$$

$$\dot{M}_{1,\rm max} = \frac{M_1}{\tau_{\rm KH,1}}. \tag{59}$$

We assume that the binary stars merge if $R_{\rm th,1} > 10R_{\rm L,1}$ for the star without the core-envelope structure since the mass transfer rate is comparable to the above upper limit.

3) Common Envelope phase

$$\Delta E_{\rm orb} = \frac{GM_{\rm c,1}M_2}{2a_{\rm f}} - \frac{GM_1M_2}{2a_{\rm i}}$$

$$E_{\rm bind} = \frac{GM_1M_{\rm env,1}}{\lambda R_1},$$

$$\alpha\left(\frac{GM_{\rm c,1}M_2}{2a_{\rm f}} - \frac{GM_1M_2}{2a_{\rm i}}\right) = \frac{GM_1M_{\rm env,1}}{\lambda R_1}, \tag{65}$$

αλ is the parameter

Condition for the merger

1) Conservative

$$R_1' + R_2' > a_{\rm f}$$

2)optimisitic

$$R_1' > R_{\rm L,1}' \ \text{or}\ R_2' > R_{\rm L,2}'$$

4) Effect of Super Nova explosion : condition of disruption of the binary.

$$\mathbf{v} = (-v\sin\beta, -v\cos\beta, 0), \tag{67}$$

$$v = \sqrt{GM_{\rm total}\left(\frac{2}{r} - \frac{1}{a}\right)},$$

$$M_{\rm total} \to M_{\rm total}' = M_{\rm total} - \Delta M_1$$

$$v' = \sqrt{GM_{\rm total}'\left(\frac{2}{r} - \frac{1}{a'}\right)}$$

69

$$a' = \left(\frac{v^2}{GM_{\rm total}} - \frac{v^2}{GM_{\rm total}'} + \frac{1}{a}\right)^{-1}$$

$$e' = \sqrt{1 - \frac{|\mathbf{r}\times\mathbf{v}|^2}{GM_{\rm total}'a'}}.$$

Before explosion e=0

$$a' = \left(\frac{2}{a} - \frac{M_{\rm total}}{M_{\rm total}'a}\right)^{-1}$$

$$e' = \frac{M_{\rm total}}{M_{\rm total}'} - 1.$$

If

$$M_{\rm total}' < \frac{1}{2}M_{\rm total}$$

The binary becomes unbound

5) The effect of the gravitational wave

$$\frac{\dot{J}}{J} = -\frac{32G^3M_1M_2M_{\rm total}}{5c^5a^4}\frac{1+\frac{7}{8}e^2}{(1-e^2)^{5/2}}, \tag{75}$$

$$\frac{\dot{a}}{a} = -\frac{64G^3M_1M_2M_{\rm total}}{5c^5a^4}\frac{1+\frac{73}{24}e^2+\frac{37}{96}e^4}{(1-e^2)^{7/2}}, \tag{76}$$

and

$$\frac{\dot{e}}{e} = -\frac{304G^3M_1M_2M_{\rm total}}{15c^5a^4}\frac{1+\frac{121}{304}e^2}{(1-e^2)^{5/2}}. \tag{77}$$

From Eqs. (76) and (77), we can express a by e as

$$\frac{a}{a_0} = \frac{1-e_0^2}{1-e^2}\left(\frac{e}{e_0}\right)^{12/19}\left(\frac{1+\frac{121}{304}e^2}{1+\frac{121}{304}e_0^2}\right)^{870/2299}, \tag{78}$$

where a_0 and e_0 are the initial values of a and e, respectively. For $a/a_0 \ll 1$, Eq. (78) is approximated by

$$e \sim \left(\frac{a}{a_0(1-e_0^2)}\right)^{19/12} e_0. \tag{79}$$

For $e_0 = 0$, Eq. (76) is integrated as

$$t_{\rm coal}(e_0=0) = \frac{5}{256}\frac{a_0^4}{c}\left(\frac{GM_1}{c^2}\right)^{-1}\left(\frac{GM_2}{c^2}\right)^{-1}\left(\frac{GM_{\rm total}}{c^2}\right)^{-1} \tag{80}$$

$$= 10^{10}\left(\frac{a_0}{16\ {\rm R_\odot}}\right)^4\left(\frac{M_1}{10\ {\rm M_\odot}}\right)^{-1}\left(\frac{M_2}{10\ {\rm M_\odot}}\right)^{-1}\left(\frac{M_{\rm total}}{10\ {\rm M_\odot}}\right)^{-1} \ {\rm yr}.$$

Peters & Mathews (1963) and Peters (1964) found numerically that for $e_0 > 0$, $t_{\rm merge}(e_0)$ is approximately given by

$$t_{\rm coal}(e_0) \sim (1-e_0^2)^{7/2}t_{\rm merge}(e_0=0). \tag{81}$$

However in our simulations, we solve Eqs. (75) and (77).

70

Initial conditions

- 1) Initial Mass Function (IMF)

  Salpeter or flat

  $\Psi(M_1) \propto M_1^{-2.35}$ $\Psi(M_1) \propto \text{const.}$

  mass range $10\ \mathrm{M}_\odot \leqslant M_1 \leqslant 100\ \mathrm{M}_\odot$

2) Distribution of mass ratio $M_2/M_1 = q_2 < 1$

$\Phi(q_2) \propto \text{const}$ $q_{2,\min} \equiv 10\ \mathrm{M}_\odot / M_1$

3) Distribution of eccentricity

$$\Xi(e) \propto e, \quad 0 \leqslant e \leqslant 1.$$

4) Distribution of semi-major axis a

$$\Gamma(a) \propto \frac{1}{a}, \quad A_{\min} \leqslant a \leqslant 10^6\ \mathrm{R}_\odot$$

$$A_{\min} = \frac{A_\mathrm{L}}{1-e} = \frac{0.6q_1^{2/3} + \ln(1+q_1^{1/3})}{0.49q_1^{2/3}} \frac{R_1}{1-e}.$$

Method of Calculation

- Monte Carlo homogeneous random number in the interval of 0 < X < 1 for IMF, for example.

$$X \equiv \frac{\int_{M_{\min}}^{M_1} \Psi(M)dM}{\int_{M_{\min}}^{M_{\max}} \Psi(M)dM} \qquad 0 \leqslant X \leqslant 1$$

Convergence check

Table 11. The convergence check of Monte Carlo simulations for Model III.s. Each column means the number of binaries, the number of the coalescing NS-NSs, NS-BHs, and BH-BHs, respectively.

Total number	NSNS	NSBH	BHBH
10^5	0	11	2593
10^6	5	64	25536
10^7	27	562	254346

Results with 10^6 binary

Table 1. The model description for the Monte Carlo simulations. Each column represents the name of the model, population of stars, IMF, mass range of the primary star and that of the secondary star, respectively. Models III.s and III.f are simulations of Pop III binaries with the mass range of 10 $M_\odot \leqslant M \leqslant 100\ M_\odot$. For Models III.s and III.f, the Salpeter and flat IMF is adopetd, respectively. Models I.h and I.l are simulations of Pop I binaries with Hurley's single stellar fitting formulae (Hurley, Pols & Tout 2000) for comparison. In both models, the Salpeter IMF is adopted. For Model I.h, the initial mass range is 10 $M_\odot \leqslant M \leqslant 100\ M_\odot$. For Model I.l, the initial mass range is 1 $M_\odot \leqslant M \leqslant 100\ M_\odot$ to take into account the typical mass of a Pop I star is $\sim 1 M_\odot$.

model	population	IMF	primary mass range	secondary mass range
III.s	III	Salpeter	$10\ M_\odot \leqslant M_1 \leqslant 100\ M_\odot$	$10\ M_\odot \leqslant M_2 \leqslant M_1$
III.f	III	Flat	$10\ M_\odot \leqslant M_1 \leqslant 100\ M_\odot$	$10\ M_\odot \leqslant M_2 \leqslant M_1$
I.h	I	Salpeter	$10\ M_\odot \leqslant M_1 \leqslant 100\ M_\odot$	$10\ M_\odot \leqslant M_2 \leqslant M_1$
I.l	I	Salpeter	$1\ M_\odot \leqslant M_1 \leqslant 100\ M_\odot$	$0.5\ M_\odot \leqslant M_2 \leqslant M_1$

Table 2. The number of the compact binaries formed in each model. Each column represents the model name, and the number of NS-NSs, NS-BHs, and BH-BHs, respectively. The numbers in the parenthesis are for the case of the conservative core-merger criterion while those without the parenthesis are for the case of the optimistic core-merger criterion. The definition of optimistic and conservative core-merger criteria are shown in Sec. 2.2.3.

	NS-NS	NS-BH	BH-BH
Model III.s	5(1994)	93085 (93793)	132534 (133485)
Model III.f	0 (279)	185335 (187638)	517067 (522581)
Model I.h	58724 (60715)	73193 (76277)	108184 (108734)
Model I.l	1847 (1865)	2264 (2354)	3559 (3578)

Pop I is the star like sun with metalicity 2% of the total mass.

73

Table 3. The number of the compact binaries with coalescence time less than 15 Gyr among those in Table 2. Notations are the same as Table 2.

	NS-NS	NS-BH	BH-BH
Model III.s	5 (1994)	64 (164)	25536 (26468)
Model III.f	0 (279)	50 (149)	115056 (120532)
Model I.h	20149 (21155)	2703 (3664)	3928 (3976)
Model I.l	776 (785)	99 (134)	150 (151)

Table 4. The formation channels of each compact binaries which merge within 15 Gyr for the case of Model III.s. Each column represents the formation channel, the fraction which each channel occupies, and the evolution history. Here, RLOF, CE, DCE, SN, CE+SN, and DCE+SN represents the Roche lobe over flow, CE phase, double CE phase, supernova explosion or direct collapse, supernova explosion or direct collapse as soon as after the CE phase, and supernova explosion or the direct collapse as soon as after the double CE phase, respectively.

Channel	Fraction	Evolution History
NSNS 1	80.0% (0.4%)	SN:1, CE+SN:2
NSNS 2	20% (99.6%)	RLOF:1→2, SN:1, CE+SN:2
NSNS others	0% (0%)	The others
NSBH 1	86.8% (90.5%)	RLOF:1→2, SN:1, CE+SN:2
NSBH 2	8.8% (3.6%)	RLOF:1→2, SN:1, RLOF:2→1, SN:2
NSBH 3	2.9% (1.2%)	SN:1, CE+SN:2
NSBH 4	1.5% (0.6%)	CE:1, SN:1, RLOF:2→1, SN:2
NSBH 5	0% (1.8%)	CE:1, RLOF:1→2, SN:1, RLOF:2→1, SN:2
NSBH 6	0% (1.8%)	CE+SN:1, RLOF:2→1, SN:2
NSBH others	0% (0.5%)	The others
BHBH 1	55.3% (53.5%)	RLOF:1→2, SN:1, RLOF:2→1, SN:2
BHBH 2	13.3% (12.7%)	RLOF:1→2, SN:1, RLOF:2→1, CE+SN:2
BHBH 3	8.1% (7.9%)	RLOF:1→2, CE+SN:1, RLOF:2→1, SN:2
BHBH 4	6.2% (6.0%)	CE:1, SN:1, RLOF:2→1, SN:2
BHBH 5	5.5% (5.3%)	RLOF:1→2, CE+SN:1, RLOF:2→1, CE+SN:2
BHBH 6	2.9% (2.8%)	CE:1, SN:1, RLOF:2→1, CE+SN:2
BHBH 7	1.5% (1.7%)	CE+SN:1, RLOF:2→1, SN:2
BHBH 8	1.3% (1.3%)	RLOF:1→2, DCE+SN:1, SN:2
BHBH 9	1.1% (1.1%)	DCE+SN:1, SN:2
BHBH 10	1.1% (1.1%)	DCE, SN:1, SN:2
BHBH 11	1.1% (1.1%)	RLOF:1→2, SN:1, CE+SN:2
BHBH others	2.6% (5.5%)	The others

Table 5. The same as Table 4, but for Model III.f.

Channel	Fraction	Evolutionary History
NSNS 2	0% (100%)	RLOF:1→2, SN:1, CE+SN:2
NSNS others	0% (0%)	The others
NSBH 1	54.4% (52.2%)	RLOF:1→2, SN:1, CE+SN:2
NSBH 2	12.3% (4.5%)	RLOF:1→2, SN:1, RLOF:2→1, SN:2
NSBH 3	1.7% (0.6%)	SN:1, CE+SN:2
NSBH 4	28.1% (10.2%)	CE:1, SN:1, RLOF:2→1, SN:2
NSBH 5	3.5% (29.9%)	CE:1, RLOF:1→2, SN:1, RLOF:2→1, SN:2
NSBH 6	0% (1.9%)	CE+SN:1, RLOF:2→1, SN:2
NSBH others	0% (0.7%)	The others
BHBH 1	36.9% (35.4%)	RLOF:1→2, SN:1, RLOF:2→1, SN:2
BHBH 2	16.3% (15.7%)	RLOF:1→2, SN:1, RLOF:2→1, CE+SN:2
BHBH 3	8.6% (8.3%)	RLOF:1→2, CE+SN:1, RLOF:2→1, SN:2
BHBH 4	8.5% (8.2%)	CE:1, SN:1, RLOF:2→1, SN:2
BHBH 5	11.8% (11.3%)	RLOF:1→2, CE+SN:1, RLOF:2→1, CE+SN:2
BHBH 6	6.3% (6.1%)	CE:1, SN:1, RLOF:2→1, CE+SN:2
BHBH 7	0.8% (0.9%)	CE+SN:1, RLOF:2→1, SN:2
BHBH 8	2.2% (2.1%)	RLOF:1→2, DCE+SN:1, SN:2
BHBH 9	1.9% (1.8%)	DCE+SN:1, SN:2
BHBH 10	2.3% (2.2%)	DCE, SN:1, SN:2
BHBH 11	0.8% (0.8%)	RLOF:1→2, SN:1, CE+SN:2
BHBH others	3.6% (7.2%)	The others

Table 6. The same as Table 4, but for Model I.h.

Channel	Fraction	Evolutionary History
NSNS 3	51.2% (49.7%)	RLOF:1→2, SN:1, CE:2, CE+SN:2
NSNS 4	24.7% (24.0%)	CE:1, SN:1, CE:2, CE+SN:2
NSNS 5	6.9% (8.7%)	CE:1, CE+SN:1, CE+SN:2
NSNS 6	4.5% (4.4%)	CE:1, SN:1, CE:2, RLOF:2→1 CE+SN:2
NSNS 7	4.0% (4.1%)	DCE, CE+SN:1, CE+SN:2
NSNS others	8.7% (9.1%)	The others
NSBH 7	47.7% (37.7%)	CE:1, SN:1, CE:2, CE+SN:2
NSBH 8	13.2% (13.9%)	RLOF:1→2, SN:1, CE:2, SN:2
NSBH 9	10.0%(16.2%)	CE:1, SN:1, CE:2, SN:2
NSBH 10	9.1% (10.8%)	RLOF:1→2, SN:1, CE:2, CE+SN:2
NSBH 11	7.5% (5.3%)	CE:1, SN:1, RLOF:2→1, CE+SN:2
NSBH others	12.5% (16.1%)	The others
BHBH 8	6.2% (6.0%)	RLOF:1→2, DCE+SN:1, SN:2
BHBH 12	80.5% (78.4%)	RLOF:1→2, SN:1, CE:2, SN:2
BHBH 13	8.4% (9.1%)	DCE+SN:1, RLOF:2→1, SN:2
BHBH others	4.9% (6.5%)	The others

Table 7. The same as Table 4, but for Model I.l.

Channel	Fraction	Evolutionary History
NSNS 3	66.9% (66.4%)	RLOF:1→2, SN:1, CE:2, CE+SN:2
NSNS 4	19.9% (19.7%)	CE:1, SN:1, CE:2, CE+SN:2
NSNS 5	1.1% (1.4%)	CE:1, CE+SN:1, CE+SN:2
NSNS 6	3.8% (3.7%)	CE:1, SN:1, CE:2, RLOF:2→1 CE+SN:2
NSNS 7	1.5% (1.5%)	DCE, CE+SN:1, CE+SN:2
NSNS others	7.8% (7.3%)	The others
NSBH 7	51.3% (43.5%)	CE:1, SN:1, CE:2, CE+SN:2
NSBH 8	10.1% (12.4%)	RLOF:1→2, SN:1, CE:2, SN:2
NSBH 9	10.9%(18.0%)	CE:1, SN:1, CE:2, SN:2
NSBH 10	6.7% (6.2%)	RLOF:1→2, SN:1, CE:2, CE+SN:2
NSBH 11	6.7% (7.5%)	CE:1, SN:1, RLOF:2→1, CE+SN:2
NSBH others	14.3% (12.4%)	The others
BHBH 12	80.0% (76.7%)	RLOF:1→2, SN:1, CE:2, SN:2
BHBH 14	11.5% (12.2%)	RLOF:1→2, SN:1, CE:2, CE+SN:2
BHBH others	18.5% (11.1%)	The others

Distribution of merging time

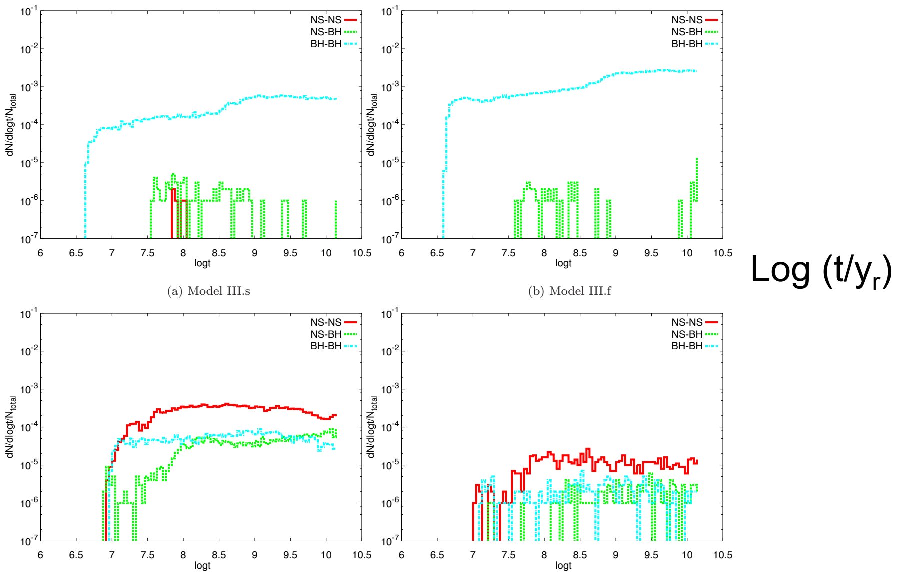

(a) Model III.s (b) Model III.f

(c) Model I.h (d) Model I.l

Figure 5. The normalized coalescence time distribution of compact binaries for each model. Each panel corresponds to Models III.s (a), III.f (b), I.h (c), and I.l (d), respectively. In each figure, the red, green, and blue lines correspond to the NS-NSs, NS-BHs, and BH-BHs, respectively.

77

Distribution of total mass

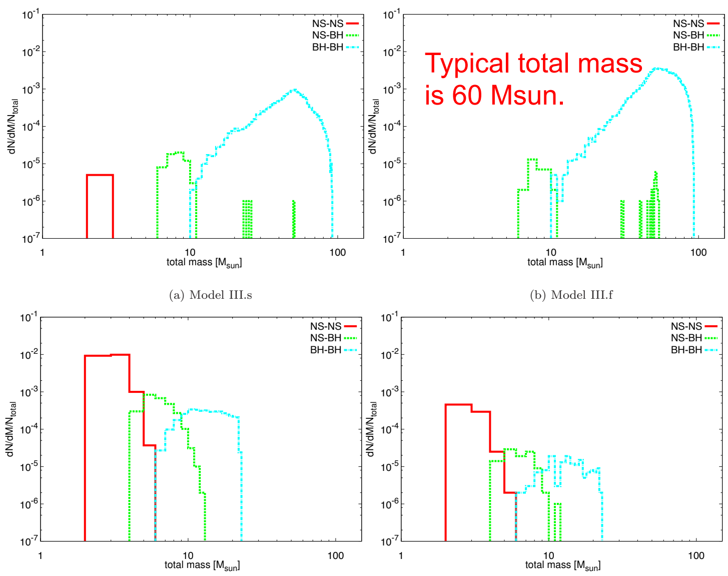

(a) Model III.s (b) Model III.f

(c) Model I.h (d) Model I.l

Figure 6. The normalized distribution of the total mass ($M_{\mathrm{tot}} = M_1 + M_2$) of compact binaries for each model . Each panel corresponds to Models III.s (a), III.f (b), I.h (c), and I.l (d), respectively. In each figure, the red, green, and blue lines correspond to the NS-NSs, NS-BHs, and BH-BHs, respectively.

78

Distribution of Chirp mass

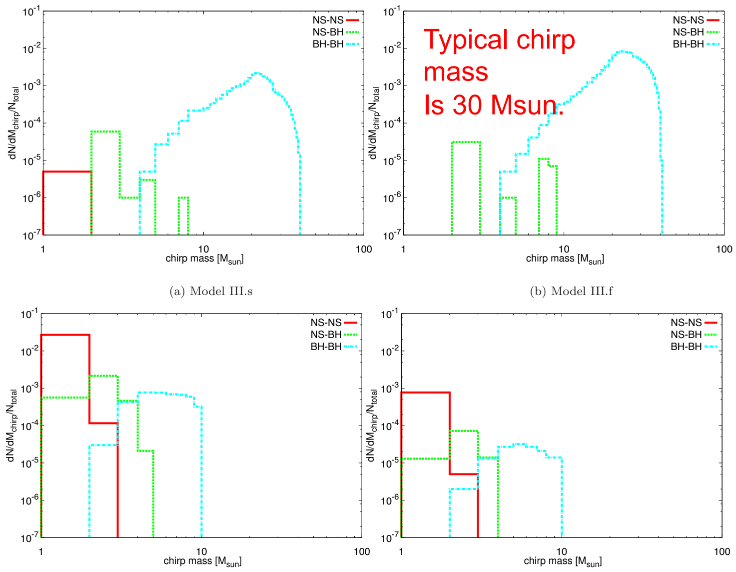

(a) Model III.s (b) Model III.f

(c) Model I.h (d) Model I.l

Figure 7. The same as Fig. 6, but for distribution of the chirp mass ($M_{\rm chirp} = (M_1 M_2)^{3/5}/(M_1 + M_2)^{1/5}$).

PopIII Star Formation Rate

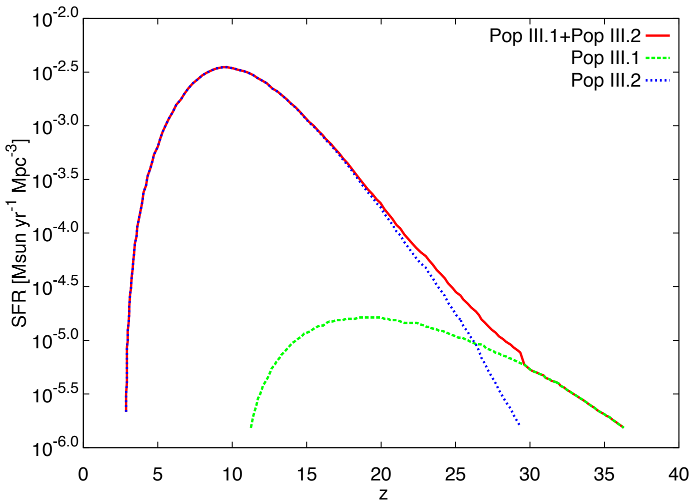

Figure 8. The star formation rate density (comoving) calculated by de Souza et al. (2011). The unit of the rate is $M_\odot$ per comoving volume per proper time. The red line is the the total SFR density of Pop III stars, and the green and blue lines are those of Pop III.1 and Pop III.2 stars, respectively.

Time evolution of merging rate

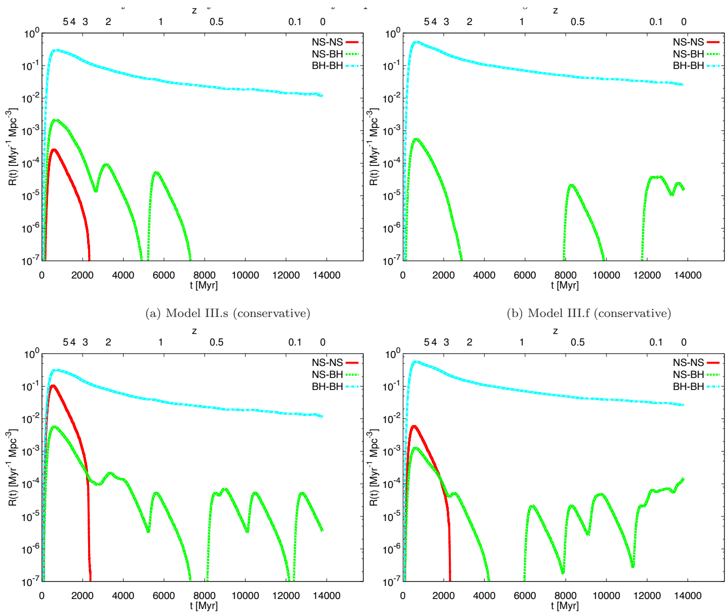

(a) Model III.s (conservative)
(b) Model III.f (conservative)
(c) Model III.s (optimistic)
(d) Model III.f (optimistic)

Figure 9. The evolution of merger rate density of each compact binary. The horizontal axis is the cosmic time.

81

Detection rate by adV LIGO, Virgo and KAGRA

$$140(68)\ \mathrm{events/yr}\ (\mathrm{SFR_p}/(10^{-2.5}\mathrm{M_\odot/yr/Mpc^3}))\cdot \mathrm{Err_{sys}}$$

Flat IMF

Salpeter IMF

Possible systematic error
in the choice of IMF, IEF, mass ratio,
semi-major axis distribution, parameters
of Common envelope, RLOF, tidal interaction
And so on.

$\mathrm{Err_{sys}}$=1 for our model at present .

82

Cumulative detection rate as a function of cosmological redshift z

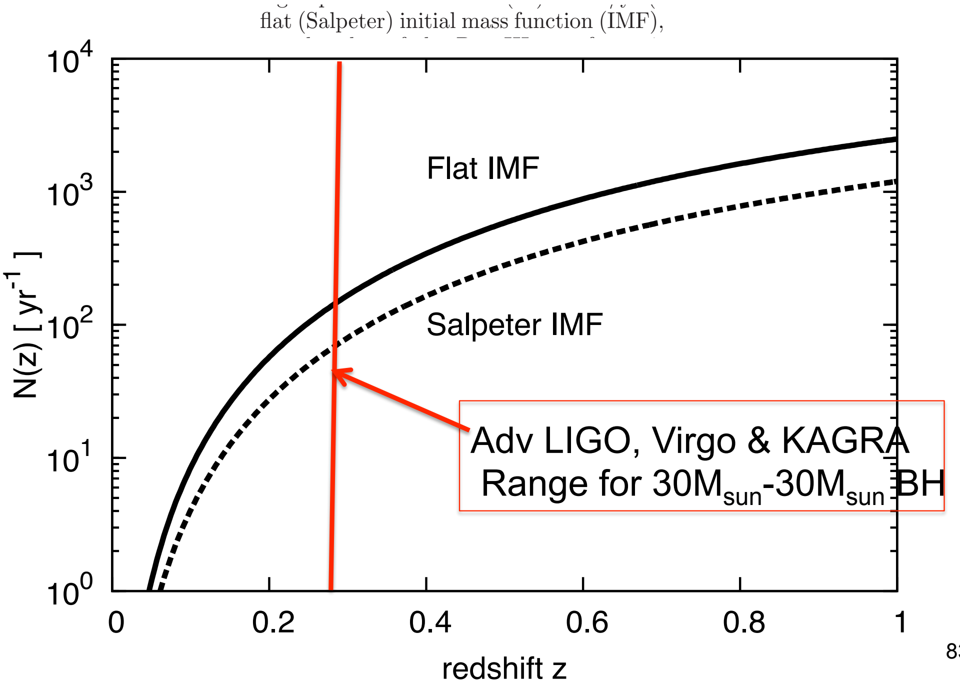

Comparison with other case

PopIII' IMF、mass ratio distribution 、eccentricity distribution 、semi-major axis distribution are unknown since Pop III stars have not been observed.

We adopted distributions and parameters of Pop I
Therefore the systematic error should exist so that we introduced $Err_{sys.}$

Our present model corresponds to $Err_{sys}=1$

Table 8. The comparison of the merger rate density of the BH-BHs and typical chirp mass between previous studies and our study. The second and third columns show the results of Dominik et al. (2012) for metallicity $Z_\odot$ and 0.1 $Z_\odot$ stars. Here, Models A and B correspond to the standard case of submodels A and B in Dominik et al. (2012). The last column show our results for Pop III binaries. Here, we take the fiducial parameter values: $Err_{sys} = 1$ and $SFR_p = 10^{-2.5}$ $M_\odot$ yr^{-1} Mpc^{-3}.

	$Z_\odot$	0.1 $Z_\odot$	Pop III
Model A [10^{-8} events yr^{-1} Mpc^{-3}]	8.2	73.3	2.5 (flat)
Model B [10^{-8} events yr^{-1} Mpc^{-3}]	1.9	13.6	1.2 (Salpeter)
chirp mass [$M_\odot$]	6.7	13.2	30

What is the range of Err_{sys} ?

Results from Kinugawa et al. 2015

1) 3 IMF: Flat, Salpeter, log flat

2) 3 IEF:IEF(Initial Eccentricity Function) 2e, const, $e^{-0.5}$

3) Kick velocity even for BH $\sigma_k = 100$ km s^{-1} and $\sigma_k = 300$ km s^{-1}

$$P(v_k) = \sqrt{\frac{2}{\pi}} \frac{v_k^2}{\sigma_k^2} \exp\left[-\frac{v_k^2}{\sigma_k^2}\right],$$

4) Common Envelope Parameter $\alpha\lambda = 0.01,\ \alpha\lambda = 0.1\ and\ \alpha\lambda = 10$

5) Roche lobe overflow parameter β =0, 0.5, 1.0

$$\dot{M}_2 = -(1-\beta)\dot{M}_1$$

6) Mass range : three cases because of the lack of stellar evolution above $100M_{su}$

In some cases the extrapolation of the fitting formulae are used .

under100	$10M_{sun} < M < 100M_{sun}$	If $M > 100M_{sun}$, Stop
over100	$10M_{sun} < M < 100M_{sun}$	If $M > 100M_{sun}$, Continue
The 140	$10M_{sun} < M < 140M_{sun}$	

85

Models

Table 1. The model parameters. Each column represents the model name, the IMF (Initial Mass Function), the IEF (Initial Eccentricity Function) , the kick velocity of supernova, the common envelope parameter $\alpha\lambda$ and the lose fraction β of transfer of stellar matter at the RLOF (Roche Lobe Over Flow) in each model. Model name "worst" means the worst combination of the parameter and distribution functions.

model	IMF	IEF	kick velocity (km/s)	$\alpha\lambda$	β
our standard	flat	e	0	1	function
IMF:logflat	M^{-1}	e	0	1	function
IMF:Salpeter	Salpeter	e	0	1	function
$f(e) =$ const.	flat	const.	0	1	function
$f(e) = e^{-0.5}$	flat	$e^{-0.5}$	0	1	function
kick 100 km/s	flat	e	100	1	function
kick 300 km/s	flat	e	300	1	function
$\alpha\lambda = 0.01$	flat	e	0	0.01	function
$\alpha\lambda = 0.1$	flat	e	0	0.1	function
$\alpha\lambda = 10$	flat	e	0	10	function
$\beta = 0$	flat	e	0	1	0
$\beta = 0.5$	flat	e	0	1	0.5
$\beta = 1$	flat	e	0	1	1
Worst	Salpeter	$e^{-0.5}$	300	0.01	1

Table 2. our standard model

	under100	over100	140
NSNS	0 (279)	0 (279)	0 (195)
NSBH	185335 (187638)	185335 (187638)	153435 (155694)
BHBH	517067 (522581)	534693 (540316)	595894 (604930)
merged NSNS	0 (279)	0 (279)	0 (195)
merged NSBH	50 (149)	50 (149)	825 (1255)
merged BHBH	115056 (120532)	131060 (136645)	128894 (137903)

Table 3. IMF:M^{-1}

	under100	over100	140
NSNS	2 (789)	2 (789)	1 (693)
NSBH	168100 (169794)	168100 (169794)	157106 (158831)
BHBH	350169 (353524)	357989 (361378)	405922 (410802)
merged NSNS	2 (789)	2 (789)	1 (693)
merged NSBH	68 (183)	68 (183)	374 (579)
merged BHBH	74745 (78054)	81786 (85129)	87590 (92450)

Table 4. IMF:Salpeter

	under100	over100	140
NSNS	5 (1994)	5 (1994)	3 (1957)
NSBH	93085 (93793)	93085 (93793)	92861 (93603)
BHBH	132534 (133485)	133880 (134835)	144096 (145294)
merged NSNS	5 (1994)	5 (1994)	3 (1957)
merged NSBH	64 (164)	64 (164)	97 (216)
merged BHBH	25536 (26468)	26720 (27656)	28378 (29564)

Table 5. $f(e) = \text{const.}$

	under100	over100	140
NSNS	0 (358)	0 (358)	0 (255)
NSBH	183460 (184761)	183460 (184761)	152099 (153548)
BHBH	522809 (526892)	541264 (545459)	602071 (608210)
merged NSNS	0 (358)	0 (358)	0 (255)
merged NSBH	43 (130)	43 (130)	843 (1087)
merged BHBH	111106 (1115171)	127904 (132081)	124714 (130831)

Table 6. $f(e) = e^{-0.5}$

	under100	over100	140
NSNS	0 (365)	0 (365)	0 (258)
NSBH	181650 (182388)	181650 (182388)	150779 (151805)
BHBH	523285 (526534)	542015 (545389)	602575 (607054)
merged NSNS	0 (365)	0 (365)	0 (258)
merged NSBH	38 (100)	38 (100)	774 (964)
merged BHBH	107594 (110832)	124620 (127983)	121494 (125955)

Table 7. kick 100 km s^{-1}

	under100	over100	140
NSNS	283 (794)	283 (794)	180 (516)
NSBH	32701 (34778)	32701 (34778)	32014 (34144)
BHBH	191755 (197327)	208268 (213962)	234117 (243348)
merged NSNS	17 (526)	17 (526)	6 (342)
merged NSBH	2527 (3016)	2527 (3016)	3218 (3762)
merged BHBH	117415 (122830)	132066 (137603)	135758 (144554)

Table 8. kick 300 km s^{-1}

	under100	over100	140
NSNS	8 (112)	8 (112)	4 (78)
NSBH	11922 (13133)	11941 (13152)	12115 (13330)
BHBH	70728 (75011)	78058 (82496)	86876 (93481)
merged NSNS	1 (85)	1 (85)	1 (60)
merged NSBH	3893 (4483)	3900 (4490)	4406 (5002)
merged BHBH	51928 (56021)	58793 (63041)	64084 (70252)

Table 9. $\alpha\lambda = 0.01$

	under100	over100	140
NSNS	0 (0)	0 (0)	0 (0)
NSBH	148290 (148770)	148290 (148770)	116548 (117117)
BHBH	340893 (352047)	345140 (363191)	365526 (382686)
merged NSNS	0 (0)	0 (0)	0 (0)
merged NSBH	0 (294)	0 (294)	30 (412)
merged BHBH	32283 (43437)	36530 (54581)	27790 (44950)

Table 10. $\alpha\lambda = 0.1$

	under100	over100	140
NSNS	0 (0)	0 (0)	0 (0)
NSBH	162814 (173016)	162814 (173016)	130556 (138835)
BHBH	434590 (464369)	448847 (480217)	480520 (520031)
merged NSNS	0 (0)	0 (0)	0 (0)
merged NSBH	45 (181)	45 (181)	1065 (1877)
merged BHBH	111696 (141356)	125953 (157204)	124830 (164240)

Table 11. $\alpha\lambda = 10$

	under100	over100	140
NSNS	1116 (2215)	1116 (2215)	840 (1616)
NSBH	198408 (198758)	198408 (198758)	166173 (166408)
BHBH	542399 (542603)	560156 (560360)	624631 (624958)
merged NSNS	890 (1949)	890 (1949)	6[illegible] (1381)
merged NSBH	767 (975)	767 (975)	506 (645)
merged BHBH	91787 (91989)	104656 (104858)	93729 (94055)

Table 12. $\beta = 0$

	under100	over100	140
NSNS	0 (279)	0 (279)	0 (195)
NSBH	185335 (187638)	185335 (187638)	153435 (155694)
BHBH	517067 (522581)	534693 (540316)	595894 (604930)
merged NSNS	0 (279)	0 (279)	0 (195)
merged NSBH	50 (149)	50 (149)	825 (1255)
merged BHBH	115056 (120532)	131060 (136645)	128894 (137903)

Table 13. $\beta = 0.5$

	under100	over100	140
NSNS	5 (380)	5 (380)	6 (272)
NSBH	193921 (196094)	193921 (196094)	158518 (160442)
BHBH	549893 (554150)	554966 (559228)	628253 (635698)
merged NSNS	5 (380)	5 (380)	6 (272)
merged NSBH	199 (286)	199 (286)	766 (1082)
merged BHBH	117094 (121310)	119758 (123979)	126090 (133512)

Table 14. $\beta = 1$

	under100	over100	140
NSNS	1359 (2006)	1359 (2006)	898 (1344)
NSBH	218311 (220521)	218311 (220522)	178444 (180375)
BHBH	531452 (536579)	531484 (536611)	610732 (619230)
merged NSNS	1358 (2005)	1358 (2005)	898 (1344)
merged NSBH	119 (255)	119 (255)	578 (917)
merged BHBH	50119 (55214)	50119 (55214)	57025 (65121)

Table 15. Worst

	under100	over100	140
NSNS	1637 (1637)	1637 (1637)	1604 (1604)
NSBH	4345 (4345)	4345 (4345	4283 (4285)
BHBH	5227 (5235)	5227 (5235)	5560 (5586)
merged NSNS	1562 (1562)	1562 (1562)	1532 (1532)
merged NSBH	1645 (1645)	1645 (1645)	1604 (1606)
merged BHBH	3195 (3203)	3195 (3203)	3376 (3399)

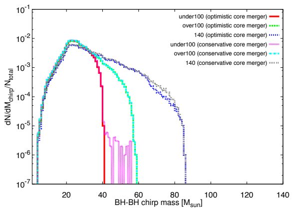

Figure 1. our standard model

Each line is the normalized distribution of the BH-BH chirp mass. The red, green, blue, pink, light blue and grey lines are the under100 case with optimistic core-merger criterion, the over100 case with optimistic core-merger criterion, the 140 case with optimistic core-merger criterion, the under100 case with conservative core-merger criterion, the over100 case with conservative core-merger criterion and the 140 case with conservative core-merger criterion, respectively.

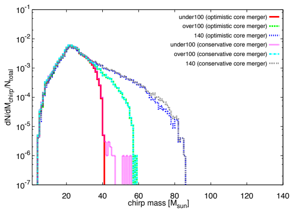

Figure 2. IMF:logflat

Same as Fig.1 but for IMF:logflat model.

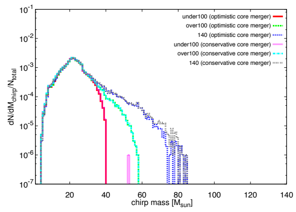

Figure 3. IMF:Salpeter

Same as Fig.1 but for IMF:Salpeter model.

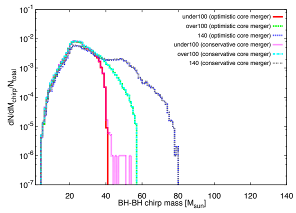

Figure 4. $f(e) = \text{const.}$

Same as Fig.1 but for $f(e) = \text{const.}$ model.

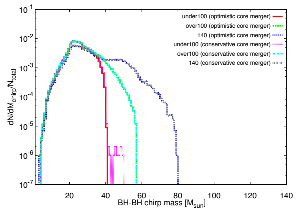

Figure 5. $f(e) = e^{-0.5}$.

Same as Fig.1 but for $f(e) = e^{-0.5}$ model.

89

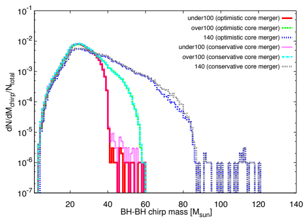

Figure 6. kick 100 km s^{-1}

Same as Fig.1 but for kick 100 km s^{-1} model.

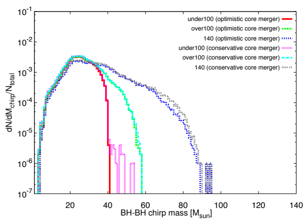

Figure 7. kick 300 km s^{-1}

Same as Fig.1 but for kick 300 km s^{-1} model.

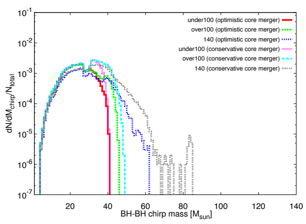

Figure 8. $\alpha\lambda = 0.01$

Same as Fig.1 but for $\alpha\lambda = 0.01$ model.

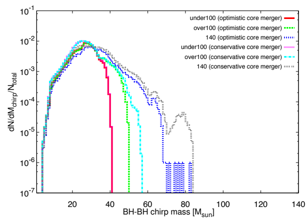

Figure 9. $\alpha\lambda = 0.1$

Same as Fig.1 but for $\alpha\lambda = 0.1$ model.

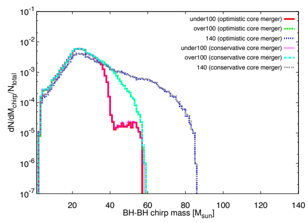

Figure 10. $\alpha\lambda = 10$

Same as Fig.1 but for $\alpha\lambda = 10$ model.

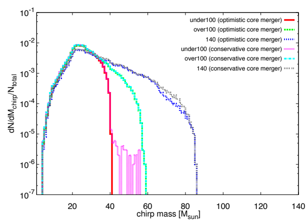

Figure 11. $\beta = 0$

Same as Fig.1 but for $\beta = 0$ model.

90

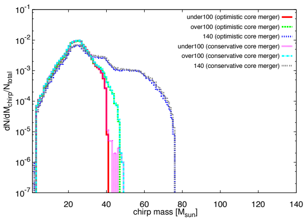

Figure 12. $\beta = 0.5$

Same as Fig.1 but for $\beta = 0.5$ model.

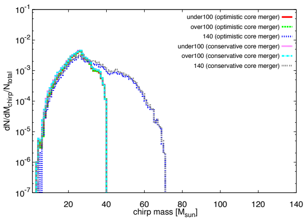

Figure 13. $\beta = 1$

Same as Fig.1 but for $\beta = 1$ model.

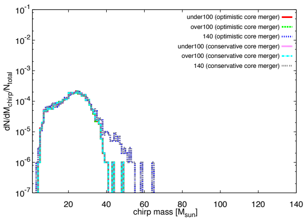

Figure 14. Worst

Same as Fig.1 but for Worst model.

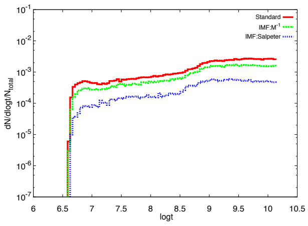

Figure 15. merger time:IMF

This figure describes the merger time distributions of Pop III BH-BHs. The red line, the green line and the blue line are our standard model, the logflat model and the Salpeter model.

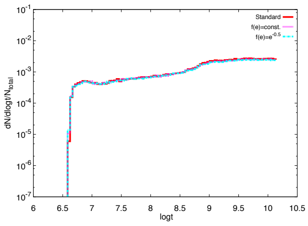

Figure 16. merger time:e

This figure describes the merger time distributions of Pop III BH-BHs. The red line, the pink line and the light blue line are our standard model, $f(e) = \mathrm{const.}$ model and $f(e) = e^{-0.5}$ model.

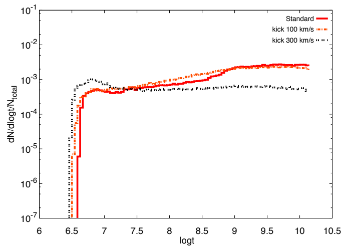

Figure 17. merger time:kick

This figure describes the merger time distributions of Pop III BH-BHs. The red line, the orange line and the black line are our standard model, the kick 100 km s^{-1} model and the kick 300 km s^{-1} model.

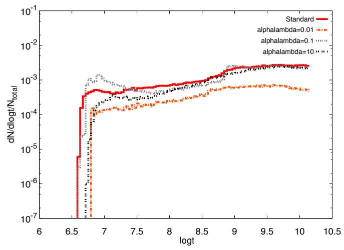

Figure 18. merger time:$\alpha\lambda$

This figure describes the merger time distributions of Pop III BH-BHs. The red line, the orange line, the grey line and the black line are our standard model, the $\alpha\lambda = 0.01$ model, the $\alpha\lambda = 0.1$ and the $\alpha\lambda = 10$ model.

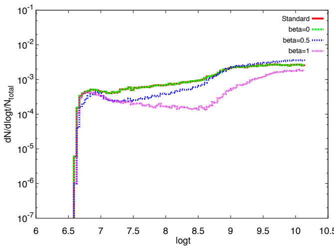

Figure 19. merger time:β

This figure describes the merger time distributions of Pop III BH-BHs. The red line, the green line, the blue line and the pink line are our standard model, the $\beta = 0$ model, the $\beta = 0.5$ and the $\beta = 1$ model.

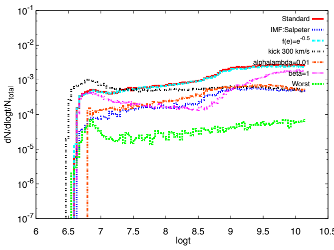

Figure 20. merger time:Worst

This figure describes the merger time distributions of Pop III BH-BHs. The red line, the blue line, the light blue line, the black line, the orange line, the pink line and the green line are our standard model, the Salpeter model, the $f(e) = e^{-0.5}$ model, the $\alpha\lambda = 0.01$ model, the $\beta = 1$ model and the Worst model.

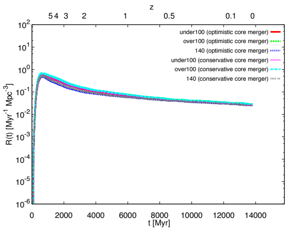

Figure 21. our standard

The red, green, blue, pink, light blue and grey lines are the under100 case with optimistic core-merger criterion, the over100 case with optimistic core-merger criterion, the 140 case with optimistic core-merger criterion, the under100 case with conservative core-merger criterion, the over100 case with conservative core-merger criterion and the 140 case with conservative core-merger criterion, respectively.

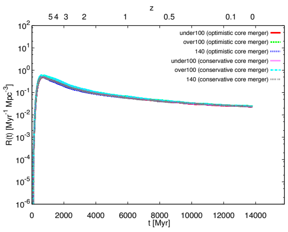

Figure 22. IMF:logflat

The same as Fig. 21 but for IMF:logflat model.

merger rate density of each model for under100 case. Table 17 describes the peak redshift of the BH-BHs merger rate density of each model in under100 case. It is seen that the peak redshift of the BH-BHs merger rate density ranges from 8.8 to 7.15. These peak redshifts are near the peak of the star formation rate at $z \sim 9$. In the following , we discuss the difference of each model.

The IMF dependence of the peak redshift of the merger rate density is clear seen. Namely for the steeper IMF the peak redshift is small although the difference is not so large ($\sim$0.45 in z). Since BH-BH progenitors whose initial mass is lower than 50 $M_\odot$ tend to evolve via the RLOF but not via

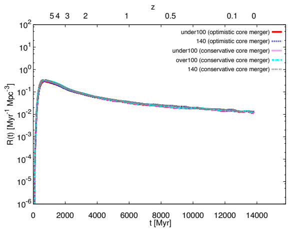

Figure 23. IMF:Salpeter

The same as Fig. 21 but for IMF:Salpeter model.

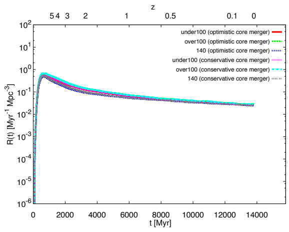

Figure 24. $f(e) = \text{const.}$

The same as Fig. 21 but for $f(e) = \text{const.}$ model.

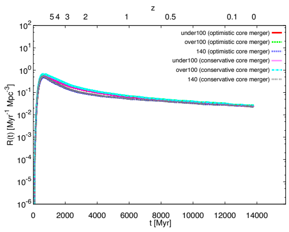

Figure 25. $f(e) = e^{-0.5}$

The same as Fig. 21 but for $f(e) = e^{-0.5}$ model.

Results

Table 16. The merger rate density [/Myr/Mpc^3] at $z = 0$

	under100	over100	140
our standard	0.0258 (0.0260)	0.0277 (0.0279)	0.0251 (0.0252)
IMF:logflat	0.0230 (0.0232)	0.0240 (0.0245)	0.0232 (0.0236)
IMF:Salpeter	0.0116 (0.0117)	0.0121 (0.0122)	0.0131 (0.0132)
$f(e) = \text{const.}$	0.0267 (0.0267)	0.0288 (0.0288)	0.0242 (0.0242)
$f(e) = e^{-0.5}$	0.0252 (0.0252)	0.0270 (0.0271)	0.0228 (0.0228)
kick 100 km s^{-1}	0.0210 (0.0212)	0.0223 (0.0226)	0.0203 (0.0207)
kick 300 km s^{-1}	0.00726 (0.00732)	0.00747 (0.00754)	0.00657 (0.00672)
$\alpha\lambda = 0.01$	0.00542 (0.00542)	0.00542 (0.00542)	0.00290 (0.00290)
$\alpha\lambda = 0.1$	0.0249 (0.0255)	0.0249 (0.0255)	0.0207 (0.0210)
$\alpha\lambda = 10$	0.0229 (0.0229)	0.0253 (0.0253)	0.0192 (0.0192)
$\beta = 0$	0.0258 (0.0260)	0.0277 (0.0279)	0.0251 (0.0252)
$\beta = 0.5$	0.0361 (0.0362)	0.0369 (0.0370)	0.0320 (0.0321)
$\beta = 1$	0.0186 (0.0187)	0.0186 (0.0187)	0.0159 (0.0161)
Worst	0.00194 (0.00194)	0.00194 (0.00194)	0.00169 (0.00169)

The redshift when merger rate is maximum

Table 17. The peak redshift of the BH-BHs merger rate density

model	peak redshift
our standard	7.85
IMF:logflat	7.75
IMF:Salpeter	7.4
$f(e) = \mathrm{const.}$	7.85
$f(e) = e^{-0.5}$	7.8
kick 100 km s^{-1}	7.5
kick 300 km s^{-1}	8.65
$\alpha\lambda = 0.01$	7.2
$\alpha\lambda = 0.1$	8.5
$\alpha\lambda = 10$	6.85
$\beta = 0$	7.85
$\beta = 0.5$	7.15
$\beta = 1$	8.8
Worst	8.3

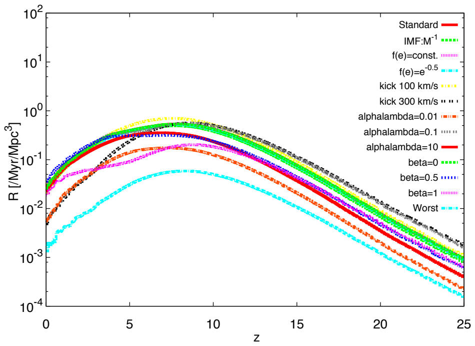

Figure 35. The merger rate densities

Detection rate for 10yr
by adv LIGO, Virgo and KAGRA for chirp and QNM signal

Table 18. under100 cases with optimistic core-merger criterion, 10year

This table shows the detection rates of Pop III BH-BHs for under100 cases with the optimistic core-merger criterion. The first column shows the name of the model. The second , the third, the fourth , the fifth and the sixth columns show the detection rate only by the inspiral chirp signal, the detection rate only by the quasi normal mode (QNM) with Kerr parameter $a/M = 0.70$, the detection rate by the inspiral chirp signal and the QNM with $a/M = 0.70$, the detection rates only by the QNM with $a/M = 0.98$ and the detection rate by the inspiral chirp signal and the QNM with $a/M = 0.98$, respectively. When signal-to-noise ratio of event that is calculated by matched filtering equation, over threshold signal-to-noise ratio, $S/N = 8$, the event is detected. For the fourth and sixth columns, their S/N are calculated by the linear summation of S/N of the inspiral and the QNM with $a/M = 0.70$ and 0.98, respectively. All the rates are based on ten years Monte Carlo simulations.

14models	Inspiral	QNM(0.70)	Inspiral + QNM(0.70)	QNM(0.98)	Inspiral + QNM(0.98)
our standard	659	474	2618	80	1539
IMF:logflat	628	341	2138	60	1298
IMF:Salpeter	314	111	955	17	569
$f(e)$= const	681	497	2560	101	1530
$f(e) = e^{-0.5}$	637	445	2519	78	1474
kick 100 km/s	526	420	2067	75	1242
kick 300 km/s	160	141	703	30	417
$\alpha\lambda$=0.01	153	92	501	19	300
$\alpha\lambda$=0.1	583	545	2463	86	1451
$\alpha\lambda$=10	637	409	2255	79	1362
β=0	694	484	2473	76	1540
β=0.5	970	523	3367	99	2011
β=1	448	329	1840	46	1098
Worst	44	24	146	5	94

Table 19. over100 cases with the optimistic core-merger criterion, 10year

The same as Table 18 but for over100 cases with the optimistic core-merger criterion.

14models	Inspiral	QNM(0.70)	Inspiral + QNM(0.70)	QNM(0.98)	Inspiral + QNM(0.98)
our standard	615	1100	3408	247	1822
IMF:logflat	631	732	2680	180	1478
IMF:Salpeter	334	220	1163	42	692
$f(e)$= const	671	1271	3665	282	1944
$f(e) = e^{-0.5}$	589	1162	3408	256	1728
kick 100 km/s	506	804	2614	174	1394
kick 300 km/s	186	308	913	76	491
$\alpha\lambda$=0.01	135	147	624	35	346
$\alpha\lambda$=0.1	502	989	3048	212	1591
$\alpha\lambda$=10	596	954	3043	232	1591
β=0	620	1113	3434	239	1741
β=0.5	930	689	3539	116	2032
β=1	432	285	1728	55	1014
Worst	44	20	163	3	101

Remember that typical total mass and chirp mass are 60 Msun and 30 Msun, respectively.

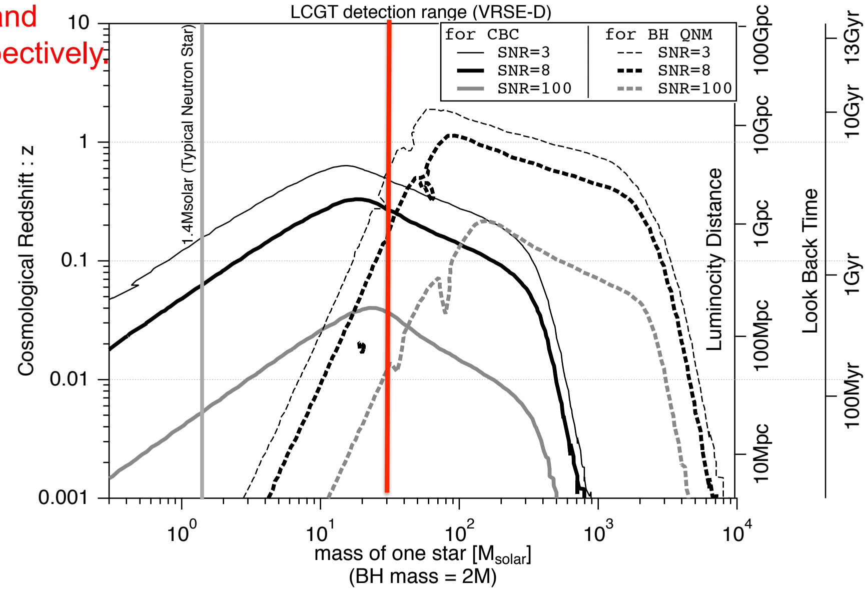

From Kanda and LCGT(KAGRA now)
Astro-ph/1112.3092 a=0.9 for QNM

97

Table 20. 140 cases with the optimistic core-merger criterion, 10year

The same as Table 18 but for 140 cases with the optimistic core-merger criterion

14models	Inspiral	QNM(0.70)	Inspiral + QNM(0.70)	QNM(0.98)	Inspiral + QNM(0.98)
our standard	474	2851	4936	1232	2786
IMF:logflat	554	1737	3743	675	2076
IMF:Salpeter	362	471	1502	140	846
$f(e)$= const	432	2822	4870	1172	2668
$f(e) = e^{-0.5}$	408	2784	4737	1151	2517
kick 100 km/s	361	2526	4239	926	2198
kick 300 km/s	109	837	1433	369	809
$\alpha\lambda$=0.01	60	130	385	34	185
$\alpha\lambda$=0.1	360	1589	3396	469	1653
$\alpha\lambda$=10	404	2155	3727	1084	2259
β=0	457	2831	5000	1221	2725
β=0.5	588	3389	5993	1392	3271
β=1	292	1619	3001	496	1424
Worst	36	33	153	9	86

Table 21. under100 cases with the conservative core-merger criterion, 10year

The same as Table 18 but for under100 cases with the conservative core-merger criterion

14models	Inspiral	QNM(0.70)	Inspiral + QNM(0.70)	QNM(0.98)	Inspiral + QNM(0.98)
our standard	627	485	2575	90	1526
IMF:logflat	652	300	2156	52	1329
IMF:Salpeter	346	90	977	12	625
$f(e)$= const	731	529	2666	101	1609
$f(e) = e^{-0.5}$	654	468	2468	95	1433
kick 100 km/s	515	395	2007	80	1209
kick 300 km/s	188	144	739	32	455
$\alpha\lambda$=0.01	128	135	571	34	334
$\alpha\lambda$=0.1	542	470	2361	75	1355
$\alpha\lambda$=10	584	404	2127	73	1244
β=0	647	496	2499	97	1492
β=0.5	879	567	3354	96	1971
β=1	487	345	1839	64	1058
Worst	47	20	163	3	97

98

Table 22. over100 cases with the conservative core-merger criterion, 10year

The same as Table 18 but for over100 cases with the conservative core-merger criterion

14models	Inspiral	QNM(0.70)	Inspiral + QNM(0.70)	QNM(0.98)	Inspiral + QNM(0.98)
our standard	619	1183	3481	251	1840
IMF:logflat	612	761	2653	173	1486
IMF:Salpeter	355	238	1167	42	703
$f(e)$= const	659	1264	3729	311	2005
$f(e) = e^{-0.5}$	654	1265	3522	297	1853
kick 100 km/s	549	790	2666	180	1443
kick 300 km/s	158	260	901	61	481
$\alpha\lambda$=0.01	124	253	719	80	403
$\alpha\lambda$=0.1	552	926	2996	174	1539
$\alpha\lambda$=10	601	991	3068	244	1641
β=0	625	1105	3492	248	1837
β=0.5	956	659	3571	104	2043
β=1	472	330	1824	64	1061
Worst	52	19	160	4	97

Table 23. 140 cases with the conservative core-merger criterion, 10year

The same as Table 18 but for 140 cases with the conservative core-merger criterion

14models	Inspiral	QNM(0.70)	Inspiral + QNM(0.70)	QNM(0.98)	Inspiral + QNM(0.98)
our standard	421	2895	5004	1273	2742
IMF:logflat	488	1892	3796	733	2049
IMF:Salpeter	330	474	1430	169	826
$f(e)$= const	455	2914	4980	1334	2814
$f(e) = e^{-0.5}$	374	2714	4611	1189	2515
kick 100 km/s	364	2620	4387	959	2317
kick 300 km/s	119	855	1414	437	852
$\alpha\lambda$=0.01	56	253	513	63	246
$\alpha\lambda$=0.1	389	1750	3479	566	1795
$\alpha\lambda$=10	358	2110	3665	1019	2173
β=0	420	2956	4959	1286	2765
β=0.5	593	3358	5926	1474	3310
β=1	277	1628	2967	506	1462
Worst	38	27	148	8	89

We also taken into account QNM so that the Standard Model is the model with Under100 and a/M=0.7. The rate becomes

$$261.8 \ \ \text{events} \ \ \text{yr}^{-1} \ \ (\text{SFR}_\text{P}/(10^{-2.5} \ \ \text{M}_\odot \ \ \text{yr}^{-1} \ \ \text{Mpc}^{-3}))$$

Expressing the rate of the other model by

$$261.8 \ \ \text{events} \ \ \text{yr}^{-1} \ \ (\text{SFR}_\text{P}/(10^{-2.5} \ \ \text{M}_\odot \ \ \text{yr}^{-1} \ \ \text{Mpc}^{-3}))\,\text{Err}_\text{sys}$$

Then $0.056 < \text{Err}_\text{sys} < 2.3$

That is :

$$14.6 - 599.3 \ \text{events yr}^{-1} \ (\text{SFR}_\text{p}/(10^{-2.5}\text{M}_\odot \ \text{yr}^{-1} \ \text{Mpc}^{-3})).$$

Typical Mass of BH is ～30Msun+30Msun.

This means in O1 event rate is 0.15-6.

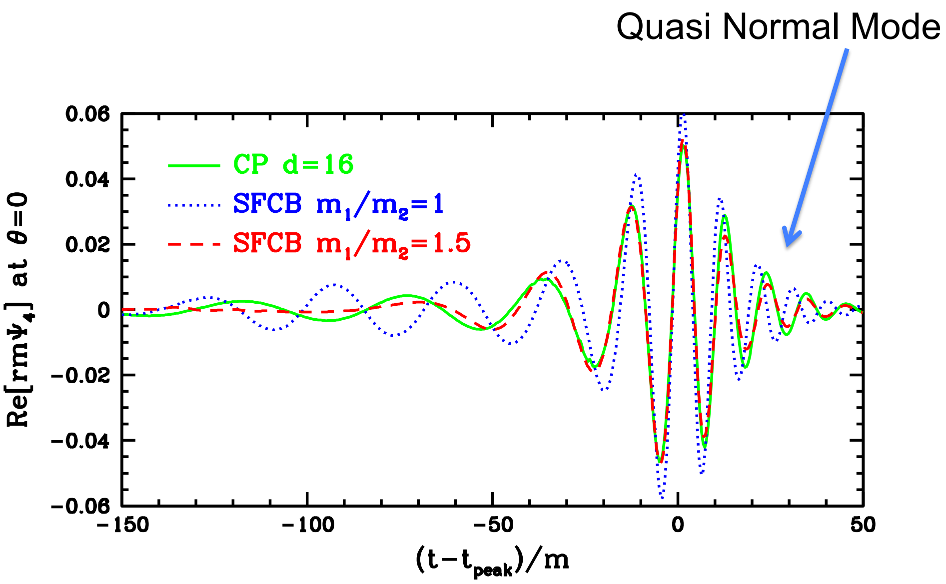

www.ligo.org/pdf_public/baumgarte01.pdf

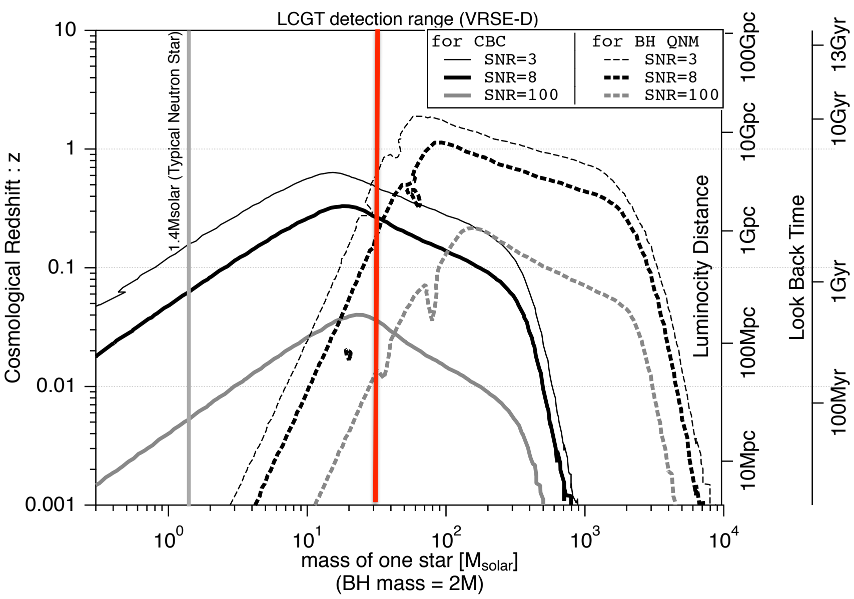

Kanda and LCGT(KAGRA now) a=0.9 for QNM

If Quasi Normal Mode of BH is detected and consistent with the Einstein theory, that is an important evidence of physics in the strong gravity region. If it is different , we should ask the true theory of gravity.

$$h_+(t;\iota,\phi) = \frac{\mathcal{A}}{r}(1+\cos^2\iota)e^{-\pi f_0(t-t_0)/Q} \times \cos[2\pi f_0(t-t_0)+\phi_0], \quad (4)$$

$$h_\times(t;\iota,\phi) = \frac{\mathcal{A}}{r}(2\cos\iota)e^{-\pi f_0(t-t_0)/Q} \times \sin[2\pi f_0(t-t_0)+\phi_0], \quad (5)$$

Berti, Cardoso and Will 2006

$$f_0 = \frac{1}{2\pi}\frac{c^3}{GM}[1.5251 - 1.1568(1-\hat{a})^{0.1292}], \quad (7)$$

$$Q = 0.7000 + 1.4187(1-\hat{a})^{-0.4990}. \quad (8)$$

Kerr parameter a/M

$M=60M_{sun}$, a=0, f_0=198Hz, Q=2.1

What we confirm by the detection of QNM?
Existence of event horizon ?

103

$$\frac{\partial^2}{\partial t^2}\chi_\ell + \left(-\frac{\partial^2}{\partial r_*^2} + V_\ell(r)\right)\chi_\ell = 0, \qquad r_* = r + 2M\log(r/2M-1).$$

$$V_\ell(r) = \left(1-\frac{2M}{r}\right)\left[\frac{\ell(\ell+1)}{r^2} + \frac{2\sigma M}{r^3}\right]$$

For GW σ=-3

WKB approximation (Schutz & Will) for a=0

$$(M\omega_n)^2 = V_\ell(r_0) - i\left(n+\frac{1}{2}\right)\left[-2\frac{d^2V_\ell(r_0)}{dr_*^2}\right]^{1/2}$$

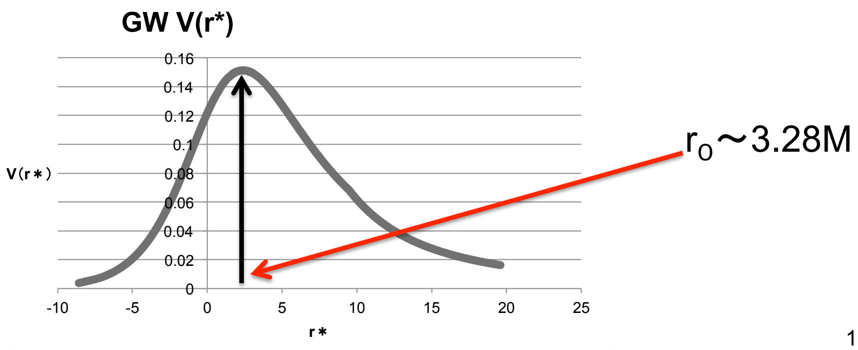

104

We can confirm the space time at r=3.28M and around there from the curvature of V.

Nakano, Tanaka & Nakamura 2015

They showed in what case , we can determine QNM and say Einstein theory is correct or not?

From chirp signal, we can determine each mass.

Numerical Relativity will tell us M and a/M after the merger as

$$
\begin{aligned}
\frac{M_{\rm rem}}{M} &= (4\eta)^2 \left(M_0 + K_{2d}\,\delta m^2 + K_{4f}\,\delta m^4\right) + \left[1+\eta(\tilde{E}_{\rm ISCO}+11)\right]\delta m^6 \\
\alpha_{\rm rem} &= \frac{S_{\rm rem}}{M_{\rm rem}^2} = (4\eta)^2 \left(L_0 + L_{2d}\,\delta m^2 + L_{4f}\,\delta m^4\right) + \eta \tilde{J}_{\rm ISCO}\delta m^6\,,
\end{aligned}
$$

$\delta m = (m_1 - m_2)/M$ $\quad M_0,\ K_{2d},\ \tilde{K}_{4f},\ L_0,\ \tilde{L}_{2d}$ and $\tilde{L}_{4f}$ are fitting parameters

equal mass cases,

$$
\begin{aligned}
\frac{M_{\rm rem}}{M} &= 0.951507 \pm 0.000030 \\
\alpha_{\rm rem} &= 0.686710 \pm 0.000039
\end{aligned}
$$

Healy, Lousto &Zlochower 2014

QNM (Quasi Normal Mode) $f_R = f_c\,, \quad f_I = -\dfrac{f_c}{2Q}$

Fitting formula Berti, Cardoso and Will 2006

$$
\begin{aligned}
f_c &= \frac{1}{2\pi M_{\rm rem}}\left[1.5251 - 1.1568(1-\alpha_{\rm rem})^{0.1292}\right] \\
&= 538.4\left(\frac{M}{60M_\odot}\right)^{-1}\left[1.5251 - 1.1568(1-\alpha_{\rm rem})^{0.1292}\right]\ [\mathrm{Hz}] \\
Q &= 0.7000 + 1.4187(1-\alpha_{\rm rem})^{-0.4990}\,.
\end{aligned}
$$

$M = 60M_\odot$, $\eta = 1/4$, we have $M_{\rm rem} = 57.0904M_\odot$ and $\alpha_{\rm rem} = 0.686710$

$$f_c = 299.5\mathrm{Hz} \text{ and } Q = 3.232$$

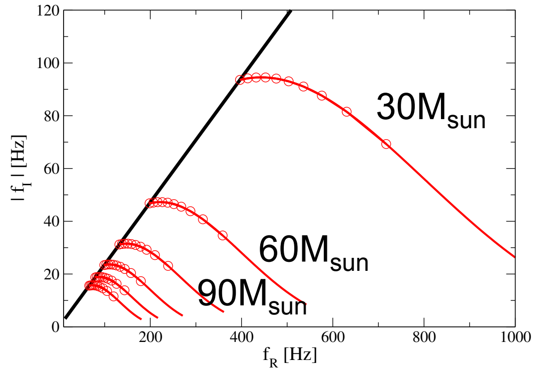

FIG. 2: Real (f_R) and imaginary (f_I) parts of QNM frequencies for the dominant ($\ell = 2$, $m = 2$) least-damped ($n = 0$) mode. The (black) thick line shows the Schwarzschild limit, and the (red) curves are for various mass cases terminated at the spin $\alpha = 0.998$ [36]. From the top of the (red) curves, we are considering BH masses, $M/M_\odot = 30$, 60, 90, 120, 150 and 180, respectively. The (red) circles for each line denote the spin dependence $\alpha = 0$, 0.1, 0.2, 0.3, 0.4, 0.5, 0.6, 0.7, 0.8 and 0.9 from the left.

107

$$\langle a|b\rangle = 4\Re \int_0^\infty \frac{\tilde{a}(f)\tilde{b}^*(f)}{S_n(f)} df$$

$$\begin{aligned} \mathrm{SNR} &= \langle h|h\rangle^{1/2} \\ &= 2\left[\int_0^\infty \frac{|\tilde{h}(f)|^2}{S_n(f)} df\right]^{1/2} \end{aligned}$$

$$S_n(f)^{1/2} = 10^{-26}\left(6.5\times 10^{10} f^{-8} + 6\times 10^6 f^{-2.3} + 1.5 f^1\right)\ [\mathrm{Hz}^{-1/2}]$$

$$\Gamma_{ij} = \left\langle \frac{\partial h}{\partial \theta^i} \middle| \frac{\partial h}{\partial \theta^j} \right\rangle\Bigg|_{\theta=\theta_{\mathrm{true}}} \qquad (\Delta\theta^i)_{\mathrm{RMS}} \ = \ \sqrt{(\Gamma^{-1})^{ii}}$$

108

KAGRA Noise Curve

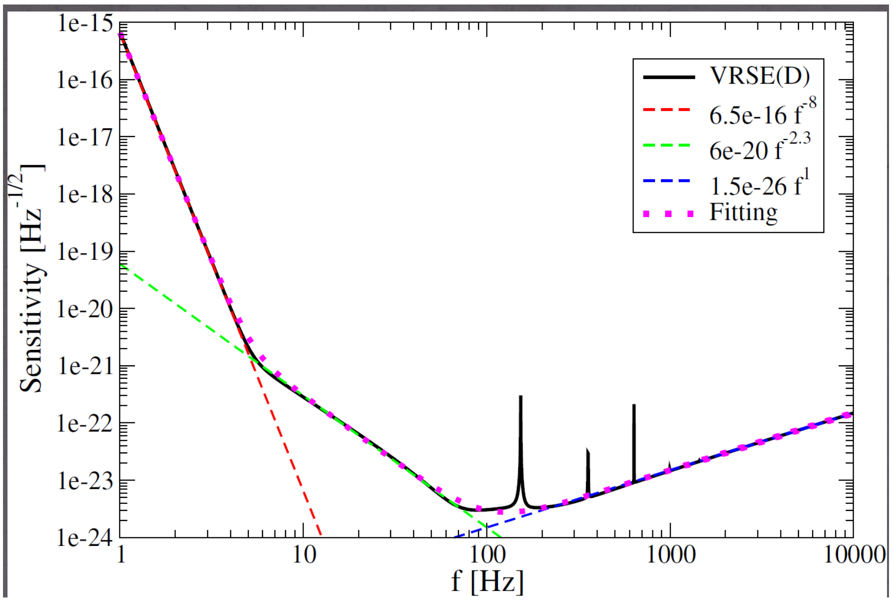

109

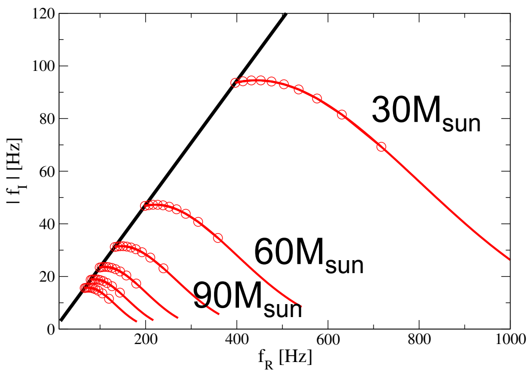

FIG. 2: Real (f_R) and imaginary (f_I) parts of QNM frequencies for the dominant ($\ell = 2$, $m = 2$) least-damped ($n = 0$) mode. The (black) thick line shows the Schwarzschild limit, and the (red) curves are for various mass cases terminated at the spin $\alpha = 0.998$ [36]. From the top of the (red) curves, we are considering BH masses, $M/M_\odot = 30$, 60, 90, 120, 150 and 180, respectively. The (red) circles for each line denote the spin dependence $\alpha = 0$, 0.1, 0.2, 0.3, 0.4, 0.5, 0.6, 0.7, 0.8 and 0.9 from the left.

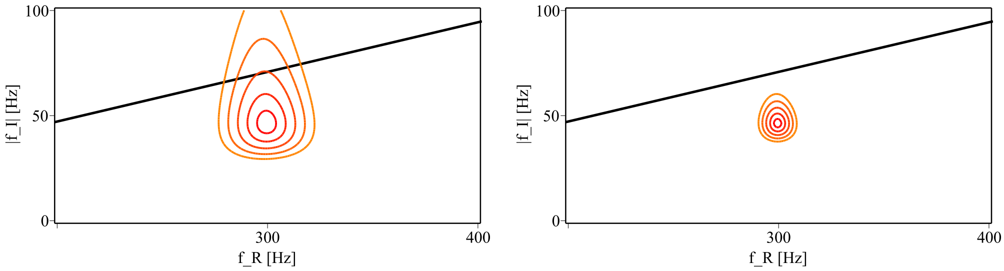

FIG. 3: In the (f_R, f_I) plane, the left and right panels show the parameter estimation in the cases with SNR = 20 and 50 for the typical case (with $M_{\rm rem} = 57.0904 M_\odot$ and $\alpha_{\rm rem} = 0.686710$), respectively. The (black) thick line shows the Schwarzschild limit which is same as that in Fig. 2, and the ellipses are the contours of 1σ, 2σ, 3σ, 4σ, and 5σ. Here, the time and phase parameters (t_0, ϕ_0) have been marginalized out.

SNR=35 is good enough to say QNM follows Einstein Theory

This is 1.2% of all events. The detection will allow us to confirm or refute Einstein's general relativity.

Event rate of this confirmation is

0.17-7.2 events yr^{-1} $(\mathrm{SFR_p}/(10^{-2.5}\ \mathrm{M_\odot\ yr^{-1}\ Mpc^{-3}}))$

111

Pop I and PopII cases

Dominik et al. 2012

Nanjing: Xu&Li 2010
Computed λ

Pop I : stars like sun

PopII stars with 0.1-0.01 metal of PopI

Table 1
Summary of Models[a]

Model	Parameter	Description
S	Standard	λ = *Nanjing*, $M_{\rm NS,max} = 2.5\,M_\odot$, $\sigma = 265$ km s^{-1} BH kicks: variable, SN: Rapid half-cons mass transfer (β=0.5)
V1	$\lambda = 0.01$	Very low λ: fixed
V2	$\lambda = 0.1$	Low λ: fixed
V3	$\lambda = 1$	High λ: fixed
V4	$\lambda = 10$	Very high λ: fixed
V5	$M_{\rm NS,max} = 3.0\,M_\odot$	High maximum NS mass
V6	$M_{\rm NS,max} = 2.0\,M_\odot$	Low maximum NS mass
V7	$\sigma = 132.5$ km s^{-1}	Low kicks: NS/BH
V8	Full BH kicks	High natal kicks: BH
V9	No BH kicks	No natal kicks: BH
V10	Delayed SN	NS/BH formation: delayed SN engine
V11	Weak winds	Wind mass-loss rates reduced to 50%
V12	Cons MT	Fully conservative mass transfer
V13	Non-cons MT	Fully non-conservative mass transfer
V14	$\lambda \times 5$	*Nanjing* λ increased by 5
V15	$\lambda \times 0.2$	*Nanjing* λ decreased by 5

Note. [a] All parameters, except for the one listed under "Description," retain their Standard model ("S") values.

112

Table 2
Galactic Merger Rates, $Z_\odot$ (Myr^{-1})[a]

Model	NS–NS	BH–NS	BH–BH
S	23.5 (7.6)	1.6 (0.2)	8.2 (1.9)
V1	0.4 (0.4)	0.002 (0.002)	1.1 (1.1)
V2	11.8 (1.1)	2.4 (0.08)	15.3 (0.4)
V3	48.8 (14.3)	4.6 (0.03)	5.0 (0.03)
V4	20.8 (0.3)	0.9 (0.0)	0.3 (0.0)
V5	24.1 (8.1)	1.4 (0.2)	8.3 (2.0)
V6	24.1 (8.3)	1.4 (0.2)	8.0 (1.9)
V7	32.4 (9.5)	1.9 (0.3)	10.4 (2.1)
V8	23.3 (7.7)	0.03 (0.004)	0.05 (0.005)
V9	23.4 (8.0)	1.4 (0.2)	16.9 (4.2)
V10	25.6 (8.9)	0.07 (0.03)	0.6 (0.08)
V11	24.2 (6.5)	1.2 (0.2)	29.7 (3.6)
V12	77.4 (0.3)	0.06 (0.02)	8.9 (1.6)
V13	26.1 (6.2)	10.6 (3.9)	5.8 (0.5)
V14	28.2 (3.7)	3.4 (0.05)	23.0 (0.07)
V15	39.8 (17.8)	0.01 (0.007)	1.1 (1.0)
Range	0.4–77.4 (0.3–17.8)	0.002–10.6 (0.0–3.9)	0.05–29.7 (0.0–4.2)

Notes. [a] Rates are calculated for a synthetic galaxy similar to the Milky Way (solar metallicity, and 10 Gyr of continuous star formation at the level of 3.5 $M_\odot$ yr^{-1}). Rates are presented for submodel A (CE HG donor allowed), with the rates for submodel B (CE HG donor forbidden) listed in parentheses; see Section 2.3.1 for details. The range presents the minimum and maximum value for each DCO type.

Table 3
Galactic Merger Rates, 0.1 $Z_\odot$ (Myr^{-1})[a]

	NS–NS	BH–NS	BH–BH
S	8.1 (2.5)	3.4 (2.3)	73.3 (13.6)
V1	0.06 (0.06)	0.03 (0.03)	12.5 (8.1)
V2	65.9 (6.9)	0.5 (0.4)	56.7 (16.1)
V3	44.1 (4.2)	15.8 (8.4)	90.2 (7.9)
V4	29.5 (1.4)	8.8 (1.6)	5.9 (0.3)
V5	8.0 (2.3)	3.4 (2.1)	73.4 (13.7)
V6	7.8 (2.4)	3.5 (2.0)	74.5 (13.8)
V7	8.3 (2.2)	6.1 (4.3)	83.7 (15.1)
V8	8.2 (2.5)	0.7 (0.2)	4.2 (0.8)
V9	8.1 (2.1)	5.2 (3.7)	92.3 (19.3)
V10	8.6 (2.6)	2.3 (2.0)	62.0 (11.5)
V11	7.7 (2.3)	3.8 (2.4)	79.2 (17.1)
V12	17.1 (4.4)	4.1 (3.0)	68.8 (6.6)
V13	5.9 (1.4)	33.0 (30.1)	39.0 (28.9)
V14	47.0 (1.0)	15.5 (5.7)	90.5 (14.9)
V15	54.4 (7.8)	0.4 (0.3)	21.7 (10.2)
Range	0.06–65.9 (0.06–7.8)	0.03–33.0 (0.03–30.1)	4.2–92.3 (0.3–28.9)

Note. [a] Same as Table 3 but for sub-solar metallicity.

time. Additional models and DCO population properties are available online at www.syntheticuniverse.com.

For each model we calculate the Galactic merger rates. These are defined as the number of coalescences of DCOs per unit

These calculations are based on the assumption that the galaxy like ours have a single metalicity with star formation rate of $3.5 M_{sun}/y$
Metalicity of the sun is Z_{sun}=0.02 in mass percentage.

Table 4
Formation Channels of DCOs for $Z_\odot$[a]

	Channel	Fraction
NSNS01	NC:a→b, SN:a, CE:b→a, NC:b→a, SN:b	79.3%
NSNS02	NC:a→b, CE:b→a, NC:b→a, AIC(WD→NS):a, NC:b→a, SN:b	8.0%
NSNS03	NC:a→b, SN:a, CE:b→a, CE:b→a,[b] SN:b	6.9%
NSNS04	Other	5.8%
BHNS01	NC:a→b, SN:a, CE:b→a, SN:b	95.4%
BHNS02	NC:a→b, SN:a, CE:b→a, NC:b→a, SN:b	1.8%
BHNS03	Other	2.8%
BHBH01	NC:a→b, SN:a, CE:b→a, SN:b	98.9%
BHBH02	Other	1.1%

Notes. [a] Coalescing DCOs' formation channels for the Standard model, submodel A at solar metallicity. NC: non-conservative mass transfer; SN: supernova; CE: common envelope; AIC: accretion-induced collapse of oxygen/neon white dwarf into NS. The arrows show the direction of transfer and "a" stands for the primary (initially more massive) component, "b" for the secondary.
[b] The first CE is initiated by the H-rich Hertzsprung gap donor (allowed in model A). The second starts when the exposed core of the donor becomes an evolved helium star.

Table 5
Formation Channels of DCOs for 0.1 $Z_\odot$[a]

	Channel	Fraction
NSNS01	NC:a→b, SN:a, CE:b→a, CE:b→a, SN:b	49.1%
NSNS02	NC:a→b, SN:a, CE:b→a, NC:b→a, SN:b	21.2%
NSNS03	NC:a→b, SN:a, CE:b→a, SN:b	18.2%
NSNS04	NC:a→b, CE:b→a, SN:a, CE:b→a, SN:b	3.3%
NSNS05	Other	8.2%
BHNS01	CE:a→b, SN:a, CE:b→a, NC:b→a, SN:b	40.8%
BHNS02	CE:a→b, SN:a, CE:b→a, SN:b	17.4%
BHNS03	NC:a→b, SN:a, CE:b→a, SN:b	13.4%
BHNS04	NC:a→b, SN:a, CE:b→a, NC:b→a, SN:b	12.2%
BHNS05	NC:a→b, CE:b→a, NC:a→b, SN:a, SN:b	8.8%
BHNS06	Other	6.4%
BHBH01	NC:a→b, SN:a, CE:b→a, SN:b	90.6%
BHBH02	CE:a→b, SN:a, CE:b→a, SN:b	4.0%
BHBH03	NC:a→b, SN:a, NC:b→a, CE:b→a, SN:b	1.4%
BHBH04	Other	4.0%

Note. [a] Same as Table 4 but for sub-solar metallicity.

Sub Model B:
Assuming that red giant makes Common Envelope to merge binary.
In this case the number of NS-NS,NS-BH,BH-BH will decrease.

Sub Model A:
No assumption like Model B.

Mass distribution progenitor

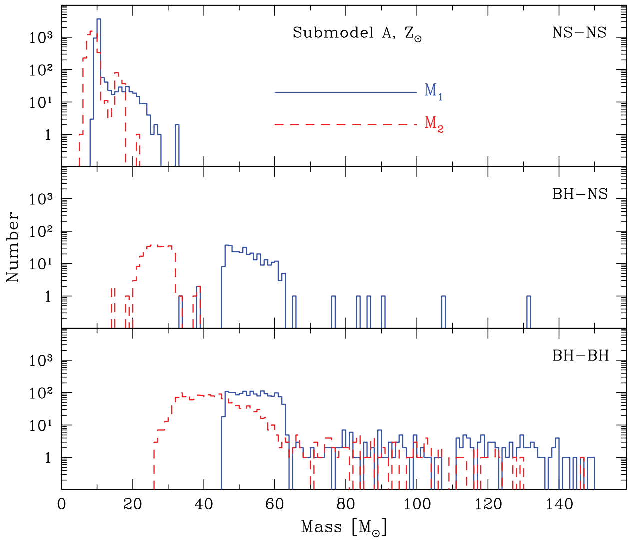

Figure 5. Distribution of progenitor (ZAMS) masses of coalescing DCOs for the Standard model, submodel A (for submodel details, see Section 2.3.1), $Z_\odot$. The top panel presents the distribution for NS–NS, the middle panel for BH–NS, and the bottom panel for BH–BH progenitors. M_1 stands for the primary component (initially more massive, solid, blue line) and M_2 for the secondary (initially less massive, dashed, red line). The average mass for NS–NS progenitors is 11–9 $M_\odot$, for BH–NS progenitors is 52–27 $M_\odot$, and for BH–BH progenitors is 58–44 $M_\odot$ (M_1–M_2). Note that binary evolution blurs the ZAMS mass limits for NS/BH formation (see Section 4.1).

Mass distribution of Remnants

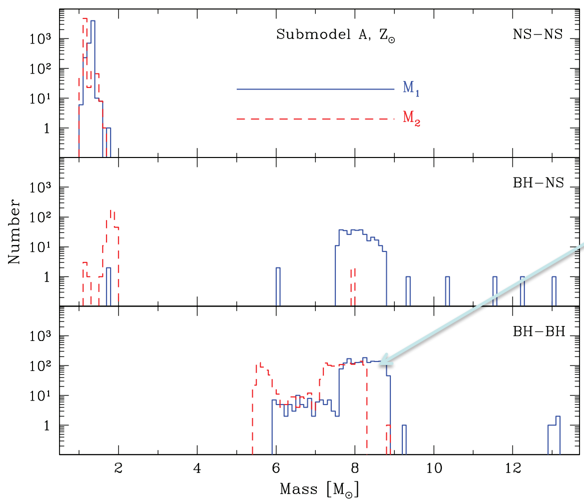

Smaller than PopIII case

Figure 6. Distribution of remnant masses of coalescing DCOs for the Standard model, submodel A, $Z_\odot$. The top panel presents the distribution for NS–NS, the middle panel for BH–NS, and the bottom panel for BH–BH systems. M_1 represents the primary remnant (corresponding to M_1 in Figure 5, solid, blue line), while M_2 is the secondary (corresponding to M_2 in Figure 5, dashed, red line). The average mass for NS–NS systems is 1.3–1.1 $M_\odot$, for BH–NS systems is 8.0–1.8 $M_\odot$, and for BH–BH systems is 8.2–7.2 $M_\odot$ (M_1–M_2). The gap between the upper mass of NSs (2 $M_\odot$) and the lowest mass of BHs (5 $M_\odot$) results from the use of the Rapid SN engine (see Section 2.4).

Chirp Mass distribution of remnant

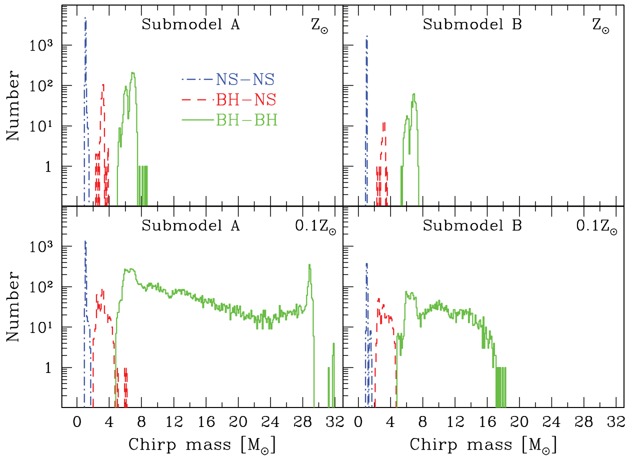

Figure 7. Distribution of chirp masses of coalescing DCOs for the Standard model. The average chirp masses for NS–NS and BH–NS systems are ∼1.1 $M_\odot$ and 3.2 $M_\odot$, respectively, for both submodels and metallicities. The average chirp mass for BH–BH systems, for $Z_\odot$, is ∼6.7 $M_\odot$ for both submodels. For 0.1 $Z_\odot$ the masses are 13.2–9.7 $M_\odot$ for submodels A and B, respectively. The maximum chirp mass increases with metallicity as wind mass-loss rates decrease, allowing for the formation of heavier BHs (see Belczynski et al. 2010b and Section 4.1).

117

Distribution of Delay time

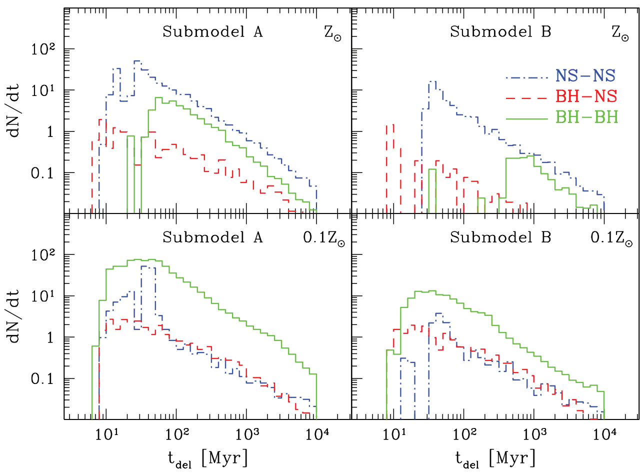

Figure 8. Distribution of delay times for coalescing DCOs for the Standard model. The vertical axis presents the number of DCOs per linear time. The average delay time for all binaries is ∼1 Gyr.

Distribution of Chirp Mass in each model

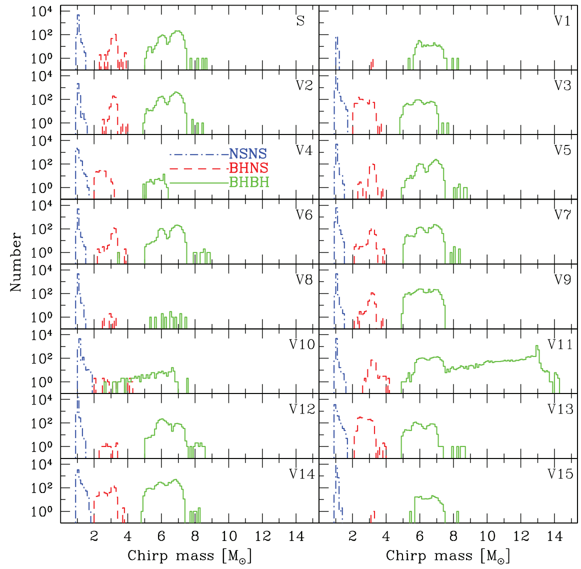

Figure 10. Chirp-mass distribution of coalescing DCOs for all variations for submodel A (for submodel details, see Section 2.3.1) and $Z = Z_\odot$. The maximum chirp mass is found for BH–BH systems, and may reach as high as $\sim 14\,M_\odot$. The typical chirp mass for BH–NS systems is ~ 2–$3\,M_\odot$, while the chirp mass for NS–NS systems peaks around $\sim 1\,M_\odot$ independent of the model. Note that the chirp masses of BH–NS systems are separated from the BH–BH values. The only exception to this rule is the (most likely unphysical) V10 model, which employs the Delayed supernova engine (see Section 4.10 for details).

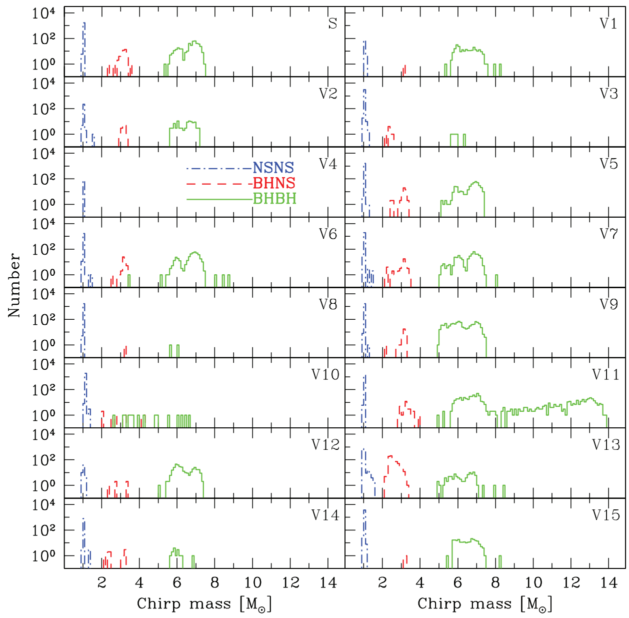

Figure 11. Chirp-mass distribution of coalescing DCOs for all variations for submodel B and $Z = Z_\odot$.
(A color version of this figure is available in the online journal.)

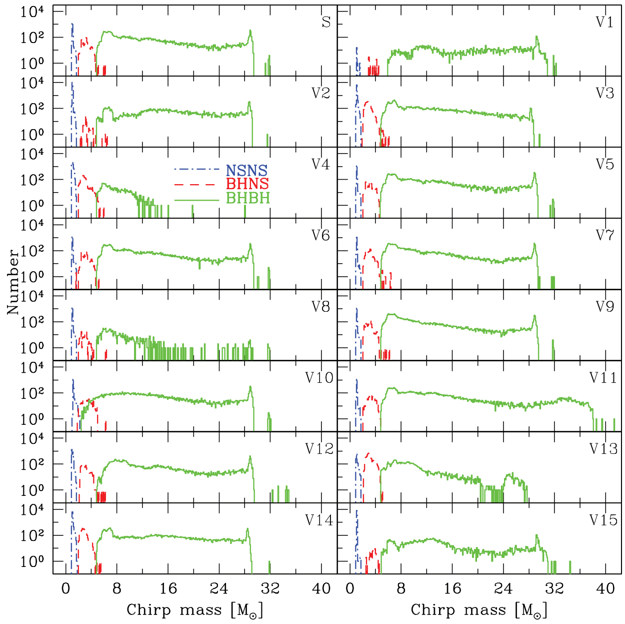

Figure 12. Chirp-mass distribution of coalescing DCOs for all variations for submodel A and $Z = 0.1\,Z_\odot$. Note the dramatic increase of the maximum chirp mass with decreasing metallicity. For solar metallicity, the chirp mass was always below 15 $M_\odot$ (Figure 10), while for the majority of models shown here the chirp mass reaches $\sim$30 $M_\odot$ for sub-solar metallicity. The lack of high chirp-mass systems in model V4 is explained in Section 4.5.

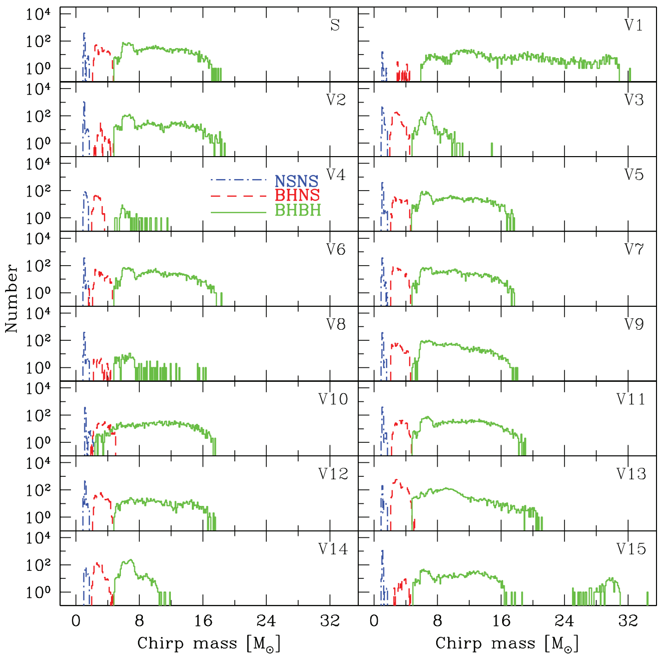

Figure 13. Chirp-mass distribution of coalescing DCOs for all variations for submodel B and $Z = 0.1\,Z_\odot$. The maximum chirp mass for submodel B typically reaches only $\sim$15 $M_\odot$, as contrasted with $\sim$30 $M_\odot$ for submodel A (see Figure 12). The reason why the V1 model allows for chirp mass as high as $\sim$30 $M_\odot$, even for submodel B, is explained in Section 4.2. For the same reason V15 harbors a large chirp-mass range.

Characteristics of Chirp Mass

Table 6
Chirp-mass Characteristics for $Z_\odot$, Submodel A[a]

	NS–NS			BH–NS			BH–BH		
	Min	Avg	Max	Min	Avg	Max	Min	Avg	Max
S	0.96	1.05	1.40	2.3	3.2	3.7	5.1	6.7	8.7
V1	1.08	1.09	1.14	3.2	3.2	3.2	5.3	6.5	8.3
V2	0.96	1.08	1.53	2.5	3.2	4.0	5.0	6.6	8.4
V3	0.94	1.06	1.69	2.1	2.7	3.6	4.9	6.0	7.7
V4	0.95	1.03	1.64	2.1	2.5	3.1	5.0	5.8	6.3
V5	0.96	1.05	1.42	2.4	3.2	3.8	5.0	6.7	8.7
V6	0.96	1.05	1.44	2.2	3.2	3.9	3.5	6.7	8.8
V7	0.96	1.05	1.45	2.1	3.1	3.9	5.0	6.5	8.7
V8	0.96	1.05	1.42	2.6	3.0	3.2	5.4	6.5	7.4
V9	0.96	1.05	1.44	2.2	3.1	3.7	5.0	6.3	7.5
V10	1.01	1.14	1.86	2.0	3.1	4.2	2.7	5.7	7.6
V11	0.96	1.05	1.50	2.7	3.2	4.2	4.9	10.5	14.3
V12	0.96	1.07	1.44	2.4	2.9	3.6	5.0	6.3	8.6
V13	0.94	1.02	1.63	2.1	2.7	4.0	4.9	6.1	8.6
V14	0.96	1.07	1.70	2.1	2.9	3.8	4.9	6.4	8.3
V15	0.95	1.07	1.40	3.1	3.2	3.2	5.5	6.5	8.2
Range		0.94–1.86			2.0–4.2			2.7–14.3	

Notes. [a] The chirp-mass distribution for merging DCOs, for $Z_\odot$ and submodel A. The values of chirp mass presented are minimum, average, and maximum in units of $M_\odot$. The range represents the minimum–maximum value of the chirp mass from the entire suite of models for each DCO type. This table corresponds to Figure 10.

Table 7
Chirp-mass Characteristics for $Z_\odot$, Submodel B[a]

	NS–NS			BH–NS			BH–BH		
	Min	Avg	Max	Min	Avg	Max	Min	Avg	Max
S	0.96	1.05	1.17	2.3	3.2	3.3	5.2	6.7	7.4
V1	1.08	1.09	1.14	3.2	3.2	3.2	5.3	6.5	8.3
V2	0.96	1.06	1.53	3.0	3.2	3.3	5.6	6.5	7.2
V3	0.96	1.05	1.22	2.2	2.4	2.6	5.7	5.9	6.4
V4	1.03	1.03	1.04		No systems			No systems	
V5	0.96	1.05	1.28	2.4	3.1	3.3	5.2	6.7	7.4
V6	0.96	1.05	1.43	2.6	3.2	3.4	3.5	6.7	8.7
V7	0.96	1.05	1.45	2.2	3.1	3.5	5.1	6.5	8.0
V8	0.96	1.05	1.08	3.2	3.2	3.2	5.6	5.9	6.1
V9	0.96	1.05	1.21	2.2	3.1	3.3	5.0	6.2	7.4
V10	1.04	1.13	1.34	2.0	3.0	4.2	2.7	4.6	6.6
V11	0.96	1.05	1.09	2.9	3.3	4.0	4.9	9.1	13.8
V12	0.96	1.04	1.17	2.4	2.9	3.4	5.0	6.3	7.4
V13	0.95	1.00	1.59	2.1	2.6	3.3	4.9	6.3	8.4
V14	0.96	1.05	1.34	2.2	2.8	3.3	5.7	6.0	6.9
V15	0.95	1.05	1.13	3.1	3.2	3.2	5.5	6.5	8.2
Range		0.95–1.59			2.0–4.2			2.7–13.8	

Notes. [a] Same as Table 6 but for submodel B. This table corresponds to Figure 11.

Table 8
Chirp-mass Characteristics for 0.1 $Z_\odot$, Submodel A[a]

	NS–NS			BH–NS			BH–BH		
	Min	Avg	Max	Min	Avg	Max	Min	Avg	Max
S	0.96	1.09	1.67	2.1	3.2	6.1	4.8	13.2	31.8
V1	1.08	1.11	1.56	2.9	3.6	4.4	5.9	20.0	32.3
V2	0.96	1.09	1.66	2.3	3.5	6.5	4.8	17.2	31.6
V3	0.96	1.09	1.68	2.0	2.9	6.1	4.8	12.5	29.7
V4	0.95	1.10	1.64	2.1	2.9	5.9	4.8	7.6	28.1
V5	0.96	1.09	1.66	2.0	3.1	4.6	4.8	13.3	31.8
V6	0.97	1.09	1.65	1.7	3.1	5.2	4.8	13.1	31.8
V7	0.96	1.08	1.70	2.0	3.1	6.4	4.9	12.4	32.0
V8	0.96	1.09	1.64	2.0	3.0	6.4	4.8	9.0	31.9
V9	0.97	1.08	1.66	2.0	3.0	6.1	4.9	12.1	31.9
V10	1.10	1.20	2.16	1.8	3.4	6.3	2.4	14.4	32.0
V11	0.97	1.08	1.61	2.0	3.3	4.7	4.8	14.3	41.4
V12	0.96	1.06	1.64	2.1	3.1	6.4	4.9	14.4	34.9
V13	0.96	1.10	1.68	2.1	3.1	5.0	4.8	9.7	27.7
V14	0.96	1.10	1.70	2.0	2.9	5.4	4.8	14.6	31.8
V15	0.96	1.09	1.64	2.4	3.7	4.6	4.9	15.0	34.5
Range		0.95–2.16			1.7–6.4			2.4–41.4	

Notes. [a] Same as Table 6 but for 0.1 $Z_\odot$. This table corresponds to Figure 12.

Table 9
Chirp-mass Characteristics for 0.1 $Z_\odot$, Submodel B[a]

	NS–NS			BH–NS			BH–BH		
	Min	Avg	Max	Min	Avg	Max	Min	Avg	Max
S	0.96	1.09	1.67	2.2	3.1	4.6	4.8	9.7	18.3
V1	1.08	1.11	1.56	2.9	3.6	4.4	5.9	16.1	32.3
V2	0.96	1.07	1.66	2.3	3.3	4.6	4.8	9.3	18.8
V3	0.99	1.12	1.68	2.0	2.9	4.5	4.8	6.8	14.9
V4	0.98	1.20	1.60	2.1	2.7	3.6	5.0	6.7	11.5
V5	0.96	1.08	1.66	2.2	3.2	4.6	4.8	9.8	17.7
V6	0.98	1.09	1.65	1.7	3.2	4.6	4.8	9.7	18.3
V7	0.96	1.08	1.60	2.1	3.1	4.6	4.9	9.7	17.7
V8	0.96	1.09	1.64	2.2	3.0	4.4	4.8	7.2	16.3
V9	0.98	1.08	1.55	2.1	3.0	4.5	4.9	9.3	18.1
V10	1.10	1.20	2.13	2.0	3.4	5.0	2.4	10.2	17.5
V11	0.97	1.08	1.61	2.3	3.4	4.7	4.8	10.6	19.1
V12	0.96	1.18	1.65	2.1	3.2	4.6	4.9	10.1	17.5
V13	0.96	1.10	1.66	2.1	3.1	5.0	4.8	9.4	21.2
V14	1.00	1.26	1.68	2.1	2.8	4.8	4.9	6.7	11.8
V15	0.96	1.06	1.64	2.5	3.7	4.6	4.9	11.8	34.5
Range		0.96–2.13			1.7–5.0			2.4–34.5	

Notes. [a] Same as Table 8 but for submodel A. This table corresponds to Figure 13.

123

orbital energy remaining above the 10 Gyr merger time. Ad-

merger rate in galaxy

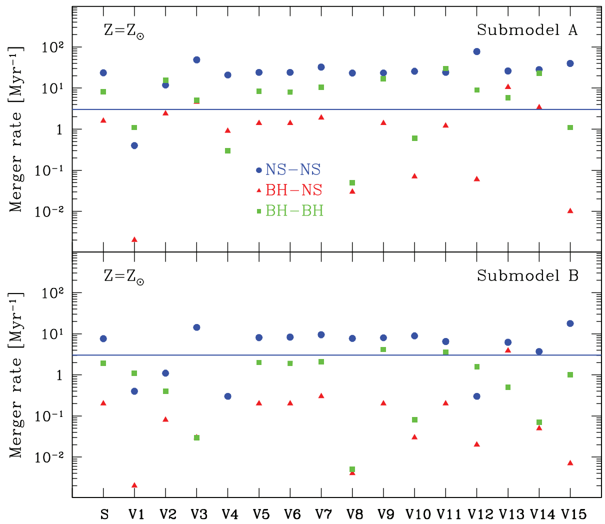

Figure 19. Galactic merger rates from all of our models, with submodel A in the top panel and submodel B in the bottom, for $Z = Z_\odot$. The blue solid line represents the lower limit for predicted merger rates of NS–NS systems observed in our Galaxy (at 3 Myr^{-1}) as shown in Kim et al. (2010). Models yielding merger rates of NS–NS systems lower than this value are disfavored; these are: V1, submodel A; V1, submodel B; V2, submodel B; V4, submodel B; and V12, submodel B. *Reminder:* the models described are: V1–V4, changing λ from 0.01 to 10; V5–V6, changing $M_{\mathrm{NS,max}}$ from 3.0 $M_\odot$ to 2.5 $M_\odot$; V7, reducing natal kicks for all DCOs; V8–V9, full and no natal kicks for BHs, respectively; V10, investigating the Delayed SN engine; V11, reducing wind mass-loss rates by half; V12–V13, investigating fully conservative and non-conservative mass transfer episodes, respectively; V15–V16, boosting and reducing the physical *Nanjing* λ value by a factor of five, respectively.

124

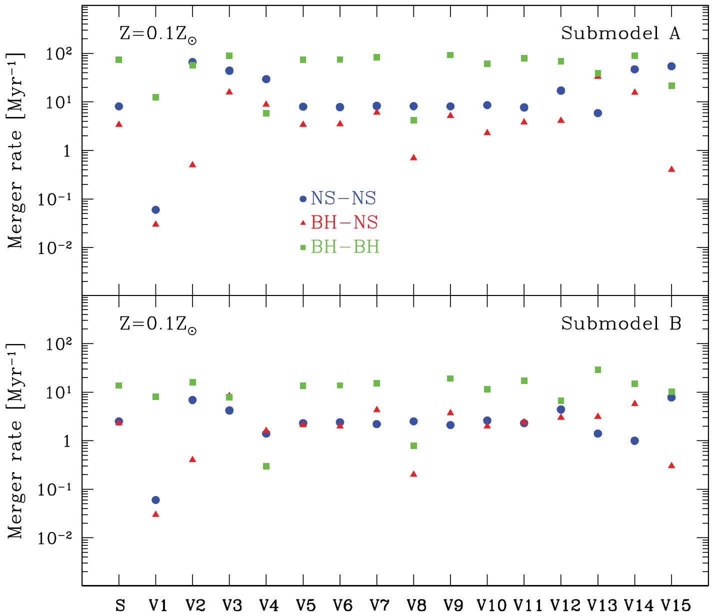

Figure 20. Same as Figure 19 but for $Z = 0.1\ Z_\odot$.

Include the chemical evolution of galaxy

Dominik et al. 2013

$$\mathrm{SFR} = 10^9 a \left(t^b e^{-t/c} + d e^{d(t-t_0)/c}\right) M_\odot\ \mathrm{yr}^{-1}\ \mathrm{Gpc}^{-3}, \quad (1)$$

where t is the age of the universe (Gyr) as measured in the rest frame, t_0 is the present age of the universe (13.47 Gyr; see Section 4), and the parameters have values $a = 0.182$, $b = 1.26$, $c = 1.865$, and $d = 0.071$. The SFR described above is expressed in comoving units of length and time.

$$\Phi(M_{\mathrm{gal,z}}) = \Phi^*(z) \ln(10) a^{1+\alpha(z)} e^{-a}, \quad (2)$$

where $\Phi^*(z) = 0.0035(1+z)^{-2.2}$, $a = M_{\mathrm{gal}} \cdot 10^{-M_z}$ ($M_z = 11.16 + 0.17z - 0.07z^2$), and $\alpha(z) = -1.18 - 0.082z$. A galaxy mass is drawn from this distribution in solar units ($M_\odot$) and in the range $7 < \log(M_{\mathrm{gal}}) < 12$. Beyond redshift $z = 4$, we assume no further evolution in galaxy mass, fixing the mass distribution to the value at $z = 4$. This assumption reflects the

Table 1
Summary of Models[a]

Model	Description
Standard	$\lambda =$ *Nanjing*/physical, BH kicks: decreased, SN: Rapid HG CE donors not allowed
Optimistic CE	HG CE donors allowed
Delayed SN	Delayed supernova engine
High BH Kicks	Full kicks of BHs

2.3. Galaxy Metallicity

We assume the average oxygen-to-hydrogen number ratio ($F_{\mathrm{OH}} = \log(10^{12}\mathrm{O/H})$) in a typical galaxy to be given by

$$\log(F_{\mathrm{OH}}) = s + 1.847 \log(M_{\mathrm{gal}}) - 0.08026(\log(M_{\mathrm{gal}}))^2. \quad (3)$$

As suggested by Erb et al. (2006) and Young & Fryer (2007), the functional form of this mass–metallicity relation is redshift independent, with only the normalization factor s varying with redshift. We describe the redshift dependence of galaxy metallicity using the average metallicity relation from Pei et al. (1999):

$$Z \propto \begin{cases} 10^{-a_2 z} & z < 3.2 \\ 10^{-b_1 - b_2 z} & 3.2 \leqslant z < 5 \\ 10^{-c_1 - c_2 z} & z \geqslant 3.2 \end{cases}, \quad (4)$$

which implies the evolution of s with redshift:

$$s \propto \begin{cases} -a_2 z - 1.492 & z < 3.2 \\ -b_2 z - 3.2(a_2 - b_2) - 1.492 & 3.2 \leqslant z < 5 \\ -c_2 z - 5(b_2 - c_2) - 3.2(a_2 - b_2) - 1.492 & z \geqslant 3.2 \end{cases}. \quad (5)$$

We assume that the oxygen abundance (used in F_{OH}) correlates linearly with the average abundance of elements heavier than helium (encapsulated in the metallicity measure, Z).

In this paper, we employ two distinct scenarios for metallicity evolution with redshift in order to investigate the uncertainties of the chemical evolution of the universe. The construction of these scenarios consists of several steps. (1) We utilize two normalizations of Equation (3). In the first, provided by Pei et al. (1999), the coefficients are $a_2 = 0.5$, $b_1 = 0.8$, $b_2 = 0.25$, $c_1 = 0.2$, and $c_2 = 0.4$. This grants a rate of average metallicity evolution, which we label *slow*. The second, provided by Young & Fryer (2007), uses $a_2 = 0.12$, $b_1 = -0.704$, $b_2 = 0.34$, $c_1 = 0.0$, and $c_2 = 0.1992$. It is based on ultraviolet *Galaxy*

Results of chemical evolution

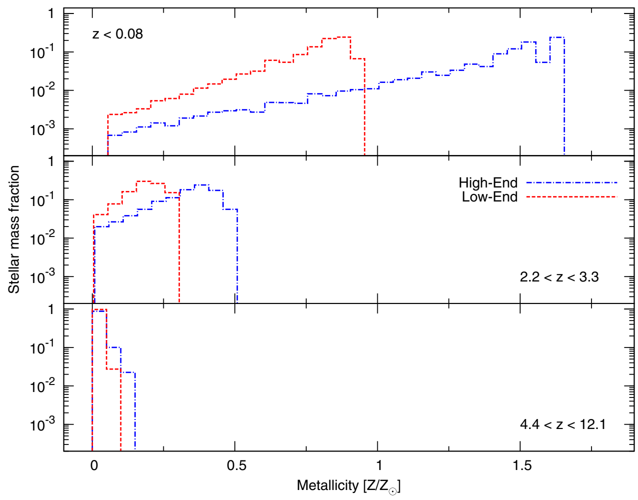

Figure 1. Distribution of metallicity for $z < 0.08$ (local universe), $2.2 < z < 3.3$ (star formation peak), and $4.4 < z < 12.1$ (high-redshift universe). The y-axis shows the fraction of the total stellar mass in the given redshift range. The dashed and dash–dotted lines represent the distributions for the final *low-end* and *high-end* metallicity profiles, respectively. The redshift ranges correspond to a 1 Gyr time bin. Each distribution is normalized to unity within each redshift range. See Section 2.3 for details.

127

Evolution of Merger Rate Density

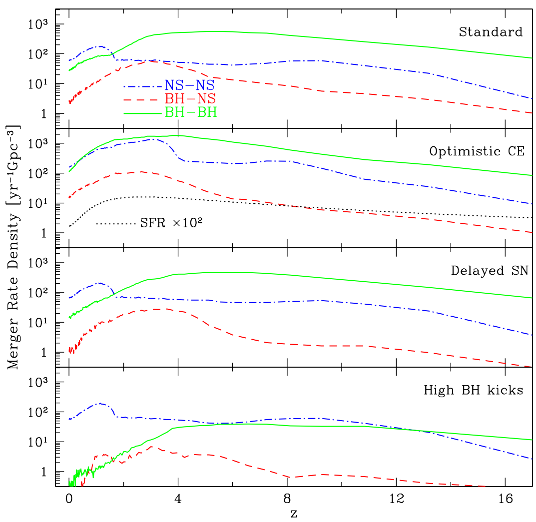

Figure 3. DCO merger rate densities in the rest frame (intrinsic), for *high-end* metallicity. Each panel shows a different model, as listed (for details, see Section 3.2). The dash–dotted, dashed, and solid lines represent NS–NS, BH–NS, and BH–BH systems, respectively. The dotted line in the second panel from the top represents the SFR (see Equation (1)) multiplied by a factor of 100 for clarity; it is in units of $M_{\odot}/100\,\mathrm{Mpc}^{-3}\,\mathrm{yr}^{-1}$. This figure demonstrates: (1) a clear domination of NS–NS systems for the Standard model for $z \lesssim 1.6$, as these systems merge copiously in the relatively metal-rich, local universe, (2) significantly increased merger rates for the Optimistic CE model, where CE events on the HG are allowed, and (3) a drastic drop in rates for the High BH Kicks model.

128

Detection Rate

Dominik et al. 2015 $10^{-4} \leq Z \leq 0.03$

Noise spectrum

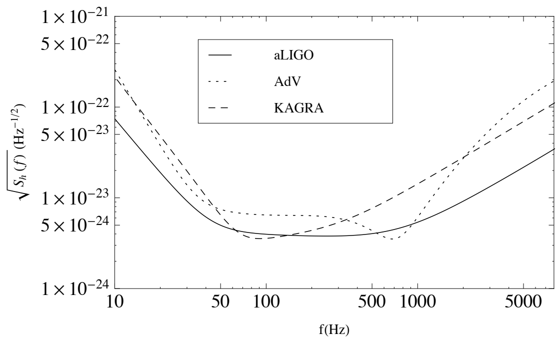

FIG. 1.— **Noise models**: we use an analytical approximation to the aLIGO zero-detuning high power (ZDHP) noise power spectral density given in Eq. (4.7) of Ajith (2011) (we verified that this approximation gives results in excellent agreement with the "official" tabulated aLIGO ZDHP noise PSD given in Shoemaker, D. for the LIGO Scientific Collaboration (2010). For AdV we use the fit in Eq. (3.4) of Ajith & Bose (2009) to Virgo Collaboration (2009), and for KAGRA we use the PSD fit from the Appendix of Pannarale et al. (2013) to Somiya (2012).

129

TABLE 2
DETECTION RATES FOR SECOND-GENERATION DETECTORS IN THE *high-end* METALLICITY SCENARIO

Model	AdV [$\rho \geq 8$] $f_{\rm cut} = 20$ Hz		KAGRA [$\rho \geq 8$] $f_{\rm cut} = 10$ Hz		aLIGO [$\rho \geq 8$] $f_{\rm cut} = 20$ Hz			3-det network [$\rho \geq 10(12)$] $f_{\rm cut} = 20$ Hz	
	Insp $\rm yr^{-1}$	PhC (EOB) $\rm yr^{-1}$	Insp $\rm yr^{-1}$	PhC (EOB) $\rm yr^{-1}$	Insp $\rm yr^{-1}$	PhC (EOB) $\rm yr^{-1}$	PhC (spin) $\rm yr^{-1}$	Insp $\rm yr^{-1}$	PhC $\rm yr^{-1}$
NS-NS									
Standard	0.3	0.3	0.8	0.7	1.2	1.1	-	2.5 (1.5)	2.4 (1.4)
Optimistic CE	0.9	0.9	2.1	1.9	3.3	3.1	-	6.9 (4.0)	6.5 (3.8)
Delayed SN	0.4	0.4	1.0	0.9	1.6	1.5	-	3.3 (1.9)	3.1 (1.8)
High BH Kicks	0.3	0.3	0.7	0.7	1.1	1.1	-	2.3 (1.4)	2.2 (1.3)
BH-NS									
Standard	0.2	0.2	0.5	0.4	0.7	0.6	0.8	1.5 (0.9)	1.2 (0.7)
Optimistic CE	1.1	1.0	2.9	2.2	4.4	3.6	4.4	9.2 (5.4)	7.4 (4.3)
Delayed SN	0.09	0.07	0.2	0.2	0.4	0.3	0.5	0.8 (0.5)	0.6 (0.3)
High BH Kicks	0.01	0.007	0.02	0.02	0.04	0.03	0.1	0.09 (0.05)	0.07 (0.04)
BH-BH									
Standard	35	41 (38)	70	93 (86)	117	148 (142)	348	236 (144)	306 (177)
Optimistic CE	126	144 (133)	281	366 (333)	491	618 (585)	1554	1042 (588)	1338 (713)
Delayed SN	27	34 (32)	50	81 (75)	90	129 (124)	320	182 (110)	270 (155)
High Kick	0.6	1.0 (0.9)	0.9	2.5 (2.3)	2.1	3.8 (3.8)	12	4.2 (2.7)	8.2 (4.7)

[a] Detection rates computed for the high-end metallicity evolution scenario using the inspiral ("Insp") and PhC or EOB IMR models for nonspinning binaries. For aLIGO we also list rough upper limits on the rates computed with the IMR PhC model by assuming that BHs have near-maximal aligned spins ($\chi_1 = \chi_2 = 0.998$ for BH-BH systems; $\chi_1 = 0.998$ and $\chi_2 = 0$ for BH-NS systems). The inspiral is calculated using the restricted PN approximation, which overestimates the amplitude (and therefore the detection rates) for low-mass systems (NS-NS) when compared to the full IMR calculations; cf. Section 3 for details. The last two columns were computed assuming a minimum *network* SNR of 10 (or 12, in parentheses) for a three-detector network composed of three instruments located at the LIGO Hanford, LIGO Livingston, and Virgo sites, all with aLIGO sensitivity. For each detector, $f_{\rm cut}$ is the assumed low-frequency cutoff in the power spectral density: see section 5.2.

Yonetoku et al. 2014
From SGRB rate
If SGRB=NS-NS > 4event/y
If SGRB=NS-BH >150event/y

Kinugawa et al. 2015(PopIII)
PopIII BH-BH
$14.6 - 599.3$ events $\rm yr^{-1}$ $(\mathrm{SFR_p}/(10^{-2.5}\ \mathrm{M_\odot\ yr^{-1}\ Mpc^{-3}}))$

Kim et al. 2015 NS-NS merging rate from NS-NS observation $8^{+10}_{-5}\ \mathrm{yr}^{-1}$ at 95 per cent confidence

130

TABLE 3
DETECTION RATES FOR SECOND-GENERATION DETECTORS IN THE *low-end* METALLICITY SCENARIO

Model	AdV [$\rho \geq 8$] $f_{\rm cut} = 20$ Hz		KAGRA [$\rho \geq 8$] $f_{\rm cut} = 10$ Hz		aLIGO [$\rho \geq 8$] $f_{\rm cut} = 20$ Hz			3-det network [$\rho \geq 10(12)$] $f_{\rm cut} = 20$ Hz	
	Insp yr^{-1}	PhC (EOB) yr^{-1}	Insp yr^{-1}	PhC (EOB) yr^{-1}	Insp yr^{-1}	PhC (EOB) yr^{-1}	PhC (spin) yr^{-1}	Insp yr^{-1}	PhC yr^{-1}
NS-NS									
Standard	0.3	0.3	0.7	0.6	1.1	1.0	-	2.3 (1.3)	2.2 (1.3)
Optimistic CE	0.8	0.7	1.8	1.7	2.9	2.7	-	6.0 (3.5)	5.6 (3.3)
Delayed SN	0.4	0.4	1.0	0.9	1.5	1.4	-	3.2 (1.8)	2.9 (1.7)
High BH Kicks	0.3	0.3	0.7	0.6	1.0	1.0	-	2.1 (1.3)	2.0 (1.2)
BH-NS									
Standard	0.3	0.2	0.7	0.5	1.1	0.8	1.2	2.3 (1.3)	1.8 (1.0)
Optimistic CE	1.4	1.2	3.6	2.8	5.5	4.4	5.7	12 (6.7)	9.4 (5.4)
Delayed SN	0.2	0.1	0.5	0.4	0.8	0.6	0.9	1.7 (0.9)	1.3 (0.7)
High BH Kicks	0.04	0.03	0.09	0.07	0.1	0.1	0.3	0.6 (0.2)	0.5 (0.2)
BH-BH									
Standard	56	66 (61)	106	153 (140)	183	246 (235)	610	369 (226)	514 (292)
Optimistic CE	287	324 (297)	629	828 (745)	1124	1421 (1339)	3560	2384 (1336)	3087 (1633)
Delayed SN	53	64 (59)	97	152 (139)	171	241 (231)	596	345 (213)	501 (291)
High Kick	0.9	1.5 (1.4)	1.4	3.8 (3.6)	3.2	5.9 (5.8)	19	6.6 (4.0)	13 (7.2)

[a] Same as Table 2, but for the *low-end* metallicity scenario.

TABLE 1
LOCAL MERGER RATES AND SIMPLY-SCALED DETECTION RATE PREDICTIONS[a]:

Model	$\left\langle \mathcal{M}_c{}^{15/6} \right\rangle$ $M_\odot^{15/6}$	$\mathcal{R}(0)$ $\mathrm{Gpc}^{-3}\,\mathrm{yr}^{-1}$	R_D (aLIGO $\rho \geq 8$) yr^{-1}	R_D (3-det network $\rho \geq 10$) yr^{-1}
NS-NS				
Standard	1.1 (1.1)	61 (52)	1.3 (1.1)	3.2 (2.7)
Optimistic CE	1.2 (1.2)	162 (137)	3.9 (3.3)	9.2 (7.7)
Delayed SN	1.4 (1.4)	67 (60)	1.9 (1.7)	4.5 (4.0)
High BH Kicks	1.1 (1.1)	57 (52)	1.2 (1.1)	3.0 (2.7)
BH-NS				
Standard	18 (19)	2.8 (3.0)	1.0 (1.2)	2.4 (2.7)
Optimistic CE	17 (16)	17 (20)	5.7 (6.5)	13.8 (15.4)
Delayed SN	24 (20)	1.0 (2.4)	0.5 (0.9)	1.1 (2.3)
High BH Kicks	19 (13)	0.04 (0.3)	0.01 (0.08)	0.04 (0.2)
BH-BH				
Standard	402 (595)	28 (36)	227 (427)	540 (1017)
Optimistic CE	311 (359)	109 (221)	676 (1585)	1610 (3773)
Delayed SN	829 (814)	14 (24)	232 (394)	552 (938)
High Kick	2159 (3413)	0.5 (0.5)	22 (34)	51 (81)

[a] Detection rates computed using the basic scaling of Eq. (3) for both the *high-end* and *low-end* (the latter in parentheses) metallicity scenarios (see Section 2.2). These rates should be compared with those from more careful calculations presented in Tables 2 and 3.

Yonetoku et al. 2014
From SGRB Rate
$R(0) >$
$115\mathrm{Gpc}^{-3}\mathrm{y}^{-1}$

Section 3: Speed of GW is c ?

Finn&Romano 2013

They apply the method of Olaus Romer in 1676
to determine the velocity of light.

Occultation time of Io by Jupiter depends on the time of the light to
pass the earth orbit around the sun. This is about 1000s。

They adopted GW from the white dwarf binary or
non-axisymmetric pulsar

The detectors are LISA,LIGO, Virgo, KAGRA and possibly DECIGO.

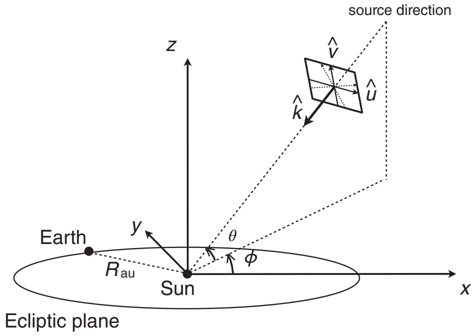

FIG. 1. The relevant geometric quantities used in the calculation: $\hat{k}$ is the unit vector pointing in the direction of wave propagation; θ is the ecliptic latitude (i.e., the angle that $-\hat{k}$ makes with the plane of the ecliptic); ϕ is the azimuthal angle of the source with respect to the Earth's orbital position at $t = 0$. The detector antenna pattern functions F_+ and $F_\times$ from Eq. (2) are defined with respect to the polarization tensors constructed from $\hat{u}$ and $\hat{v}$, which are proportional to the unit vectors $\hat{\phi}$ and $\hat{\theta}$, respectively.

Defining $\delta c = c - v_g$

100Hz Pulsar SNR=10

$\delta c/c = 10^{-6}$

LISA 10mHz SNR=100

$\delta c/c = 10^{-3}$

Nishizawa & Nakamura 2014

If we add the astronomical information

$\delta c/c = \delta_g$ should be restricted more:

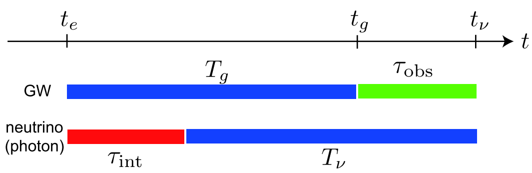

FIG. 1 (color online). GW and neutrino (photon) propagation times. GW is emitted at the time $t = t_e$ and detected on the Earth at $t = t_g$. For instance, we refer the merger time of a NS binary or the core bounce time of a core-collapsed SN to the emission time of a GW, while a neutrino (photon) is emitted at $t = t_e + \tau_{\rm int}$ and detected at $t = t_\nu$. The observable is the difference of the arrival times between the GW and neutrinos(photons), $\tau_{\rm obs}$.

$$T_g \equiv L/v_g \text{ and } T_\nu \equiv L/v_\nu.$$

ν is either photon or neutrino

$$\Delta T \equiv T_\nu - T_g.$$

$$\tau_{\rm obs} = \Delta T + \tau_{\rm int}$$

If velocity of GW is not c.

$$\Delta T + \tau_{\rm int,max} < \tau_{\rm int,min} \quad \text{for } \Delta T < 0,$$

$$\tau_{\rm int,max} < \Delta T + \tau_{\rm int,min} \quad \text{for } \Delta T > 0,$$

$$\Delta\tau_{\rm int} < |\Delta T|.$$

$$\delta_g \equiv (c - v_g)/c \text{ and } \delta_\nu \equiv (c - v_\nu)/c.$$

$$\frac{\Delta T}{T_0} \approx \delta_\nu - \delta_g.$$

where $T_0 = L/c$

$\Delta\tau_{\rm int} \equiv \tau_{\rm int,max} - \tau_{\rm int,min}$. from theoretical prediction

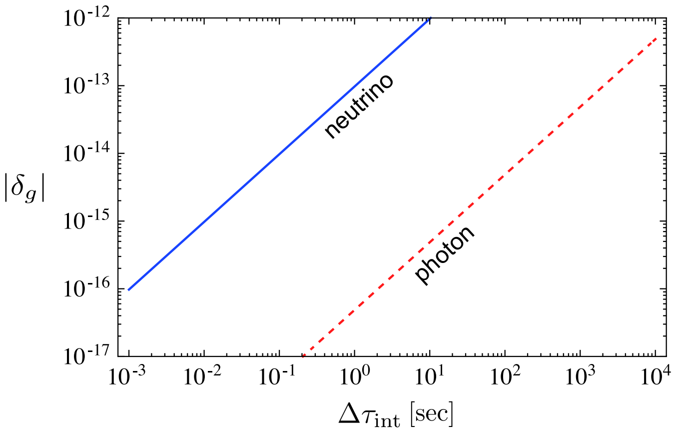

$$\Delta\tau_{\rm int} < T_0|\delta_\nu - \delta_g|,$$

$$\delta_\nu = \frac{m_\nu^2 c^4}{2E_\nu^2}.$$

For photon δ_ν=0

FIG. 4 (color online). Constraint on the propagation speed of a GW as a function of intrinsic time delay from multimessenger observations of a GW and SN neutrinos (blue, solid) or SGRB photons (red, dashed). For SN, the neutrino energy is 10 MeV, and the distance to the source is 100 kpc. For SGRB, the distance to the source is 200 Mpc.

Null result means

observations, we have the constraint on δ_g for an SN event at $L = 100$ kpc,

$$|\delta_g| < 9.7 \times 10^{-16}. \qquad (11)$$

As for a SGRB, typical time lag is $\Delta\tau_{\rm int} = 10$ sec, and conservative time lag is $\Delta\tau_{\rm int} = 500$ sec. If the finite deviation of δ_g is not found in the GW-photon observations of a SGRB at $L = 200$ Mpc, we would obtain the constraint on δ_g:

$$|\delta_g| < 2.4 \times 10^{-14} \quad \text{for } \Delta\tau_{\rm int} = 500 \text{ sec}, \qquad (12)$$

$$|\delta_g| < 4.9 \times 10^{-16} \quad \text{for } \Delta\tau_{\rm int} = 10 \text{ sec}. \qquad (13)$$

If the velocity of GW is not the light velocity , what is the explanation？

- Mass of graviton？

It was theoretically impossible for graviton to have mass before 2011.

- Let us consider scalar field φ's mass term like $-1/2m^2\varphi^2$
- In gravity $g_{\mu\nu}$ is the variable so that the covariant mass term should be $-1/2m^2 g_{\mu\nu}g^{\mu\nu}=-2m^2=$constant, which is meaningless.
- Fierz & Pauli in 1939 considered the non-covariant case.
- $g_{\mu\nu}=\eta_{\mu\nu}+h_{\mu\nu}$ and if the mass terms is $m^2(h_{\mu\nu}h^{\mu\nu}-h^2)$, no ghost, which has negative energy state, exists.
- However Boulware & Deser 1972 showed that in non-linear regimes the ghost exists.

Based on dRGT theory (2011), Hassan & Rosen(2012) showed that no ghost massive gravity theory is possible as follows;

Hassen & Rosen 2012

$$ds^2 = g_{\mu\nu}dx^\mu dx^\nu, \quad \text{This world metric}$$
$$d\tilde{s}^2 = \tilde{g}_{\mu\nu}dx^\mu dx^\nu \quad \text{Heaven's metric}$$

$$S = \int d^4x\{\sqrt{-g}(M_{pl}^2(R-2m_g^2V)+L_{matt})+\kappa M_{pl}^2\sqrt{-\tilde{g}}\tilde{R}\},$$
$$M_{pl}^2 = \frac{1}{16\pi G},$$
$$V = \sum_{n=0}^{4} a_n V_n(Y_\nu^\mu),$$
$$Y_\alpha^\mu Y_\nu^\alpha = g^{\mu\alpha}\tilde{g}_{\alpha\nu},$$

To guarantee the equivalence principle, the matter in this world can interact only with this world metric but not with heaven's metric.

Let $\lambda_1, \lambda_2, \lambda_3, \lambda_4$ be 4 eigen values of Y_ν^μ, we have

$$V_0 = 1,$$
$$V_1 = \lambda_1+\lambda_2+\lambda_3+\lambda_4,$$
$$V_2 = 2(\lambda_1\lambda_2+\lambda_1\lambda_3+\lambda_1\lambda_4+\lambda_2\lambda_3+\lambda_2\lambda_4+\lambda_3\lambda_4),$$
$$V_3 = 6(\lambda_1\lambda_2\lambda_3+\lambda_1\lambda_2\lambda_4+\lambda_1\lambda_3\lambda_4+\lambda_2\lambda_3\lambda_4),$$
$$V_4 = 24(\lambda_1\lambda_2\lambda_3\lambda_4) = 24\frac{\sqrt{-\tilde{g}}}{\sqrt{-g}}.$$

$$[Y^n] = tr(Y^n) = Y_{\alpha_1}^{\alpha_0}Y_{\alpha_2}^{\alpha_1}..........Y_{\alpha_0}^{\alpha_{n-1}},$$

$$V_0 = 1,$$
$$V_1 = [Y],$$
$$V_2 = [Y]^2-[Y^2],$$
$$V_3 = [Y]^3-3[Y][Y^2]+2[Y^3],$$
$$V_4 = [Y]^4-6[Y]^2[Y^2]+8[Y][Y^3]+3[Y^2]^2-6[Y^4].$$

We have Einstein equations of this world and heaven as

$$R_{\mu\nu}-\frac{1}{2}g_{\mu\nu}R+B_{\mu\nu} = 8\pi G T_{\mu\nu},$$
$$\kappa\{\tilde{R}_{\mu\nu}-\frac{1}{2}\tilde{g}_{\mu\nu}\tilde{R}\}+\tilde{B}_{\mu\nu} = 0,$$

Energy momentum tensor exist only in this world to guarantee the equivalence Principle.

$$B_{\mu\nu} = m_g^2\Big[a_0 g_{\mu\nu}+a_1\{g_{\mu\nu}[Y]-\frac{1}{2}(g_{\mu\alpha}Y_\nu^\alpha+g_{\nu\alpha}Y_\mu^\alpha)\}+a_2\{g_{\mu\nu}([Y]^2-[Y^2])-[Y](g_{\mu\alpha}Y_\nu^\alpha+g_{\nu\alpha}Y_\mu^\alpha)+2\tilde{g}_{\mu\nu}\}$$
$$+a_3\{g_{\mu\nu}([Y]^3-3[Y][Y^2]+2[Y^3])-\frac{3}{2}([Y]^2-[Y^2])(g_{\mu\alpha}Y_\nu^\alpha+g_{\nu\alpha}Y_\mu^\alpha)+6[Y]\tilde{g}_{\mu\nu}-3(\tilde{g}_{\mu\alpha}Y_\nu^\alpha+\tilde{g}_{\nu\alpha}Y_\mu^\alpha)\}\Big], \quad ($$

$$\tilde{B}_{\mu\nu} = m_g^2\frac{\sqrt{-g}}{\sqrt{-\tilde{g}}}\Big[\frac{a_1}{2}(\tilde{g}_{\mu\alpha}Y_\nu^\alpha+\tilde{g}_{\nu\alpha}Y_\mu^\alpha)+a_2\{[Y](\tilde{g}_{\mu\alpha}Y_\nu^\alpha+\tilde{g}_{\nu\alpha}Y_\mu^\alpha)-(\tilde{g}_{\mu\alpha}Y_\beta^\alpha Y_\nu^\beta+\tilde{g}_{\nu\alpha}Y_\beta^\alpha Y_\mu^\beta)\}$$
$$+a_3\{\frac{3}{2}([Y]^2-[Y^2])(\tilde{g}_{\mu\alpha}Y_\nu^\alpha+\tilde{g}_{\nu\alpha}Y_\mu^\alpha)-3[Y](\tilde{g}_{\mu\alpha}Y_\beta^\alpha Y_\nu^\beta+\tilde{g}_{\nu\alpha}Y_\beta^\alpha Y_\mu^\beta)+3(\tilde{g}_{\mu\alpha}Y_\beta^\alpha Y_\gamma^\beta Y_\nu^\gamma+\tilde{g}_{\nu\alpha}Y_\beta^\alpha Y_\gamma^\beta Y_\mu^\gamma)\}\Big]$$
$$+24m^2\tilde{g}_{\mu\nu}a_4 \quad ($$

$$\nabla_\mu B^\mu_\nu = 0, \qquad \Theta_{\mu\nu} = -\frac{1}{8\pi G} B_{\mu\nu},$$
$$\nabla_\mu T^\mu_\nu = 0,$$
$$\tilde{\nabla}_\mu \tilde{B}^\mu_\nu = 0, \qquad \tilde{\Theta}_{\mu\nu} = -\frac{1}{\kappa 8\pi G}\tilde{B}_{\mu\nu}$$

$$R_{\mu\nu} - \frac{1}{2} g_{\mu\nu} R = 8\pi G (T_{\mu\nu} + \Theta_{\mu\nu}),$$
$$\tilde{R}_{\mu\nu} - \frac{1}{2}\tilde{g}_{\mu\nu}\tilde{R} = 8\pi G \tilde{\Theta}_{\mu\nu}.$$

De-Felice, Tanaka & Nakamura 2014

They considered the propagation of gravitational wave in bi-gravity theory where κ is the ratio of the gravitational constants between the heaven and this world.
First they solve the background cosmological model as

$$ds^2 = a^2(-dt^2 + d\boldsymbol{x}^2), \quad d\tilde{s}^2 = \tilde{a}^2(-\tilde{c}^2 dt^2 + d\boldsymbol{x}^2)$$

$$3H^2 = \frac{\rho_\mathrm{m} + \rho_V}{M_\mathrm{G}^2} \qquad M_\mathrm{G}^2 = 1/(8\pi G_N)$$

$$\rho_V(\xi) \equiv M_\mathrm{G}^2 m^2 (c_0 + 3\xi c_1 + 6\xi^2 c_2 + 6\xi^3 c_3) \qquad \xi \equiv \tilde{a}/a$$

$$\frac{3}{\tilde{c}^2 a^2}\left(\frac{\dot{\tilde{a}}}{\tilde{a}}\right)^2 = \frac{m^2}{\kappa}\left(\frac{c_1}{\xi} + 6c_2 + 18\xi c_3 + 24\xi^2 c_4\right). \quad (3)$$ Heaven's Universe

From $\nabla_\mu B^\mu_\nu = 0$, We have $3\Gamma(\xi)[\tilde{c}aH - (\dot{\tilde{a}}/\tilde{a})] = 0$

We adopt $[\tilde{c}aH - (\dot{\tilde{a}}/\tilde{a})] = 0$ $\quad \Gamma(\xi) \equiv c_1\xi + 4c_2\xi^2 + 6c_3\xi^3$

Combining this condition with Eqs. (2) and (3)

We have
$$\frac{\rho_\mathrm{m}}{M_\mathrm{G}^2 m^2} = \left[\frac{c_1}{\kappa\xi} + \left(\frac{6c_2}{\kappa} - c_0\right) + \left(\frac{18c_3}{\kappa} - 3c_1\right)\xi + \left(\frac{24c_4}{\kappa} - 6c_2\right)\xi^2 - 6c_3\xi^3\right]. \quad (4)$$

If $m^2 \gg \rho_\mathrm{m}/M_\mathrm{G}^2$, the r.h.s. of Eq. (4) should be very small.

Denoting a value of ξ at which the right- hand side vanishes by ξ_c

After some algebra, we have $\tilde{c} \approx 1 + \dfrac{\kappa\xi_c^2(\rho_\mathrm{m} + P_\mathrm{m})}{\Gamma_c m^2 \tilde{M}_\mathrm{G}^2}$

Let us consider the propagation of gravitational wave in
this back ground. As this world metric interact with Heaven's metric
the propagation gw is this world is different from the usual case as
Omitting +, x mode sign,

$$\ddot{h} - \triangle h + m^2\Gamma_c(h - \tilde{h}) = 0,$$

$$\ddot{\tilde{h}} - \tilde{c}^2\triangle\tilde{h} + \frac{m^2\Gamma_c}{\kappa\xi_c^2}(\tilde{h} - h) = 0$$

Assuming $\tilde{c} - 1 \ll 1$ and defining

$$x \equiv \frac{2(2\pi f)^2(\tilde{c} - 1)}{\mu^2} \qquad \mu^2 \equiv \lambda_\mu^{-2} = \frac{(1+\kappa\xi_c^2)\Gamma_c m^2}{\kappa\xi_c^2}$$

Where F is the frequency of GW.

for a given gravitational wave frequency f, two eigen wave numbers are given by

$$k_{1,2}^2 = (2\pi f)^2 - \frac{\mu^2}{2}\left(1 + x \mp \sqrt{1 + 2x\frac{1-\kappa\xi_c^2}{1+\kappa\xi_c^2} + x^2}\right),$$

$$h_1 = \cos\theta_g h + \sin\theta_g\sqrt{\kappa}\xi_c\tilde{h}, \qquad \theta_g = \frac{1}{2}\cot^{-1}\left(\frac{1+\kappa\xi_c^2}{2\sqrt{\kappa}\xi_c}x + \frac{1-\kappa\xi_c^2}{2\sqrt{\kappa}\xi_c}\right)$$

$$h_2 = -\sin\theta_g h + \cos\theta_g\sqrt{\kappa}\xi_c\tilde{h},$$

In the limit of $x \to 0$ h_1 is massless and h_2 is massive

phase shifts after the propagation distance of D are given by

$$\delta\Phi_{1,2} = -\frac{\mu D\sqrt{\tilde{c}-1}}{2\sqrt{2x}}\left(1 + x \mp \sqrt{1 + x^2 + 2x\frac{1-\kappa\xi^2}{1+\kappa\xi^2}}\right)$$

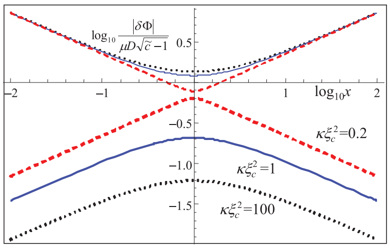

Fig. 1. $|\delta\Phi_{1,2}|$ as a function of x for $\kappa\xi_c^2 = 0.2$ (dotted, black), 1 (blue), and 100 (dashed, red). Thick and thin curves represent $|\delta\Phi_1|$ and $|\delta\Phi_2|$, respectively.

We can measure only h in this world.

However h_1 and h_2 propagate with different velocity.

$$h(f) = A(f)e^{i\Phi(f)}\left[B_1 e^{i\delta\Phi_1(f)} + B_2 e^{i\delta\Phi_2(f)}\right], \tag{10}$$

where the amplitude $A(f)$ (after angular average), $B_{1,2}$, and the phase function $\Phi(f, g)$ (truncated at 1.5PN order) are given by

$$A(f) = \sqrt{\frac{5\pi}{24}}\frac{\mathcal{M}^2}{(8\pi M_G^2)^2 D}y^{-7/6},$$
$$B_1 = \cos\theta_g(\cos\theta_g + \sqrt{\kappa}\xi_c\sin\theta_g),$$
$$B_2 = \sin\theta_g(\sin\theta_g - \sqrt{\kappa}\xi_c\cos\theta_g),$$
$$\Phi(f) \equiv 2\pi f t_c - \Phi_c - \pi/4 + \frac{3}{128}y^{-5/3} + \frac{5}{96}\left(\frac{743}{336} + \frac{11}{4}\eta\right)\eta^{-2/5}y^{-1} - \frac{3\pi}{8}\eta^{-3/5}y^{-2/3},$$

with $y \equiv \mathcal{M}f/(8\tilde{M}_G^2)$, the chirp mass $\mathcal{M} \equiv (m_1 m_2)^{3/5}/(m_1+m_2)^{1/5}$, and the reduced mass ratio $\eta = m_1 m_2/(m_1+m_2)^2$. The first and second terms in Eq. (10) show the contributions of h_1 and h_2, respectively. Here we plot $B_{1,2}$ in Fig. 2 for $\kappa\xi_c^2 = 0.2$, 1, and 100.

Arrival time of chirp signal

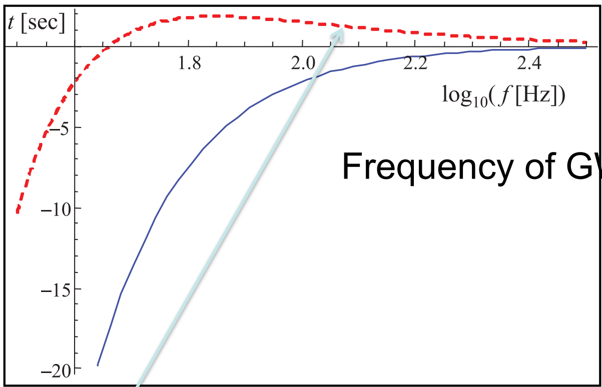

Fig. 3. The arrival time as a function of the frequency f for respective modes of a $1.4\,M_\odot + 1.4\,M_\odot$ binary inspiral with $\kappa\xi_c^2 = 100$, $D = 300$ Mpc, $H = 67.3$ km s^{-1} Mpc^{-1}, $\Omega_0 = 0.315$, and $\lambda_\mu = 0.001$ pc. The blue solid curve is for the first mode, while the dashed red one is for the second mode.

Wave with high frequency arrives earlier->Inverse chirp signal.

Usually low frequency GW is emitted earlier so that it arrives Earlier but not in this case.

GW
$$(-\omega^2 + k^2 + m_g{}^2)h^{TT} - m_g{}^2\tilde{h}^{TT} = 0,$$
$$-\tilde{m}_g^2 h^{TT} + (-\omega^2 + \tilde{c}^2k^2 + \tilde{m}_g^2)\tilde{h}^{TT} = 0,$$

1. one is massless ,the other is massive in the limit of vacuum.
2. flavor eigen state is different from mass eigen state where flavor means “This world” or “Heaven”
3. Just like neutrino oscillation, graviton oscillation is expected so that the group velocity of massive one is smaller than the light velocity.

In extreme case
Inverse Chirp

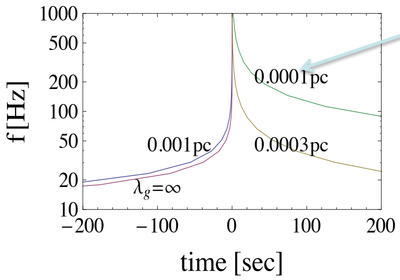

Compton length Of massive graviton.

Seto 2014

FIG. 1: The observed “chirp” signals for a NS-NS binary at $D = 300$Mpc. The curve with the label $\lambda_g = \infty$ shows the massless mode (identical to GR). The other three curves are given for finite Compton lengths.

What is the heaven’s metric $\tilde{g}_{\mu\nu}$???

Yamashita & Tanaka 2014 suggest each metric corresponds to that in different brane.

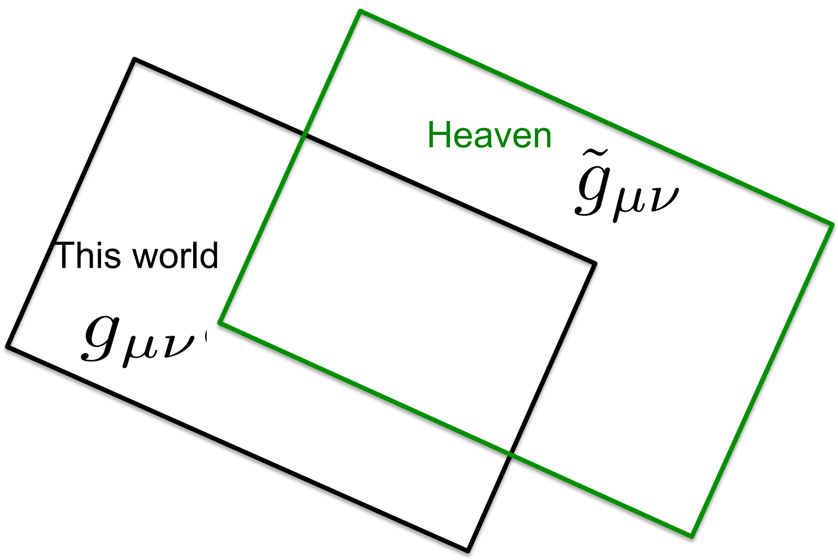

Why not massive graviton!!

- Let us count the number of bosons which are responsible for four forces
- Electro magnetic forces

  4: photon、Z、W^+、W^-

- QCD

  8 glueones

- Why not more than one graviton for gravitational force?

Section 4: My last night dream of press conference

"In the press conference , LIGO team is presenting that we discovered the gravitational wave signals from the coalescence of 30 Msun-30Msun black hole binary which could be remnants of the first stars in our universe. However quasi normal mode is completely different from the prediction based on Einstein theory. We must seek the true theory of gravity in the strong gravity region."

I hope
that this does not remain for ever as a scientific fiction.

Section 5: What is next for me ?

- I am now PI of DECIGO(DECi herz Gravitational wave Observatory) group. v～0.1Hz GW
- The title of the adopted project A of JSPS(Japan Society for the Promotion of Science) is
- " Completion of Test Model of DECIGO on the earth." from 2015.4-2020.3 with 3.2×10^7yen.
- We will perform zero-gravity experiments

20 times using freely falling air plane with the help of Mitsubishi company.

DECIGO（DECi hertz Interferometer Gravitational wave Observatory）

This was proposed by Seto, Kawamura & Nakamura in 2001.
DECIGO means also "Decide and Go".

VOLUME 87, NUMBER 22 PHYSICAL REVIEW LETTERS 26 NOVEMBER 2001

Possibility of Direct Measurement of the Acceleration of the Universe Using 0.1 Hz Band Laser Interferometer Gravitational Wave Antenna in Space

Naoki Seto,[1] Seiji Kawamura,[2] and Takashi Nakamura[3]
[1]*Department of Earth and Space Science, Osaka University, Toyonaka 560-0043, Japan*
[2]*National Astronomical Observatory, Mitaka 181-8588, Japan*
[3]*Yukawa Institute for Theoretical Physics, Kyoto University, Kyoto 606-8502, Japan*
(Received 4 June 2001; published 9 November 2001)

It may be possible to construct a laser interferometer gravitational wave antenna in space with $h_{\rm rms} \sim 10^{-27}$ at $f \sim 0.1$ Hz in this century. Using this antenna, (1) typically 10^5 chirp signals of coalescing binary neutron stars per year may be detected with $S/N \sim 10^4$; (2) we can directly measure the acceleration of the universe by a 10 yr observation of binary neutron stars; and (3) the stochastic gravitational waves of $\Omega_{\rm GW} \gtrsim 10^{-20}$ predicted by the inflation may be detected by correlation analysis. Our formula for phase shift due to accelerating motion might be applied for binary sources of LISA.

Targets of DECIGO

1) $\sim 10^5$ NS-NS binary up to z=1

2) Prediction of the merging position
A few arc minutes and 0.1s in time
about a week before the merger.
This situation looks like a solar eclipse.

3) Direct measurement of the acceleration of the universe to clarify dark energy.

4) Inflation origin GW at $\sim$0.1Hz up to $\Omega_{GW}=10^{-20}$

5) Intermediate Mass BH

6) EMRI

7) Mass spectrum of NS &BH

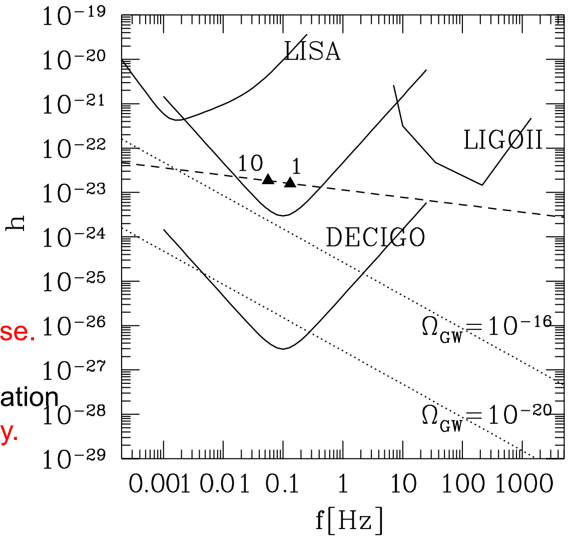

FIG. 1. Sensitivity (effectively S/N = 1) for various detectors (LISA, DECIGO, LIGOII, and a detector 10^3 times less sensitive than DECIGO) in the form of $h_{\rm rms}$ (solid lines). The dashed line represents evolution of the characteristic amplitude h_c for NS-NS binary at $z = 1$ (filled triangles: wave frequencies at 1 and 10 yr before coalescence). The dotted lines represent the required sensitivity for detecting stochastic background with $\Omega_{\rm GW} = 10^{-16}$ and $\Omega_{\rm GW} = 10^{-20}$ by 10 yr correlation analysis (S/N = 1).

DECIGO Members

DECIGO

Masaki Ando, Seiji Kawamura, Naoki Seto, Takashi Nakamura, Kimio Tsubono, Shuichi Sato, Takahiro Tanaka, Ikkoh Funaki, Kenji Numata, Nobuyuki Kanda, Kunihito Ioka, Takeshi Takashima, Jun'ichi Yokoyama, Tomotada Akutsu, Mitsuru Musha, Akitoshi Ueda, Koh-suke Aoyanagi, Kazuhiro Agatsuma, Hideki Asada, Yoichi Aso, Koji Arai, Akito Araya, Takeshi Ikegami, Takehiko Ishikawa, Hideharu Ishizaki, Hideki Ishihara, Kiwamu Izumi, Kiyotomo Ichiki, Hiroyuki Ito, Yousuke Itoh, Kaiki T. Inoue, Ken-ichi Ueda, Takafumi Ushiba, Masayoshi Utashima, Satoshi Eguchi, Yumiko Ejiri, Motohiro Enoki, Toshikazu Ebisuzaki, Yoshiharu Eriguchi, Naoko Ohishi, Masashi Ohkawa, Masatake Ohashi, Kenichi Oohara, Yoshiyuki Obuchi, Kenshi Okada, Norio Okada, Koki Okutomi, Nobuki Kawashima, Fumiko Kawazoe, Isao Kawano, Kenta Kiuchi, Naoko Kishimoto, Hitoshi Kuninaka, Hiroo Kunimori, Kazuaki Kuroda, Sachiko Kuroyanagi, Hiroyuki Koizumi, Feng-Lei Hong, Kazunori Kohri, Wataru Kokuyama, Keiko Kokeyama, Yoshihide Kozai, Yasufumi Kojima, Kei Kotake, Shiho Kobayashi, Rina Gondo, Motoyuki Saijo, Ryo Saito, Shin-ichiro Sakai, Masaaki Sakagami, Shihori Sakata, Norichika Sago, Misao Sasaki, Takashi Sato, Masaru Shibata, Kazunori Shibata, Ayaka Shoda, Hisaaki Shinkai, Aru Suemasa, Naoshi Sugiyama, Rieko Suzuki, Yudai Suwa, Kentaro Somiya, Hajime Sotani, Tadashi Takano, Kakeru Takahashi, Keitaro Takahashi, Hirotaka Takahashi, Fuminobu Takahashi, Ryuichi Takahashi, Ryutaro Takahashi, Takamori Akiteru, Hideyuki Tagoshi, Hiroyuki Tashiro, Nobuyuki Tanaka, Keisuke Taniguchi, Atsushi Taruya, Takeshi Chiba, Dan Chen, Shinji Tsujikawa, Yoshiki Tsunesada, Morio Toyoshima, Yasuo Torii, Kenichi Nakao, Kazuhiro Nakazawa, Shinichi Nakasuka, Hiroyuki Nakano, Shigeo Nagano, Kouji Nakamura, Yoshinori Nakayama, Atsushi Nishizawa, Erina Nishida, Yoshito Niwa, Taiga Noumi, Tatsuaki Hashimoto, Kazuhiro Hayama, Tomohiro Harada, Wataru Hikida, Yoshiaki Himemoto, Hisashi Hirabayashi, Takashi Hiramatsu, Mitsuhiro Fukushima, Ryuichi Fujita, Masa-Katsu Fujimoto, Toshifumi Futamase, Mizuhiko Hosokawa, Hideyuki Horisawa, Kei-ichi Maeda, Hideo Matsuhara, Nobuyuki Matsumoto, Yuta Michimura, Osamu Miyakawa, Umpei Miyamoto, Shinji Miyoki, Shinji Mukohyama, Toshiyuki Morisawa, Mutsuko Y. Morimoto, Shigenori Moriwaki, Kent Yagi, Hiroshi Yamakawa, Toshitaka Yamazaki, Kazuhiro Yamamoto, Shijun Yoshida, Taizoh Yoshino, Chul-Moon Yoo, Yaka Wakabayashi

(On June 18th, 2015)

GWPAW2015 (June 19th, 2015, INTEX-Osaka, Osaka) by Ando

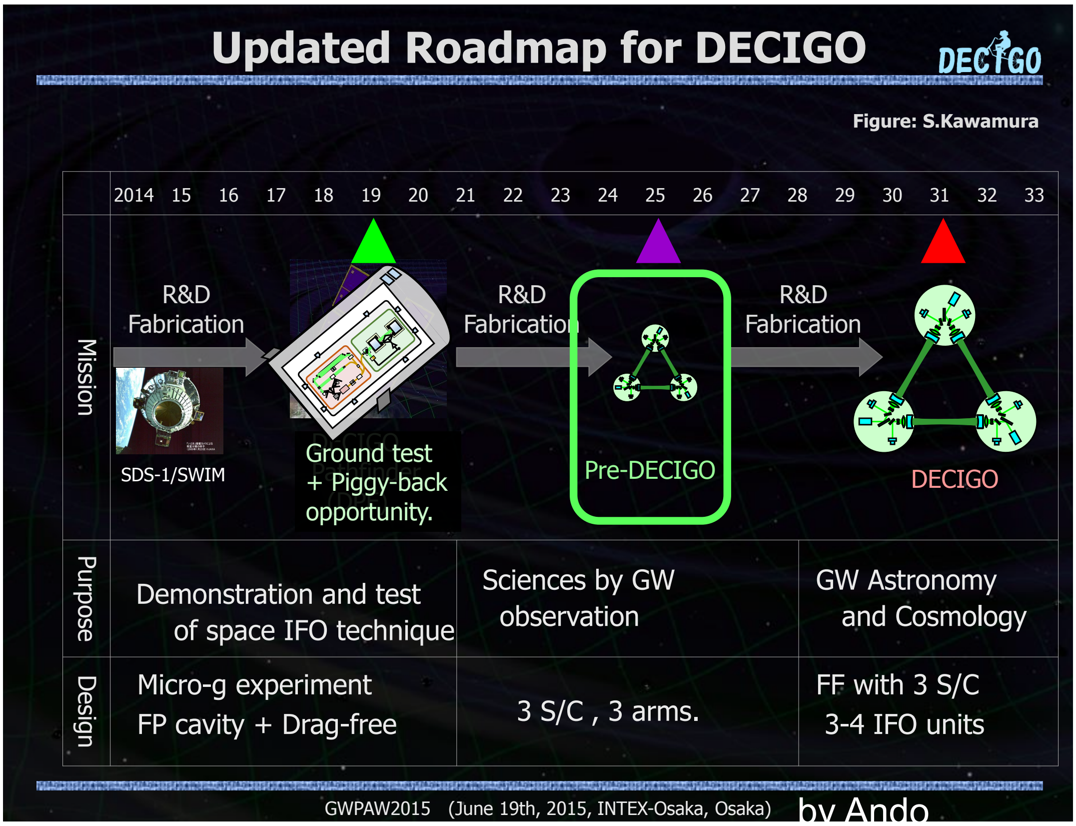
Updated Roadmap for DECIGO
DECIGO
Figure: S.Kawamura
2014 15 16 17 18 19 20 21 22 23 24 25 26 27 28 29 30 31 32 33
Mission
R&D
Fabrication
SDS-1/SWIM
Ground test
+ Piggy-back
opportunity.
R&D
Fabrication
Pre-DECIGO
R&D
Fabrication
DECIGO
Purpose
Demonstration and test
of space IFO technique
Sciences by GW
observation
GW Astronomy
and Cosmology
Design
Micro-g experiment
FP cavity + Drag-free
3 S/C , 3 arms.
FF with 3 S/C
3-4 IFO units
GWPAW2015 (June 19th, 2015, INTEX-Osaka, Osaka)
by Ando

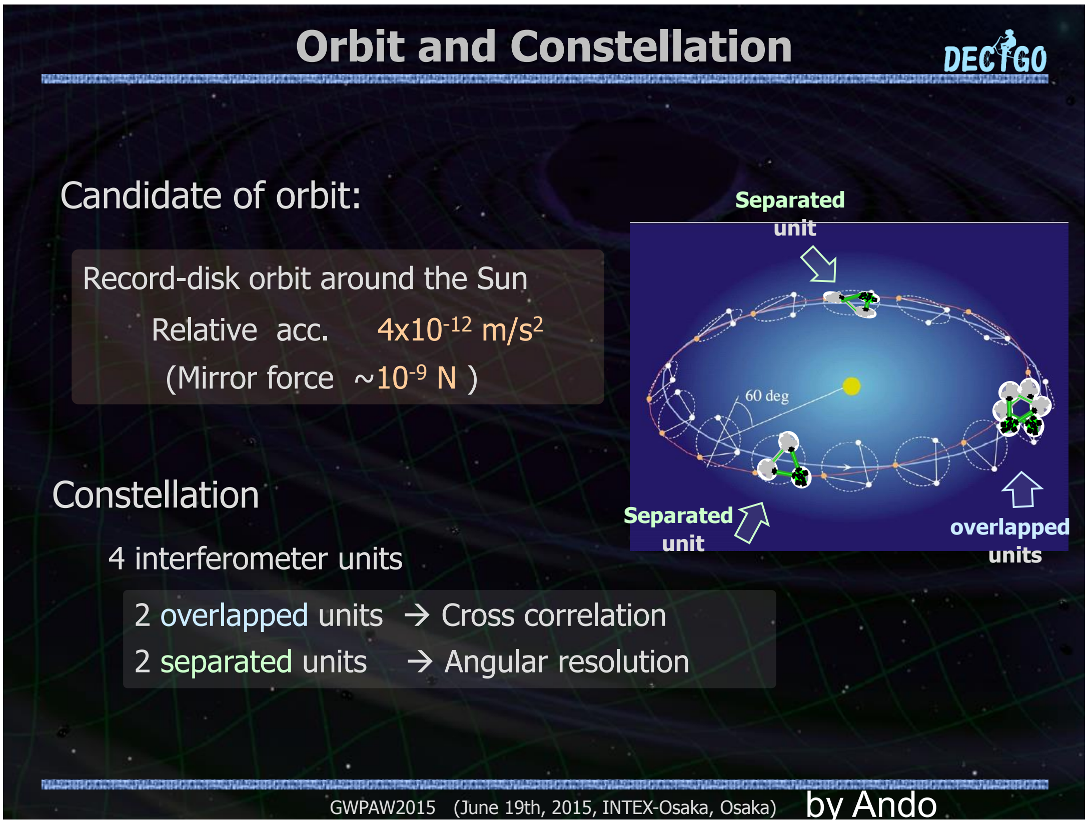
Orbit and Constellation
DECIGO
Candidate of orbit:
Record-disk orbit around the Sun
Relative acc. 4x10^-12 m/s^2
(Mirror force ~10^-9 N)
Separated
unit
60 deg
Separated
unit
overlapped
units
Constellation
4 interferometer units
2 overlapped units → Cross correlation
2 separated units → Angular resolution
GWPAW2015 (June 19th, 2015, INTEX-Osaka, Osaka)
by Ando

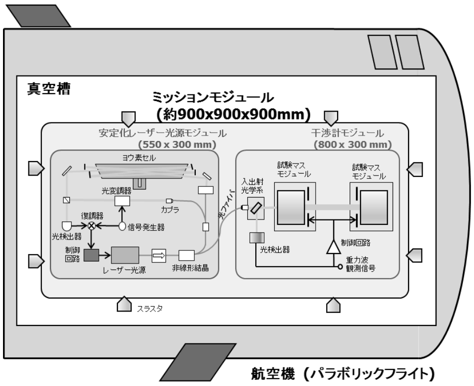

Project A

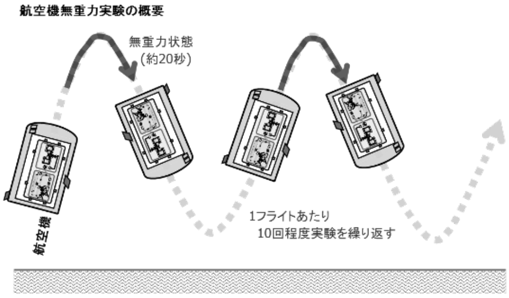

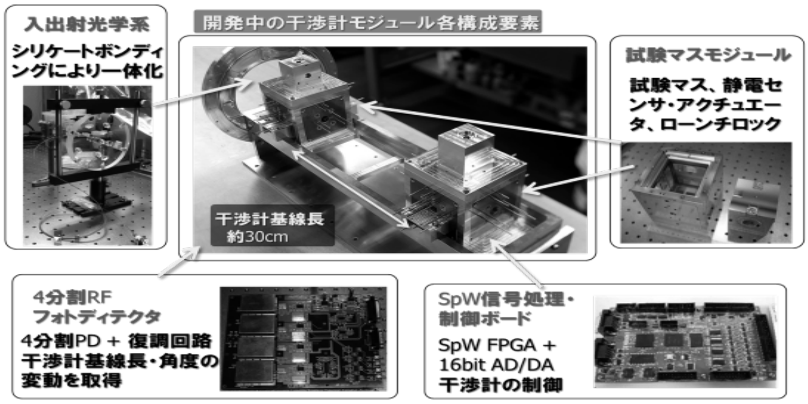

Project A

Thank you for your attention

Narikawa et al.2015 argued the possibility of detecting graviton oscillation

C. Modified inspiral waveforms due to graviton oscillations

Here we discuss only the inspiral phase of gravitational waves from CCB systems in the ghost-free bigravity model. Both h and $\tilde{h}$ are excited exactly as in the case of GR [24]. By using the stationary phase approximation, the observed signal in the frequency domain is given as[2]

$$h(f) = \mathcal{A}(f)e^{i\Phi(f)}[B_1 e^{i\delta\Phi_1(f)} + B_2 e^{i\delta\Phi_2(f)}], \quad (10)$$

where the amplitude $\mathcal{A}(f)$ (up to Newtonian order), the bigravity corrections $B_{1,2}$ and the phase function $\Phi(f)$ (up to 3.5PN order), and the phase corrections $\delta\Phi_{1,2}$ are given as

$$\mathcal{A}(f) = \sqrt{\frac{5\pi}{24}} \frac{\mathcal{M}^2}{(8\pi M_{\mathrm{G}}^2)^2 D_L} y^{-7/6}, \quad (11)$$

$$B_1 = \cos\theta_g(\cos\theta_g + \sqrt{\kappa}\xi_c \sin\theta_g), \quad (12)$$

$$B_2 = \sin\theta_g(\sin\theta_g - \sqrt{\kappa}\xi_c \cos\theta_g), \quad (13)$$

$$\begin{aligned}\Phi(f) \equiv\ & 2\pi f t_c - \Phi_c - \pi/4 + \frac{3}{128} y^{-5/3}\left\{1 + \left(\frac{3715}{756} + \frac{55}{9}\eta\right)\eta^{-2/5}y^{2/3} - 16\pi\eta^{-3/5}y\right.\\ &+ \left(\frac{15\,293\,365}{508\,032} + \frac{27\,145}{504}\eta + \frac{3085}{72}\eta^2\right)\eta^{-4/5}y^{4/3} + \left(\frac{38\,645}{756} - \frac{65}{9}\eta\right)\left[1 + \ln\left(\frac{y}{y_{\mathrm{ISCO}}}\right)\right]\pi\eta^{-1}y^{5/3}\\ &+ \left[\frac{11\,583\,231\,236\,531}{4\,694\,215\,680} - \frac{640}{3}\pi^2 - \frac{6848}{21}\gamma_{\mathrm{E}} - \frac{6848}{63}\ln(64\eta^{-3/5}y)\right.\\ &+ \left.\left(-\frac{15\,737\,765\,635}{3\,048\,192} + \frac{2255}{12}\pi^2\right)\eta + \frac{76\,055}{1728}\eta^2 - \frac{127\,825}{1296}\eta^3\right]\eta^{-6/5}y^2\\ &+ \left.\left(\frac{77\,096\,675}{254\,016} + \frac{378\,515}{1512}\eta - \frac{74\,045}{756}\eta^2\right)\pi\eta^{-7/5}y^{7/3}\right\}, \quad (14)\end{aligned}$$

$$\delta\Phi_{1,2} = -\frac{\mu D_L\sqrt{\tilde{c} - 1}}{2\sqrt{2x}}\left(1 + x \mp \sqrt{1 + x^2 + 2x\frac{1 - \kappa\xi_c^2}{1 + \kappa\xi_c^2}}\right), \quad (15)$$

$$|h(f)| = \mathcal{A}(f)(1 + 2B_1B_2(\cos(\Delta\delta\Phi) - 1))^{1/2}, \quad (16)$$

$$\Delta\delta\Phi \equiv \delta\Phi_1 - \delta\Phi_2. \quad (17)$$

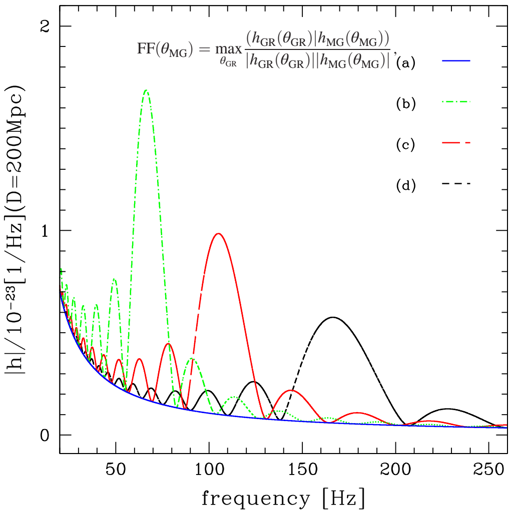

FIG. 1 (color online). The frequency-domain gravitational waves $h(f)$ for different values of the model parameter sets of $(\mu^2, \tilde{c}-1)$. The curves are plotted for (a) GR [solid (blue)] and for the bigravity models with (b) $(\mu^2, \tilde{c}-1) = (10^{-33.2}\ \mathrm{cm}^{-2}, 10^{-17.8})$ [dot-dashed (green)], (c) $(10^{-33}\ \mathrm{cm}^{-2}, 10^{-18})$ [long-dashed (red)], and (d) $(10^{-32.8}\ \mathrm{cm}^{-2}, 10^{-18.2})$ [dashed (black)], respectively, at fixed $\kappa\xi_c^2 = 100$. Here we consider BNS at the distance, $D_L = 200$ Mpc. The SNR and the fitting factor between the GR waveform and each waveform in this figure become as follows: $(\mathrm{SNR}, \mathrm{FF}) =$ (a) (8.7,1.0), (b) (31,0.50), (c) (26,0.47), (d) (21,0.53). The definition of FF is given in Eq. (23).

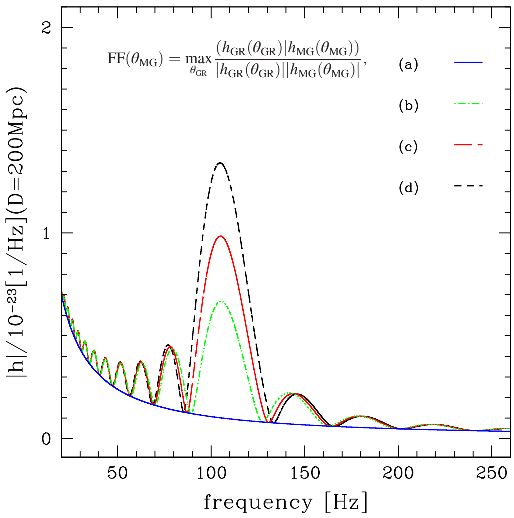

FIG. 3 (color online). The same as Fig. 1 but for different values of $\kappa\xi_c^2$ in the case of $(\mu^2, \tilde{c}-1) = (10^{-33}\ \mathrm{cm}^{-2}, 10^{-18})$. The curves are for (a) GR [solid (blue)] and the bigravity model with (b) $\kappa\xi_c^2 = 50$ [dot-dashed (green)], (c) $\kappa\xi_c^2 = 100$ [long-dashed (red)], and (d) $\kappa\xi_c^2 = 1000$ [dashed (black)], respectively. Each curve corresponds to $(\mathrm{SNR}, \mathrm{FF}) =$ (a) (8.7,1.0), (b) (19,0.58), (c) (26,0.47), (d) (34,0.41).

$$f_{\mathrm{peak}} \equiv \frac{1}{2\pi}\left(\frac{\mu^2}{2(\tilde{c}-1)}\right)^{1/2}. \tag{18}$$

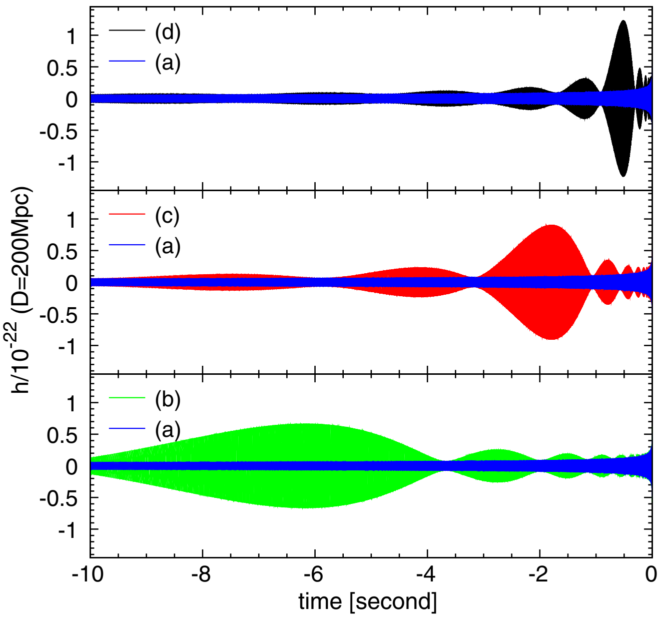

FIG. 2 (color online). The time-domain gravitational waveform $h(t)$. The coalescence time t_c is set to 0. The parameters and the definitions of the curves are the same as those of Fig. 1.

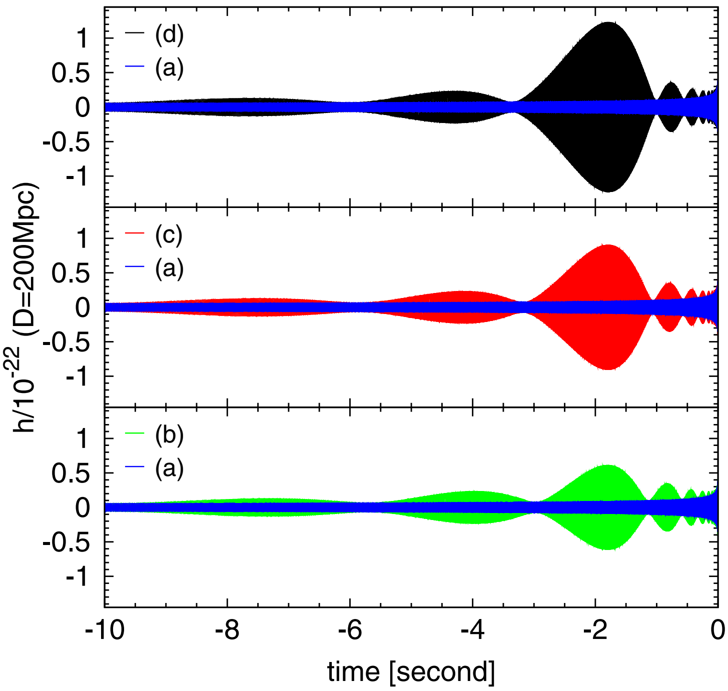

FIG. 4 (color online). The time-domain gravitational waveform $h(t)$. The parameters are the same as those of Fig. 3.

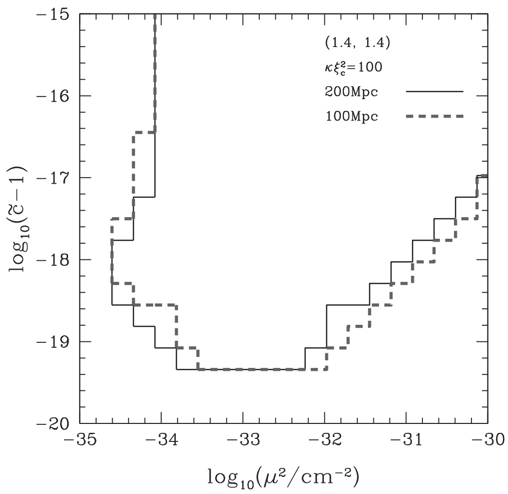

FIG. 5. The detectable region of the bigravity corrections to the waveforms in the case $(m_1, m_2) = (1.4M_\odot, 1.4M_\odot)$ and $\kappa\xi_c^2 = 100$. Curves correspond to the distance to the source at $D_L = 200$ Mpc (solid) and 100 Mpc (dashed). The detectable region is upper and right-hand side of these curves. The detectable region is defined as the region where $\mathrm{SNR} > \mathrm{SNR}_{\mathrm{req}}$ is satisfied. The false-alarm probability is set to $F = 10^{-4}$.

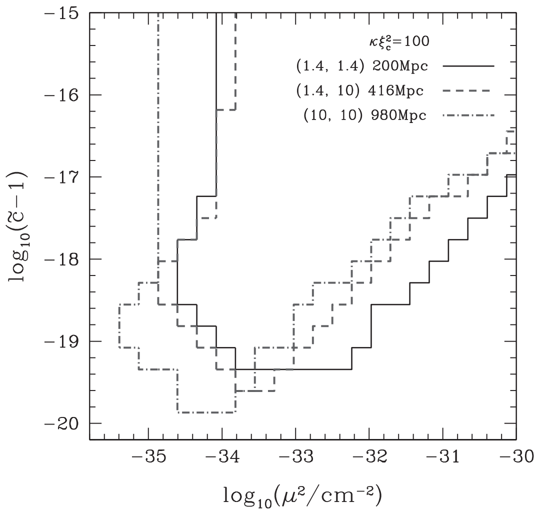

FIG. 6. A plot similar to Fig. 5 but for the waveforms from BNS with $(m_1, m_2) = (1.4M_\odot, 1.4M_\odot)$ at 200 Mpc (solid), NSBH with $(m_1, m_2) = (1.4M_\odot, 10M_\odot)$ at 416 Mpc (dashed), and BBH with $(m_1, m_2) = (10M_\odot, 10M_\odot)$ at 980 Mpc (dot-dashed), respectively. We set $\kappa\xi_c^2 = 100$. The detectable region is upper and right-hand side of these curves. SNR of the gravitational waves from these systems in GR limit are 8.7.

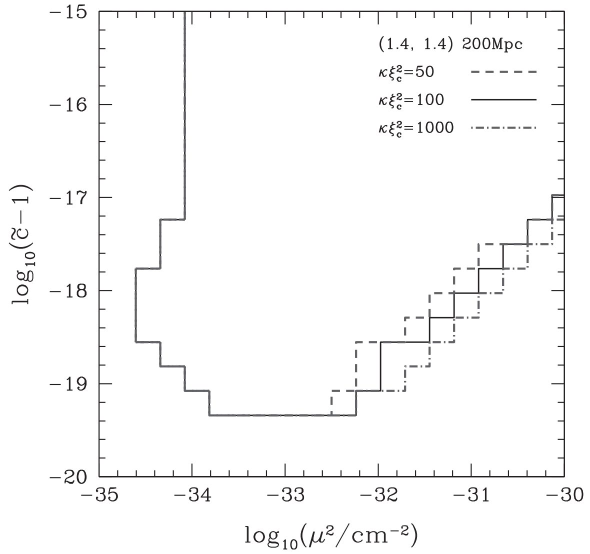

FIG. 7. A plot similar to Fig. 5, but for $\kappa\xi_c^2 = 50$ (dashed), 100 (solid), and 1000 (dot-dashed), respectively. The masses are $(m_1, m_2) = (1.4M_\odot, 1.4M_\odot)$ and the distance is 200 Mpc.

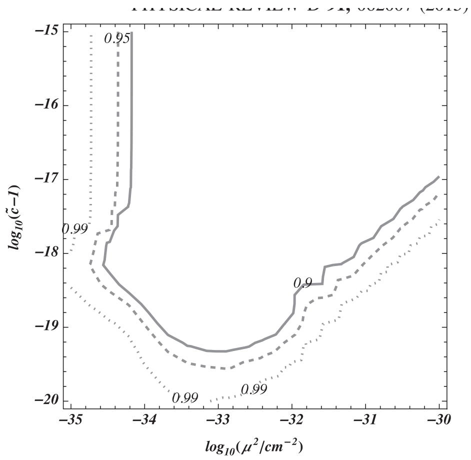

FIG. 8. Contour plots of the fitting factor between the GR and bigravity waveforms in the $(\mu^2, \tilde{c}-1)$ parameter space. Here we adopt the model $\kappa\xi_c^2 = 100$. Curves correspond to contours of FF = 0.9 (solid), FF = 0.95 (dashed), and FF = 0.99 (dotted). We assume BNS at $D_L = 200$ Mpc.

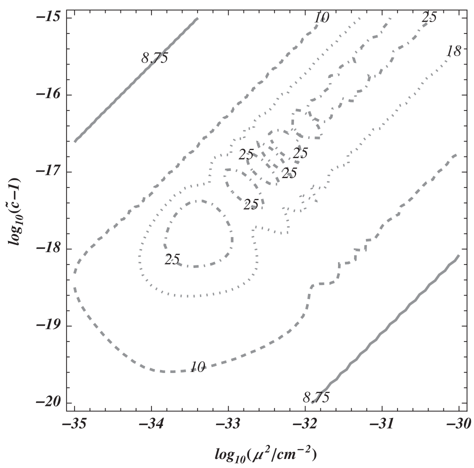

FIG. 9. Contour plots of the SNR of bigravity waveforms in the $(\mu^2, \tilde{c}-1)$ parameter space. The parameters are the same as those of Fig. 5. Curves correspond to contours of SNR = 8.75 (solid), SNR = 10 (dashed), SNR = 18 (dotted), and SNR = 25 (dot-dashed). We assume BNS at $D_L = 200$ Mpc.

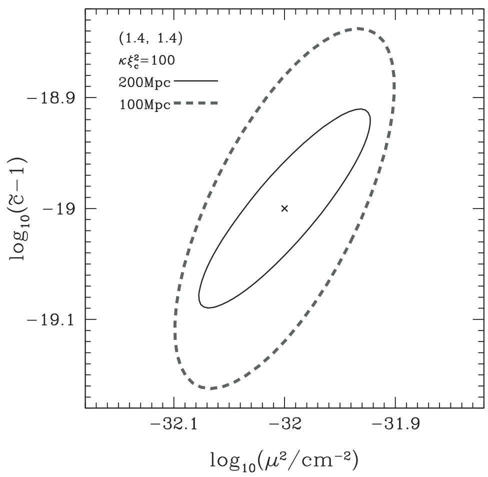

FIG. 11. Same as Fig. 10 but for the fiducial model, $(\mu^2, \tilde{c}-1) = (10^{-32}\ \mathrm{cm}^{-2}, 10^{-19})$. SNR is renormalized to SNR = 10.

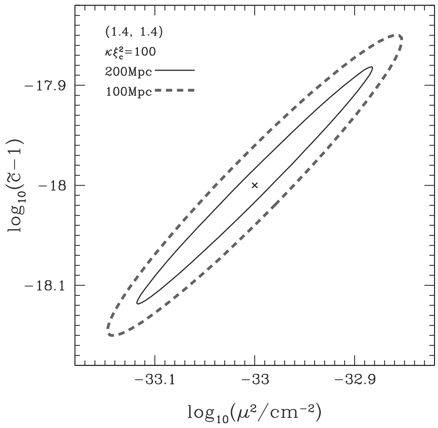

FIG. 10. Projected 1σ error contours on the $(\mu^2, \tilde{c}-1)$ plane. The results are obtained from the Fisher matrix with 8-parameters, $\log\mu^2, \log(\tilde{c}-1), \kappa\xi_c^2, \log D_L, \mathcal{M}, \eta, t_c$, and Φ_c, and marginalized over 6 parameters other than $\log\mu^2$ and $\log(\tilde{c}-1)$. The fiducial model is $(\mu^2, \tilde{c}-1) = (10^{-33}\mathrm{cm}^{-2}, 10^{-18})$, for BNS at $D_L = 200$ Mpc (solid) and at 100 Mpc (dashed). SNR is renormalized to SNR = 10.

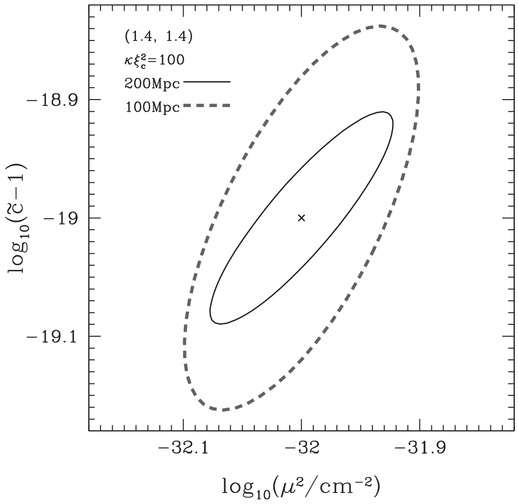

FIG. 11. Same as Fig. 10 but for the fiducial model, $(\mu^2, \tilde{c}-1) = (10^{-32}\ \mathrm{cm}^{-2}, 10^{-19})$. SNR is renormalized to SNR = 10.

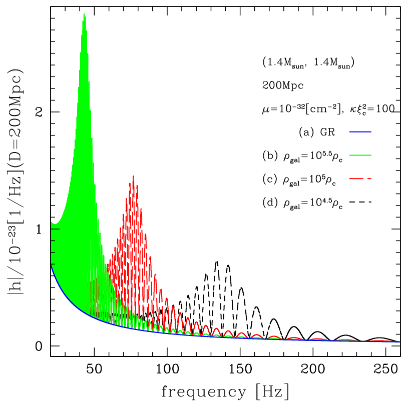

FIG. 12 (color online). The frequency-domain gravitational waves $h(f)$ for DFNT subset of the bigravity model for different values of the average density in the galaxies ρ_{gal}, where GWs are generated. The curves are plotted for (a) GR (solid (blue)) and for the DFNT subset of the bigravity model with (b) $\rho_{\mathrm{gal}} = 10^{5.5}\rho_{\mathrm{c}}$ (dot-dashed (green)), (c) $10^5\rho_{\mathrm{c}}$ (long-dashed (red)), and (d) $10^{4.5}\rho_{\mathrm{c}}$ (dashed (black)), respectively, at fixed $(\mu^2, \kappa\xi_c^2) = (10^{-32}\ \mathrm{cm}^{-2}, 100)$. Here we consider BNS at the distance, $D_L = 200$ Mpc. The SNR and the fitting factor between GR waveform and each waveform in this figure become as follows. (SNR, FF) = (a) (8.7,1.0), (b) (26,0.71), (c) (24,0.72), (d) (19,0.73).

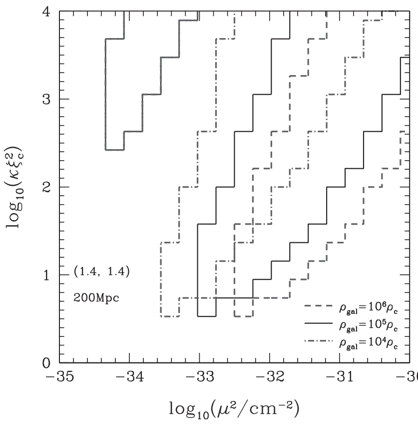

FIG. 13. The detectable region of the bigravity corrections to the waveforms for DFNT subset of the bigravity model in the case $(m_1, m_2) = (1.4M_\odot, 1.4M_\odot)$ and $D_L = 200$ Mpc. Curves correspond to the average density in the galaxies $\rho_{\mathrm{gal}} = 10^{5.5}\rho_{\mathrm{c}}$ (dashed), $10^5\rho_{\mathrm{c}}$ (solid), and $10^{4.5}\rho_{\mathrm{c}}$ (dot-dashed).

significant. The left region does not exist in the phenomenological model. As an example, if we pick up one point in the left region at $(\mu^2, \kappa\xi_c^2) = (10^{-34}\ \mathrm{cm}^{-2}, 10^{3.2})$, we have $f_{\mathrm{peak}} = 0.20$ Hz for $\rho_{\mathrm{Gal}} = 10^5\rho_c$, which is out of the detector sensitivity band. While the amplitude and

$$\tilde{c} - 1 = 3H_0^2 \frac{\rho_{\mathrm{m}}}{\rho_c} \frac{1 + \kappa\xi_c^2}{\mu^2}$$

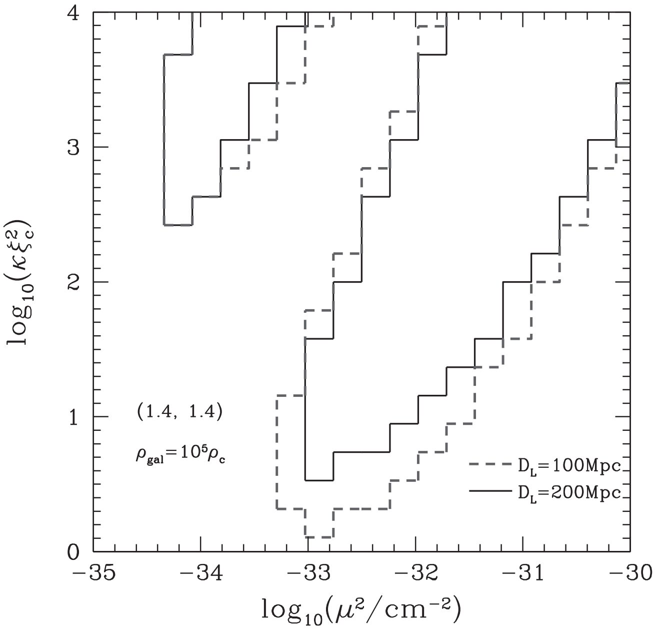

FIG. 14. A plot similar to Fig. 13, but for $D_L = 100$ Mpc (dashed) and 200 Mpc (solid), respectively. The masses are $(m_1, m_2) = (1.4M_\odot, 1.4M_\odot)$. We set $\rho_{\rm gal} = 10^5\rho_{\rm c}$.